2.5.3 Surface Faulting

NAPS COL 2.0-28-A

The information needed to address DCD COL Item 2.0-28-A is included in SSAR Section 2.5.3, which is incorporated by reference with the following variance and supplements.

NAPS ESP VAR 2.0-4

The last sentence of the first paragraph of this SSAR section is replaced as follows.

Information contained in these sections is consistent with RG 1.208 (Reference 2.5-226), and is intended to satisfy 10 CFR 100.23, “Geologic and Seismic Siting Criteria” (SSAR Reference 4).

2.5.3.2.1 Chopawamsic and Spotsylvania Thrust Faults

The following is added to the end of the second paragraph of this SSAR section as follows.

Recent geologic mapping by Hughes and Hibbard (Reference 2.5-246) at a scale of 1:24,000 in the northern half of the Ferncliff, VA 7.5’ quadrangle indicates that the Chopawamsic fault may not be folded as had been interpreted by previous investigators (SSAR References 66 and 105). Mapping by Hughes and Hibbard (Reference 2.5-246) also indicates that the Ellisville pluton appears to cross-cut the Chopawamsic fault suggesting it is younger than the sinistral motion and thrust faulting that occurred approximately 471-440 million years ago. This mapping simplifies the geometry of the Chopawamsic fault and has the effect of moving the surface trace of the fault further to the northwest (Reference 2.5-246) than had been mapped by previous investigators (SSAR References 66 and 105).

2.5.3.2.4 Other Faults Within the Chopawamsic Terrane

Two sentences are added to the end of the fourth paragraph of this SSAR section as follows.

The mainshock and several deep aftershock epicenters associated with the Mineral earthquake are located near the mapped Long Branch fault (Figure 2.5.1-205). However, the up-dip projection of the aftershock rupture surface places the location of potential surface rupture several miles west of the Long Branch fault (Figures 2.5.1-203 and 2.5.1-205).

NAPS COL 2.0-28-A

2.5.3.2.5 Unit 3 Subsurface Investigation

Borehole data, from the supplemental subsurface investigation described in Section 2.5.4.3, were reviewed for evidence of Quaternary fault movement. No such evidence was exhibited by the borehole data.

2.5.3.4 Ages of Most Recent Deformations

Two paragraphs are added to the end of this SSAR section as follows.

The subsurface structure defined by aftershocks resulting from the Mineral earthquake is located beyond the 5-mile radius site area (Figures 2.5.1-204 and 2.5.1-205).

- No evidence of surface rupture, surface fault features, or geomorphic expression of surface rupture or coseismic surface tectonic deformation exists for the Mineral earthquake. Based on reconnaissance performed by other researchers immediately following the earthquake and the field reconnaissance of the epicentral region on April 19-21, 2012, the **M** 5.8 earthquake did not produce any discernible rupture or deformation at the ground surface.
- The Mineral earthquake does not appear to have occurred on a previously mapped fault. The surface projection of fault rupture crosses the trace of the Chopawamsic thrust and is near to the southeast margin of the Ellisville pluton tail. Hughes and Hibbard (Reference 2.5-246) reinterpreted the Chopawamsic fault as being truncated where it intersects the Ellisville pluton, making the sub-parallel contact between the Chopawamsic Formation and the Ellisville pluton the nearest mapped structural surface on which a fault could be located. It has been suggested that this contact is faulted, based on offset dikes mapped in the region and is a possible candidate for the causative fault for the Mineral earthquake.
- The mainshock and deep aftershock epicenters are located near the mapped Long Branch fault. However, the up-dip projection of the aftershock rupture plane places the surface rupture several miles west of the Long Branch fault.

The earthquake epicenter, the surface projection of the aftershock rupture and any known potentially related faults are all located outside the 5-mile radius site area (Figures 2.5.1-204, 2.5.1-205, and 2.5.1-206).

2.5.4 Stability of Subsurface Materials and Foundations

NAPS COL 2.0-29-A

The information needed to address DCD COL Item 2.0-29-A is included in SSAR Section 2.5.4, which is incorporated by reference with the following supplements.

SSAR Section 2.5.4 has been supplemented by integrating information on the additional Unit 3 borings into a single section with the same numbering as the SSAR.

2.5.4.1 Geologic Features

SSAR Section 2.5.1.1 describes the regional geology, including regional physiography and geomorphology, regional geologic history, regional stratigraphy, and the regional tectonic setting. SSAR Section 2.5.1.2 addresses site-specific geology and structural geology, including site physiography and geomorphology, site geologic history, site stratigraphy, site structural geology, and a site geologic hazard evaluation.

2.5.4.2 Properties of Subsurface Materials

2.5.4.2.1 Introduction

This section describes the static and dynamic engineering properties of the Unit 3 site subsurface materials. An overview of the subsurface profile and materials is given in Section 2.5.4.2.2. The field investigations are described in Section 2.5.4.2.3. The laboratory tests on soil and rock samples from the investigation and their results are presented in Section 2.5.4.2.4. The engineering properties of the subsurface materials are given in Section 2.5.4.2.5.

2.5.4.2.2 Description of Subsurface Materials

The following is a brief description of the subsurface materials, giving the soil and rock constituents, and their range of thicknesses encountered at the Unit 3 site. The information was taken from the 93 borings made at the site (outlined in Section 2.5.4.2.3). For reference, the existing site ground surface elevations in the areas explored range from about Elevation 250 ft to Elevation 335 ft, with a median of about Elevation 296 ft. The design plant grade elevation for Unit 3 is Elevation 290 ft. Vertical datum is with reference to NAVD88 throughout Section 2.5.4, unless stated otherwise. Also, directions are with respect to Plant North, unless stated otherwise.

a. **Zone III-IV and Zone IV Bedrock**

The Unit 3 subsurface investigation (Appendices 2.5.4AA, 2.5.4BB, and 2.5.4CC) describes the bedrock underlying the power block area mostly as quartz gneiss, biotite quartz gneiss, quartz biotite gneiss, or biotite gneiss. A detailed description of the bedrock is provided in Section 2.5.1.2.3.

The top of Zone IV bedrock encountered in the borings made for Unit 3 ranges from about Elevation 171 ft to Elevation 278 ft. Top of Zone IV rock contours beneath the Unit 3 power block area are shown on Figure 2.5.4-201. The top of Zone III-IV bedrock ranges from about Elevation 187 ft to Elevation 292 ft. Top of Zone III-IV rock contours beneath the Unit 3 power block area are shown on Figure 2.5.4-202.

b. **Zone III Weathered Rock**

The top of Zone III bedrock encountered in the borings made for Unit 3 ranges from about Elevation 206 ft to Elevation 292 ft. The maximum thickness measured is about 77 ft. Top of Zone III rock contours beneath the Unit 3 power block area are shown on Figure 2.5.4-203.

c. **Zone IIA and IIB Saprolites**

Distribution of Zone IIA and IIB saprolites varies throughout the Unit 3 site. The Zone IIB saprolites represent about 25 percent of the saprolites on site and are typically very dense silty sands with from 10 to 50 percent core stone. The thickest Zone IIB deposit encountered in the Unit 3 borings was 43 ft while the median thickness was about 8 ft. The top of Zone IIB saprolite encountered ranges from about Elevation 215 ft to Elevation 302 ft. Top of Zone IIB saprolite contours beneath the Unit 3 power block area are shown on Figure 2.5.4-204.

The overlying Zone IIA saprolites comprise, at the Unit 3 site, about 75 percent of the saprolitic materials on site. About 80 percent of the Zone IIA saprolites are classified as coarse grained (sands, silty sands), while the remainder are fine grained (clayey sands, sandy and clayey silts, and clays). The thickest Zone IIA deposit encountered in the Unit 3 borings was 94 ft while the median thickness was about 30 ft. The top of Zone IIA saprolite ranges from about Elevation 232 ft to Elevation 335 ft. Top of Zone IIA saprolite contours beneath the Unit 3 power block area are shown on Figure 2.5.4-205.

d. **Zone I and Fill**

For Unit 3 foundations, Zone I soils and existing fills will be excavated. Thus, they are not considered further here.

e. **Subsurface Profiles**

Figures 2.5.4-207 through 2.5.4-216 illustrate typical subsurface profiles across the Unit 3 power block area. The locations of these profiles are shown in Figure 2.5.4-206. These profiles, with structure cross-sections added, are presented to illustrate foundation interfaces in Section 2.5.4.3. They also are used to illustrate the Unit 3 excavation in Section 2.5.4.5, and for bearing capacity considerations in Section 2.5.4.10.

2.5.4.2.3 Field Investigations

The borings, observation wells, and cone penetrometer tests (CPTs) from the Unit 3 site exploration program are summarized in Tables 2.5.4-201, 2.5.4-202, and 2.5.4-203, respectively. The elevations, depths and thicknesses of the subsurface zones observed from the individual borings are shown in Table 2.5.4-204. Geophysical surveys are described in Section 2.5.4.4.

The initial subsurface field investigation (900-series borings, observation wells, etc.) was performed during August through November 2006. Two supplemental subsurface investigations were performed later, one in September and early October 2009 (M-series borings) and the other in October 2009 (W-series borings). The W-series borings were labeled as Investigation Supplement No. 1 and the M-series borings were labeled as Investigation Supplement No. 2. Most of the initial investigation and all of the supplemental investigations were conducted in the power block area with the number and depth of investigation points conforming to the guidance provided in RG 1.132 (SSAR Reference 153). Additional exploration points were located outside the power block area, e.g., at the proposed locations for the cooling towers.

The Unit 3 exploration point locations in the power block area are shown in Figure 2.5.4-217. Selected borings from previous exploration programs are also shown. Exploration points outside the power block area are shown on Figure 2.5.4-218.

The scope of work and the special methods used to collect field data are listed below:

- 93 exploratory borings (MACTEC Engineering and Consulting, Raleigh, North Carolina) including 55 borings in the 900-series, 10 W-series borings, and 28 M-series borings
- 7 observation wells with permeability (slug) tests in 4 wells (MACTEC Engineering and Consulting, Raleigh, North Carolina, and Bedford Well Drilling, Bedford, Virginia)
- 4 packer tests (Miller Well Drilling, Hayesville, North Carolina, under MACTEC supervision)
- 23 CPTs including 4 down-hole seismic cone tests and pore pressure dissipation tests in 4 CPTs (Gregg InSitu, Inc., Columbia, South Carolina)
- 6 test pits (MACTEC Engineering and Consulting, Raleigh, North Carolina)
- 5 sets of borehole geophysical logging and 5 sets of suspension P-S velocity logging (GEOVision, Corona, California) including 3 sets in the 900-series and 2 M-series sets
- 2 sets of electrical resistivity tests (MACTEC Engineering and Consulting, Raleigh, North Carolina)
- Survey of exploration points (McKim and Creed, Virginia Beach, Virginia) for all the investigations

The exploration program was performed using the guidance in RG 1.132 (SSAR Reference 153). The fieldwork was performed under an audited and approved quality assurance program and work procedures developed specifically for the Unit 3 project. MACTEC Engineering and Consulting, contracted to Dominion to perform the subsurface investigation, worked under MACTEC's Quality Assurance Plan that met the requirements of 10 CFR 50, Appendix B. This Plan included meeting the requirements of Subpart 2.20 of ASME NQA-1, 1994 edition (Reference 2.5-204).

The subsurface investigation and sample/core collection was directed by the MACTEC site manager who was on site at all times during the field operations. A Bechtel geotechnical engineer or geologist, along with a Dominion representative, was also on site continuously during these operations. MACTEC's QA/QC engineer was on site part of the time. The

draft boring and well logs were prepared in the field by MACTEC geologists.

Sample and core storage and handling were in accordance with ASTM D 4220 (Reference 2.5-205). For the initial investigation, an on-site storage facility for soil samples and rock cores was established before the fieldwork began. This facility was in the limited access and climate controlled "A" Level area of the Units 1 and 2 warehouse. Samples and cores were stored either within a 12-ft square area surrounded by a 6-ft high chain link fence, or in an adjacent secured area. For the supplemental subsurface investigations, samples were stored in an on-site lockable, climate controlled 20 ft by 8 ft trailer, with a high security door system and security bars over each window. Each sample and core in each storage area was logged into an inventory control system. Samples removed from the facility were noted in the sample inventory logbook. A chain-of-custody form was also completed for samples removed from the facility.

Details and results of the exploration program are contained in Appendices 2.5.4AA (900-series), 2.5.4BB (W-series), and 2.5.4CC (M-series). The borings, observation wells, CPTs and test pits are summarized below. The laboratory tests are summarized and the results presented in Section 2.5.4.2.4. The geophysical tests are summarized and the results presented in Section 2.5.4.4.

a. **Borings and Samples/Cores**

The 93 borings drilled ranged from 22 ft to 300-ft in depth. The 300-ft deep boring was drilled at the center of the Reactor Building (RB) location, to about 215 ft depth in sound rock beneath the bottom of the basemat level. The borings were advanced in soil using rotary wash drilling techniques until standard penetration test (SPT) refusal (defined as 50 blows per 1 in. or less for start of rock coring) occurred. Steel casing was then set into the rock, and the holes were advanced using wireline rock coring equipment consisting of a 5-ft long "HQ" or "NQ" core barrel with a split inner barrel.

The soil was sampled using an SPT sampler at 2.5 ft intervals to about 15 ft depth and at 5 ft intervals below 15 ft. The SPT was performed using an automatic hammer, and was conducted in accordance with ASTM D 1586 (SSAR Reference 155). The recovered soil samples were visually described and classified by the onsite geologist. A selected

portion of the soil sample was placed in a glass sample jar with a moisture-proof lid. The sample jars were labeled, placed in boxes, and transported to the on-site storage area.

A set of energy measurements was made on each of the automatic SPT hammers used by the drill rigs that performed the borings. The nine sets of energy measurements were made in accordance with ASTM D 4633 (Reference 2.5-206). The average energy transfer ratio (ETR) for each rig ranged from 75.2 percent to 87.4 percent, with an overall average of 82.1 percent. The N-values shown on the boring logs (Appendices 2.5.4AA, 2.5.4BB, and 2.5.4CC) are not adjusted for hammer energy. N-values used in engineering analysis (e.g., liquefaction analysis) are adjusted for hammer energy, i.e., N_{60} was used in these situations.

Intact samples were obtained in accordance with ASTM D 1587 (Reference 2.5-220) using a Shelby tube sampler or a rotary Pitcher sampler. Upon sample retrieval, the disturbed portions at both ends of the tube were removed, both ends were trimmed square to establish an effective seal, and pocket penetrometer (PP) tests were performed on the trimmed lower end of the samples. Both ends of the sample were then sealed with hot wax, covered with plastic caps, and sealed once again using electrician tape and wax. The tubes were labeled and transported to the sample storage area. Undisturbed samples are identified on the boring logs included in Appendix 2.5.4AA.

Rock coring was performed in accordance with ASTM D 2113 (SSAR Reference 156). After removal from the split inner barrel, the recovered rock was carefully placed in wooden core boxes. The onsite geologist visually described the core, noting the presence of joints and fractures, and distinguishing natural breaks from mechanical breaks. The geologist also computed the percentage recovery and the RQD. Photographs of the cores were taken in the field. Filled and labeled core boxes were transported to the on-site sample storage facility.

The boring logs and the photographs of the rock cores are provided in Appendices 2.5.4AA, 2.5.4BB and 2.5.4CC, along with details of the automatic hammer energy measurements. Borehole locations, depths, etc. are summarized in Table 2.5.4-201. The soil and rock materials encountered in the Unit 3 borings were similar to those found in the previous sets of borings conducted at the NAPS site. The elevations, depths and thicknesses of the subsurface zones observed from the

individual borings are shown in Table 2.5.4-204. These values are based on SPT N-values, rock recovery values, and RQD depending on the zone for all 93 borings, except that the five shear wave velocity (V_S) borings (B-901, B-907, B-909, M-10 and M-30) also consider V_S measurement data. Section 2.5.4.4.4 presents the results of V_S measurements and summarizes the range of V_S values for each zone of rock. Section 2.5.4.7.1 describes the use of V_S ranges to determine top of zone elevations and thicknesses of subsurface zones.

b. **Observation Wells**

Each of the seven observation wells was installed adjacent to a sample boring. Three of the wells were screened in the soil/weathered rock zone, while four were screened in rock. Each well depth was selected in the field after a review of the borehole record. For the wells screened in rock, the screen depth was also based on the rock core description and packer test results. Boreholes for the wells in soil/weathered rock were advanced with hollow stem augers while the boreholes for all but one of the wells in rock were advanced using air-rotary drilling techniques. The borehole for the fourth well in rock (OW-951) was advanced with hollow stem augers until auger refusal, and was completed in rock using an “HQ” core barrel with a split inner barrel. This was after repeated cave-ins during attempts to advance the hole with air-rotary drilling.

After the designated depth of each well was reached, and the PVC screen and casing set, the sand pack and bentonite seal were placed, and then a grout plug was placed from the top of the bentonite seal to the ground surface. (In OW-951, a filter sock was placed over the screen, above which a formation packer and bentonite seal were set.) Each well was capped with a lockable steel cap and surrounded with a concrete pad.

Each well was developed by pumping. Two or three standing well volumes of water were purged initially by pumping, cycling the pump on and off to create a surging effect. The well was considered developed when the pH and conductivity stabilized and the pumped water was reasonably free of suspended sediment.

Permeability tests were performed in each of the three wells screened in soil/weathered rock, and in one of the wells screened in rock (OW-949) in accordance with ASTM D 4044, Section 8 (SSAR Reference 157) using a procedure that is commonly termed the slug test method. Slug testing

involves establishing a static water level, lowering a solid cylinder (slug) into the well to cause an increase in water level in the well, and monitoring the time rate for the well water to return to the pre-test static level. The slug is then rapidly removed to lower the water level in the well, and the time rate for the water to recover to the pre-test static level is again measured. Electronic transducers and data loggers were used to measure the water levels and times during the test.

Permeability testing by the packer method was conducted in the borings adjacent to the four wells screened in rock. Test procedures used are described in ASTM D 4630 (Reference 2.5-207), as modified by U.S. Army Corps of Engineers in their Rock Testing Handbook (Reference 2.5-208) to use a manually read flowmeter rather than a digitally recorded one. The packer testing method, known as the constant head injection test, involved establishing and maintaining a constant pressure in the test length, measured by an electronic transducer, to determine the rate of inflow associated with maintaining the pressure.

Appendix 2.5.4AA contains the boring logs for the observation wells, the well installation records, the well development records, and the well permeability and packer test results. Observation well locations, depths, etc., are summarized in Table 2.5.4-202.

c. **Cone Penetrometer Tests**

The 23 CPTs were advanced using a track-mounted 20 ton self-contained cone rig. Each CPT was advanced to refusal, to depths ranging from about 3 ft to 60 ft. Tip resistance, sleeve friction and porewater pressure were measured. The CPTs were performed in accordance with ASTM D 5778 (SSAR Reference 158). The pore pressure filter was located immediately behind the cone tip.

Down-hole seismic testing was performed at approximately 3 ft intervals in four of the CPTs (C-902, C-916, C-921 and C-923, see Section 2.5.4.4). One pore pressure dissipation test was performed in each of four CPTs (C-902, C-904b, C-911 and C-917) at depths ranging from about 13 ft to 29 ft.

The CPT logs, shear wave time of arrival records, and pore pressure versus time plots are contained in Appendix 2.5.4AA. CPT locations, depths, etc., are summarized in Table 2.5.4-203.

d. **Test Pits**

Six test pits were excavated to depths ranging from about 2 ft to 4.5 ft to obtain bulk samples of site soils to test for suitability as backfill. A rubber-tired backhoe was used to excavate the test pits. Bulk samples were collected in new 5 gallon plastic buckets. Small portions of the samples were placed in glass jars and sealed for moisture retention.

2.5.4.2.4 Laboratory Testing

Numerous laboratory tests of soil and rock samples were performed for Unit 3. The types and numbers of these tests are shown in Table 2.5.4-205.

The laboratory testing investigation was performed in accordance with the guidance presented in RG 1.138 (SSAR Reference 148). The laboratory work was performed under an approved quality assurance program with work procedures developed specifically for the Unit 3 project. Soil and rock samples were shipped under chain-of-custody protection from the storage area (described in Section 2.5.4.2.3) to the testing laboratory. When required, samples sent to the testing laboratory were divided and/or shipped to an appropriate testing laboratory under chain-of-custody rules. Laboratory testing of soil and rock samples, except for chemical tests and resonant column torsional shear (RCTS) tests, was performed at the MACTEC laboratories in Charlotte and Raleigh, North Carolina and Atlanta, Georgia. Chemical testing for pH, sulfates and chlorides in selected soil samples was conducted by Severn Trent Laboratories in Earth City, Missouri. RCTS testing of selected soil samples was performed by Fugro Inc. in Houston, Texas, under the technical direction of Dr. K. H. Stokoe of the University of Texas in Austin.

Since the Unit 3 power block area is approximately 1500 ft southwest of the center of the Unit 2 Containment Building, the tests focused on verifying that the properties of the soil and rock beneath the Unit 3 power block area were similar to those beneath Units 1 and 2 as determined during previous studies. In addition, chemical tests (for corrosiveness toward buried steel and aggressiveness toward buried concrete) and RCTS tests (for shear modulus and damping ratio variation with cyclic strain) were run on selected saprolite samples.

The details and results of the laboratory testing are included in Appendices 2.5.4AA and 2.5.4CC, except for the RCTS test results which are included in Appendix 2.5.4AAS1. Appendices 2.5.4AA

and 2.5.4CC include references to the industry standards used for each specific laboratory test. The results of the tests on soil samples (excluding strength and RCTS tests) are summarized in Tables 2.5.4-206a, 2.5.4-206b, and 2.5.4-206c. Table 2.5.4-207 gives the results of the unconfined compression tests on the rock cores. The results of the RCTS tests are shown in Figure 2.5.4-219.

The results of the laboratory tests as they relate to the engineering properties of the soil and rock are described in Section 2.5.4.2.5.

2.5.4.2.5 Engineering Properties

The engineering properties for Zones IIA, IIB, III, III-IV, and IV derived from the Unit 3 field exploration and laboratory testing programs are provided in Table 2.5.4-208 and described in the following paragraphs. These engineering properties are similar to those obtained from the previous field and laboratory testing programs (as shown in SSAR Table 2.5-45), with some differences. Where there are differences, the impact from an engineering standpoint is usually either the same or more favorable.

The following paragraphs discuss selected properties shown in Table 2.5.4-208 under the subheadings: a) rock properties, including concrete fill; b) soil properties, including structural fill; c) RCTS results; and d) chemical properties.

a. **Rock and Concrete Fill Properties**

Rock

In general, the rock strength and stiffness values, derived from the field and laboratory testing of the Unit 3 rock, are higher than given in the SSAR. This could reflect less fractured or weathered rock beneath the Unit 3 area, and/or better rock coring equipment and techniques that produced better quality cores.

The Recovery and RQD are based on the results presented for each core in the boring logs in Appendices 2.5.4AA, 2.5.4BB and 2.5.4CC. The RQDs from the borings for Strata III, III-IV and IV are plotted versus elevation in Figure 2.5.4-220. For Stratum III, RQD generally ranges from zero to around 50 percent, with some higher values. The average value is about 20 percent. For Stratum III-IV, RQD generally ranges from around 50 to 90 percent. The average value is about 65 percent (compared to 50 percent in the SSAR). For Stratum IV, RQD is generally above 80 percent and mostly above 90 percent. The average value is

about 95 percent. The average recovery values for Zone III, III-IV and IV are 55 percent, 90 percent, and 98 percent, respectively.

The unconfined compressive strengths and unit weights in Table 2.5.4-208 are based on the rock strength test results shown in Table 2.5.4-207. The elastic modulus values are also based on the values shown in Table 2.5.4-207. The shear modulus values are derived from the elastic modulus values using the Poisson's ratio values tabulated in Table 2.5.4-208. These higher strain shear modulus values agree well with the low strain values derived from the geophysical tests performed for the Unit 3 exploration program described in Section 2.5.4.4. These high and low strain shear modulus values are essentially the same for high strength rock, certainly for the Zone IV and Zone III-IV rock. Some strain softening has been allowed in the case of the Zone III rock, as described in Section 2.5.4.7. Low strain is defined here as 10^{-4} percent while high strain is taken as 0.25 to 0.5 percent, the amount of strain frequently associated with settlement of structures on soil.

Best estimate values of V_S and compression wave velocity V_P in Table 2.5.4-208 are based on suspension P-S velocity logging performed as part of the Unit 3 exploration program (Appendices 2.5.4AA and 2.5.4CC). These results are summarized in Section 2.5.4.4.4.

Concrete Fill

All of the saprolitic soils will be excavated from within the temporary wall that will be constructed around the power block area. As stated in Section 2.5.4.10, if Zone III rock is encountered at foundation subgrade level of the RB/FB, CB, or FWSC, it will be removed and replaced with concrete fill. The concrete fill will have a minimum strength of 2,500 psi, with a unit weight of 145 pcf and Poisson's ratio of 0.15. The bearing capacity of concrete fill is addressed in Section 2.5.4.10.1.

The top of Zone III-IV rock contours superimposed on the structure footprints in Figure 2.5.4-202 are used to estimate the thickness of Zone III rock that will be removed from beneath the RB/FB, CB or FWSC foundations and replaced with concrete fill. Up to 10 ft of concrete fill will be required under the northern edge of the RB, and up to 15 ft will be required under the southeast corner of the FB. Up to 30 ft of concrete fill will be required under the southeast portion of the CB while over 50 ft of concrete fill will be needed beneath most of the FWSC. Typical

thicknesses of concrete fill are illustrated on most of the subsurface profiles in Figures 2.5.4-207 through 2.5.4-216. Analysis indicates that if the top 25 ft of rock beneath the RB/FB foundation is replaced with concrete fill, the seismic response at foundation level decreases with increasing V_s of the concrete fill. Based on the calculated log-mean V_S value at and below the RB/FB foundation (shown in Figure 2.5.4-242), the V_S of the in-situ rock at 25 ft below the RB/FB foundation base is approximately 5000 ft/sec. Therefore, the V_S of the concrete fill should be equal to or greater than 5000 ft/sec to ensure that the seismic response of the column that includes the concrete fill is equal to or less than the response from the original analysis of the in-situ rock. Further analysis indicates that concrete with strength of 2500 psi has a best estimate V_S of 7000 ft/sec.

Construction, QA, and engineering properties of the concrete fill, including strength and durability, are controlled through project specifications. The project specifications provide controls on the construction process (including placement techniques), material properties (including mix design and concrete properties during placement; for example slump, air content, and mix temperature) and other variables. The concrete fill is required by project specifications to conform to the pertinent provisions of ACI 349 (Reference 2.5-215) including provisions contained in ASTM standards and ACI Committee 201 and 207 publications referenced within ACI 349.

b. **Soil Properties**

Zone IIA Saprolite

Grain size curves from sieve analyses of Zone IIA silty and clayey sand, and sandy silt samples are shown in Appendices 2.5.4AA and 2.5.4CC. The tests were run mainly on the silty sand samples with more than 90 percent having fines contents of less than 50 percent. Figure 2.5.4-221 shows fines content versus depth from these tests. The median fines content for the Zone IIA saprolite is about 24 percent, with the majority of samples having a Unified Soil Classification System (USCS) classification (Reference 2.5-209) of SM.

The median natural moisture content from 100 tests performed is 19 percent. For the relatively small percentage of samples that exhibited plasticity, the median liquid limit was 38 percent while the plasticity index (PI) was 11 percent.

The measured SPT N-values from 656 tests ranged from 2 to refusal (defined as >100 blows/ft), with a median value of 15 blows/ft. These are plotted versus depth on Figure 2.5.4-222. The N_{60} median value adjusted for hammer energy is 20 blows/ft. The effective angle of internal friction of a medium dense coarse-grained saprolite (N = 20 blows/ft) would typically be taken as around 35 degrees (SSAR Reference 150). However, the relatively high silt content and the presence of low plasticity clay minerals reduce this angle. Consolidated-undrained (C-U) triaxial tests reported in UFSAR Appendices 2C and 3E (SSAR Reference 5) produced internal friction angles (φ') ranging from 23 to 33 degrees, with a median of 30.8 degrees. The average effective cohesive (c') component from the Appendix 2C tests was 0.275 ksf. A series of C-U tests performed for the Unit 3 program gave effective internal friction angles ranging from about 31 to 36 degrees, with a median of 33 degrees, and very little effective cohesion. The values of φ' = 33 degrees and c' = 0.125 ksf were adopted for the Zone IIA saprolite. This compares with φ' = 30 degrees and c' = 0.25 ksf used in the SSAR.

A large amount of testing was performed after low unit weights were measured in the Zone IIA saprolites in the Units 1 and 2 Service Water Reservoir area. The testing details and results are given in UFSAR Appendix 3E, Attachment 4 (SSAR Reference 5). It was concluded that there are isolated lower densities, but these are not typical. UFSAR Table 3.8-13 (SSAR Reference 5) identifies 125 pcf as a design total unit weight. A value of 125 pcf is shown in Table 2.5.4-208.

The V_S versus depth measured in the soil by suspension P-S velocity logging and CPT seismic testing during the Unit 3 field investigation are shown in Figure 2.5.4-223. The average V_S ranges from about 500 ft/sec to 1200 ft/sec in the upper 40 ft, with a best estimate of about 850 ft/sec. This is presented in more detail in Section 2.5.4.4 and Section 2.5.4.7.

The high strain (i.e., in the range of 0.25 to 0.5 percent) elastic modulus value has been derived using the relationship with SPT N-value given in SSAR Reference 151. The shear modulus value has been obtained from the elastic modulus values using the relationship between elastic modulus, shear modulus and Poisson's ratio (SSAR Reference 150). The best estimate low strain (i.e., 10^{-4} percent) shear modulus has been derived from the V_S of 850 ft/sec. The low strain elastic modulus value has been obtained from this shear modulus value using the relationship

between elastic modulus, shear modulus, and Poisson's ratio (SSAR Reference 150).

In Table 2.5.4-208, the value of unit coefficient of subgrade reaction is based on the value for medium dense sand provided by Terzaghi (SSAR Reference 152), while the earth pressure coefficients are Rankine values, assuming level backfill and a zero friction angle between the soil and the wall (see also Section 2.5.4.10.3).

All of the bulk samples obtained from the test pits were Zone IIA saprolite, since the test pits only sampled near-surface soils. Details of the results of the modified Proctor compaction tests and the California Bearing Ratio (CBR) tests run on these samples are provided in Appendix 2.5.4AA. The maximum dry density ranged from about 100 pcf to 126 pcf, with a median value of 116 pcf. The corresponding optimum moisture content ranged from 9 to 22 percent, with a median value of 13 percent. A plot of molded dry density versus CBR (soaked samples) is given in Figure 2.5.4-224.

Zone IIB Saprolite

Grain size curves from 19 sieve analyses of Zone IIB silty sand samples are shown in Appendices 2.5.4AA and 2.5.4CC. The samples had fines contents ranging from about 15 to 27 percent. These fines contents are shown versus depth in Figure 2.5.4-221. The Zone IIB USCS classification is SM.

The measured SPT N-values from 206 tests ranged from 24 to refusal (defined as >100 blows/ft), with a median value of 75 blows/ft. These are plotted versus depth on Figure 2.5.4-222. The N_{60} median value adjusted for individual hammer energy is 100 blows/ft. The effective angle of internal friction of a very dense sand (N = 100 blows/ft) would typically be taken as over 40 degrees (SSAR Reference 150). However, with the moderately high silt content, φ' has been limited to 40 degrees with c' = 0. The unit weight of 130 pcf reflects the very dense nature of the Zone IIB saprolite.

The shear wave velocities measured in the soil by suspension P-S velocity logging and CPT seismic testing during the Unit 3 field investigation are shown in Figure 2.5.4-223. The average shear wave velocity ranges from about 1200 ft/sec to 2500 ft/sec with a best estimate of about 1600 ft/sec. This is presented in more detail in Section 2.5.4.4 and Section 2.5.4.7.

The high strain (i.e., in the range of 0.25 to 0.5 percent) elastic modulus value has been derived using the relationship with SPT N-value given in SSAR Reference 151. The shear modulus value has been obtained from the elastic modulus values using the relationship between elastic modulus, shear modulus and Poisson's ratio (SSAR Reference 150). The low strain (i.e., 10^{-4} percent) shear modulus has been derived from the best estimate shear wave velocity of 1600 ft/sec.

In Table 2.5.4-208, the value of unit coefficient of subgrade reaction is based on the value for dense sand provided by Terzaghi (SSAR Reference 152). The earth pressure coefficients are Rankine values, assuming level backfill and a zero friction angle between the soil and the wall (see also Section 2.5.4.10.3).

Structural Fill

Structural fill for placing around major power block structures is obtained from crushing the sound rock removed from the deep excavation for some of these structures, including the RB/FB, CB, and Radwaste Building. If there is an insufficient quantity of on-site sources, similar material will be obtained from offsite. The rock is crushed down to well-graded, angular or sub-angular sand and gravel-sized particles conforming to the gradation of Size No. 21A in the Virginia Department of Transportation (VDOT) Road and Bridge Specifications (SSAR Reference 166). It is compacted with heavy equipment in thin lifts to a dry density that is at least 95 percent of the maximum dry density obtained from ASTM D 1557 (SSAR Reference 165) (see also Section 2.5.4.5). Based on this, N_{60} = 50 blows/ft and φ' = 40 degrees were selected as reasonable and conservative.

Zone IIB saprolite material may be used as secondary structural fill as described in Section 2.5.4.5.3.

Additional details about the structural fill and the laboratory and field testing programs proposed for the backfill are presented in Section 2.5.4.5.3.

c. **RCTS Testing**

The results of the three RCTS tests are presented in Appendix 2.5.4AAS1 and illustrated in Figure 2.5.4-219. Two of the tests were on Zone IIA saprolites (each an SM sample, obtained using a Shelby tube) and one test was on a sample of Zone IIB saprolite (also SM, obtained using a rotary Pitcher barrel sampler). The test results on

Figure 2.5.4-219 show normalized shear modulus (G/G_{max}) and material damping ratio, D, versus shear strain, for both the resonant column and torsional shear modes. The results are shown for a confining pressure approximately equal to the in-situ confining pressure.

Comparison of the RCTS results with the generic curves used in the seismic soil column analyses is illustrated and discussed in Section 2.5.4.7.

d. **Electrical Resistivity and Chemical Properties**

When assessing the corrosion potential of soils, electrical resistivity and selected chemical testing results are typically used in combination. Field electrical resistivity and laboratory chemical tests were performed on the Zone IIA and Zone IIB saprolites during the Unit 3 subsurface investigation, and the results of the tests are given in Appendix 2.5.4AA. The results of the chemical tests are also shown in Table 2.5.4-206. The results are described in the following paragraphs.

Zone IIA Saprolite

The electrical resistivity measured in two arrays ranges from over 100 ohm-m close to the surface to around 500 ohm-m at 30 ft depth. The chloride content of the soil, measured in 15 tests, ranges from about ≤ 2 to 210 parts per million (ppm), with a median value of about 6 ppm. These results suggest very low corrosion potential. The pH, measured in 15 tests, ranges from 4.8 to 7, with a median of 5.8. These pH results indicate a higher corrosion potential than the resistivity or chloride results. The sulfate content measured in 15 tests ranges from about ≤ 3 to 11 ppm, indicating that no special sulfate resisting cement is required.

Zone IIB Saprolite

The electrical resistivity measured in two arrays was about 450 ohm-m at 50 ft depth. The chloride content, measured in 5 tests, is less than 10 ppm, while the pH ranges from 6.7 to 7.4. These results suggest very low corrosion potential. The sulfate content measured in 5 tests ranges from ≤ 2 to 9 ppm, indicating that no special sulfate resisting cement is required.

2.5.4.3 Foundation Interfaces

NAPS ESP COL 2.5-2

The locations of site exploration points for the Unit 3 subsurface investigation, including borings, observation wells, CPTs, electrical resistivity tests, and test pits made in the power block area are shown on

Figure 2.5.4-217. Borings from previous exploration programs are also shown. Exploration points outside the power block area are shown on Figure 2.5.4-218.

NAPS ESP COL 2.5-3

Figure 2.5.4-206 shows the excavation plan for the safety-related and other major facilities. Also shown in Figure 2.5.4-206 are the locations of the 10 subsurface profiles shown on Figures 2.5.4-207 through 2.5.4-216. The cross sections of the structure foundations and the proposed excavation and backfilling limits are superimposed on Figures 2.5.4-207 through 2.5.4-216 to produce Figures 2.5.4-225 through 2.5.4-234.

NAPS COL 2.0-29-A

Logs of the core borings are in Appendices 2.5.4AA, 2.5.4BB, and 2.5.4CC, and logs of observation wells, CPTs and test pits are in Appendix 2.5.4AA.

2.5.4.4 Geophysical Surveys

The geophysical testing for Unit 3 consisted of field electrical resistivity testing, geophysical down-hole testing, and seismic CPTs.

2.5.4.4.1 Field Electrical Resistivity Testing

Field electrical resistivity testing was conducted along two crossing lines located as shown on Figure 2.5.4-217. The Wenner four-electrode method was used to perform the tests in accordance with ASTM G 57 (Reference 2.5-210). In this method, four electrodes, two for current and two for voltage, are spaced an equal distance apart and inserted about 1 ft into the ground. A current is sent through the two outer electrodes and voltage is measured at the two inner electrodes. Electrode spacing ("A" spacing) ranged from 3 ft to 100 ft. The results of the testing are given in Appendix 2.5.4AA and are described relative to corrosion potential in Section 2.5.4.2.5.d.

2.5.4.4.2 Geophysical Down-Hole Testing

This suite of tests was performed in borings B-901 (300.0 ft depth), B-907 (200.5 ft depth), B-909 (201.9 ft depth), M-10 (201.9 ft) depth), and M-30 (201.7 ft depth). The tests conducted were natural gamma, three arm caliper, resistivity, spontaneous potential, borehole acoustic televiewer logging, boring deviation, and suspension P-S velocity logging. The results of all of these tests and detailed descriptions of the test methods are in Appendices 2.5.4AA and 2.5.4CC. Plots of the V_S and V_P results

versus depth are presented in Section 2.5.4.4.4. The descriptions below are summarized from the more detailed descriptions in Appendices 2.5.4AA and 2.5.4CC.

For all of the tests, all five borings were logged as partially-cased borings, filled with clear water or polymer-based drilling mud, with a 4-in diameter PVC or steel casing placed in the top 40 ft (B-901 and B-907), 44 ft (M-30), 80 ft (B-909), or 90 ft (M-10) of soil above bedrock contact during the measurements in the lower rock portions of the borings. The casing was then removed and measurements were performed in the upper soil portion of the borings. The instrument probe receives control signals from, and sends the digitized receiver signals to, instrumentation on the surface via an armored 4-conductor cable. The cable is wound onto the drum of a winch and is used to support the probe.

a. **Natural Gamma and 3-Arm Caliper**

Natural gamma and caliper data were collected using a Model 3ACS 3-leg caliper probe, manufactured by Robertson Geologging, Ltd. With this tool, caliper measurements were collected concurrently with the measurement of natural gamma emission from the borehole wall. The probe is 6.82 ft long and 1.5 in. in diameter and can:

- Measure boring diameter and volume
- Locate hard and soft formations
- Locate fissures, caving, pinching and casing damage
- Identify bed boundaries
- Correlate strata between borings
- Provide natural gamma measurements

Natural gamma measurements rely upon small quantities of radioactive material contained in all rocks to emit gamma radiation as they decay. The measurement is useful because the radioactive elements are concentrated in certain rock types, e.g., clay or shales, and depleted in others, e.g., sandstone or coal.

For testing, the probe was lowered to the bottom of the boring where the caliper legs were opened, and data collection was begun. The probe was returned to the surface at a rate of 10 ft/minute, collecting data continuously at 0.05 ft spacing.

b. **Resistivity, Spontaneous Potential and Natural Gamma**

Resistivity, spontaneous potential, and natural gamma data were collected using a Model ELXG electric log probe, manufactured by Robertson Geologging, Ltd. The probe, which is 8.2 ft long and 1.73 in. in diameter, measures single point resistance, short and long normal resistivity, spontaneous potential, and natural gamma, and can:

- Identify bed boundaries
- Correlate strata between borings
- Identify strata geometry (shale indication)
- Provide natural gamma measurements

For testing, the probe was lowered to the bottom of the boring, and data collection was begun. The probe was returned to the surface at a rate of 10 ft/minute, collecting data continuously at 0.05 ft spacing.

c. **Acoustic Televiewer and Borehole Deviation Measurement**

Acoustic image and boring deviation data were collected using a High Resolution Acoustic Televiewer probe, manufactured by Robertson Geologging, Ltd. The probe, which is 7.58 ft long and 1.9 in. in diameter, is fitted with upper and lower four-band centralizers, and can:

- Measure boring inclination and deviation from vertical
- Determine need to correct soil and geophysical log depths to true vertical depths
- Provide acoustic imaging of the borehole to identify fractures, dikes, and weathered zones, and determine dip and azimuth of these features

This system produces images of the borehole wall based on the amplitude and travel time of an ultrasonic beam reflected from the formation wall. The strength of the reflected signal from the formation wall depends primarily upon the impedance contrast between the clear water or drilling fluid and the wall. In the North Anna rock borings, the contrast between the fluid and the rock formation generally provided high contrast. The acoustic wave propagates along the axis of the probe and is then reflected perpendicular to this axis by a reflector that focuses the beam to a 0.1 in. diameter spot about 2 in. from the central axis of the probe. This reflector is able to rotate. During the survey, data were collected at 360 samples per revolution.

The probe contains a fluxgate magnetometer to monitor magnetic north, and all raw televiewer data are referenced to magnetic north. In addition, a 3-axis accelerometer is enclosed in the probe, and boring deviation data are recorded during the logging runs, to permit correction of structure dip angle from apparent dip to true dip in non-vertical borings.

For testing, the probe was lowered to the bottom of the boring, and data collection was begun. The probe was returned to the surface at a rate of 3 ft/minute, collecting data continuously at 0.008 ft intervals. The data were presented on a computer screen for operator review during the logging run, and stored on hard disk for later processing.

d. **Suspension P-S Logger**

Suspension soil and rock velocity measurements were performed using the Robertson Geologging USB Micrologger II digital recorder with a digital OYO Suspension P-S Logging Probe. This system directly determines the average in-situ horizontal V_S and V_P measurements of a 3.3 ft high segment of the soil and rock column surrounding the borehole by measuring the elapsed time between arrivals of a wave propagating upwards through the soil and rock column.

Suspension P-S velocity logging uses a 23-ft long cable suspended probe containing a source near the bottom, and two geophone receivers spaced 3.3 ft apart. The probe is lowered into the borehole to a specified depth where the source generates a pressure wave in the borehole fluid (drilling mud). The pressure wave is converted to seismic waves (P-wave and S-wave) at the borehole wall. At each receiver location, the P- and S-waves are converted to pressure waves in the fluid and received by the geophones mounted in the probe, which in turn send the data to a recorder on the surface. At each measurement depth, two opposite horizontal records and one vertical record are obtained. This procedure is typically repeated every 1.65 ft or 3.3 ft as the probe is moved from the bottom of the borehole towards the ground. The elapsed time between arrivals of the waves at the geophone receivers is used to determine the average velocity of a 3.3 ft high column of soil or rock around the borehole. For quality assurance, analysis is also performed on source-to-receiver data.

2.5.4.4.3 Seismic Tests with Cone Penetrometer

The tests were performed at 5 ft intervals in C-902, C-916, C-921 and CPT-923. Shear waves were generated by striking a heavy beam

adjacent to the CPT location. Only shear waves were generated. The wave arrival was recorded by a geophone attached near the bottom of the cone string. The results of these seismic CPTs are provided in Appendix 2.5.4AA, and discussed in Section 2.5.4.4.4.

2.5.4.4.4 Results of Shear and Compression Wave Velocity Tests

a. **Soil**

The measurements of V_S from suspension P-S logging and seismic CPT tests in the Zone IIA and Zone IIB saprolite (and top of Zone III weathered rock) are shown versus depth in Figure 2.5.4-223. The corresponding measurements of V_P, from the suspension P-S logging are shown in Figure 2.5.4-235. Low strain Poisson's ratio can be determined from a relationship between V_s and V_p (SSAR Reference 150). A plot of Poisson's ratio versus depth derived from the suspension P-S logging V_s and V_p measurements is shown in Figure 2.5.4-236. Note that on these plots, the Zone IIA saprolite extends to about 29 ft depth in boring B-909, to about 34 ft depth in boring M-10, to about 35 ft depth in borings B-901 and B-907, and to about 59 ft depth in boring M-10.

For the Zone IIA saprolite, the average shear wave velocity generally increases with depth from around 500 ft/sec at the ground surface to 1200 ft/sec as it transitions to Zone IIB saprolite. The median value within the layer is about 850 ft/sec. This compares with a median of about 950 ft/sec noted in the SSAR. The results of the compression wave tests in Zone IIA saprolite are fairly consistent at around 1800 ft/sec, while the low strain Poisson's ratio can be taken as 0.35.

For the Zone IIB saprolite, the average V_S generally ranges from around 1200 ft/sec to 2500 ft/sec as it transitions to Zone III. The median value within the layer is about 1600 ft/sec which is the same as noted in the SSAR. The results of the compression wave tests in Zone IIB saprolite in Figure 2.5.4-235 reflect the V_P of water. The V_P from SSAR Table 2.5-45 of 3500 ft/sec was used, with a low strain Poisson's ratio of 0.37.

b. **Rock**

Figure 2.5.4-237 shows the measurements of V_S from suspension P-S logging in the Zone III, Zone III-IV and Zone IV bedrock versus elevation. Figure 2.5.4-238 shows the corresponding measurements of V_P, while Figure 2.5.4-239 shows Poisson's ratio versus elevation derived from V_S and V_P. These measurements were taken in the power block area at the

R/B/FB (B-901 and B-907), and CB (B-909) and to the south of the power block area (M-10 and M-30).

Based on a review of the V_S versus elevation information in Figure 2.5.4-237, and the RQD data in Figure 2.5.4-220 as described in Section 2.5.4.2.5.a, it was concluded that the overall V_S of the rock as defined by the three rock zones (III, III-IV and IV) is somewhat higher at the Unit 3 plant location than described in the SSAR. For Zone III weathered rock, the range of V_S is approximately 2000 ft/sec to 4000 ft/sec, with a best estimate value of 3000 ft/sec. For Zone III-IV partially weathered rock, the range of V_S is approximately 4000 ft/sec to 8000 ft/sec, with a best estimate value of 6000 ft/sec. For Zone IV fresh rock, the range of V_S is approximately 8000 ft/sec to 11000 ft/sec, with a best estimate value of 9000 ft/sec. These best estimate V_S values are provided in Table 2.5.4-208 and represent a best estimate for each rock zone based on all five V_S borings. Section 2.5.4.7.1 describes the development of V_S profiles for Seismic Category I structures based on the proximity of the V_S measurements to the structure.

In Figure 2.5.4-237, Zone IV bedrock extends consistently up to around Elevation 184 ft, although the V_S values indicate that Zone IV extends above this elevation in some of the borings, and well above it in M-30. Conversely, B-901 shows Zone III rock extending from this elevation up to about Elevation 205 ft before grading to Zone III-IV rock. From Elevation 205 ft to about Elevation 225 ft, all the borings show Zone III-IV, except for the two borings to the south of the power block – M-10 indicates Zone III while M-30 indicates Zone IV. Above about Elevation 225 ft, B-907 and B-909 show mostly Zone III and lower end Zone III-IV rock material, while B-901 shows Zone III-IV rock and M-30 indicates mostly Zone IV rock. These V_S profiles demonstrate that, whereas previously the “top of competent rock” was the top of the Zone III-IV (SSAR), the shear wave velocities in the Zone III rock can be high enough (e.g., in B-907) that, in some instances, Zone III can be included in the “competent rock” description. The V_S profiles also demonstrate, along with the RQD profile in Figure 2.5.4-220, that above about Elevation 184 ft, weathered/fractured zones can be encountered; however, there is no pattern to where these zones occur, indicating the randomized process of weathering.

2.5.4.5 Excavation and Backfill

NAPS ESP COL 2.5-3

This section describes the following topics:

- The extent (horizontally and vertically) of Seismic Category I excavations, fills and slopes
- Excavation methods and stability
- Backfill sources, quantities, compaction specifications and quality control (QC)

2.5.4.5.1 Extent of Excavations, Fills and Slopes

Figure 2.5.4-206, the excavation plan, shows the extent of excavations, fills and slopes for Unit 3. These are shown in cross-section in Figures 2.5.4-225 through 2.5.4-234. To obtain the finish ground level grade of Elevation 289.5 ft, considerable quantities of soil will be excavated. The location of original ground surface is shown in the cross-sections. There are some lower areas to the northeast that will be backfilled. The total estimated cut within the power block area is about 625,380 cubic yards, while the amount of backfilling with compacted structural fill is about 241,750 cubic yards and concrete fill is about 109,620 cubic yards. Benched 3-horizontal to 1-vertical (3H:1V) slopes extend up from finish ground level grade around the southern and eastern perimeter of the area.

To the northeast of the Turbine Building, going towards the existing Units 1 and 2, ground surface elevation reduces at an approximately 5 percent slope down to Elevation 280 ft at the Service Water Building. Stormwater management pond #1 is between these structures and the boundary of Units 1 and 2 with yard grade at Elevation 270 ft. As existing grade falls off from the power block area northeast towards Units 1 and 2 some backfilling will be required to achieve final grade. As much as 30 ft of backfill will be needed to bring grade up to the planned ground surface area of the originally planned Units 3 and 4, where ground level is presently at around Elevation 250 ft.

Figures 2.5.4-206 and 2.5.4-217 show the outline of the power block foundations. As shown in Figures 2.5.4-225 through 2.5.4-234, temporary excavation for Unit 3 construction will be supported by a wall system. This wall will be supported by tie-backs or other means.

2.5.4.5.2 Excavation Methods and Stability

a. **Excavation in Soil**

Excavation in the soils (Zones IIA and IIB) and any existing fills is achieved with conventional excavating equipment. Excavation of less than 20 ft in height will adhere to OSHA regulations (SSAR Reference 162). As noted in the previous section, a temporary vertical wall system will be used to support the power block excavation. The slopes around the perimeter of the power block area are no steeper than 3H to 1V, with a bench at approximately 25 ft height. Since the saprolitic soils can be highly erosive, even temporary slopes cut into the saprolite are sealed and protected.

b. **Excavation in Rock**

Excavation in the Zone III moderately to severely weathered rock is achieved using conventional earthmoving equipment. A temporary vertical wall system will be used to support the excavation, where necessary.

Excavation made for the originally planned Units 3 and 4 in the slightly to moderately weathered rock (Zone III-IV) and fresh to slightly weathered rock (Zone IV) is documented in SSAR Reference 163. Techniques employed were similar to those used for Units 1 and 2 (SSAR Reference 164) but with “lessons learned” applied. The methods of rock excavation outlined below for Unit 3 are based, in part, on the methods that worked successfully for Units 1 and 2 and the originally planned Units 3 and 4. Unit 3 is approximately 1500 ft from the center of the Unit 2 R/B, whereas the originally planned Unit 3 R/B was only about 300 ft from the Unit 2 R/B. Thus, the following techniques to reduce vibrations that worked for the originally planned Unit 3 will be used and will be effective for the new Unit 3:

- Controlled blasting techniques, including cushion blasting, pre-splitting and line drilling may be used, with appropriately dimensioned bench lifts. The blasted faces are vertical except where the foliation dip is into the excavation. There, the excavation may be parallel to the foliation dip (typically about 1-H to 1-V).

- Any blasting is strictly controlled to preserve the integrity of the rock outside the excavations and to prevent damage to existing structures, equipment, and freshly poured concrete. Peak particle velocity is measured and kept within specified limits that are a function of distance from the blast.
- The rock is reinforced to ensure adequate support and safety. Reinforcing includes installation of rock bolts in finished rock faces (typically at around 5 ft centers), and the use of welded wire mesh. Necessary measures are taken when weathered or fractured zones are encountered. Instrumentation such as slope indicators and extensometers are installed to monitor rock movements, especially on the foliation dip slopes.

NAPS ESP PC 3.E(6)

- The excavation for safety-related structures will be geologically mapped and photographed by experienced geologists. Unforeseen geologic features that are encountered will be evaluated. The NRC will be notified no later than 30 days before any excavations for safety-related structures are open to allow for NRC staff examination and evaluation.
- There is no measurable rebound or heave of the sound rock subgrade, and monitoring is not needed.

NAPS ESP PC 3.E(5)

2.5.4.5.3 Structural Fill Sources, Compaction and Quality Control

Although a large amount of Zone IIA soil will be excavated for Unit 3, this material will not be used as structural fill to support Seismic Category I or II structures.

Structural fill is either concrete fill or a sound, well-graded granular material. The anticipated extent of the concrete and granular fill is shown on the foundation cross-sections on Figures 2.5.4-225 through 2.5.4-234. The concrete fill is used to replace any moderately to severely weathered rock (Zone III) exposed at the bottom of the excavations for the Seismic Category I RB/FB, CB, and FWSC foundation mats. As noted in Section 2.5.4.2.5.a, the concrete fill will have a minimum strength of 2500 psi, a best estimate shear wave velocity of 7000 ft/sec, and a unit weight and Poisson's ratio of 145 pcf and 0.15, respectively.

The granular structural fill material that will be used as backfill around Seismic Category I as well as around and beneath Seismic Category II structures does not exist naturally on site. However, given the large amount of rock that will need to be excavated for Unit 3, it will be

economical to set up a crushing and blending plant onsite to produce crushed aggregate to the required gradation to specifications for use as structural fill. The onsite source will consist of crushed Zone III, Zone III-IV, and/or Zone IV rock. The rock will be crushed down to well-graded, angular or sub-angular sand and gravel-sized particles conforming to the gradation of Size No. 21A specified by the VDOT Road and Bridge Specifications (SSAR Reference 166). This gradation is shown in Figure 2.5.4-240. The soundness of the aggregate will be confirmed using sulfate soundness and Los Angeles abrasion tests. This structural fill will be placed in lifts not exceeding 12 inches loose thickness and compacted to at least 95 percent of the maximum dry density as determined by ASTM D 1557 (SSAR Reference 165) to within 3 percent of its optimum moisture content. Compaction will be performed with a heavy steel-drummed vibratory roller, except within 5 ft of a structure wall, where smaller compaction equipment will be used in conjunction with reduced lift thickness to minimize excess pressures against the wall. As noted in Section 2.5.4.2.5.b, based on the type of material and its degree of compaction, N_{60} = 50 blows/ft and φ' = 40 degrees were considered as reasonable and conservative for this structural fill.

Although proposed structural fill material from the site is not presently available, bulk samples of similar material will be obtained from a quarry in the site vicinity that crushes the native rock (sound gneiss or schist) to the VDOT Size 21A gradation. Laboratory tests will be used to confirm the properties of the structural fill, and will include:

- Confirmatory gradation tests
- Modified Proctor compaction tests to provide values of maximum density and optimum moisture content
- Consolidated-undrained (CU) triaxial compression tests, with porepressure measurements, on compacted samples at different confining pressures to verify the angle of internal friction

Since the gradation of the fill material falls within a relatively narrow band, the test results should be consistent, and so the number of laboratory tests can be limited. Two each of the modified Proctor and C-U triaxial tests should provide sufficient data.

As an alternative or supplement to the onsite crushed rock, dense-graded aggregate can be used as structural fill material. Dense-graded aggregate will conform to VDOT Size 21A (SSAR Reference 166) as noted in the previous paragraph.

Zone IIB saprolite material may be used as secondary structural fill under and around structures (excluding Seismic Category I and II structures) and under roads. This material may be used either on its own or mixed with excess finer materials from crushing Zone III, Zone III-IV, and Zone IV material.

Fill placement and compaction control procedures will be addressed in a technical specification that includes requirements for suitable fill, sufficient testing to address potential material variations, and in-place density testing frequency. Compacted structural fill placement and testing will follow the guidelines of ASME NQA-1 (Reference 2.5-221). At least one field density test will be performed per lift and for no more than every 250 cubic yards of fill placed. The technical specification also includes requirements for an on-site testing laboratory for QC (gradation, moisture-density, placement, compaction, etc.) and requirements to ensure that the fill operations conform to the earthwork specification. The soil testing firm is required to be independent of the earthwork contractor and to have an approved Quality Assurance Program. Sufficient laboratory compaction tests (modified Proctor) and grain size distribution tests will be performed to ensure that variations in the fill material are accounted for. (Variations in the crushed and blended rock are expected to be minimal.)

A test fill program is also included for the purposes of determining an optimum size of roller, number of passes, lift thickness, and other relevant data for achievement of the specified compaction.

2.5.4.5.4 Control of Groundwater During Excavation

Construction dewatering is presented in Section 2.5.4.6.2. Since the saprolitic soils can be highly erosive, sumps and ditches constructed for dewatering are lined. The tops of excavations are sloped back to prevent runoff down the excavated slopes during heavy rainfall.

NAPS COL 2.0-29-A

2.5.4.6 Groundwater Conditions

2.5.4.6.1 Groundwater Measurements and Elevations

Groundwater is present in unconfined conditions in both the surficial sediments and underlying bedrock at the Unit 3 site. Seven observation wells installed for the Unit 3 investigation (along with nine wells installed at the site as part of the ESP subsurface investigation program) have exhibited groundwater levels ranging from about Elevation 238 ft to Elevation 314 ft between December 2002 and August 2007. (The groundwater generally occurs at depths ranging from about 18 ft to 25 ft below the present-day ground surface in the main Unit 3 power block area.)

The logs and details of these seven wells, and tests in the wells, are given in Appendix 2.5.4AA. Details of measured groundwater levels and their fluctuations are given in Section 2.4.12. Hydraulic conductivity values for the saprolite based on slug tests performed in eleven of the observation wells range from 0.25 ft to 9.9 ft/day, with a geometric mean value of 1.74 ft/day. The hydraulic conductivity of the underlying shallow bedrock as determined from slug tests performed in two of the wells and packer tests performed in one of the wells is estimated to range from about 0.5 ft to 6.3 ft/day, with a geometric mean value of 2.05 ft/day. Groundwater movement at the site is generally to the north and east, towards Lake Anna. A detailed description of groundwater conditions is provided in Section 2.4.12.

Groundwater levels at the site require temporary dewatering of foundation excavations extending below the water table during construction of Unit 3. This construction dewatering is performed in a manner that minimizes drawdown effects on the surrounding environment. Drawdown effects are expected to be limited to the NAPS site. The relatively low permeability of the saprolite and underlying rock means that sumps and pumps should be sufficient for successful construction dewatering, as presented in Section 2.5.4.6.2.

The maximum allowable ground water level for operation of the power block area of Unit 3 is Elevation 288 ft which is at 2 ft below design plant grade at Elevation 290 ft. Section 2.4.12.4 indicates that the maximum predicted groundwater level in the power block area of Unit 3 increases from north to south, ranging from about Elevation 271 ft at the north end

of the Turbine Building to about Elevation 282.5 ft at the south end of the RB/FB.

2.5.4.6.2 Construction Dewatering and Seepage

Dewatering for all major excavations is achieved by gravity-type systems.

a. **Soils**

Due to the relatively impermeable nature of even the coarse-grained saprolite, sump-pumping of ditches is adequate to dewater the soil. These ditches are advanced below the progressing excavation grade.

During the construction of Units 1 and 2 and originally planned Units 3 and 4, plant excavation and dewatering was significant in causing local groundwater levels to decline. However, the extent of the area of influence of the construction dewatering was estimated to be a radius of less than 500 ft due to the low permeability of the materials being dewatered (SSAR Reference 164).

b. **Rock**

Sump-pumping is used to collect water from relief drains that are installed in the major rock excavation walls to prevent hydrostatic pressure buildup behind the walls. Such relief wells were spaced on 20 ft centers around the perimeters of the originally planned Units 3 and 4 containment excavations.

Although an approximately 40 ft head existed between excavation grade and the North Anna Reservoir during the final stages of excavation for the originally planned Units 3 and 4, no dewatering difficulties were encountered, due to the tight nature of the joints in the rock below about Elevation 240 ft. The excavation for Unit 3 is at least 1000 ft from Lake Anna, and so negligible seepage effects from the lake are anticipated.

2.5.4.6.3 Effect of Groundwater Conditions on Foundation Stability

NAPS ESP COL 2.5-4

Maximum allowable groundwater level is at least 2 ft below design plant grade, i.e., Elevation 288 ft. A water level at Elevation 290 ft was conservatively used in bearing capacity and settlement analyses and in computing hydrostatic pressures on the buried structure walls (Section 2.5.4.10). As described in Section 2.5.4.10, there are no buoyancy issues with deep buried structures because of the appreciable dead loads imposed by these structures. Large diameter buried piping

such as the circulating water pipes are designed to resist buoyancy when empty.

No permanent dewatering system is required for Unit 3.

NAPS COL 2.0-29-A

2.5.4.7 Response of Soil and Rock to Dynamic Loading

The RB/FB common basemat at Unit 3 is founded on Zone III-IV or Zone IV bedrock or on concrete placed on Zone III-IV or Zone IV bedrock after removing Zone III weathered rock. A similar scheme is followed for the CB and FWSC foundations. The foregoing foundation subgrades are illustrated on Figures 2.5.4-225 through 2.5.4-234.

The seismic acceleration at the hard bedrock (V_S > 9200 ft/sec) level is amplified or attenuated up through the rock column, or the rock and soil column. To estimate this amplification or attenuation, the following data are required:

- Shear wave velocity profiles of the rock and soil overlying hard rock
- Variation with strain of the shear modulus and damping values of the weathered rock and soil
- Site-specific seismic acceleration-time histories

2.5.4.7.1 Shear Wave Velocity Profile

NAPS ESP COL 2.5-9

Various measurements were made at the Unit 3 site to obtain estimates of the shear wave velocity in the soil and rock. These are summarized in Section 2.5.4.4. The materials of interest here are the Zone IIA and Zone IIB saprolitic soils, the structural fill, the Zone III weathered rock, the concrete fill, the Zone III-IV slightly to moderately weathered rock, and the Zone IV slightly weathered to fresh rock.

V_S of the bedrock at the RB/FB basemat (B-901 and B-907) and the CB (B-909) as well as the two profiles south of the power block area (M-10 and M-30) are shown versus elevation in Figure 2.5.4-237. Borings M-10 and M-30 are not considered further here because they are a significant distance from the power block structures.

The V_S profiles from B-901, B-907, and B-909 were used to develop the best estimate V_S profiles beneath the Seismic Category I RB/FB, CB, and FWSC structures. The bottom of foundation elevation for these structures is Elevation 224 ft, Elevation 241 ft, and Elevation 282 ft, respectively.

The Unit 3 site is well characterized and extensively investigated with abundant high-quality data which reduces epistemic uncertainty in the site properties. These data also provide information to characterize the aleatory variation in layer thickness and shear-wave velocity across the site. These variations will be included in considerations of aleatory uncertainties for the best estimate profile during the randomization process. No alternate profiles are considered because of the relative insignificance of epistemic uncertainty with respect to the aleatory variability for this site.

a. **Reactor Building/Fuel Building**

B-901 and B-907 are beneath the RB/FB footprint and B-909 is under the footprint of the adjacent CB. The V_S measurements from all three of these borings were used in developing the best estimate V_S profile for the RB/FB. Figure 2.5.4-241 shows Zone IV bedrock extending up to around Elevation 184 ft. Above this elevation, two distinct V_S profiles are identified, with one representing the more weathered and fractured rock profile (Profile 1) and the other the mostly unweathered and unfractured profile (Profile 2). The log mean of Profile 1 and Profile 2 is used as the best estimate profile for the RB/FB up to the average top of rock at about Elevation 273 ft. The best estimate in-situ saprolite V_S profile that extends from Elevation 273 ft to grade at about Elevation 290 ft is the average profile measured in the saprolite at the Unit 3 site and reflects the fact that the original ground surface was significantly higher in most places than Elevation 290 ft. The best estimate profile used for the RB/FB is shown in Figure 2.5.4-242.

b. **Control Building**

Since boring B-909 is directly below the footprint of the CB, the V_S profile from that boring is used as the best estimate V_S profile for the CB, and is shown in Figure 2.5.4-242. As can be seen from the figure, the V_S values are generally averaged over 10-ft intervals.

c. **Firewater Service Complex**

The FWSC is counted as a surface foundation, with the bottom of foundation approximately 8 ft below grade, at Elevation 282 ft. The soil above this elevation is ignored when developing the V_S profile. Concrete fill will be used between the bottom of the foundation and the top of Zone III-IV material. This concrete fill is of limited lateral extent and is not

used in developing the V_S. The free-field profile in the soil surrounding the structure is used above rock.

Since boring B-909 is located less than 50 ft from the edge of the FWSC, the V_S profile from that boring is used as the basis for the best estimate V_S profile for the FWSC. The average thicknesses of the various zones beneath the FWSC based on borings beneath and adjacent to the FWSC footprint differ somewhat from the zone thicknesses encountered in B-909. The V_S values from B-909 were used for the FWSC but the thickness of the zones in the FWSC profile reflect the average zone thickness beneath the structure. Thus, the best estimate V_S profile shown in Figure 2.5.4-243 for the FWSC is not identical to the V_S profile for the CB in Figure 2.5.4-242.

The FWSC is surrounded by approximately 20 to 50 ft of structural fill, as shown in the Section D-D Profile (Figure 2.5.4-228). The best estimate V_S profile for the backfill is included in Figure 2.5.4-243. The V_S of the backfill is similar to the V_S of the saprolite used in the best estimate profile.

d. **Profile for Slope**

In addition to the V_S profiles considered for the Seismic Category I structures, a V_S profile beyond the excavation for the power block is developed. This profile is employed to obtain peak ground accelerations in the free-field for use in slope stability (Section 2.5.5) and liquefaction analysis (Section 2.5.4.8). The profile is in the vicinity of boring B-947 and CPT C-916, on the planned 3H:1V slope to the east of the power block area. The ground elevation for the profile is Elevation 315 ft. The borings show the Zone II saprolite is thick in this area, with the combined thickness of the Zone IIA and Zone IIB materials being about 60 ft. The V_S profile developed for the saprolite takes into account V_S measured in C-916, the N-values measured in B-947, and the average V_S values derived from V_S measurements in saprolite sitewide. The V_S profile is shown in Figure 2.5.4-244. The V_S profile for the rock below 60 ft depth is the log mean profile derived from Profile 1 and Profile 2 (for the RB/FB from borings B-901, B-907 and B-909), adjusted to take into account the lower elevation of the top of rock in B-947, and maintaining the transition to hard rock at Elevation 184 ft.

e. **Profile for Structural Fill**

A V_S profile is also developed for the structural fill that will be used as backfill around the Seismic Category I structures. As noted in Section 2.5.4.5.3, the primary source of structural fill is crushed rock obtained from the power block excavation.

For this structural fill, there are no measured V_S values, since the backfill will be crushed rock obtained from the new plant excavation. To obtain a V_S profile range, the SPT N-value selected in Section 2.5.4.2.5.b for the structural fill, i.e., N_{60} = 50 blows/ft, is used. Relationships between N-value (adjusted for overburden pressure) and V_S developed by Seed, et al. (Reference 2.5-212) and Imai and Tonoucchi (Reference 2.5-213) are used to obtain a profile of V_S versus depth, as shown in Figure 2.5.4-245. This profile is averaged vertically in 5-ft intervals to obtain the average VS profile shown in Figure 2.5.4-246 for P-SHAKE input. The upper and lower bound values shown in this figure are 1.414 and 0.707 times the mean value of shear wave velocity, respectively, which correspond to 2.0 and 0.5 times the shear modulus.

Table 2.0-201 provides an evaluation of DCD site parameter values and corresponding Unit 3 site characteristic values for shear wave velocity.

NAPS COL 2.0-29-A

2.5.4.7.2 Variation of Shear Modulus and Damping with Strain

a. **Shear Modulus**

The shear modulus reduction curve for the Zone IIA saprolite is the same as used for the Zone IIA saprolite in the SSAR, i.e., Curve 1 in SSAR Figure 2.5-63. This curve is reproduced here in Figure 2.5.4-247, labeled “Recommended for Natural Soil.” A series of grain size tests on the Zone IIB saprolite indicated that all of the samples tested were sands, with no appreciable gravel content. Thus, Curve 1 in SSAR Figure 2.5-63 was also used for the Zone IIB saprolite, and labeled “Recommended for Natural Soil” in Figure 2.5.4-247. The typical thickness of the saprolite is about 35 ft. Curve 1 is almost identical to the average of the EPRI curves (SSAR Reference 170) for depths 0 to 20 ft, and 20 to 50 ft.

The results of the RCTS tests (normalized shear modulus (G/G_{max}) versus shear strain) from Figure 2.5.4-219 are superimposed on Curve 1 in Figure 2.5.4-248. These results show good agreement with Curve 1, and so no additional SHAKE runs were made using the RCTS shear modulus reduction curves. Note that the median thickness of the

Zone IIA saprolite encountered in the Unit 3 borings was about 25 ft, and approximately 80 percent of the material was classified as silty sand (SM). The two silty sand samples of Zone IIA saprolite tested in RCTS are thus considered sufficient and representative. Similarly, the median thickness of the Zone IIB saprolite encountered in the Unit 3 borings was about 9 ft, and all of this material was classified as silty sand (SM). Thus the sample of Zone IIB silty sand tested in RCTS is considered sufficient and representative.

As noted in Section 2.5.4.2.5.b, the primary source of structural fill is bedrock excavated to construct the Unit 3 power block, crushed down to well-graded, angular sand and gravel-sized particles. Curve 2 in SSAR Figure 2.5-63, which was derived for a gravel-type material, was selected as the shear modulus reduction curve for this structural fill and is included in Figure 2.5.4-248. Curve 3 in SSAR Figure 2.5-63 was used for the Zone III weathered rock. The shear modulus of the Zone IV and Zone III-IV weathered rock was considered non-strain dependent.

b. **Damping**

The typical thickness of the saprolite and the structural fill is about 35 ft. For the granular materials (Zone IIA and Zone IIB saprolite, and the structural fill), the average of the EPRI curves (SSAR Reference 170) for depths 0 to 20 ft, and 20 to 50 ft was selected. This curve is shown on Figure 2.5.4-249. Curve 3 in SSAR Figure 2.5-64 is used for the Zone III weathered rock. This curve is also shown on Figure 2.5.4-249.

Figure 2.5.4-248 shows the results of the RCTS tests from Figure 2.5.4-219 for material damping ratio D versus shear strain superimposed on the granular soils curve from Figure 2.5.4-249. These results show reasonable agreement, and so no additional SHAKE runs were made using the RCTS damping ratio reduction curves.

There is no variation of damping ratio of the Zone III-IV or Zone IV rock with cyclic shear strain. However, this rock has some intrinsic damping properties. A value of 1 percent was selected for the damping ratio with a variation of about ± 0.5 percent.

2.5.4.7.3 Site Specific Acceleration-Time Histories

Section 2.5.4.7.1 used the P-SHAKE computer program (Reference 2.5-222) which does not use acceleration-time histories for input.

2.5.4.7.4 Rock and Soil Column Amplification/Attenuation Analysis

NAPS ESP COL 2.5-5

The ARS derived from the P-SHAKE analyses for the Seismic Category I structures described in Section 2.5.4.7.1 are presented in Section 3.7.1.

The P-SHAKE program is used to obtain peak ground accelerations in the free-field for use in slope stability (Section 2.5.5) and liquefaction analysis (Section 2.5.4.8) using the V_S profile described in Section 2.5.4.7.1.d. Figure 2.5.4-250 shows the maximum acceleration versus depth profiles obtained from P-SHAKE for the high and low frequency earthquakes. The peak ground acceleration occur at about 42 ft depth and are about 0.56g for the high frequency earthquake and about 0.31g for the low frequency earthquake.

2.5.4.8 Liquefaction Potential

NAPS COL 2.0-29-A

The Zone IIB saprolitic soils are extremely dense and the Zone III weathered rock has over 50 percent core stone and has typically been sampled by rock coring. Neither of these materials has liquefaction potential. The primary source of structural fill is bedrock excavated for the Unit 3 power block. This consists of crushed angular or sub-angular sand and gravel-sized particles compacted in thin lifts with a heavy vibratory steel-drummed roller. This fill is not liquefiable. The only material analyzed here for liquefaction is the Zone IIA saprolitic soil.

NAPS ESP PC 3.E(7)

All of the Seismic Category I structures are founded on rock or on concrete fill on rock at the Unit 3 site. Thus, even if the Zone IIA saprolite is liquefiable, such liquefaction does not impact the stability of any Seismic Category I structure. As described in Section 2.5.4.10, the Zone IIA saprolite has relatively high resistance to bearing failure but can produce excessive settlements under certain conditions. Thus, the Zone IIA saprolite is not used to support Seismic Category I structures, whether it is potentially liquefiable or not.

The peak ground accelerations obtained from the Unit 3 P-SHAKE analyses through the natural soil profile are less than those reported in the SSAR, due to some slightly different rock and soil profiles, and the randomization process applied to these profiles. The previous liquefaction analyses are in Section 2.5.4.8.1. Section 2.5.4.8.2 presents the results of summarized liquefaction analyses performed on Zone IIA saprolites on slopes outside the power block area, based on borings and

CPTs performed for Unit 3 in these areas, i.e., analyses of soils that will generally not be excavated.

Any failure of slopes due to liquefaction could impact adjacent safety-related structures. Locations having this potential are identified, and a liquefaction analysis of the slope soils is performed.

2.5.4.8.1 Previous Liquefaction Analyses Performed

The SSAR describes liquefaction analyses performed previously for the North Anna site. The primary analysis was performed for a seismic margin assessment. This included, for the main Units 1 and 2 plant area, an analysis using a version of the simplified procedure and a threshold strain analysis. For the Units 1 and 2 Service Water Reservoir, an analysis was performed based on the results of 15 stress-controlled cyclic triaxial tests. An updated seismic margin assessment was performed for the SSAR maintaining the same assumptions as used in the original study but substituting the ESP design accelerations and moment magnitudes. As noted previously, these accelerations were higher than those being used for the present analysis (Section 2.5.4.8.2). The SSAR also describes liquefaction analysis performed using subsurface data gathered for the ESP investigation.

2.5.4.8.2 Liquefaction Analyses Performed for Unit 3

This section was developed in accordance with, and conforms to guidance in RG 1.198 (Reference 2.5-214).

As noted earlier, at the locations of the majority of the borings and CPTs in the power block area that contains the Seismic Category I structures, the Zone IIA saprolite will be excavated. Thus, analyzing the liquefaction potential of these soils prior to excavation is of little relevance.

The liquefaction analysis focuses on slopes whose failure could impact safety-related structures. The excavation plan (Figure 2.5.4-206) shows the cut slopes to the east and south of the power block are in the 30 to 35-ft high range. The bottom of the slope to the east of the FWSC is approximately 120 ft from the structures. This is the nearest point of the bottom of any slope to a Seismic Category I structure. The Seismic Category II Ancillary Diesel Building is slightly farther from the south slope. The liquefaction potential of the east and south slope soils was computed, as described below. Note that even if these slopes failed due to liquefaction (or other mechanisms) it is extremely unlikely the failed

35-ft high slopes would have any impact on structures 120 ft or more from the slope.

Six SPT sample borings were conducted on the east and south slopes (B-930, B-947, M-6, M-9, M-10 and M-11) along with two CPTs (C-909 and C-916). V_S measurements were taken in M-10 and C-916. The results from these explorations were analyzed to determine the liquefaction potential of the slope soils.

The analysis conservatively ignored mineralogy/fabric effects of the saprolite. The saprolite is estimated to be between 0.8 and 1.6 million years old, according to SSAR Reference 176. A conservative age factor of 1.4 was used in the analysis. Cohesive samples and/or samples above the groundwater table were considered non-susceptible to liquefaction.

The analysis followed the methods proposed by Youd, et al. (SSAR Reference 178). This state-of-the-art liquefaction methodology is based on the evolution of the Seed and Idriss "Simplified Procedure" since the early 1980s. Magnitude scaling factors of 1.05 and 1.93 were used in the analysis for the moment magnitude 7.4 (low frequency) and 6.0 (high frequency) earthquakes, respectively. The K_σ factor for high overburden pressures was incorporated into the analysis, using a relative density of 60 percent.

The analysis of the SPT results from the six borings gave factor of safety values against liquefaction greater than 1.1 for the approximately 80 Zone IIA saprolite samples that were potentially liquefiable, except for eight samples. For the two CPTs, the liquefaction analysis showed no measurement where the factor of safety against liquefaction was less than 1.1. For the two sets of V_S measurements, one measurement in C-916 indicated a factor of safety of less than 1.1 against liquefaction. In M-10, seven measurements indicated a factor of safety of less than 1.1 against liquefaction. Youd et al. (SSAR Reference 178) express concerns about the applicability of V_S measurements to liquefaction potential evaluation because V_S is a small strain measurement whereas pore-water pressure buildup and the onset of liquefaction are medium- to high-strain phenomena.

Using the method outlined in Tokimatsu and Seed (SSAR Reference 179), the maximum estimated dynamic settlement of the Zone IIA saprolite due to earthquake shaking was less than the 5 in. estimated based on soil encountered in one of the CPTs performed for

the ESP investigation using the same computation method. This value of 5 in. is conservatively adopted as the maximum dynamic settlement that could occur in the saprolite due to the design seismic event.

2.5.4.8.3 Conclusions about Liquefaction

Only the Zone IIA saprolites fall into the gradation and relative density categories where liquefaction would be considered possible.

Any liquefaction of the Zone IIA saprolite will not impact the stability of any Seismic Category I structure.

The conclusions from the foregoing sections on the analysis of liquefaction potential of Zone IIA saprolite are as follows. These conclusions apply to measurements taken on or close to the slopes to the east and south of the power block area. Note that all of the analysis neglected the beneficial effects against liquefaction of structure, fabric, and mineralogy. A conservative factor was adopted for age effects.

- A state-of-the-art liquefaction analysis of the SPT measurements gave factor of safety values against liquefaction greater than 1.1 for those samples that were potentially liquefiable, except for eight samples
- A state-of-the-art liquefaction analysis of the CPT measurements showed the factor of safety against liquefaction was greater than 1.1 for all measurements
- A state-of-the-art liquefaction analysis of the V_S measurements gave factor of safety values against liquefaction greater than 1.1 for all except eight measurements
- Maximum dynamic settlement of the Zone IIA saprolite due to earthquake shaking is conservatively estimated as about 5 in. based on the maximum value obtained from the ESP investigation. This settlement will be outside the zone of loading influence of any of the Seismic Category I structures

Based on the above analysis results, it can be concluded that a very small percentage of the Zone IIA saprolitic soils have a potential for liquefaction based on the low and high frequency Unit 3 seismic characteristics. The liquefaction analysis did not take into account the beneficial effects of structure, fabric, and mineralogy, and adopted a conservative factor for age; thus the chances of any liquefaction occurring are extremely low. Any liquefaction of the Zone IIA saprolite

that does occur will not impact the stability of any Unit 3 Seismic Category I structure.

2.5.4.9 Earthquake Design Basis

See Sections 2.5.2 and 3.7.1 for the GMRS and FIRS, respectively.

2.5.4.10 Static Stability

NAPS ESP COL 2.5-6

As with the Units 1 and 2, and the originally planned Units 3 and 4, the Unit 3 RB/FB is founded on Zone III-IV or Zone IV bedrock. If Zone III weathered rock or fractured rock is encountered at foundation subgrade level, then it will be removed and replaced with concrete fill. The subgrade of the other Seismic Category I structures and the Seismic Category II structures depends on their elevation and location. Table 2.5.4-209 shows the bottom of foundation elevations and depths for the Seismic Category I structures (RB/FB, CB, FWSC), the Seismic Category II structures (Turbine Building, Service Building and Ancillary Diesel Building), and the Radwaste Building. The foundation dimensions are also included in Table 2.5.4-209. The cross-sections in Figures 2.5.4-225 through 2.5.4-234 show the materials supporting these structures (except for the Ancillary Diesel Building). The average subsurface profiles beneath the Seismic Category I structures used for bearing capacity and settlement analyses are shown on Figure 2.5.4-251. The corresponding profiles beneath the Seismic Category II structures and the Radwaste Building are shown on Figure 2.5.4-252. There may be several materials immediately beneath the foundations of the larger structures (e.g., the Turbine Building) because of the variable stratigraphy and the different depths of the parts of the building, and because any Zone IIA saprolite beneath the shallow Seismic Category I or II structures (and the Radwaste Building) is removed and replaced with structural fill. Figure 2.5.4-209 also shows the static and dynamic design loads (demand) for these structures.

2.5.4.10.1 Bearing Capacity

a. **Allowable Bearing Capacity of Rock and Concrete Fill**

The allowable static bearing capacity values for each bedrock zone and concrete fill are given in Table 2.5.4-210. The Zone III allowable static bearing capacity of 20 ksf is less than the value of 20 percent of the ultimate crushing strength (or unconfined compressive strength) given in several building codes (SSAR Reference 181). The ultimate crushing

strength is given as 1.0 kips per square inch (ksi) (144 ksf)) in Table 2.5.4-208. The 20 ksf value is the same value given for weathered rock in Table 2.5-2 of the Units 1 and 2 UFSAR (SSAR Reference 5). For dynamic loading, 20 percent of the ultimate crushing strength can be used. Although the 20 ksf allowable static bearing capacity is greater than the maximum static bearing pressure from the RB/FB basemat, as noted earlier the RB/FB foundation will not be founded directly on the Zone III weathered rock. If excavation during construction for this foundation reveals any weathered or fractured zones at foundation level, such zones will be over-excavated and replaced with concrete fill.

The Zone III-IV and Zone IV bedrock have design unconfined compressive strengths of 9 ksi (1296 ksf) and 17 ksi (2448 ksf), respectively (Table 2.5.4-208). The allowable static values of the bearing capacity of 80 ksf and 160 ksf for Zone III-IV and Zone IV rock, respectively, are presumptive values based on various building codes for moderately weathered to fresh foliated rock (SSAR Reference 181). For dynamic loading, 20 percent of the ultimate crushing strength can be used, i.e., 259 ksf for Zone III-IV, and 490 ksf for Zone IV. For 2500 psi concrete fill, the computed allowable bearing capacity is 199 ksf (Reference 2.5-215) for both static and dynamic loading.

b. **Allowable Bearing Capacity of Soil**

For granular soils like the Zone IIB saprolite and the engineered structural fill, bearing capacity is based on Terzaghi's bearing capacity equations modified by Vesic (SSAR Reference 180). The ultimate (gross) bearing capacity of a footing, q_{ult}, supported on homogeneous soils can be estimated by (SSAR Reference 180):

$$q_{ult} = cN_c\zeta_c + \gamma' D_f N_q \zeta_q + 0.5\gamma' B N_\gamma \zeta_\gamma$$

where:

- c = undrained shear strength for clay (c_u) or cohesion intercept for (c,ϕ) soil
- $\gamma' D_f$ = effective overburden pressure at base of foundation
- γ' = effective unit weight of soil
- D_f = depth from ground surface to base of foundation
- B = width of foundation
- N_c, N_q, and N_γ are bearing capacity factors (defined in SSAR Reference 180), and

ζ_c, ζ_q, and ζ_γ are shape factors (defined in SSAR Reference 180)

These equations use the effective unit weight of the soil, the width and depth of the foundation, and bearing capacity and shape factors that are a function of the angle of internal friction of the soil. Consequently, each foundation has a different bearing capacity, depending on the foundation dimensions. For large foundations that are founded at large depths below grade, these equations can give very large bearing capacity values, even when a factor of safety of 3 is included for the allowable bearing value. In such situations, settlement, discussed in Section 2.5.4.10.2, normally governs.

c. **Allowable Bearing Capacity for Structures**

Table 2.5.4-211 gives the estimated allowable bearing capacity for the Seismic Category I and II structures, and the Radwaste Building based on the materials underlying the structures shown in Figures 2.5.4-251 and 2.5.4-252. Review of Figure 2.5.4-251 for the Seismic Category I structures shows that there is concrete fill beneath each structure underlain by Zone III-IV bedrock. Table 2.5.4-210 indicates that, for the static case, the Zone III-IV bearing capacity is less than that of concrete fill, while for the dynamic case, the concrete fill bearing capacity is less than that of Zone III-IV. The smaller bearing capacity is conservatively assumed in each case. Where the major structure bears on soil (Zone IIB saprolite or structural fill), the theoretical allowable capacities of the soil are very large, for the reasons explained above. The design static bearing capacity given in Table 2.5.4-211 is the minimum value for any layer beneath the structure. For structures on soil, settlement estimates are needed to determine what value of bearing pressure can be realistically applied.

Table 2.5.4-211 also contains values of allowable bearing capacity under dynamic or transient loading conditions. For bedrock subgrade, as noted earlier, these values are equivalent to 20 percent of the ultimate crushing strength. The allowable static and dynamic bearing capacity values in Table 2.5.4-211 for the Seismic Category I RB/FB, CB and FWSC foundations exceed the maximum static and dynamic bearing demand values given in Table 2.5.4-209.

The Zone IIA saprolite can be used to support relatively lightly-loaded, non-settlement sensitive structures that are not classified as Seismic Category I or II. The allowable bearing capacity value is limited to 4 ksf

because of settlement considerations. As noted in Section 2.5.4.10.2, settlement considerations usually dominate when this material is used for supporting foundations, and the actual allowable bearing capacity may be less than 4 ksf, especially for larger foundations.

d. **Buoyancy Effects**

NAPS ESP COL 2.5-4

As noted in Section 2.5.4.6.1, Section 2.4.12.4 indicates that the maximum predicted groundwater level in the power block area of Unit 3 increases from north to south, ranging from about Elevation 271 ft at the north end of the Turbine Building to about Elevation 282.5 ft at the south end of the RB/FB. Thus, there can be a hydrostatic uplift force on many of the structures founded below grade. All of the below-ground structures shown in Table 2.5.4-209 have sufficient applied foundation loads (Tables 2.5.4-209 and 2.5.4-211) that there are no net uplift forces even at the DCD site parameter for maximum groundwater level. However, such forces can be significant in the design of buried piping, particularly when the pipe is empty. In such a situation, the weight and strength of the backfill above the pipe is analyzed to confirm satisfactory resistance to the uplift forces. The normal factor of safety of 3 against soil failure is used in this analysis.

NAPS ESP COL 2.5-6

2.5.4.10.2 **Settlement Analysis**

The pseudo-elastic method of analysis was used for settlement estimates. This approach is suitable for the granular soils and bedrock at the site. The analysis is based on a stress-strain model that computes settlement of discrete layers:

$$\delta = \Sigma(\Delta p_i \times \Delta h_i)/E_i$$

where:

δ = settlement

i = 1 to n, where n is the number of soil layers

Δp_i = vertical applied pressure at center of layer i

Δh_i = thickness of layer i

E_i = elastic modulus of layer i

The stress distribution below rectangular foundations is based on a Boussinesq-type distribution for flexible foundations (Reference 2.5-216). The computation extends to a depth where the increase in vertical stress (Δp) due to the applied load is equal to or less than 10 percent of the applied foundation pressure. The Boussinesq-type vertical pressure

under a rectangular footing, σ_z, is as follows (Reference 2.5-216):

$$\sigma_z = (p/2\pi)(\tan^{-1}(lb/(zR_3)) + (lbz/R_3)(1/R_1^2 + 1/R_2^2))$$

where:

l = length of footing
b = width of footing
z = depth below footing at which pressure is computed
R1 = $(l^2 + z^2)^{0.5}$
R2 = $(b^2 + z^2)^{0.5}$
R3 = $(l^2 + b^2 + z^2)^{0.5}$

Settlement estimates were made using the preceding relationships and the soil and rock properties given in Table 2.5.4-208. These estimates were made for each Seismic Category I and II structure, and the Radwaste Building, and are presented in Table 2.5.4-212. The applied pressures from the foundations are also shown on Table 2.5.4-212.

As would be anticipated, the settlement of the structures founded on Zone III-IV or Zone IV bedrock is negligible. Similarly, settlements of structures sitting on the dense to very dense structural fill or Zone IIB saprolite overlying rock are modest in light of the large applied pressures.

The total and differential settlements under the RB/FB, CB and FWSC are well within the limits stated in Table 2.0-201. Based on the computed settlement values in Table 2.5.4-212, the average settlement of these structures is 0.1 in. or less.

2.5.4.10.3 Earth Pressures

Static and seismic lateral earth pressures are addressed for plant below-ground walls. Both active and at-rest cases are included. Active earth pressure is used for temporary retaining wall installed to facilitate construction. For these, the earth pressure coefficients are Rankine values, assuming level backfill and a zero friction angle between the soil and the wall. Hydrostatic pressures are conservatively based on the groundwater table being at grade. An area wide surcharge pressure of 500 psf is used. Lateral pressures due to compaction are not included; these pressures are controlled by compacting backfill with light equipment near structures. The soil properties used in the calculation of lateral earth pressures are from Table 2.5.4-208.

For the active lateral earth pressure case, earthquake-induced horizontal ground accelerations are addressed by the application of $k_h \cdot g$ applying

the Mononobe-Okabe method. Vertical ground accelerations ($k_v \cdot g$) are considered negligible and were ignored (Reference 2.5-217). The peak low frequency acceleration of 0.31g was used for developing the seismic active earth pressure diagram. Use of the peak high frequency acceleration was considered overly conservative given the low magnitude (energy) of this earthquake.

The method described in ASCE 4-98 Section 3.5.3.2 (Reference 2.5-218) can be used to estimate the dynamic component of seismic at-rest lateral earth pressure for the below-grade walls of the power block structures. Reference 2.5-218 provides an elastic solution that is demonstrated by a nomograph. In the nomograph, a dimensionless normalized in-situ lateral stress at 1.0g horizontal earthquake acceleration is developed for a normalized depth at a given Poisson's ratio. The appropriate site-specific at-rest pressure is calculated from the nomograph at various depth intervals using the site-specific acceleration and Poisson's ratio.

Figures 2.5.4-225 through 2.5.4-234 show structural fill between some below-ground structures, e.g., between the FWSC and CB in Figure 2.5.4-228 (Section D-D), and between structures and the temporary retaining wall installed to facilitate construction. Figure 2.5.4-225 (Section A-A) shows approximately 50 ft of excavation is required from the existing ground surface to the bottom of excavation for the Turbine Building. This wall will hold back the natural in-situ soil (Zone IIA and IIB saprolites) which will be in an active condition. This case is used as an example of active earth pressure for the lateral earth pressure diagram in Figure 2.5.4-253. This figure includes active earth pressure along with the groundwater, surcharge and seismic components of lateral pressure against the temporary wall.

The same section shows approximately 60 ft depth of structural fill against the Turbine Building wall. This case is used as an example of at-rest earth pressure against an unyielding wall for the lateral earth pressure diagram in Figure 2.5.4-254. This figure includes at-rest earth pressure along with the groundwater, surcharge and seismic components of lateral pressure against the permanent wall.

The lateral pressures in Figures 2.5.4-253 and 2.5.4-254 are best estimate pressures with a factor of safety of 1. Appropriate safety factors need to be incorporated into the wall structural design. The factor of safety against a gravity wall or structure foundation sliding is normally

taken as 1.1 when seismic pressures are included. The same factor of safety is applied against a wall overturning.

NAPS COL 2.0-29-A

2.5.4.11 Design Criteria

NAPS ESP COL 2.5-7

Applicable design criteria are covered in various sections. The criteria summarized below are geotechnical criteria and also geotechnical-related criteria that pertain to structural design.

Section 2.5.4.8 specifies that the acceptable factor of safety against liquefaction of site soils is ≥ 1.1.

Bearing capacity and settlement criteria are presented in Section 2.5.4.10. Table 2.5.4-211 provides allowable bearing capacity values for the Seismic Category I and II structures and the Radwaste Building. A minimum factor of safety of 3 is used when applying bearing capacity equations. This factor of safety is also applied against breakout failure due to uplift forces on buried piping.

Section 2.5.4.10 also discusses factors of safety related to lateral earth pressures. The lateral pressures shown in Figures 2.5.4-253 and 2.5.4-254 have a factor of safety of 1. A factor of safety of 1.1 should be used in the analyses of sliding and overturning due to these lateral loads when the seismic component is included.

Section 2.5.5.2 specifies that the minimum acceptable long-term static factor of safety against slope stability failure is 1.5. Section 2.5.5.3 specifies that the minimum acceptable long-term seismic factor of safety against slope stability failure is 1.1.

NAPS COL 2.0-29-A

2.5.4.12 Techniques to Improve Subsurface Conditions

NAPS ESP COL 2.5-8

For Unit 3, any Zone IIA and Zone IIB saprolite beneath or adjacent to Seismic Category I or II structures is removed and replaced with concrete fill. Improvement of the Zone IIA saprolite as described SSAR Section 2.5.4.12 is suitable for non-Seismic Category I and II structures.

Zones of weathered or fractured rock encountered immediately beneath the RB/FB, CB, and FWSC footprints are removed and replaced with concrete fill.

Appendix 2.5.4AA MACTEC Geotechnical Data Report, Rev. 1; September 28, 2007

Volume 1: Text, Figures, Tables and Appendices A and B

Letters

Geotechnical Data Report

Appendix A - Survey Report

Appendix B.1 - Geotechnical Boring Logs (Soil and Rocks)

Boring: B901 (pp1–10) (pp11–14)
B902
B903
B904
B905
B906
B907
B908
B909
B910
B911
B912
B913
B914
B915
B916
B917
B918
B919
B920
B921 B921A
B922 B922A
B923
B924
B925
B926
B927
B928 B928A
B929 B929A
B930
B931
B932
B933 B933A
B934
B936
B937
B939
B940
B941

B942
B943
B944
B945
B946
B947
B948
B949
B950
B951
OW951

Appendix B.2 - Test Pit Logs

Appendix B.3 - SPT Energy Measurement Reports

Volume 2: Appendices C and D

Appendix C.1 - Observation Well Logs, Development Records and Sampling Records

Appendix C.2 - Slug Test Data
OW-945 (pp1–14) (pp15–21)
OW-946 (pp1–6) (pp7–25)
OW-947 (pp1–13) (pp14–16) (pp17–27)
OW- 949 (pp1–13) (pp14–19)

Appendix C.3 - Packer Test Data (pp2–80) (pp81–195)

Appendix C.4 - Groundwater Chemistry Tests

Appendix D - Cone Penetrometer Test Results (pp2–29) (pp30–52) (pp53–68) (pp69–92)

Volume 3: Appendix E

Appendix E.1 - Field Sensitivity Test

Appendix E.2 - Geovision Downhole and P-S Logging Report (359pp)
Cover
Contents
Introduction
Scope of Work
Instrumentation
Measurement Procedures
Data Analysis
Results
Summary
Tables and Figures (pp36–56) (pp57–68)
Appendix A - Suspension Velocity Measurement: Quality Assurance
Suspension Source to Receiver Analysis Results (pp2–12) (pp13–23)

Appendix E.2 - Geovision Downhole and P-S Logging Report (continued)

Appendix B - Caliper, Natural Gamma, Resistivity, and Spontaneous Potential Logs
(pp2-9) (pp10–19) (pp20–23)

Appendix C - Acoustic Televiewer Dip Logs
Borehole: B-901 (pp1–4) (pp5–8) (pp9–12) (pp13–16) (pp17–20)
(pp21–24) (pp25–28) (pp29–32) (pp33–36)
Borehole: B-907 (pp1–4) (pp5–8) (pp9–12) (pp13–16) (pp17–20)
(pp21–22)
Borehole: B-909 (pp1–4) (pp5–8) (pp9–13) (pp14–18) (pp19–23) (pp24–28)

Appendix D - Boring Geophysical Logging Systems - NIST Traceable Calibration Procedures and Calibration Records

Appendix E - Boring Geophysical Logging Field Data Logs
B-901 (pp1–26) (pp27–28)
B-907
B-909

Appendix F - Boring Geophysical Logging Field Measurement Procedures
Procedure for OYO P-S Suspension Seismic Velocity Logging
Procedure for Using the Robertson Geologging Hi-Resolution Acoustic Viewer (HiRAT) (pp1–12) (pp13–14)
ASTM D 5753 – 05, Standard Guide for Planning and Conducting Borehole Geophysical Logging
ASTM D 6167 – 97, Standard Guide for Conducting Borehole Geophysical Logging: Mechanical Caliper
ASTM D 6274 – 98; Conducting Borehole Geophysical Logging - Gamma

Volume 4: Appendix F

Appendix F- Geotechnical Laboratory Test Assignment

Appendix F.1 - Soil Index and Particle Size Distribution Tests (pp1–208) (pp209–297)

Appendix F.2 - Soil Strength Tests

Appendix F.3 - Soil Moisture-Density and California Bearing Ration Tests (pp1–13) (pp14–27) (pp28–34)

Appendix F.4 - Soil Corrosivity Tests

Appendix F.5 - Rock Core Unconfined Strength Tests

Appendix F.6 - Rock Core Strength and Modulus Tests

Appendix 2.5.4AAS1 Supplement 1, Dynamic Laboratory Testing Results

Appendix 2.5.4AAS2 Supplement 2, Distribution Coefficients (Kd) Laboratory Test Results

Title
Introduction
Scope of Work
Methodology
Quality Assurance
Results
Table SR-1 Summary of Particle Size Dist. Test Results
Table SR-2 Summary of Soil pH and Cation Exchange Capacity Tests
Introduction
Materials and Methods
Results
Appendix A - Detailed Description: Materials and Methods for K_d Testing
Appendix B - Radioisotope Certification
Appendix C - Gamma Spectroscopy, ICP-MS, and XRF, XRD Sample Results and QA Result
Appendix D - Data Used in K_d Calculations
Appendix E - Chain of Custody Sheets for the Soil, Rock and Groundwater Samples
Appendix F - M&TE Approval of Balance
Appendix G - List of Equipment Used in Study
Appendix H - Personnel Qualifications
Appendix I - Sieve Certificates of Compliance

Appendix 2.5.4BB MACTEC Geotechnical Exploration and Testing Supplement 1, 2009

Appendix B.1 - Geotechnical Boring Logs
Boring No.: W-1
Boring No.: W-2
Boring No.: W-3
Boring No.: W-4
Boring No.: W-5 & 6
Boring No.: W-7 & 8
Boring No.: W-9 & 10
Appendix B.2 - SPT Energy Measurement Reports
CME-550x ATV
CME-55 Track RAL

Appendix 2.5.4CC MACTEC Geotechnical Exploration and Testing Supplement 2, 2010

Appendix C - Acoustic Televiewer Dip Logs (pp 2-28) (pp 1-27)
Appendix D - Geophysical Logging Systems - NIST Traceable Calibration Procedures and Calibration Records
Appendix E - Boring Geophysical Logging Field Data Logs (pp 2-32) (pp 1-15)
Appendix F - Boring Geophysical Logging Field Measurement Procedures
Appendix D - Laboratory Test Data

NAPS COL 2.0-29A

Table 2.5.4-201 Borehole Information

Boring Number	Coordinates (ft)		Ground Surface Elevation (ft)	Penetration Depth (ft)
	Northing	Easting		
B-901	3,909,777.72	11,685,928.59	309.42	300.0
B-902	3,909,874.19	11,685,884.28	302.20	201.7
B-903	3,909,812.10	11,686,028.80	301.59	151.0
B-904	3,909,692.47	11,685,970.43	316.75	151.7
B-905	3,909,732.86	11,685,821.97	306.75	150.4
B-906	3,909,670.03	11,685,795.34	311.72	150.5
B-907	3,909,607.90	11,685,938.35	322.71	200.5
B-908	3,909,716.65	11,686,060.89	307.71	151.4
B-909	3,909,695.46	11,686,107.40	304.90	201.9
B-910	3,909,667.63	11,685,883.11	316.54	148.4
B-911	3,909,919.91	11,685,992.68	299.79	101.0
B-911A	3,909,916.04	11,686,000.53	299.91	21.7
B-912	3,910,021.70	11,686,051.36	275.10	151.8
B-913	3,910,148.50	11,686,114.71	273.37	100.9
B-914	3,909,939.55	11,685,922.35	297.45	200.5
B-915	3,909,877.48	11,686,088.55	301.79	112.8
B-916	3,910,049.54	11,686,008.70	276.24	100.3
B-917	3,910,160.68	11,686,029.45	274.85	150.8
B-918	3,910,115.28	11,686,194.05	272.13	150.1
B-919	3,909,575.39	11,685,764.67	317.79	76.2
B-920	3,909,545.07	11,685,980.20	327.17	150.7
B-921	3,909,680.19	11,686,162.71	307.96	73.9
B-921A	3,909,686.89	11,686,161.68	307.39	40.4
B-922	3,909,943.65	11,686,232.99	271.30	26.0
B-922A	3,909,949.30	11,686,244.02	271.33	76.5
B-923	3,910,076.97	11,686,309.48	272.00	75.4
B-924	3,909,969.53	11,686,475.40	271.52	75.6
B-925	3,910,036.67	11,686,576.27	270.01	75.8

NAPS COL 2.0-29A

Table 2.5.4-201 Borehole Information

Boring Number	Coordinates (ft)		Ground Surface Elevation (ft)	Penetration Depth (ft)
	Northing	Easting		
B-926	3,910,043.20	11,685,709.26	289.03	155.5
B-927	3,909,966.07	11,685,878.59	292.51	100.4
B-928	3,910,222.75	11,686,159.07	272.17	75.2
B-928A	3,910,220.39	11,686,165.35	271.82	37.5
B-929	3,909,214.44	11,685,654.82	329.02	74.0
B-929A	3,909,214.15	11,685,665.51	329.03	52.5
B-930	3,909,275.95	11,685,842.87	326.12	123.6
B-931	3,910,152.94	11,685,921.54	278.52	74.0
B-932	3,910,444.31	11,686,415.70	249.88	35.1
B-933	3,909,827.41	11,685,790.97	296.48	100.3
B-933A	3,909,826.28	11,685,802.01	296.58	27.5
B-934	3,909,860.37	11,685,686.09	294.80	101.6
B-936	3,910,745.87	11,685,929.15	286.56	100.7
B-937	3,910,688.52	11,686,672.12	270.25	55.3
B-939	3,911,317.60	11,686,605.91	254.03	76.1
B-940	3,910,266.77	11,688,901.02	268.32	76.1
B-941	3,910,403.63	11,688,912.87	267.19	75.8
B-942	3,909,614.69	11,684,326.45	291.85	100.8
B-943	3,909,355.39	11,683,892.47	300.40	101.9
B-944	3,908,772.38	11,684,127.62	334.69	86.4
B-945	3,910,135.55	11,683,779.79	281.51	100.6
B-946	3,908,787.24	11,683,810.59	333.36	100.7
B-947	3,909,574.53	11,686,367.21	312.48	88.8
B-948	3,909,619.26	11,685,565.69	310.41	100.6
B-949	3,909,018.09	11,685,157.27	334.82	106.4
B-950	3,910,835.82	11,686,282.11	282.50	100.8
B-951	3,910,548.26	11,686,821.80	249.93	101.0
W-1	3,909,853.0	11,685,959.0	306.2	154.0

NAPS COL 2.0-29A

Table 2.5.4-201 Borehole Information

Boring Number	Coordinates (ft)		Ground Surface Elevation (ft)	Penetration Depth (ft)
	Northing	Easting		
W-2	3,909,822.0	11,685,864.0	298.4	143.3
W-3	3,909,714.5	11,685,899.0	312.3	150.7
W-4	3,909,749.0	11,686,002.0	311.9	150.6
W-5	3,909,978.5	11,686,141.5	273.0	100.4
W-6	3,909,830.5	11,686,205.5	301.9	123.9
W-7	3,909,730.5	11,686,146.5	303.1	151.2
W-8	3,909,767.5	11,686,273.0	307.8	150.6
W-9	3,909,600.5	11,686,022.0	320.2	151.0
W-10	3,909,598.5	11,685,820.0	319.1	153.0
M-1	3,909,611.0	11,685,483.5	314.1	151.1
M-2	3,909,531.0	11,685,586.0	315.3	153.4
M-3	3,909,538.5	11,685,678.5	313.9	152.6
M-4	3,909,456.0	11,685,694.5	321.8	154.0
M-6	3,909,401.0	11,685,759.5	327.8	150.4
M-7	3,909,504.0	11,685,835.5	326.0	151.5
M-8	3,909,413.5	11,685,847.0	329.3	150.6
M-9	3,909,333.5	11,685,946.0	327.3	153.6
M-10	3,909,243.5	11,685,962.0	323.6	201.9
M-11	3,909,351.5	11,686,038.5	325.9	148.7
M-12	3,909,723.0	11,685,560.0	307.0	151.2
M-13	3,909,519.5	11,686,025.0	326.8	151.6
M-14	3,909,451.5	11,686,111.0	323.8	60.3
M-15	3,909,531.0	11,686,166.0	311.3	60.0
M-16	3,909,989.5	11,685,801.5	284.6	61.9
M-17	3,909,775.0	11,686,213.5	306.2	151.9
M-18	3,909,608.0	11,686,213.5	304.2	60.4
M-19	3,910,052.5	11,685,855.5	280.4	151.4
M-20	3,909,793.5	11,686,067.5	302.6	151.0

NAPS COL 2.0-29A

Table 2.5.4-201 Borehole Information

Boring Number	Coordinates (ft)		Ground Surface Elevation (ft)	Penetration Depth (ft)
	Northing	Easting		
M-21	3,909,811.0	11,686,269.5	303.9	151.8
M-27	3,909,426.0	11,685,937.5	330.2	151.4
M-28	3,909,635.5	11,685,672.0	308.2	150.0
M-29	3,909,710.5	11,685,460.0	309.3	151.2
M-30	3,909,695.0	11,685,381.5	313.3	201.7
M-31	3,909,799.0	11,685,459.5	306.9	151.5
M-32	3,909,875.5	11,685,526.5	313.2	62.2
M-33	3,909,983.5	11,685,614.5	303.8	64.9
M-34	3,910,122.0	11,685,736.0	280.9	63.0

NAPS COL 2.0-29-A

Table 2.5.4-202 Observation Well Information

Well Number	Coordinates (ft)		Surface Elev. (ft)	Depth (ft)	Elev. of Top of Screen (ft)	Screen Length (ft)
	Northing	Easting				
OW-901	3,909,772	11,685,917	309.6	108.0	214.6	10
OW-945	3,910,136	11,683,793	281.6	54.5	240.1	10
OW-946	3,908,788	11,683,823	334.0	43.4	303.6	10
OW-947	3,909,580	11,686,372	313.3	58.0	268.3	10
OW-949	3,909,025	11,685,153	335.7	105.0	243.2	0
OW-950	3,910,842	11,686,285	283.0	92.0	203.0	10
OW-951	3,910,521	11,686,786	249.7	67.0	194.6	10

NAPS COL 2.0-29-A

Table 2.5.4-203 Information on the CPTs Performed

CPT Number	Coordinates (ft)		Ground Surface Elevation (ft)	Depth (ft)
	Northing	Easting		
C-901	3,909,627.77	11,686,012.67	318.56	20.0
C-902	3,909,552.59	11,685,842.21	323.66	29.0
C-903	3,909,719.02	11,685,775.66	306.84	29.0
C-904	3,910,026.29	11,685,793.52	283.92	35.5
C-905	3,910,137.61	11,685,857.21	279.29	45.6
C-906	3,910,013.77	11,686,269.94	270.75	2.6
C-907	3,910,174.67	11,686,277.14	271.66	13.1
C-908	3,910,326.76	11,686,187.39	271.91	28.1
C-909	3,909,346.74	11,685,717.77	330.26	60.0
C-910	3,909,154.43	11,685,782.42	326.99	25.1
C-911	3,910,716.79	11,685,941.76	286.69	15.3
C-912	3,909,959.42	11,686,349.77	271.16	2.8
C-913	3,910,999.95	11,686,812.54	268.65	20.0
C-914	3,910,360.20	11,688,917.62	267.86	31.0
C-915	3,909,784.60	11,686,794.40	320.92	54.0
C-916	3,909,584.68	11,686,372.70	312.91	49.1
C-917	3,909,337.29	11,686,293.79	320.37	49.2
C-918	3,909,151.49	11,685,509.11	329.55	25.1
C-919	3,909,154.30	11,685,255.41	338.06	25.1
C-920	3,909,071.70	11,685,870.40	324.73	25.1
C-921	3,910,112.20	11,685,717.17	281.10	30.0
C-922	3,909,889.28	11,684,055.95	311.73	20.3
C-923	3,910,107.49	11,683,828.42	283.03	22.2

NAPS COL 2.0-29-A

Table 2.5.4-204 Elevation, Depth, and Thickness of the Subsurface Zones

Boring Number	Top Elevation of Zones (ft)						Top Depth of Zones (ft)						Thickness of Zones (ft)				
	I	IIA	IIB	III	III-IV	IV	I	IIA	IIB	III	III-IV	IV	I	IIA	IIB	III	III-IV
B-901	309.4	309.4	279.9	269.5	229.4	174.4	0.0	0.0	29.5	39.9	80.0	135.0	0.0	29.5	10.4	40.1	55.0
B-902	302.2	302.2	283.0	283.0	-	278.4	0.0	0.0	19.2	19.2	-	23.8	0.0	19.2	0.0	4.6	-
B-903	301.6	301.6	281.9	279.0	220.8	185.6	0.0	0.0	19.7	22.6	80.8	116.0	0.0	19.7	2.9	58.2	35.2
B-904	316.8	316.8	288.3	270.0	235.1	195.1	0.0	0.0	28.5	46.8	81.7	121.7	0.0	28.5	18.3	34.9	40.0
B-905	306.7	306.7	286.8	282.9	271.4	176.2	0.0	0.0	19.9	23.8	35.3	130.5	0.0	19.9	3.9	11.5	95.2
B-906	311.7	311.7	282.8	276.8	262.0	176.2	0.0	0.0	28.9	34.9	49.7	135.5	0.0	28.9	6.0	14.8	85.8
B-907	322.7	322.7	287.7	283.7	207.2	177.2	0.0	0.0	35.0	39.0	115.5	145.5	0.0	35.0	4.0	76.5	30.0
B-908	307.7	307.7	280.7	245.0	-	241.3	0.0	0.0	27.0	62.7	-	66.4	0.0	27.0	35.7	3.7	-
B-909	304.9	304.9	275.9	258.0	225.0	195.0	0.0	0.0	29.0	46.9	79.9	109.9	0.0	29.0	17.9	33.0	30.0
B-910	316.5	316.5	294.5	274.5	226.1	-	0.0	0.0	22.0	42.0	90.4	-	0.0	22.0	20.0	48.4	-
B-911	299.8	299.8	282.8	278.8	268.7	233.8	0.0	0.0	17.0	21.0	31.1	66.0	0.0	17.0	4.0	10.1	34.9
B-911A	299.9	299.9	282.9	278.8	268.7	233.8	0.0	0.0	17.0	21.1	31.2	66.1	0.0	17.0	4.1	10.1	34.9
B-912	275.1	275.1	255.5	251.0	-	238.3	0.0	0.0	19.6	24.1	-	36.8	0.0	19.6	4.5	12.7	-
B-913	273.4	273.4	223.4	217.9	-	215.5	0.0	0.0	50.0	55.5	-	57.9	0.0	50.0	5.5	2.4	-
B-914	297.4	297.4	275.4	275.4	236.9	202.1	0.0	0.0	22.0	22.0	60.5	95.3	0.0	22.0	0.0	38.5	34.8
B-915	301.8	301.8	288.3	284.8	279.4	-	0.0	0.0	13.5	17.0	22.4	-	0.0	13.5	3.5	5.4	-
B-916	276.2	276.2	251.1	-	-	250.6	0.0	0.0	25.1	-	-	25.6	0.0	25.1	0.5	-	-
B-917	274.9	274.9	217.9	206.4	187.1	178.8	0.0	0.0	57.0	68.5	87.8	96.1	0.0	57.0	11.5	19.3	8.3
B-918	272.1	271.1	267.0	245.8	-	239.8	0.0	1.0	5.1	26.3	-	32.3	1.0	4.1	21.2	6.0	-
B-919	317.8	317.8	294.8	279.9	264.7	-	0.0	0.0	23.0	37.9	53.1	-	0.0	23.0	14.9	15.2	-

NAPS COL 2.0-29-A

Table 2.5.4-204 Elevation, Depth, and Thickness of the Subsurface Zones

Boring Number	Top Elevation of Zones (ft)						Top Depth of Zones (ft)						Thickness of Zones (ft)				
	I	IIA	IIB	III	III-IV	IV	I	IIA	IIB	III	III-IV	IV	I	IIA	IIB	III	III-IV
B-920	327.2	324.8	289.2	274.2	-	221.5	0.0	2.4	38.0	53.0	-	105.7	2.4	35.6	15.0	52.7	-
B-921	308.0	308.0	260.0	236.2	-	-	0.0	0.0	48.0	71.8	-	-	0.0	48.0	23.8	-	-
B-921A	307.4	307.4	259.4	236.2	-	-	0.0	0.0	48.0	71.2	-	-	0.0	48.0	23.2	-	-
B-922	271.3	271.3	265.0	262.5	257.3	-	0.0	0.0	6.3	8.8	14.0	-	0.0	6.3	2.5	5.2	-
B-922A	271.3	271.3	271.3	263.1	254.8	209.8	0.0	0.0	0.0	8.2	16.5	61.5	0.0	0.0	8.2	8.3	45.0
B-923	272.0	269.2	266.8	-	266.8	260.3	0.0	2.8	5.2	-	5.2	11.7	2.8	2.4	0.0	-	6.5
B-924	271.5	271.1	265.0	265.0	252.9	227.9	0.0	0.4	6.5	6.5	18.6	43.6	0.4	6.1	0.0	12.1	25.0
B-925	270.0	270.0	253.0	-	249.6	213.7	0.0	0.0	17.0	-	20.4	56.3	0.0	17.0	3.4	-	35.9
B-926	289.0	289.0	235.0	235.0	225.2	179.5	0.0	0.0	54.0	54.0	63.8	109.5	0.0	54.0	0.0	9.8	45.7
B-927	292.5	292.5	268.5	-	252.7	217.9	0.0	0.0	24.0	-	39.8	74.6	0.0	24.0	15.8	-	34.8
B-928	272.2	272.2	244.2	235.1	220.1	212.0	0.0	0.0	28.0	37.1	52.1	60.2	0.0	28.0	9.1	15.0	8.1
B-928A	271.8	271.8	243.8	235.1	220.1	212.0	0.0	0.0	28.0	36.7	51.7	59.8	0.0	28.0	8.7	15.0	8.1
B-929	329.0	329.0	283.0	265.0	-	-	0.0	0.0	46.0	64.0	-	-	0.0	46.0	18.0	-	-
B-929A	329.0	329.0	283.0	265.0	-	-	0.0	0.0	46.0	64.0	-	-	0.0	46.0	18.0	-	-
B-930	326.1	323.7	265.1	244.1	-	-	0.0	2.4	61.0	82.0	-	-	2.4	58.6	21.0	-	-
B-931	278.5	278.5	228.7	221.5	-	-	0.0	0.0	49.8	57.0	-	-	0.0	49.8	7.2	-	-
B-932	249.9	231.9	221.9	-	-	-	0.0	18.0	28.0	-	-	-	18.0	10.0	-	-	-
B-933	296.5	291.0	274.5	269.5	248.3	239.6	0.0	5.5	22.0	27.0	48.2	56.9	5.5	16.5	5.0	21.2	8.7
B-933A	296.6	291.1	274.6	269.5	248.3	239.6	0.0	5.5	22.0	27.1	48.3	57.0	5.5	16.5	5.1	21.2	8.7
B-934	294.8	294.8	252.8	252.8	-	246.4	0.0	0.0	42.0	42.0	-	48.4	0.0	42.0	0.0	6.4	-

NAPS COL 2.0-29-A

Table 2.5.4-204 Elevation, Depth, and Thickness of the Subsurface Zones

Boring Number	Top Elevation of Zones (ft)						Top Depth of Zones (ft)						Thickness of Zones (ft)				
	I	IIA	IIB	III	III-IV	IV	I	IIA	IIB	III	III-IV	IV	I	IIA	IIB	III	III-IV
B-936	286.6	286.6	266.3	253.1	190.6	-	0.0	0.0	20.3	33.5	96.0	-	0.0	20.3	13.2	62.5	-
B-937	270.3	270.3	245.3	237.0	220.0	-	0.0	0.0	25.0	33.3	50.3	-	0.0	25.0	8.3	17.0	-
B-939	254.0	254.0	215.2	-	-	-	0.0	0.0	38.8	-	-	-	0.0	38.8	-	-	-
B-940	268.3	268.3	249.8	249.8	212.1	-	0.0	0.0	18.5	18.5	56.2	-	0.0	18.5	0.0	37.7	-
B-941	267.2	267.2	258.7	219.3	-	205.8	0.0	0.0	8.5	47.9	-	61.4	0.0	8.5	39.4	13.5	-
B-942	291.8	291.8	285.8	-	-	263.0	0.0	0.0	6.0	-	-	28.8	0.0	6.0	22.8	-	-
B-943	300.4	300.4	283.9	278.0	268.5	220.1	0.0	0.0	16.5	22.4	31.9	80.3	0.0	16.5	5.9	9.5	48.4
B-944	334.7	334.7	299.7	-	281.2	-	0.0	0.0	35.0	-	53.5	-	0.0	35.0	18.5	-	-
B-945	281.5	281.5	228.1	-	221.0	210.6	0.0	0.0	53.4	-	60.5	70.9	0.0	53.4	7.1	-	10.4
B-946	333.4	333.4	301.2	-	291.6	-	0.0	0.0	32.2	-	41.8	-	0.0	32.2	9.6	-	-
B-947	312.5	312.5	260.8	248.8	-	-	0.0	0.0	51.7	63.7	-	-	0.0	51.7	12.0	-	-
B-948	310.4	310.4	288.4	281.9	274.7	-	0.0	0.0	22.0	28.5	35.7	-	0.0	22.0	6.5	7.2	-
B-949	334.8	334.8	281.9	-	258.4	-	0.0	0.0	52.9	-	76.4	-	0.0	52.9	23.5	-	-
B-950	282.5	282.5	261.8	-	232.2	218.7	0.0	0.0	20.7	-	50.3	63.8	0.0	20.7	29.6	-	13.5
B-951	249.9	249.9	230.4	209.3	-	179.9	0.0	0.0	19.5	40.6	-	70.0	0.0	19.5	21.1	29.4	-
W-1	306.2	306.2	284.2	277.9	211.2	-	0.0	0.0	22.0	28.3	95.0	-	0.0	22.0	6.3	66.7	-
W-2	298.4	298.4	279.9	275.6	275.6	212.3	0.0	0.0	18.5	22.8	22.8	86.1	0.0	18.5	4.3	0.0	63.3
W-3	312.3	312.3	283.7	278.7	241.6	231.6	0.0	0.0	28.6	33.6	70.7	80.7	0.0	28.6	5.0	37.1	10.0
W-4	311.9	311.9	275.9	273.0	241.3	201.3	0.0	0.0	36.0	38.9	70.6	110.6	0.0	36.0	2.9	31.7	40.0
W-5	273.0	273.0	273.0	269.1	268.8	228.8	0.0	0.0	0.0	3.9	4.2	44.2	0.0	0.0	3.9	0.3	40.0

NAPS COL 2.0-29-A

Table 2.5.4-204 Elevation, Depth, and Thickness of the Subsurface Zones

Boring Number	Top Elevation of Zones (ft)						Top Depth of Zones (ft)						Thickness of Zones (ft)				
	I	IIA	IIB	III	III-IV	IV	I	IIA	IIB	III	III-IV	IV	I	IIA	IIB	III	III-IV
W-6	301.9	301.9	263.2	248.2	208.0	-	0.0	0.0	38.7	53.7	93.9	-	0.0	38.7	15.0	40.2	-
W-7	303.1	303.1	253.8	243.8	226.9	201.9	0.0	0.0	49.3	59.3	76.2	101.2	0.0	49.3	10.0	16.9	25.0
W-8	307.8	307.8	253.5	233.5	227.8	216.4	0.0	0.0	54.3	74.3	80.0	91.4	0.0	54.3	20.0	5.7	11.4
W-9	320.2	320.2	291.9	251.9	187.2	-	0.0	0.0	28.3	68.3	133.0	-	0.0	28.3	40.0	64.7	-
W-10	319.1	319.1	276.1	275.8	226.1	-	0.0	0.0	43.0	43.3	93.0	-	0.0	43.0	0.3	49.7	-
M-1	314.1	314.1	280.9	273.1	260.6	255.6	0.0	0.0	33.2	41.0	53.5	58.5	0.0	33.2	7.8	12.5	5.0
M-2	315.3	315.3	282.5	272.5	251.4	241.9	0.0	0.0	32.8	42.8	63.9	73.4	0.0	32.8	10.0	21.1	9.5
M-3	313.9	313.9	299.1	289.6	274.8	171.3	0.0	0.0	14.8	24.3	39.1	142.6	0.0	14.8	9.5	14.8	103.5
M-4	321.8	321.8	292.9	287.9	252.8	207.8	0.0	0.0	28.9	33.9	69.0	114.0	0.0	28.9	5.0	35.1	45.0
M-6	327.8	327.8	263.7	253.7	231.4	211.4	0.0	0.0	64.1	74.1	96.4	116.4	0.0	64.1	10.0	22.3	20.0
M-7	326.0	326.0	302.0	291.9	219.7	184.7	0.0	0.0	24.0	34.1	106.3	141.3	0.0	24.0	10.1	72.2	35.0
M-8	329.3	329.3	275.6	250.6	242.9	-	0.0	0.0	53.7	78.7	86.4	-	0.0	53.7	25.0	7.7	-
M-9	327.3	327.3	264.6	244.6	-	203.7	0.0	0.0	62.7	82.7	-	123.6	0.0	62.7	20.0	40.9	-
M-10	323.6	323.6	264.5	221.5	212.8	172.0	0.0	0.0	59.1	102.1	110.8	151.6	0.0	59.1	43.0	8.7	40.8
M-11	325.9	325.9	232.3	212.3	-	-	0.0	0.0	93.6	113.6	-	-	0.0	93.6	20.0	-	-
M-12	307.0	305.0	269.0	263.5	243.1	240.8	0.0	2.0	38.0	43.5	63.9	66.2	2.0	36.0	5.5	20.4	2.3
M-13	326.8	326.8	-	274.8	255.8	182.7	0.0	0.0	-	52.0	71.0	144.1	0.0	52.0	-	19.0	73.1
M-14	323.8	323.8	265.0	-	-	-	0.0	0.0	58.8	-	-	-	0.0	58.8	-	-	-
M-15	311.3	311.3	267.8	-	-	-	0.0	0.0	43.5	-	-	-	0.0	43.5	-	-	-
M-16	284.6	283.8	235.3	230.3	-	224.4	0.0	0.8	49.3	54.3	-	60.2	0.8	48.5	5.0	5.9	-

NAPS COL 2.0-29-A

Table 2.5.4-204 Elevation, Depth, and Thickness of the Subsurface Zones

Boring Number	Top Elevation of Zones (ft)						Top Depth of Zones (ft)						Thickness of Zones (ft)				
	I	IIA	IIB	III	III-IV	IV	I	IIA	IIB	III	III-IV	IV	I	IIA	IIB	III	III-IV
M-17	306.2	305.7	-	252.1	214.3	204.3	0.0	0.5	-	54.1	91.9	101.9	0.5	53.6	-	37.8	10.0
M-18	304.2	304.2	245.7	244.0	-	-	0.0	0.0	58.5	60.2	-	-	0.0	58.5	1.7	-	-
M-19	280.4	280.4	222.1	-	213.8	206.7	0.0	0.0	58.3	-	66.6	73.7	0.0	58.3	8.3	-	7.1
M-20	302.6	302.1	-	265.6	246.6	193.6	0.0	0.5	-	37.0	56.0	109.0	0.5	36.5	-	19.0	53.0
M-21	303.9	303.9	260.4	255.4	222.1	207.1	0.0	0.0	43.5	48.5	81.8	96.8	0.0	43.5	5.0	33.3	15.0
M-27	330.2	330.2	286.5	261.5	215.2	208.8	0.0	0.0	43.7	68.7	115.0	121.4	0.0	43.7	25.0	46.3	6.4
M-28	308.2	308.2	292.6	284.4	265.2	183.2	0.0	0.0	15.6	23.8	43.0	125.0	0.0	15.6	8.2	19.2	82.0
M-29	309.3	309.3	277.3	-	268.3	265.1	0.0	0.0	32.0	-	41.0	44.2	0.0	32.0	9.0	-	3.2
M-30	313.3	313.3	279.6	274.6	269.6	266.6	0.0	0.0	33.7	38.7	43.7	46.7	0.0	33.7	5.0	5.0	3.0
M-31	306.9	306.9	-	-	247.9	245.4	0.0	0.0	-	-	59.0	61.5	0.0	59.0	-	-	2.5
M-32	313.2	313.2	264.6	259.6	256.0	-	0.0	0.0	48.6	53.6	57.2	-	0.0	48.6	5.0	3.6	-
M-33	303.8	303.8	259.7	-	-	-	0.0	0.0	44.1	-	-	-	0.0	44.1	-	-	-
M-34	280.9	280.9	252.1	237.0	232.9	220.9	0.0	0.0	28.8	43.9	48.0	60.0	0.0	28.8	15.1	4.1	12.0

NAPS COL 2.0-29-A

Table 2.5.4-205 Type and Number of Laboratory Tests Performed

Material	Test	Number
Soil	Natural moisture content	122
	Specific gravity	6
	Sieve and hydrometer analysis	55
	Grain size analysis with no. 200 wash	72
	Atterberg limits	23
	Chemical analysis (pH, chloride, sulfate)	19
	Triaxial consolidated-undrained compression	6
	Resonant column torsional shear	5
	California bearing ratio	5
	Moisture density (modified Proctor)	9
Rock	Unit weight	92
	Unconfined compression	65
	Unconfined compression with stress-strain measurements	27

NAPS COL 2.0-29-A

Table 2.5.4-206a Results of Laboratory Tests on Soil Samples*

Boring Number	Sample Number	Depth (ft)	Sample Type	Gravel (%) [1]	Sand (%) [1]	Fines (%) [2]	Silt (%) [1]	0.005 mm Clay (%) [1]	USCS Symbol	Natural Moisture (%)	LL	PI	G_s	pH [3]	Chloride (mg/kg) [3], [6], [7]	Sulfate (mg/kg) [3], [6], [7]
B-901	B-901-2	3.5-5.0	SPT	0.0	53.6	46.4	10.8	35.6	[8]	21.5	[8]	[8]	[8]	[8]	[8]	[8]
B-901	B-901-4	11.5-13.0	SPT	0.0	76.6	23.4	16.0	7.4		10.2				5.8	ND [5]	ND [5]
B-901	B-901-6	22.2-23.7	SPT	0.0	76.8	23.2				16.4						
B-901	B-901-9	37.2-38.7	SPT	0.7	71.9	22.5	15.2	7.3		16.4						
B-901	UD-2	9.5-11.5 [4]	UD	0.0	78.0	22.0	12.6	9.4		15.0						
B-902	B-902-2	3.5-5.0	SPT	0.0	86.1	13.9				5.6						
B-902	B-902-4	8.5-10.0	SPT	1.3	71.0	29.0	13.4	15.6	SM	23.9	33	7				
B-902	B-902-6	13.5-15.0	SPT	0.0	80.0	20.0				14.0						
B-907	B-907-2	3.5-5.0	SPT	0.0	67.0	33.0	17.7	15.3	SM	14.0	33	8				
B-907	B-907-3	5.5-7.0	SPT	0.0	74.9	25.1				16.4				4.8	51.1 J	ND [5]
B-907	B-907-5	11.0-12.5	SPT	0.0	76.0	24.0				20.2						
B-907	B-907-7	17.5-19.0	SPT	0.0	80.9	19.1	11.7	7.4		12.3						
B-907	B-907-9	27.5-29.0	SPT	0.0	73.9	26.1										
B-907	B-907-10	32.5-34.0	SPT	0.0	66.6	23.4										
B-908	B-908-3	6.0-7.5	SPT	2.0	72.6	25.4	11.6	13.8		12.3			2.62			
B-908	B-908-6	13.5-15.0	SPT	0.0	76.6	23.4							2.69			
B-908	B-908-8	23.7-25.2	SPT	0.0	68.1	31.9										
B-908	B-908-13	47.1-48.6	SPT	0.0	76.0	24.0	18.9	5.1		14.5						

* From Appendices 2.5.4AA, 2.5.4BB, and 2.5.4CC

NAPS COL 2.0-29-A

Table 2.5.4-206a Results of Laboratory Tests on Soil Samples*

Boring Number	Sample Number	Depth (ft)	Sample Type	Gravel (%) [1]	Sand (%) [1]	Fines (%) [2]	Silt (%) [1]	0.005 mm Clay (%) [1]	USCS Symbol	Natural Moisture (%)	LL	PI	G_s	pH [3]	Chloride (mg/kg) [3], [6], [7]	Sulfate (mg/kg) [3], [6], [7]
B-909	B-909-3	6.0-7.5	SPT	0.0	66.9	33.1	19.3	13.8	SM	25.9	57	12				
B-909	B-909-5	11.0-12.5	SPT	0.0	77.6	22.4				31.4				5.4	137 J	6.7
B-909	B-909-7	18.5-20.0	SPT	0.0	63.7	36.3	29.0	7.3	SM	25.1	30	4				
B-909	B-909-8	23.5-25.0	SPT	1.7	56.1	42.2				35.4						
B-909	B-909-12	41.9-43.4	SPT	0.0	75.3	24.7				17.6						
B-910	B-910-2	3.5-5.0	SPT	4.0	31.9	64.1	12.1	52.0		27.7						
B-910	B-910-5	11.0-12.5	SPT							30.5	45	13		5.8	3.6 J	5.1 B
B-910	B-910-7	18.5-20.0	SPT	0.0	46.4	53.6	43.1	10.5		33.1						
B-910	B-910-9	25.9-27.4	SPT	2.3	76.3	21.4				14.6				6.7	5.2 J	4.2 B
B-911	B-911-2	3.5-5.0	SPT	0.3	59.1	40.6				12.8						
B-911	B-911-4	8.0-9.5	SPT	0.0	70.6	29.4	13.6	15.8		19.6						
B-911	B-911-5	11.0-12.5	SPT	0.0	78.3	21.7								5.6	3.4 J	ND [5]
B-911	B-911-7	18.5-20.0	SPT	0.1	80.0	19.9				11.1						
B-912	B-912-1	9.1-10.6	SPT	0.0	73.7	26.3	20.8	5.5		24.0						
B-912	B-912-3	14.1-15.6	SPT	0.0	72.6	27.4				15.2						
B-912	B-912-4	19.1-19.9	SPT	14.5	84.9	0.6				15.7						
B-913	B-913-8	43.5-48.5	SPT	0.0	72.3	27.7										
B-914	B-914-2	3.5-5.0	SPT	0.1	52.9	47.0	21.0	26.0	SC	16.6	27	10				

* From Appendices 2.5.4AA, 2.5.4BB, and 2.5.4CC

NAPS COL 2.0-29-A

Table 2.5.4-206a Results of Laboratory Tests on Soil Samples*

Boring Number	Sample Number	Depth (ft)	Sample Type	Gravel (%) [1]	Sand (%) [1]	Fines (%) [2]	Silt (%) [1]	0.005 mm Clay (%) [1]	USCS Symbol	Natural Moisture (%)	LL	PI	G_s	pH [3]	Chloride (mg/kg) [3], [6], [7]	Sulfate (mg/kg) [3], [6], [7]
B-914	B-914-3	6.0-7.5	SPT	4.0	63.0	33.0										
B-914	B-914-5	11.0-13.5	SPT	2.1	78.0	19.9										
B-914	B-914-7	19.0-20.5	SPT	27.8	61.0	11.2	8.6	2.6		20.8						
B-914	B-914-9	35.6-37.1	SPT	5.7	70.1	24.2								6.8	8.4 J	ND [5]
B-914	B-914-10	40.6-42.1	SPT	0.1	74.4	25.5	19.5	6.0		20.5						
B-917	B-917-13	48.5-53.5	SPT	0.0	81.9	18.1	15.0	3.1								
B-918	B-918-2	1.8-3.2	SPT	1.2	85.7	13.1	7.3	5.8		15.8			2.68			
B-918	B-918-3	5.1-6.6	SPT	0.0	85.0	15.0				13.3				6.9	8.0 J	9.4
B-918	B-918-4	9.3-10.8	SPT	0.0	80.6	19.4	13.4	6.0		13.7						
B-918	B-918-6	13.2-14.7	SPT	0.0	77.7	22.3				13.9						
B-918	B-918-8	22.4-23.9	SPT	1.4	79.4	19.2				17.8						
B-919	B-919-1	1.5-3.0	SPT							18.6	32	11				
B-919	B-919-3	5.9-7.4	SPT	2.5	80.9	16.6				11.1						
B-919	B-919-5	11.0-12.5	SPT	0.6	80.4	19.0				11.2						
B-919	B-919-7	18.9-19.4	SPT	3.7	75.5	20.8	10.8	10.0		13.8						
B-919	B-919-13	51.3-52.8	SPT	0.0	65.9	34.1	26.0	8.1		17.9						
B-920	B-920-1	2.0-3.5	SPT							25.2						
B-920	B-920-2	3.8-5.3	SPT											5.9	1.5 B J	7.5

* From Appendices 2.5.4AA, 2.5.4BB, and 2.5.4CC

NAPS COL 2.0-29-A

Table 2.5.4-206a Results of Laboratory Tests on Soil Samples*

Boring Number	Sample Number	Depth (ft)	Sample Type	Gravel (%) (1)	Sand (%) (1)	Fines (%) (2)	Silt (%) (1)	0.005 mm Clay (%) (1)	USCS Symbol	Natural Moisture (%)	LL	PI	G_s	pH (3)	Chloride (mg/kg) (3), (6), (7)	Sulfate (mg/kg) (3), (6), (7)
B-920	B-920-3	6.0-7.5	SPT	0.3	58.9	40.8				24.1						
B-920	B-920-6	13.8-15.3	SPT							15.7				6.5	63.0 J	7.5
B-920	B-920-7	18.8-20.3	SPT	0.0	72.3	27.7	21.3	6.4		15.4						
B-920	B-920-9	27.3-28.8	SPT	0.0	79.9	20.1				19.5						
B-920	B-920-12	43.5-44.7	SPT							12.9				6.9	1.4 B J	2.3 B
B-921	B-921-1	1.5-3.0	SPT	11.5	52.1	36.4				12.0						
B-921	B-921-3	6.0-7.5	SPT	0.0	41.3	58.7	29.2	29.5	CL	24.8	34	14				
B-921	B-921-4	8.5-10.0	SPT	0.0	53.5	46.5	37.3	9.2		28.0				7.0	4.4 J	10.8
B-921	B-921-6	13.5-15.0	SPT	0.0	74.2	25.8	16.1	9.7		26.0						
B-921	B-921-8	23.8-25.3	SPT							32.1	38	NP				
B-921	B-921-10	33.8-35.3	SPT	0.0	75.5	24.5				20.4						
B-921	B-921-11	38.8-40.3	SPT	0.0	81.3	18.7				15.8						
B-921	B-921-16	63.8-65.3	SPT	0.0	75.1	24.9	18.2	6.7		8.5						
B-923	B-923-2	3.3-4.8	SPT	10.9	55.5	33.6	16.7	16.9	SC	22.5	33	10				
B-924	B-924-2	3.5-5.0	SPT	23.2	65.8	11.0	7.9	3.1		2.1						
B-924	B-924-3	6.0-7.5	SPT	11.1	74.5	14.4				4.8						
B-927	B-927-1	1.5-3.0	SPT	0.0	61.4	38.6	12.6	26.0	SC	14.1	28	10				
B-927	B-927-2	3.5-5.0	SPT	0.0	75.8	24.2				11.7						

* From Appendices 2.5.4AA, 2.5.4BB, and 2.5.4CC

NAPS COL 2.0-29-A

Table 2.5.4-206a Results of Laboratory Tests on Soil Samples*

Boring Number	Sample Number	Depth (ft)	Sample Type	Gravel (%) [1]	Sand (%) [1]	Fines (%) [2]	Silt (%) [1]	0.005 mm Clay (%) [1]	USCS Symbol	Natural Moisture (%)	LL	PI	G_s	pH [3]	Chloride (mg/kg) [3], [6], [7]	Sulfate (mg/kg) [3], [6], [7]
B-927	B-927-3	6.0-7.5	SPT	0.0	73.2	26.8	17.1	9.7		12.2						
B-927	B-927-4	8.5-10.0	SPT	0.0	83.3	16.7				6.8				5.8	2.8 J	4.3 B
B-927	B-927-6	13.5-15.0	SPT	0.0	81.2	18.8				11.2						
B-927	B-927-7	18.5-20.0	SPT	0.0	76.2	23.8				11.4						
B-927	B-927-8	23.5-25.0	SPT	0.0	79.7	20.3				15.7				7.4	5.6 J	3.4 B
B-928	B-928-2	3.5-5.0	SPT	0.0	78.4	21.6				17.9						
B-928	B-928-4	8.3-9.8	SPT	0.0	73.4	26.6				18.5				6.8	120.0 J	4.9 B
B-928	B-928-6	14.0-15.5	SPT	0.0	77.0	23.0	17.8	5.2		24.5						
B-928	B-928-8	22.1-23.6	SPT	0.0	78.7	21.3				17.0						
B-928	B-928-9	27.1-28.6	SPT	0.0	74.7	25.3	19.2	6.1		16.4						
B-928 A	UD-3	20-22 [4]	UD	0.0	82.0	18.0	13.2	4.8								
B-929	B-929-1	1.5-3.0	SPT	12.2	43.7	44.1	16.6	27.5	SC	14.5	36	17				
B-929	B-929-2	3.5-5.0	SPT								54	16				
B-929	B-929-4	8.7-10.2	SPT	0.0	65.5	34.5				18.9				5.9	2.8 J	2.7 B
B-929	B-929-5	13.5-15.0	SPT	0.0	73.8	26.2				19.6						
B-929	B-929-7	23.0-24.5	SPT	0.0	76.9	23.1	17.0	6.1		18.8						
B-929	B-929-9	33.0-34.5	SPT	0.0	82.7	17.3				16.9						
B-929	B-929-11	43.0-44.5	SPT	0.7	81.4	17.9				17.2						

* From Appendices 2.5.4AA, 2.5.4BB, and 2.5.4CC

NAPS COL 2.0-29-A

Table 2.5.4-206a Results of Laboratory Tests on Soil Samples*

Boring Number	Sample Number	Depth (ft)	Sample Type	Gravel (%) (1)	Sand (%) (1)	Fines (%) (2)	Silt (%) (1)	0.005 mm Clay (%) (1)	USCS Symbol	Natural Moisture (%)	LL	PI	G_s	pH (3)	Chloride (mg/kg) (3), (6), (7)	Sulfate (mg/kg) (3), (6), (7)
B-929	B-929-13	53.0-54.5	SPT	0.0	80.0	20.0				13.8						
B-929A	UD-1	15.0-16.8 (4)	UD	0.0	78.6	21.4	15.1	6.3		13.1						
B 929A	UD-6	40-41.8 (4)	UD	0.0	83.3	16.7	11.7	5.0		16.9						
B-931	B-931-10	47.3-48.8	SPT	0.0	78.5	21.5	15.9	5.6								
B-932	B-932-5	19.0-20.5	SPT	0.0	77.7	22.3	15.7	6.6		21.5						
B-933	B-933-3	6.0-7.5	SPT	0.0	62.3	37.7	22.6	15.1	SM	24.2	28	3				
B-933	B-933-5	11.2-12.7	SPT	0.0	58.8	41.2				25.9				5.4	210 J	3.0 B
B-933	B-933-7	19.5-21.0	SPT	0.0	76.6	23.4				26.7						
B-933	B-933-8	24.5-25.0	SPT	0.0	80.5	19.5				18.7						
B-945	B-945-1	1.5-3.0	SPT	0.0	82.0	18.0				14.5						
B-945	B-945-3	4.7-6.2	SPT	0.0	75.5	24.5	16.2	8.3		15.9						
B-945	B-945-5	11.3-12.8	SPT	0.0	84.2	15.8				21.6				6.4	6.9 J	3.1 B
B-945	B-945-7	19.4-20.9	SPT	0.0	84.8	15.2				27.6			2.58			
B-945	B-945-9	27.8-29.4	SPT	0.0	82.9	17.1	10.2	6.9		24.1						
B-945	B-945-11	39.4-40.9	SPT	0.0	90.1	9.9				20.4						
B-945	B-945-13	49.4-50.9	SPT	0.0	90.3	9.7				15.6						
B-947	B-947-1	1.5-3.0	SPT							16.7	55	25	2.60			
B-947	B-947-3	4.5-6.0	SPT	0.0	38.3	61.7	23.5	38.2	MH	36.0	56	19				

* From Appendices 2.5.4AA, 2.5.4BB, and 2.5.4CC

NAPS COL 2.0-29-A

Table 2.5.4-206a Results of Laboratory Tests on Soil Samples*

Boring Number	Sample Number	Depth (ft)	Sample Type	Gravel (%) [1]	Sand (%) [1]	Fines (%) [2]	Silt (%) [1]	0.005 mm Clay (%) [1]	USCS Symbol	Natural Moisture (%)	LL	PI	G_s	pH [3]	Chloride (mg/kg) [3], [6], [7]	Sulfate (mg/kg) [3], [6], [7]
B-947	B-947-4	8.5-10.0	SPT	0.0	60.0	40.0			SM	20.7	38	9				
B-947	B-947-5	9.5-11.0	SPT	1.6	55.9	42.5	21.1	21.4		28.2			2.78			
B-947	B-947-6	13.5-15.0	SPT	0.0	30.5	69.5				22.5						
B-947	B-947-7	17.2-18.7	SPT	0.0	75.8	24.2				21.1				6.4	21.4 J	6.4
B-947	B-947-8	22.2-23.7	SPT	0.6	79.4	20.0	10.7	9.3		24.3						
B-947	B-947-9	28.7-30.2	SPT	0.0	66.6	33.4				28.8	33	NP				
B-947	B-947-10	33.7-35.2	SPT	0.0	81.3	18.7				20.2						
B-947	B-947-11	38.7-40.2	SPT	0.0	85.8	14.2				16.9						
B-947	B-947-12	42.2-43.7	SPT	0.0	79.7	20.3	13.4	6.9		20.5						
B-948	B-948-1	1.5-3.0	SPT	0.0	54.7	45.3				83.7						
B-948	B-948-3	6.0-7.5	SPT	0.0	51.1	48.9				16.2				5.7	3.8 J	ND [5]
B-948	B-948-5	9.5-11.0	SPT	0.0	31.0	69.0	61.9	7.1		13.7						
B-948	B-948-7	18.5-20.0	SPT	0.0	35.9	64.1				15.2						
B-948	B-948-8	23.5-24.4	SPT	0.0	77.7	22.3				13.6						
B-951	B-951-8	23.0-24.5	SPT	0.2	82.9	16.9	10.5	6.4		13.9						
M-10 (DH)	SS-2	11.7-13.2		0	57.5	42.5	30.2	12.3	SM	48.5	59	9				
M-10 (DH)	SS-4	19.2-20.7		0	61.9	38.1	29.4	8.7	SM	35.9	54	6				

* From Appendices 2.5.4AA, 2.5.4BB, and 2.5.4CC

NAPS COL 2.0-29-A

Table 2.5.4-206a Results of Laboratory Tests on Soil Samples*

Boring Number	Sample Number	Depth (ft)	Sample Type	Gravel (%) (1)	Sand (%) (1)	Fines (%) (2)	Silt (%) (1)	0.005 mm Clay (%) (1)	USCS Symbol	Natural Moisture (%)	LL	PI	G_s	pH (3)	Chloride (mg/kg) (3), (6), (7)	Sulfate (mg/kg) (3), (6), (7)
M-10 (DH)	SS-5	24.2-25.7		0	61.3	38.7	28.4	10.3	SM	53.7	59	12				
M-10 (DH)	SS-6	29.2-30.7		0	56.6	43.4	31.9	11.5	SM	66.7	51	7				
M-10 (DH)	SS-8	39.1-40.6		0	53.5	46.5	42.4	4.1	SM	30.6	42	6				
M-10 (DH)	SS-10	49.1-50.6		0	79.9	20.1			SM(9)	16.4						
M-10 (DH)	SS-12	59.1-60.6		0.7	77.2	22.1			SM(9)	15.1						
M-10 (DH)	SS-15	74.1-75.6		0	72.6	27.4			SM(9)	29.9						
M-10 (DH)	SS-17	84.1-85.6		0	79	21			SM(9)	15.1						
M-30 (DH)	SS-1	8.7-10.2		0.6	72.3	27.1			SM(9)	17						
M-30 (DH)	SS-3	13.7-15.2		0	64	36			SM(9)	19.8						
M-30 (DH)	SS-5	23.7-25.2		0	82	18			SM(9)	18.5						
M-30 (DH)	SS-7	33.7-35.2		0	77.1	22.9			SM(9)	14.8						

* From Appendices 2.5.4AA, 2.5.4BB, and 2.5.4CC

NAPS COL 2.0-29-A

Table 2.5.4-206a Results of Laboratory Tests on Soil Samples*

(1) Due to computer roundoff, particle size fractions may total 100 ±1. Fines include silt plus clay.
(2) Fines include silt plus clay.
(3) Tests performed by STL - St. Louis, MO
(4) Depth interval shown reflects total pushed depth of UD tube.
(5) ND indicates analyte not detected at or above the Method Detection Limit
(6) B = Estimated Result. Analyte detected above the Method Detection Limit but not above the Reporting Limit.
(7) J = Method blank contamination. The associated method blank contains the target analyte at a reportable level
(8) Shaded cells indicate that information not obtained.
(9) Classification is based on quantitative and qualitative (visual inspection) information. LL= Liquid Limit, PI = Plasticity Index, Gs = Specific Gravity

* From Appendices 2.5.4AA, 2.5.4BB, and 2.5.4CC

NAPS COL 2.0-29-A

Table 2.5.4-206b Results of Laboratory Tests on Soil Samples; Consolidated-Undrained Triaxial Tests*

Source of Sample	Sample No.	Sample Depth (1) (ft)	Sample Type	Test Type	C' (psf)	Φ' (degree)	C (psf)	Φ' (degree)	Comment
B-901	UD-2	9.5-11.5	UD Tube	CU	0.0	33.6	0.0	37.5	
B-928 A	UD-3	20-22	UD Tube	CU	423.4	31.4	103.7	41.2	
B-929 A	UD-1	15-16.75	UD Tube	CU	5.4	32.4	178.6	35.8	Only 2 points tested due to limited sample
B-929 A	UD-4	30-31.5	UD Tube	CU	0.0	33.0	0.0	33.0	Only 2 points tested due to limited sample
B-929 A	UD-6	40-41.5	UD Tube	CU	0.0	36.1	318.2	36.4	
B-933 A	UD-2	15-16.25	UD Tube	CU	55.0	32.6	479.5	30.5	Only 2 points tested due to limited sample

(1) Sample depth shown reflects the depth of start of push plus the length of the recovered sample

* From Appendices 2.5.4AA, 2.5.4BB, and 2.5.4CC

NAPS COL 2.0-29-A **Table 2.5.4-206c Results of Laboratory Tests on Soil Samples Moisture-Density and CBR Tests***

		Moisture/Density Results [A]					CBR Results [B]	
Source of Sample	Sample No.	Natural Moisture (%)	Maximum Dry Density (pcf)	Optimum Moisture (%)	Molded Density (pcf)	Molded Moisture (%)	Soaked CBR (0.10") (%)	Soaked CBR (0.20") (%)
Test Pit 1	TP-1-1	23.4	108.7	17.6	Not Tested			
Test Pit 1	TP-1-2	22.6	108.8	17.1	90.3	17.0	1.2	1.6
					94.4	17.0	6.3	5.5
					105.3	17.2	14.7	15.6
Test Pit 2	TP-2	22.6	100.4	22.3	83.0	22.8	1.1	1.1
					89.1	22.0	1.3	1.2
					101.0	22.0	6.2	6.5
Test Pit 3	TP 3-1	16.1	124.9	9.5	Not Tested			
Test Pit 3	TP 3-2	12.4	124.5	10.9	117.5	10.7	5.9	6.0
					122.9	10.6	3.2	5.0
					125.6	10.5	4.2	8.4
Test Pit 4	TP 4-1	30.2	108.6	17.1	Not Tested			
Test Pit 4 [C]	TP 4-2	15.2	125.5	10.8	119.4	11.0	4.9	7.3
					121.5	10.6	8.8	11.9
Test Pit 5	TP 5	9.4	126	9.2	Not Tested			
Test Pit 6	TP 6	18.2	116.1	13.2	110.3	12.3	6.9	8.0
					111.7	12.7	6.4	9.5
					115.1	12.3	12.1	13.8

A Proctor Test results, ASTM D 1557-02 Method A Modified

B California Bearing Ratio Test results, ASTM D 1883-05 (Section 7.12)

C Insufficient Material for three tests

* From Appendices 2.5.4AA, 2.5.4BB, and 2.5.4CC

NAPS COL 2.0-29-A

Table 2.5.4-207 Results of Unconfined Compression Tests on Rock*

Boring No.	Run Number	Sample Top Depth (ft)	Sample Length (L) (Inches)	Sample Diameter (D) (inches)	L/D Ratio	Unit Weight (pcf)	Type of Break (1)	Unconfined Compressive Strength (psi)(2)	Young's Modulus (psi)	Poisson's Ratio
B-901	5	54.0	5.27	2.49	2.1	160	Shear	4,375	(ND) 3	(ND)
B-901	7	60.3	5.27	2.49	2.1	162	Columnar	15,425	3,970,000	* (4)
B-901	14	97.9	5.34	2.50	2.1	162	C&S	12,629	(ND)	(ND)
B-901	25	129.5	5.35	2.49	2.1	164	C&S	14,171	(ND)	(ND)
B-901	34	170.5	5.33	2.40	2.2	168	Shear	10,865	5,360,000	0.31
B-901	42	208.5	5.32	2.40	2.2	163	Shear	12,777	(ND)	(ND)
B-901	51	240.5	5.35	2.39	2.2	165	C&S	23,619	(ND)	(ND)
B-901	59	280.5	5.36	2.39	2.2	164	C&S	25,335	8,320,000	0.39
B-902	3	27.3	5.29	2.38	2.2	162	C&S	14,947	4,090,000	* (4)
B-902	9	47.4	5.35	2.40	2.2	163	Shear	21,007	(ND)	(ND)
B-902	14	72.3	5.34	2.40	2.2	164	C&S	25,100	(ND)	(ND)
B-902	18	92.8	5.32	2.40	2.2	164	Shear	6,030	1,840,000	0.42
B-902	28	141.9	5.31	2.40	2.2	170	Shear	6,982	(ND)	(ND)
B-902	38	184.6	5.36	2.40	2.2	163	C&S	27,303	(ND)	(ND)
B-907	3	51.9	5.29	2.45	2.2	152	Shear	957	(ND)	(ND)
B-907	12	90.0	5.23	2.46	2.1	155	Shear	751	(ND)	(ND)
B-907	24	116.8	5.27	2.47	2.1	173	Shear	4,599	(ND)	(ND)
B-907	27	131.8	5.32	2.48	2.1	173	C&S	8,519	(ND)	(ND)

* From Appendices 2.5.4AA, 2.5.4BB, and 2.5.4CC

NAPS COL 2.0-29-A

Table 2.5.4-207 Results of Unconfined Compression Tests on Rock*

Boring No.	Run Number	Sample Top Depth (ft)	Sample Length (L) (Inches)	Sample Diameter (D) (inches)	L/D Ratio	Unit Weight (pcf)	Type of Break (1)	Unconfined Compressive Strength (psi)(2)	Young's Modulus (psi)	Poisson's Ratio
B-907	33	160.8	5.32	2.50	2.1	163	Columnar	19,333	7,700,000	0.30
B-907	40	200.0	5.35	2.50	2.1	165	C&S	20,166	(ND)	(ND)
B-908	2	67.5	5.32	2.38	2.2	163	Shear	5,476	(ND) 3	(ND)
B-908	4	79.4	5.25	2.39	2.2	164	C&S	14,695	3,400,000	0.41
B-908	7	96.0	5.31	2.39	2.2	163	Shear	17,164	(ND)	(ND)
B-908	11	112.7	5.32	2.38	2.2	178	Shear	15,284	(ND)	(ND)
B-908	17	135.7	5.28	2.38	2.2	187	Shear	5,670	3,180,000	0.21
B-908	20	146.8	5.31	2.38	2.2	173	Shear	7,687	(ND)	(ND)
B-909	11	82.4	5.32	2.39	2.2	176	C&S	9,464	3,520,000	* (4)
B-909	14	96.5	5.28	2.39	2.2	190	Shear	5,897	(ND)	(ND)
B-909	17	107.4	5.35	2.39	2.2	179	Shear	3,938	(ND)	(ND)
B-909	21	127.4	5.35	2.39	2.2	174	Shear	8,167	(ND)	(ND)
B-909	26	152.3	5.27	2.38	2.2	184	C&S	6,467	4,600,000	0.39
B-909	33	187.3	5.32	2.39	2.2	175	Shear	9,305	(ND)	(ND)
B-910	5	53.1	5.27	2.15	2.2	159	Shear	6,935	(ND)	(ND)
B-910	13	91.1	5.24	2.15	2.2	159	Shear	4,821	670,000	* (4)
B-910	20	120.9	5.27	2.40	2.2	163	Columnar	9,395	(ND)	(ND)
B-910	24	142.1	5.35	2.40	2.2	168	C&S	28,834	(ND)	(ND)

* From Appendices 2.5.4AA, 2.5.4BB, and 2.5.4CC

NAPS COL 2.0-29-A

Table 2.5.4-207 Results of Unconfined Compression Tests on Rock*

Boring No.	Run Number	Sample Top Depth (ft)	Sample Length (L) (Inches)	Sample Diameter (D) (inches)	L/D Ratio	Unit Weight (pcf)	Type of Break (1)	Unconfined Compressive Strength (psi)(2)	Young's Modulus (psi)	Poisson's Ratio
B-911	3	34.3	5.27	2.37	2.2	161	Shear	5,558	1,230,000	* (4)
B-911	5	44.3	5.28	2.38	2.2	162	Cone	10,209	(ND)	(ND)
B-911	10	66.5	5.35	2.39	2.2	164	Cone	24,646	(ND)	(ND)
B-911	13	82.1	5.36	2.40	2.2	164	C&S	20,431	5,730,000	0.40
B-911	16	97.6	5.36	2.40	2.2	163	Shear	6,561	(ND) 3	(ND)
B-912	3	37.1	5.32	2.39	2.2	170	C&S	3,524	2,570,000	(ND)
B-912	5	48.9	5.26	2.40	2.2	163	C&S	12,992	(ND)	(ND)
B-912	8	62.2	5.26	2.40	2.2	164	C&S	32,680	(ND)	(ND)
B-912	12	82.4	5.25	2.40	2.2	163	Shear	27,356	(ND)	(ND)
B-912	17	111.4	5.32	2.40	2.2	163	Shear	16,702	8,220,000	0.31
B-912	24	143.9	5.26	2.40	2.2	161	Columnar	15,996	(ND)	(ND)
B-914	8	63.8	5.34	2.40	2.2	169	Cone	17,866	(ND)	(ND)
B-914	10	75.3	5.32	2.40	2.2	164	C&S	36,600	(ND)	(ND)
B-914	15	95.8	5.37	2.40	2.2	164	C&S	29,776	8,980,000	0.31
B-914	20	120.6	5.32	2.39	2.2	169	C&S	17,942	(ND)	(ND)
B-914	26	151.4	5.31	2.40	2.2	166	C&S	16,517	8,930,000	0.32
B-914	34	192.7	5.32	2.40	2.2	163	Cone	30,162	(ND)	(ND)
B-918	2	31.7	5.29	2.39	2.2	164	Shear	19,038	(ND)	(ND)

* From Appendices 2.5.4AA, 2.5.4BB, and 2.5.4CC

NAPS COL 2.0-29-A

Table 2.5.4-207 Results of Unconfined Compression Tests on Rock*

Boring No.	Run Number	Sample Top Depth (ft)	Sample Length (L) (Inches)	Sample Diameter (D) (inches)	L/D Ratio	Unit Weight (pcf)	Type of Break (1)	Unconfined Compressive Strength (psi)(2)	Young's Modulus (psi)	Poisson's Ratio
B-918	4	37.1	5.32	2.40	2.2	164	C&S	29,636	9,530,000	0.35
B-918	7	51.6	5.29	2.40	2.2	165	Cone	15,409	(ND)	(ND)
B-918	9	60.7	5.32	2.40	2.2	164	Columnar	21,064	(ND)	(ND)
B-918	15	88.1	5.28	2.40	2.2	165	Shear	21,944	7,850,000	0.24
B-918	22	122.0	5.25	2.40	2.2	166	C&S	33,610	(ND)	(ND)
B-920	7	90.2	5.28	2.39	2.2	160	Shear	1,021	(ND)	(ND)
B-920	11	107.7	5.32	2.39	2.2	163	Cone	29,621	8,500,000	0.34
B-920	13	119.1	5.33	2.39	2.2	181	Shear	9,456	(ND)	(ND)
B-920	18	141.1	5.35	2.40	2.2	166	Cone	18,040	5,970,000	* (4)
B-923	6	20.0	5.35	2.39	2.2	164	C&S	28,911	8,510,000	0.28
B-923	9	30.8	5.35	2.39	2.2	162	C&S	26,779	(ND)	(ND)
B-923	12	45.7	5.33	2.39	2.2	163	Shear	13,477	(ND)	(ND)
B-923	16	65.7	5.35	2.39	2.2	164	Cone	21,069	7,150,000	0.29
B-924	1	21.7	5.33	2.39	2.2	162	Shear	10,588	(ND) 3	(ND)
B-924	3	30.2	5.35	2.39	2.2	163	C&S	15,110	(ND)	(ND)
B-924	6	44.0	5.33	2.39	2.2	174	Shear	6,384	2,620,000	* (4)
B-924	12	75.1	5.33	2.40	2.2	179	C&S	5,681	(ND)	(ND)
B-927	2	43.0	5.35	2.39	2.2	163	C&S	19,288	(ND)	(ND)

* From Appendices 2.5.4AA, 2.5.4BB, and 2.5.4CC

NAPS COL 2.0-29-A

Table 2.5.4-207 Results of Unconfined Compression Tests on Rock*

Boring No.	Run Number	Sample Top Depth (ft)	Sample Length (L) (Inches)	Sample Diameter (D) (inches)	L/D Ratio	Unit Weight (pcf)	Type of Break [1]	Unconfined Compressive Strength (psi)[2]	Young's Modulus (psi)	Poisson's Ratio
B-927	6	51.6	5.35	2.39	2.2	163	C&S	27,239	6,550,000	0.49
B-927	13	74.9	5.33	2.39	2.2	164	Cone	30,297	(ND)	(ND)
B-927	18	96.3	5.35	2.39	2.2	164	C&S	28,266	(ND)	(ND)
B-928	2	52.6	5.33	2.39	2.2	153	Shear	1,318	(ND)	(ND)
B-928	6	74.7	5.35	2.39	2.2	162	Cone	20,333	5,070,000	0.35
B-933	3	50.5	5.33	2.39	2.2	163	Cone	19,395	(ND)	(ND)
B-933	7	66.6	5.34	2.38	2.2	162	Columnar	15,764	8,600,000	* [4]
B-933	11	90.1	5.32	2.39	2.2	164	Cone	30,993	(ND)	(ND)
B-948	6	56.8	5.28	2.39	2.2	162	C&S	17,089	(ND)	(ND)
B-948	10	76.1	5.25	2.40	2.2	167	C&S	22,435	(ND)	(ND)
M-10 (DH)	R-7	117.45	5.15	2.41	2.1	160.1	S	7960	(ND)	(ND)
M-10 (DH)	R-10	133.75	5.09	2.41	2.1	161.9	S	19640[5]	(ND)	(ND)
M-10 (DH)	R-15	153.7	5.08	2.41	2.1	163.5	C	33830[5]	(ND)	(ND)
M-10 (DH)	R-20	177.6	5.14	2.39	2.2	163.3	S	20880[5]	(ND)	(ND)
M-10 (DH)[6]	R-24	196.7	5.18	2.39	2.2	163.7	C	30780	(ND)	(ND)
M-30 (DH)[6]	R-4	57	5.18	2.4	2.2	162.8	C	28650	(ND)	(ND)
M-30 (DH)	R-18	95.4	5.06	2.39	2.1	162.7	C	23700	(ND)	(ND)

* From Appendices 2.5.4AA, 2.5.4BB, and 2.5.4CC

NAPS COL 2.0-29-A

Table 2.5.4-207 Results of Unconfined Compression Tests on Rock*

Boring No.	Run Number	Sample Top Depth (ft)	Sample Length (L) (Inches)	Sample Diameter (D) (inches)	L/D Ratio	Unit Weight (pcf)	Type of Break (1)	Unconfined Compressive Strength (psi)(2)	Young's Modulus (psi)	Poisson's Ratio
M-30 (DH)(6)	R-26	134.9	5.26	2.39	2.2	163.7	S	26200	(ND)	(ND)
M-30 (DH)	R-34	166.9	5.06	2.4	2.1	164.6	C/S	24820	(ND)	(ND)
M-30 (DH)	R-40	197.05	5.16	2.4	2.2	162.6	C	33040	(ND)	(ND)

(1) Type of Breaks: Columnar; Cone (C); Shear (S); Cone & Shear (C&S)
(2) Unconfined compressive strength corrected for L/D Ratio
Compressive strength testing was performed in general accordance with ASTM D7012-04.
(3) (ND) indicates that information was not determined
(4) Value of Poisson's ratio is greater than 0.5 which indicates inelastic behavior probably due to presence of fractures or discontinuities affecting lateral strain.
(5) Test duration exceeded 15 minute maximum time as indicated by ASTM D 7012-07e1.
(6) Core samples did not meet the dimensional tolerances for straightness or perpendicularity per ASTM D 4543-08.

* From Appendices 2.5.4AA, 2.5.4BB, and 2.5.4CC

NAPS COL 2.0-29-A

Table 2.5.4-208 Best Estimate Engineering Properties of Subsurface Materials

Stratum	Structural Fill	Concrete Fill	Zone IIA	Zone IIB	Zone III	Zone III-IV	Zone IV
Description	**Gravelly materials derived from crushing rock material**		**Saprolite – core stone less than 10% of volume of overall mass**	**Saprolite – core stone 10% to 50% of volume of overall mass**	**Weathered rock – core stone more than 50% of volume of overall mass**	**Moderately weathered to slightly weathered rock**	**Parent rock – slightly weathered to fresh rock**
USCS symbol	GW	-	SM, SC	SM	-	-	-
Total unit weight, g (pcf)	130	145	125	130	150	163	164
Fines Content (%)	6-12	-	25	20	-	-	-
Natural water content, w_N (%)	-	-	19	15	-	-	-
Atterberg limits		-					
Liquid limit, LL	-	-	-	-	-	-	-
Plastic limit, PL	-	-	-	-	-	-	-
Plasticity index, PI	-	-	-	-	-	-	-
Measured SPT N-value (blows/ft)	-	-	15	75	Ref	-	-
Adjusted SPT N_{60}-value (blows/ft)	50	-	20	100	Ref	-	-
Undrained properties							
Undrained shear strength, s_u (ksf)	-	-	-	-	-	-	-
Unconfined compressive strength, q_u(ksi)	-	2.5	-	-	1.0	9.0	17.0

NAPS COL 2.0-29-A

Table 2.5.4-208 Best Estimate Engineering Properties of Subsurface Materials

Stratum	Structural Fill	Concrete Fill	Zone IIA	Zone IIB	Zone III	Zone III-IV	Zone IV
Description	**Gravelly materials derived from crushing rock material**		**Saprolite – core stone less than 10% of volume of overall mass**	**Saprolite – core stone 10% to 50% of volume of overall mass**	**Weathered rock – core stone more than 50% of volume of overall mass**	**Moderately weathered to slightly weathered rock**	**Parent rock – slightly weathered to fresh rock**
Drained properties							
Effective cohesion, c' (ksf)	0	-	0.125	0	-	-	-
Effective friction angle, ' (degrees)	40	-	33	40	-	-	-
Shear wave velocity, V_s (ft/sec)	1,100	7,000	850	1,600	3,000	6,000	9,000
Compression wave velocity, V_p (ft/sec)	2,400	10,900	1,800	3,500	7,300	12,000	16,000
Poisson's ratio, u (high strain)	0.3	0.15	0.35	0.3	0.4	0.33	0.27
Poisson's ratio, u (low strain)	0.37	0.15	0.35	0.37	0.4	0.33	0.27
Elastic modulus (high strain), E_h	1,800 ksf	2,850 ksi	720 ksf	3,600 ksf	400 ksi	1,900 ksi	7,250 ksi
Elastic modulus (low strain), E_l	13,000 ksf	2,850 ksi	7,500 ksf	28,000 ksf	800 ksi	1,900 ksi	7,250 ksi
Shear modulus (high strain), G_h	700 ksf	1,240 ksi	270 ksf	1,400 ksf	150 ksi	700 ksi	2,900 ksi
Shear modulus (low strain), G_l	5,000 ksf	1,240 ksi	2,800 ksf	10,000 ksf	300 ksi	700 ksi	2,900 ksi
Consolidation characteristics							
Compression ratio, CR		-			-	-	-
Recompression ratio, RR		-			-	-	-

NAPS COL 2.0-29-A

Table 2.5.4-208 Best Estimate Engineering Properties of Subsurface Materials

Stratum	Structural Fill	Concrete Fill	Zone IIA	Zone IIB	Zone III	Zone III-IV	Zone IV
Description	**Gravelly materials derived from crushing rock material**		**Saprolite – core stone less than 10% of volume of overall mass**	**Saprolite – core stone 10% to 50% of volume of overall mass**	**Weathered rock – core stone more than 50% of volume of overall mass**	**Moderately weathered to slightly weathered rock**	**Parent rock – slightly weathered to fresh rock**
Coefficient of subgrade reaction, k_1 (kcf)	2,000	-	260	2,000	-	-	-
Coefficient of sliding	0.55	0.7	0.35	0.45	0.6	0.65	0.7
Static earth pressure coefficients							
Active, K_a	0.22	-	0.30	0.22	-	-	-
Passive, K_p	4.60	-	3.40	4.60	-	-	-
At-rest, K_0	0.36	-	0.50	0.36	-	-	-
Optimum moisture content, w_{opt} (%)	-	-	14	-	-	-	-
Maximum dry unit weight, g_{max} (pcf)	-	-	116	-	-	-	-
Rock Quality Designation, RQD (%)	-	-	-	-	20	65	95

NAPS ESP COL 2.5-6

Table 2.5.4-209 Size, Depth and Loading of Structures

Structure	Seismic Cate-gory[2]	Approximate Dimensions (ft)	Bottom of Foundation Elevation[1] (ft)	Embed-ment Depth (ft)	Design Load (ksf)	
					Static	Dynam-ic
Reactor/Fuel Building	I	161 x 230	223.9	65.6	14.6	23.0
Control Building	I	78 x 99	240.6	48.9	6.1	8.8
Fire Water Service Complex	I	66 x 171	281.8	7.7	3.45	25.1
Turbine Building	II	194 x 377	263.6	25.9	6	—
Radwaste Building	NS	108 x 213	237.5	52.0	6	—
Service Building	II	111 x 163	274.1	15.4	4	—
Ancillary Diesel Building	II	61 x 71	286.2	3.3	4	—

Note: (1) The bottom of foundation is derived from the finished ground level grade at Elevation 289.5 ft.
(2) See DCD Table 3.2-1.

NAPS ESP COL 2.5-6

Table 2.5.4-210 Allowable Bearing Capacities of Rock and Concrete

Rock Type	Unconfined Compressive Strength, q_u (ksi)	$q_a = 0.2\ q_u$ (ksf)	Recommended q_a (ksf)
Zone III	1	29	20
Zone III-IV	9	259	80
Zone IV	17	490	160
Concrete	2.5	40	199

NAPS ESP COL 2.5-6

Table 2.5.4-211 Bearing Demand and Capacity

Structure	Calculated Allowable Static (Dynamic) Bearing Capacity, q_a (ksf)					Selected q_a (ksf)	
	Structural Fill (1)	Concrete Fill	Zone III	Zone III-IV	Zone IV	Static	Dynamic
Reactor/Fuel Building	—	199 (199)	—	80 (259)	160 (490)	80	199
Control Building	—	199 (199)	—	80 (259)	160 (490)	80	199
Fire Water Service Complex	—	199 (199)	—	80 (259)	160 (490)	80	199
Turbine Building	242 (323)	—	20 (29)	80 (259)	160 (490)	20	29
Radwaste Building	214 (285)	—	20 (29)	80 (259)	160 (490)	20	29
Service Building	135 (180)	—	20 (29)	80 (259)	160 (490)	20	29
Ancillary Diesel Building	58 (78)	—	20 (29)	80 (259)	160 (490)	20	29

Note:

(1) This value also applies to structures on Zone IIB, where applicable.

NAPS ESP COL 2.5-6

Table 2.5.4-212 Estimated Settlements

Structure	Applied Load (ksf)	Calculated Settlement (in.)			
		Center	Edge	Average[(1)]	Corner
Reactor/Fuel Building	14.6	0.12	0.075	0.10	0.05
Control Building	6.1	0.022	0.014	0.018	0.010
Fire Water Service Complex	3.45	0.011	0.008	0.010	0.005
Turbine Building	6	2.23	1.14	1.69	0.58
Radwaste Building	6	0.75	0.38	0.57	0.27
Service Building	4	0.68	0.35	0.52	0.27
Ancillary Diesel Building	4	0.13	0.065	0.10	0.034

Note: (1) Average is average of center and edge settlements

NAPS COL 2.0-29-A **Figure 2.5.4-201 Contours of Top of Zone IV**

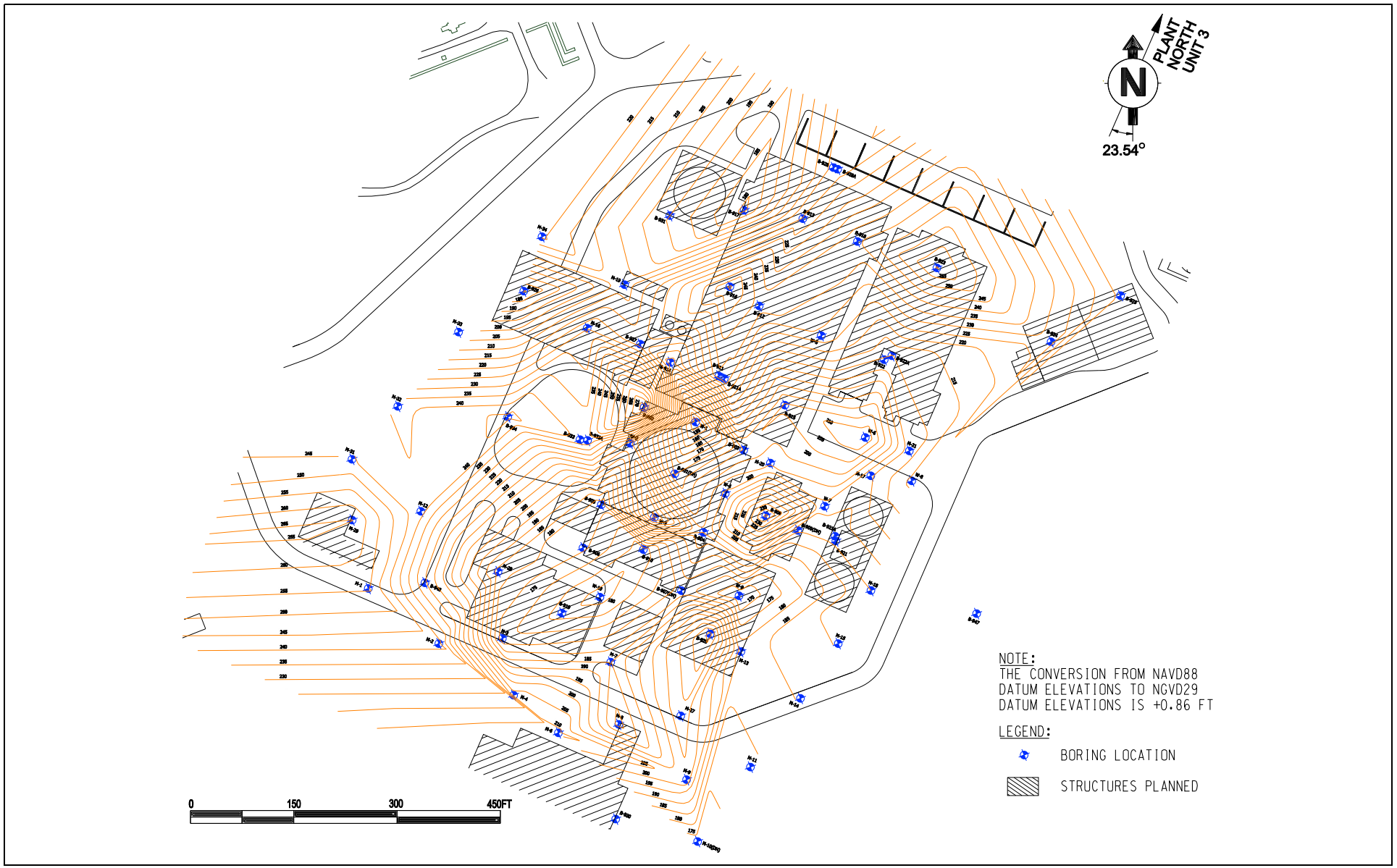

NAPS COL 2.0-29-A **Figure 2.5.4-202 Contours of Top of Zone III-IV**

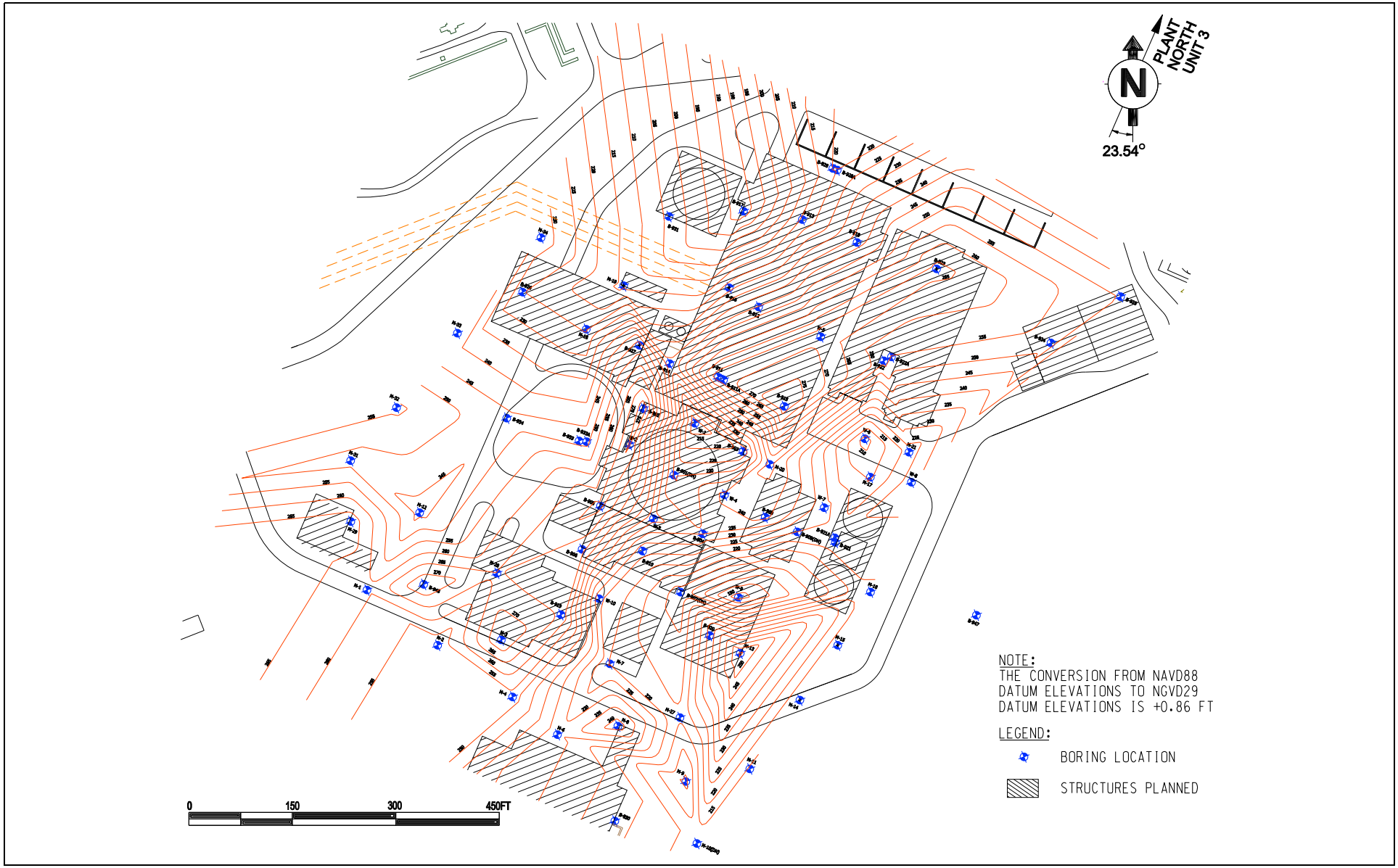

NAPS COL 2.0-29-A **Figure 2.5.4-203 Contours of Top of Zone III**

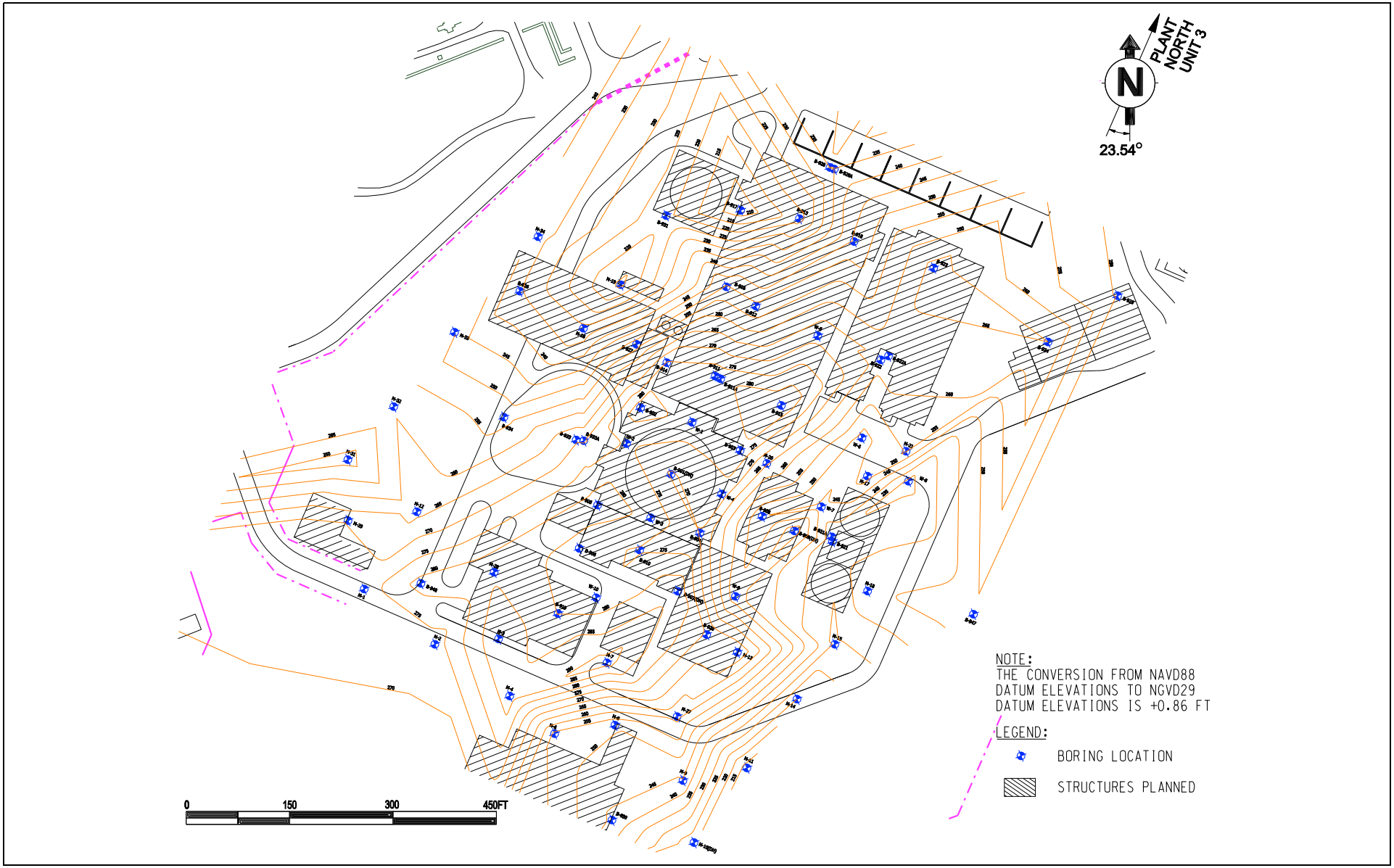

NAPS COL 2.0-29-A **Figure 2.5.4-204 Contours of Top of Zone IIB**

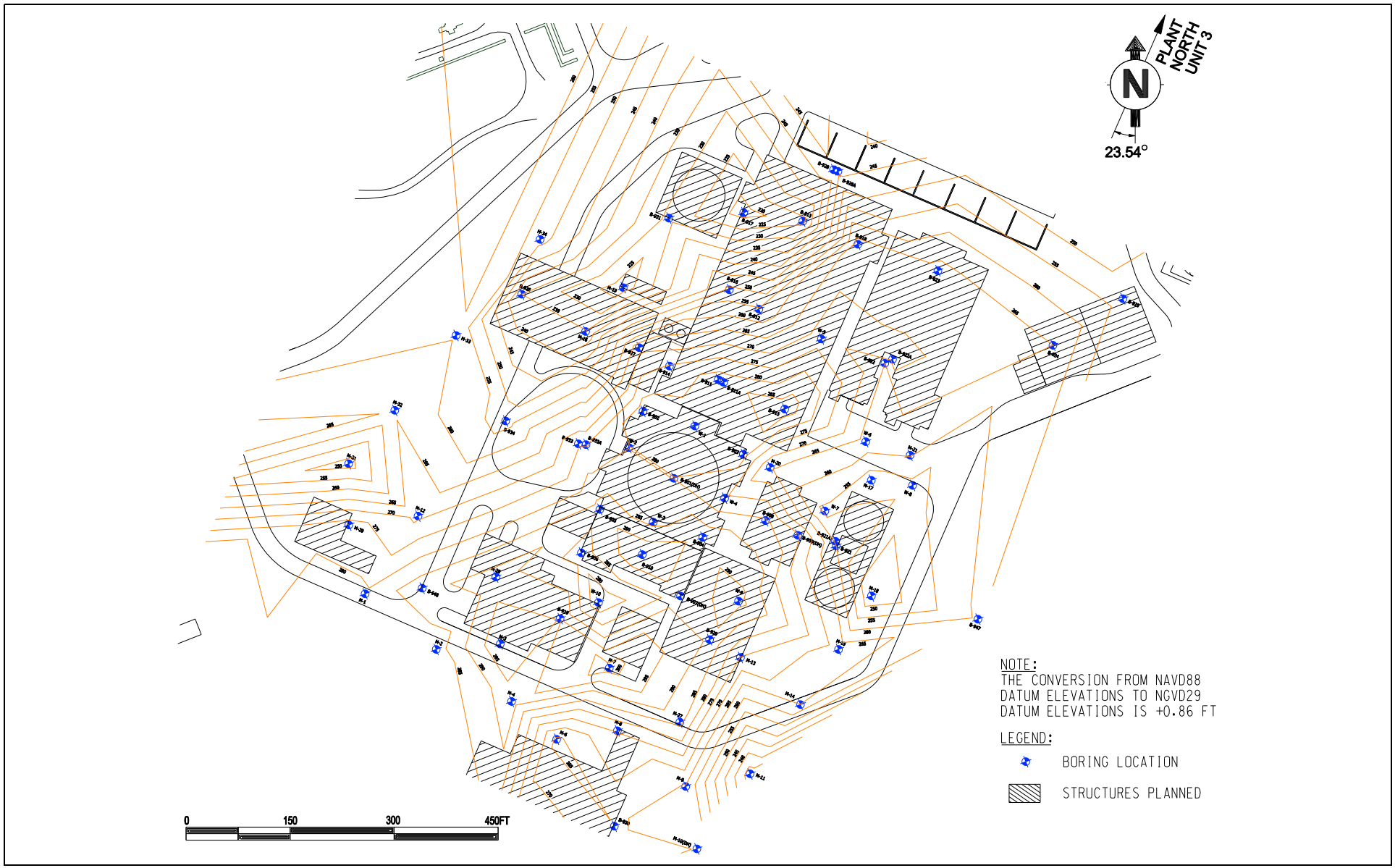

NAPS COL 2.0-29-A **Figure 2.5.4-205 Contours of Top of Zone IIA**

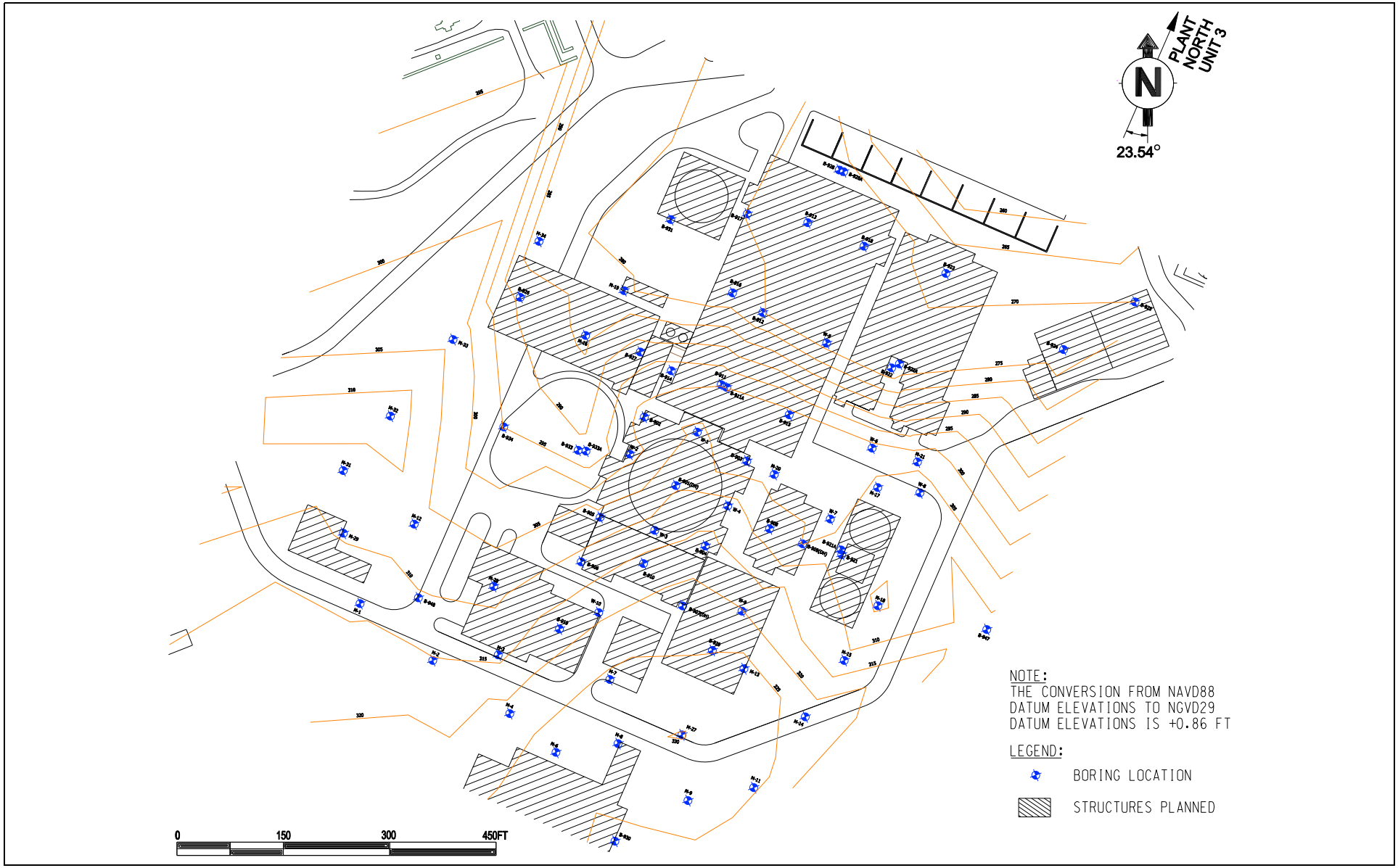

NAPS COL 2.0-29-A **Figure 2.5.4-206 Excavation Plan and Locations of Profiles**

NAPS COL 2.0-29-A **Figure 2.5.4-207 Subsurface Profile A-A**

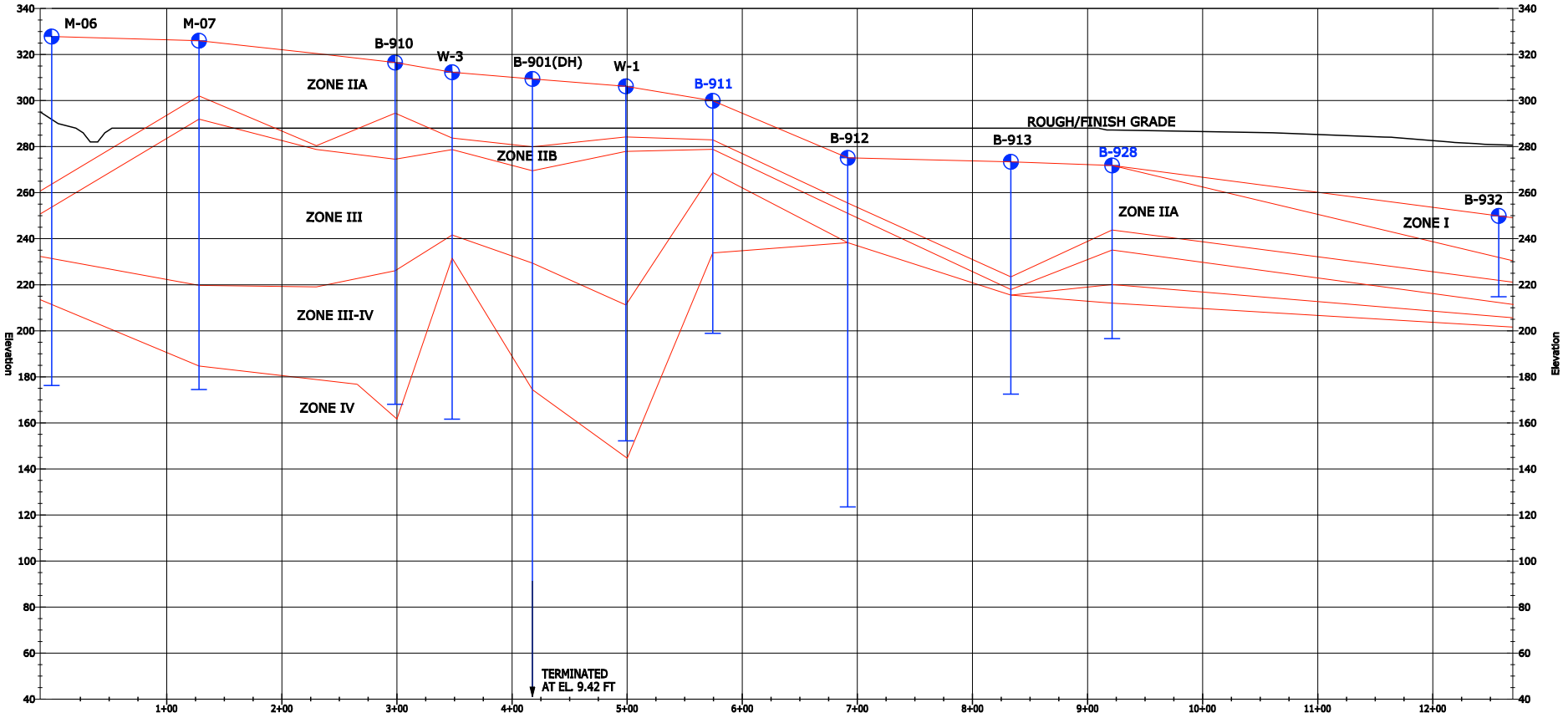

NOTE:
THE CONVERSION FROM NAVD88 DATUM ELEVATIONS TO NGVD29 DATUM ELEVATIONS IS +0.86 FT

SUBSURFACE PROFILE A-A

0 40 80 160 240FT

VERTICAL EXAGGERATION = 2:1

NAPS COL 2.0-29-A **Figure 2.5.4-208 Subsurface Profile B-B**

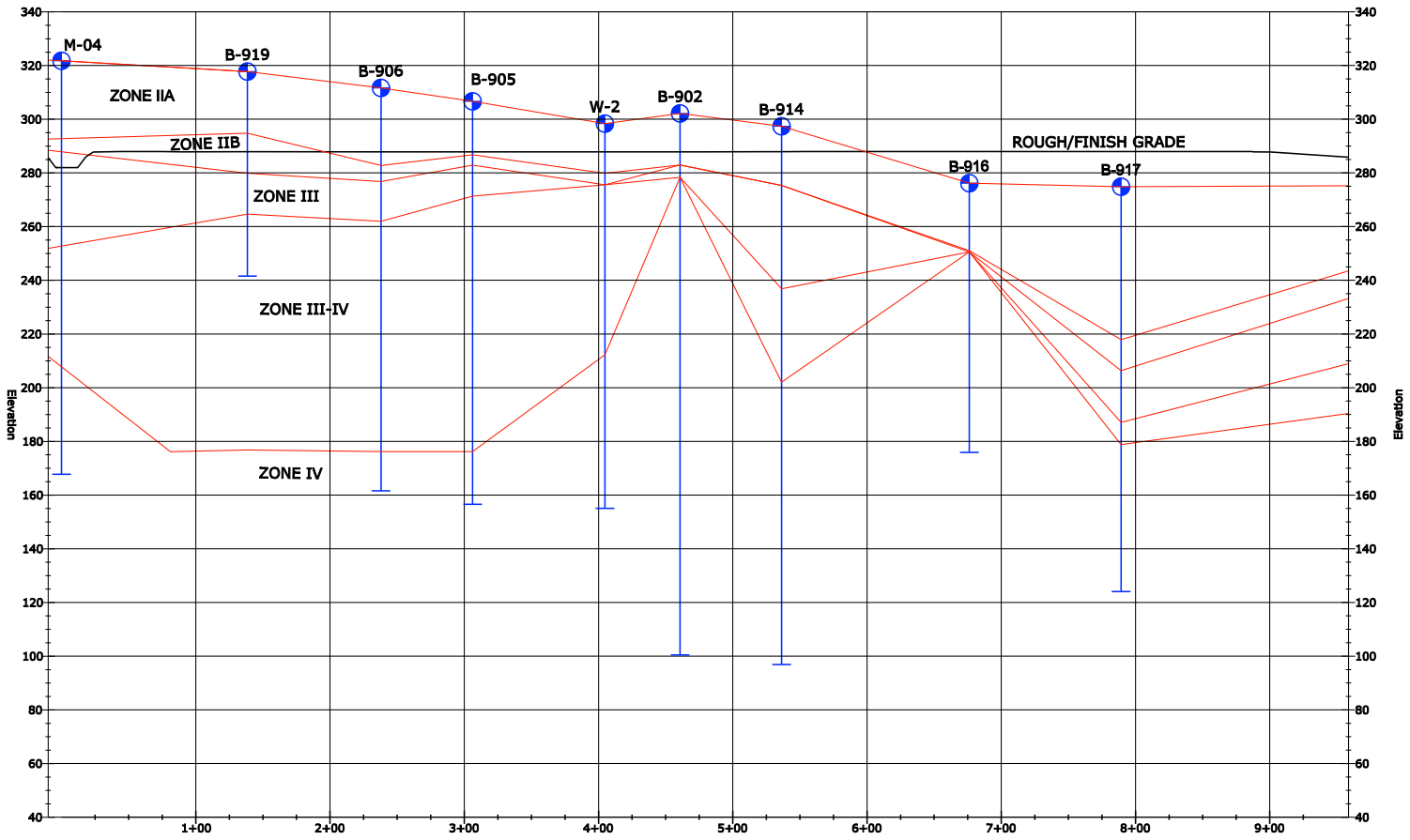

NOTE:
THE CONVERSION FROM NAVD88 DATUM ELEVATIONS
TO NGVD29 DATUM ELEVATIONS IS +0.86 FT

SUBSURFACE PROFILE B-B

0 40 80 160 240FT

VERTICAL EXAGGERATION = 2:1

NAPS COL 2.0-29-A **Figure 2.5.4-209 Subsurface Profile C-C**

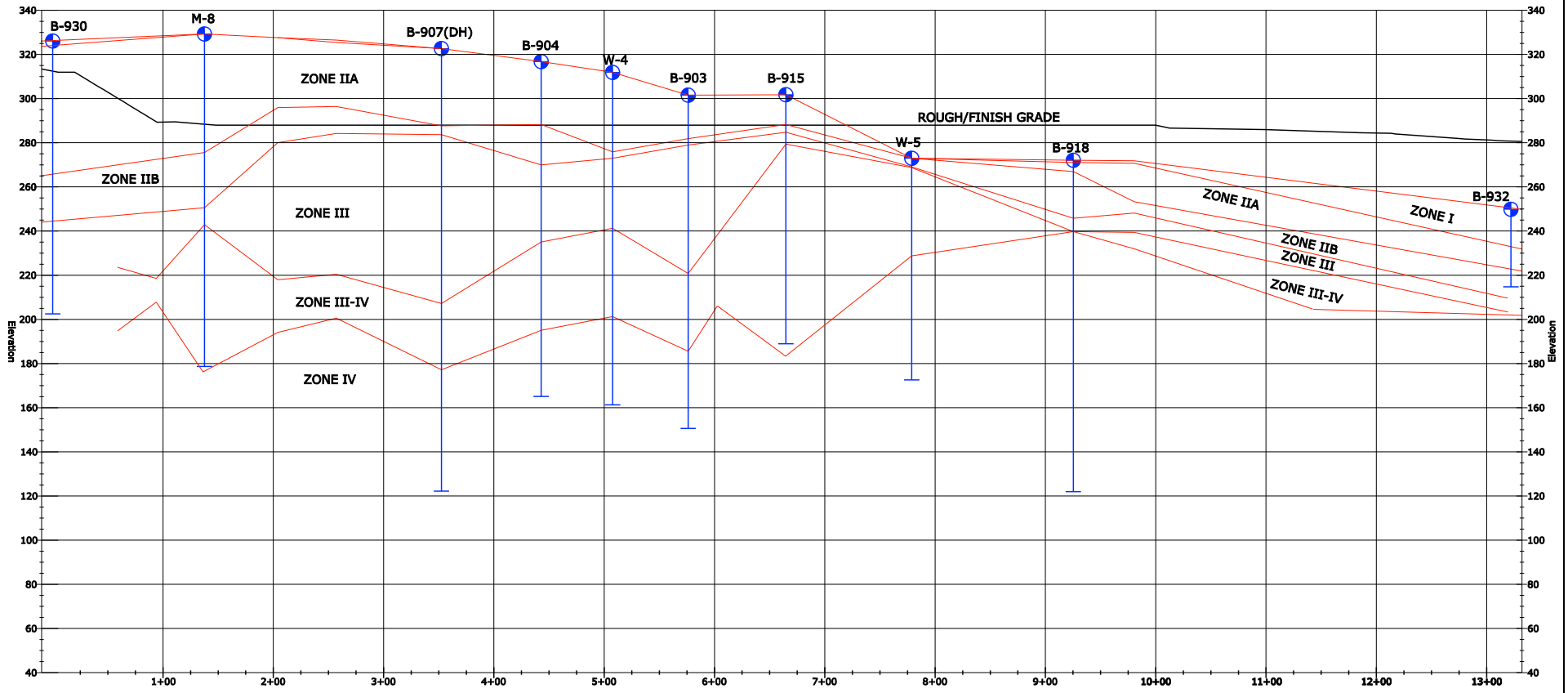

NOTE:
THE CONVERSION FROM NAVD88 DATUM ELEVATIONS
TO NGVD29 DATUM ELEVATIONS IS +0.86 FT

SUBSURFACE PROFILE C-C

0 40 80 160 240FT

VERTICAL EXAGGERATION = 2:1

NAPS COL 2.0-29-A **Figure 2.5.4-210 Subsurface Profile D-D**

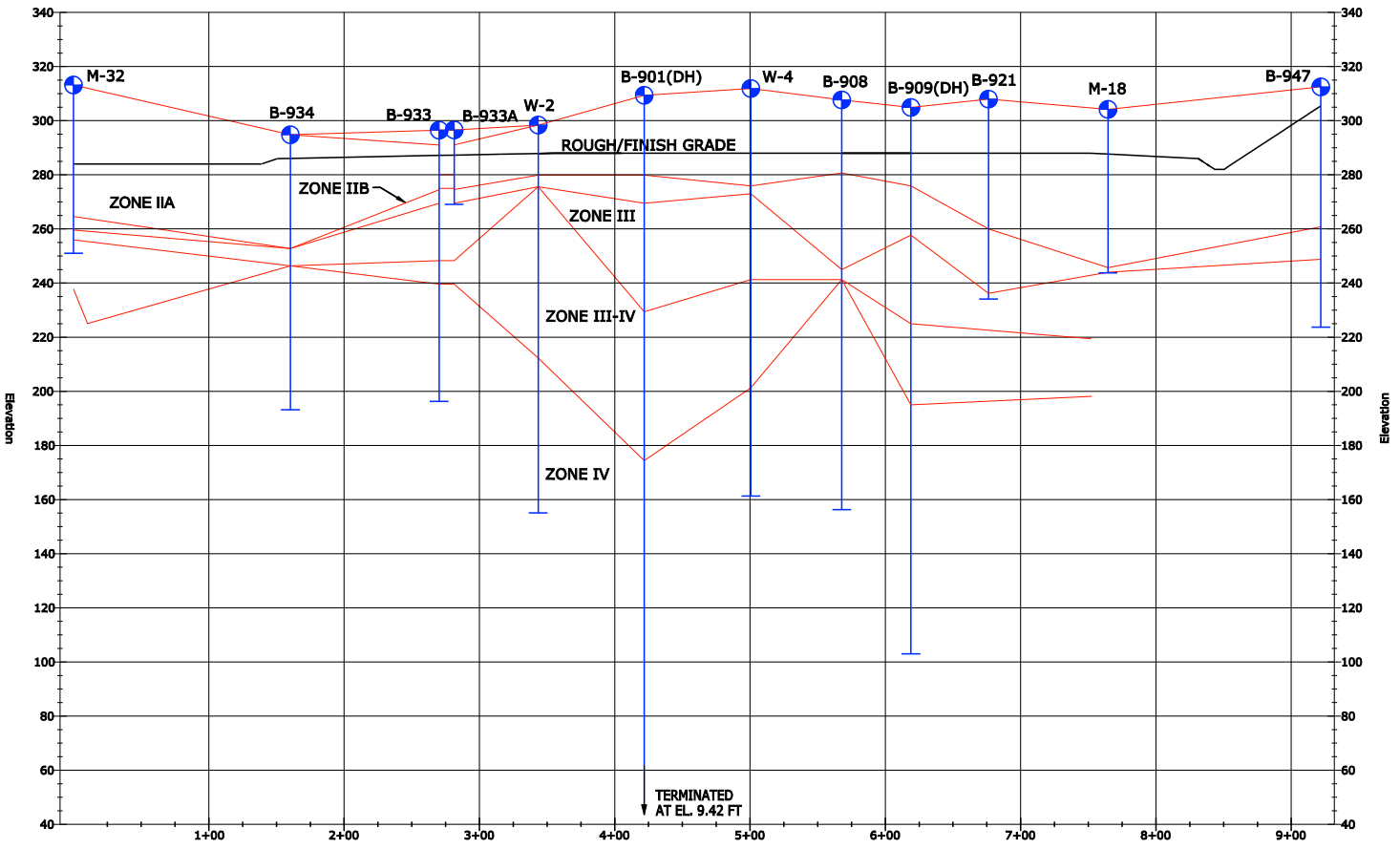

NOTE:
THE CONVERSION FROM NAVD88 DATUM ELEVATIONS TO NGVD29 DATUM ELEVATIONS IS +0.86 FT

SUBSURFACE PROFILE D-D

0 40 80 160 240FT

VERTICAL EXAGGERATION = 2:1

NAPS COL 2.0-29-A **Figure 2.5.4-211 Subsurface Profile E-E**

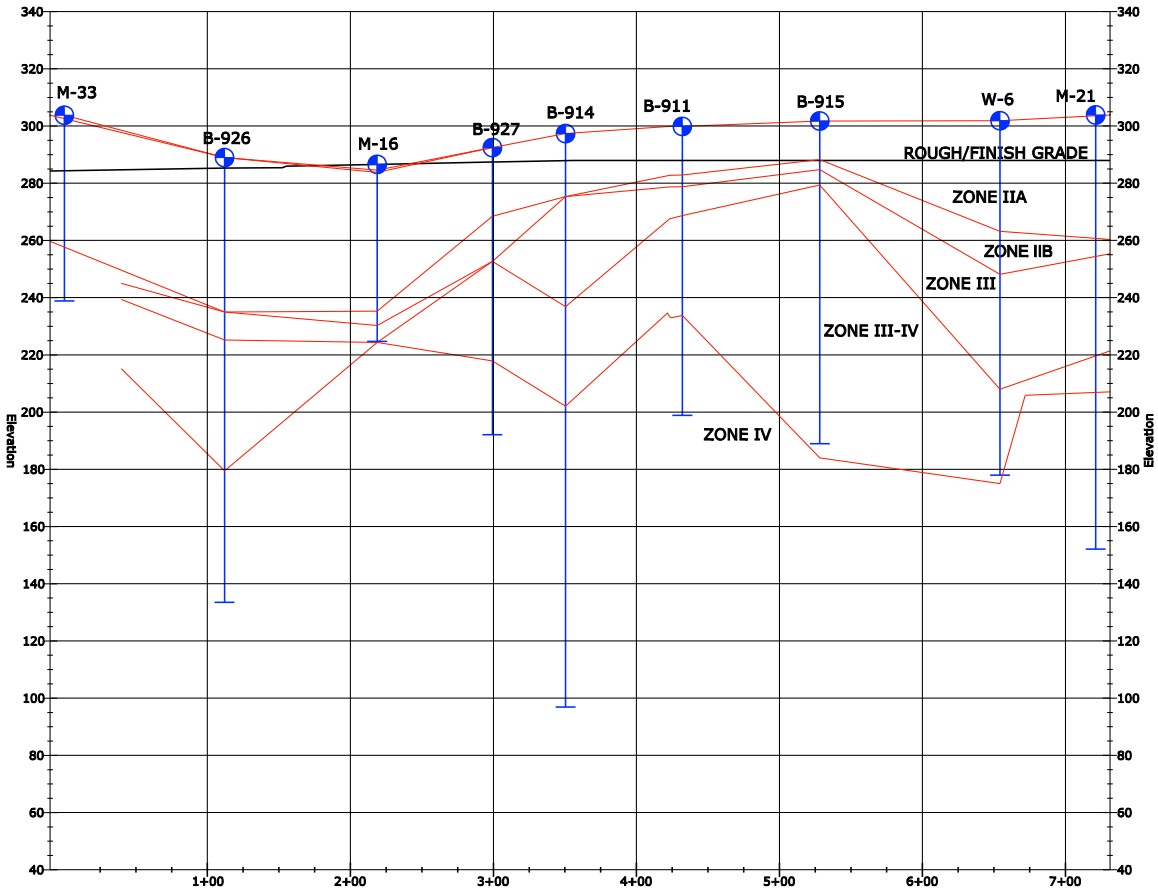

NOTE:
THE CONVERSION FROM NAVD88 DATUM ELEVATIONS
TO NGVD29 DATUM ELEVATIONS IS +0.86 FT

SUBSURFACE PROFILE E-E

0 40 80 160 240FT

VERTICAL EXAGGERATION = 2:1

NAPS COL 2.0-29-A **Figure 2.5.4-212 Subsurface Profile F-F**

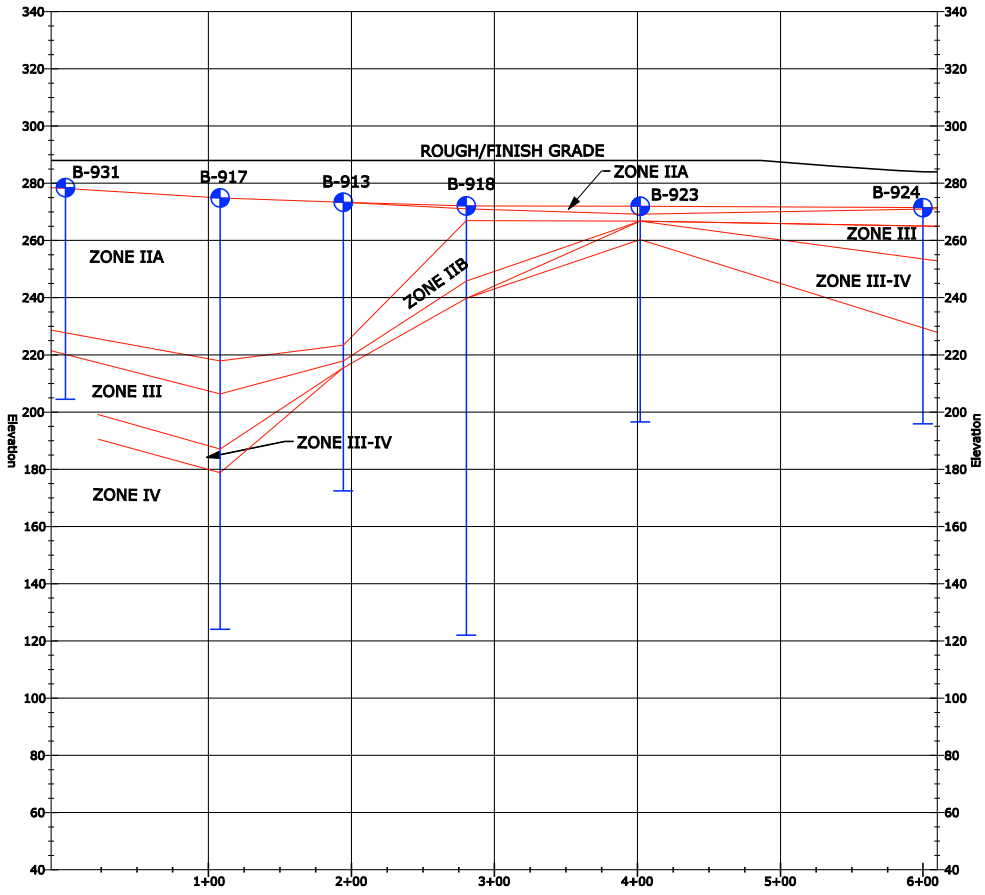

NOTE:
THE CONVERSION FROM NAVD88 DATUM ELEVATIONS
TO NGVD29 DATUM ELEVATIONS IS +0.86 FT

SUBSURFACE PROFILE F-F

0 40 80 160 240FT

VERTICAL EXAGGERATION = 2:1

NAPS COL 2.0-29-A **Figure 2.5.4-213 Subsurface Profile G-G**

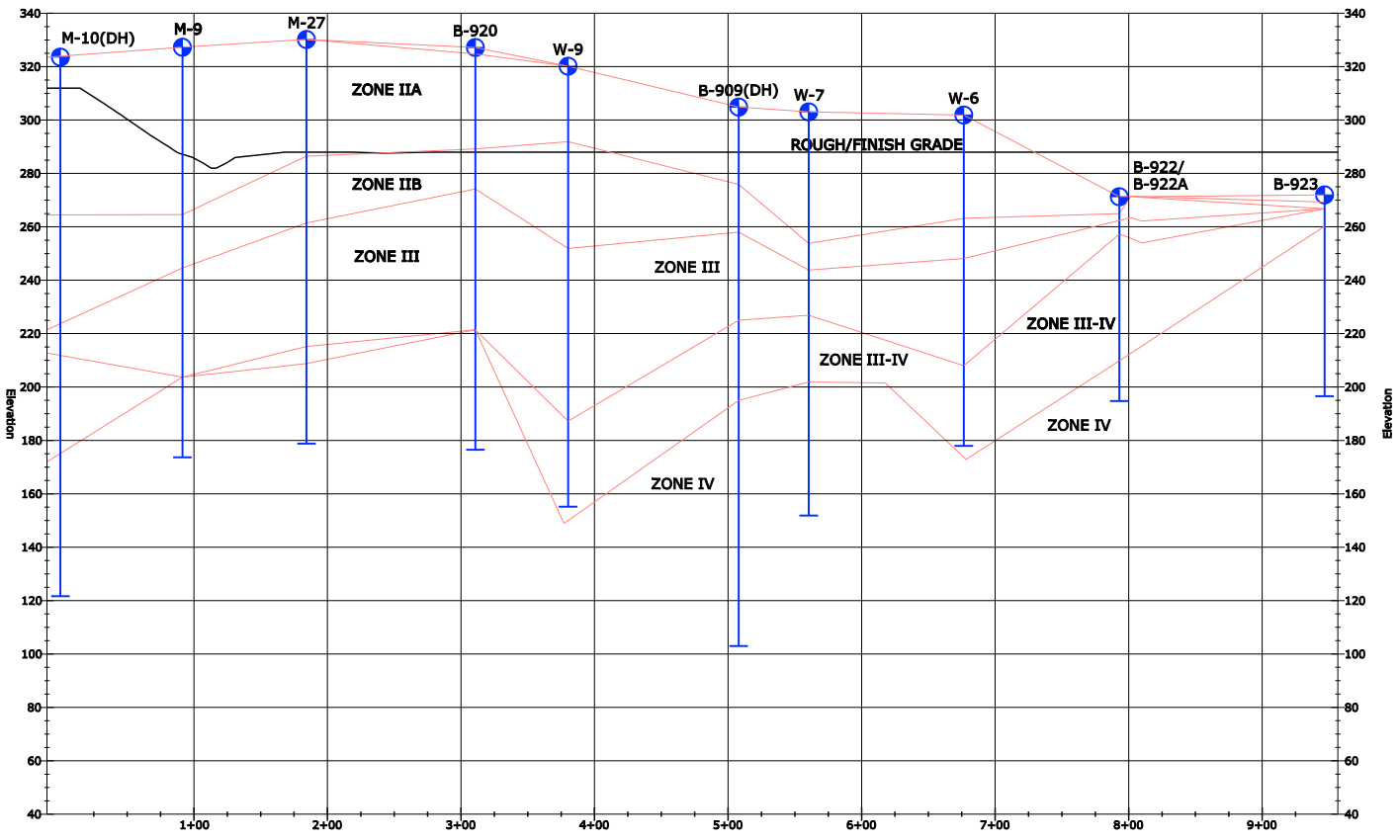

NOTE:
THE CONVERSION FROM NAVD88 DATUM ELEVATIONS
TO NGVD29 DATUM ELEVATIONS IS +0.86 FT

SUBSURFACE PROFILE G-G

0 40 80 160 240FT

VERTICAL EXAGGERATION = 2:1

NAPS COL 2.0-29-A **Figure 2.5.4-214 Subsurface Profile H-H**

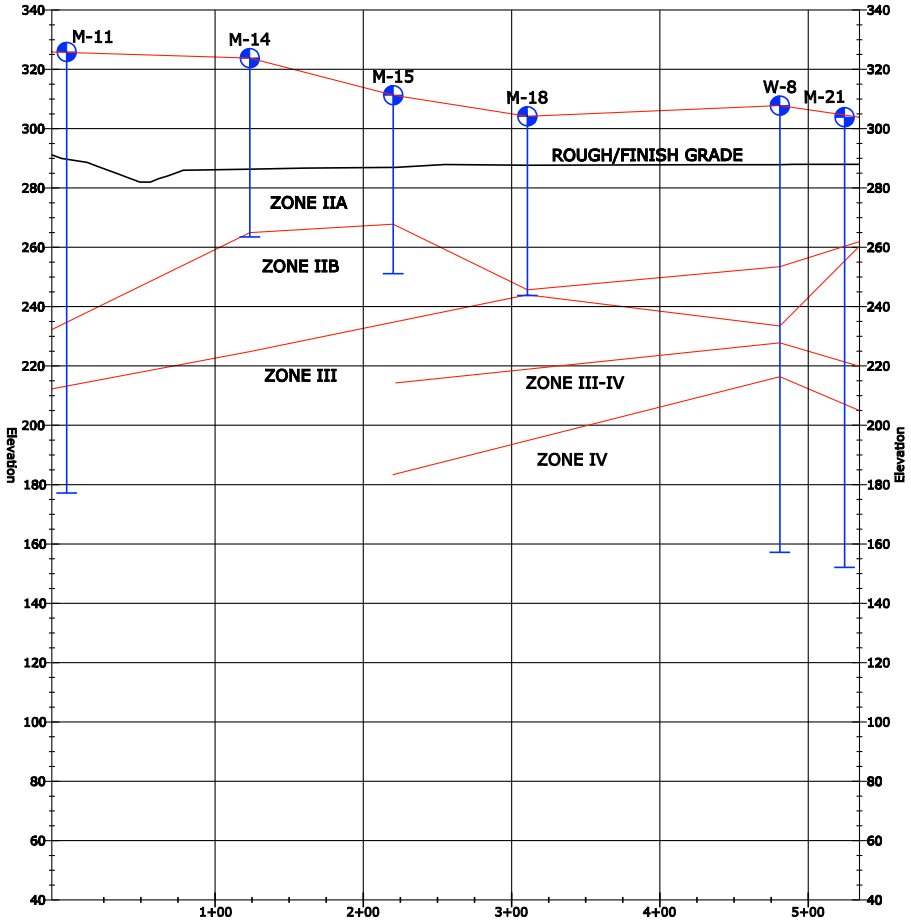

NOTE:
THE CONVERSION FROM NAVD88 DATUM ELEVATIONS
TO NGVD29 DATUM ELEVATIONS IS +0.86 FT

SUBSURFACE PROFILE H-H

0 40 80 160 240FT

VERTICAL EXAGGERATION = 2:1

NAPS COL 2.0-29-A **Figure 2.5.4-215 Subsurface Profile J-J**

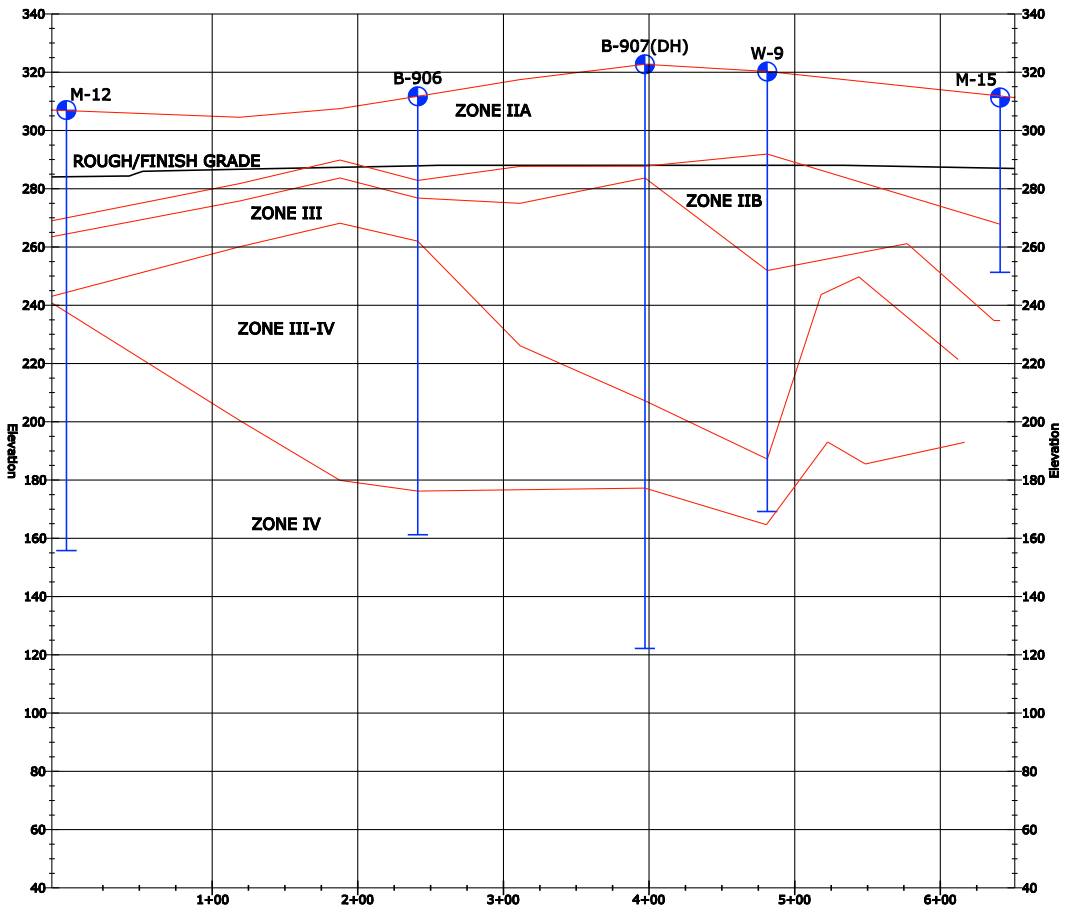

NOTE:
THE CONVERSION FROM NAVD88 DATUM ELEVATIONS
TO NGVD29 DATUM ELEVATIONS IS +0.86 FT

SUBSURFACE PROFILE J-J

0 40 80 160 240FT

VERTICAL EXAGGERATION = 2:1

NAPS COL 2.0-29-A **Figure 2.5.4-216 Subsurface Profile K-K**

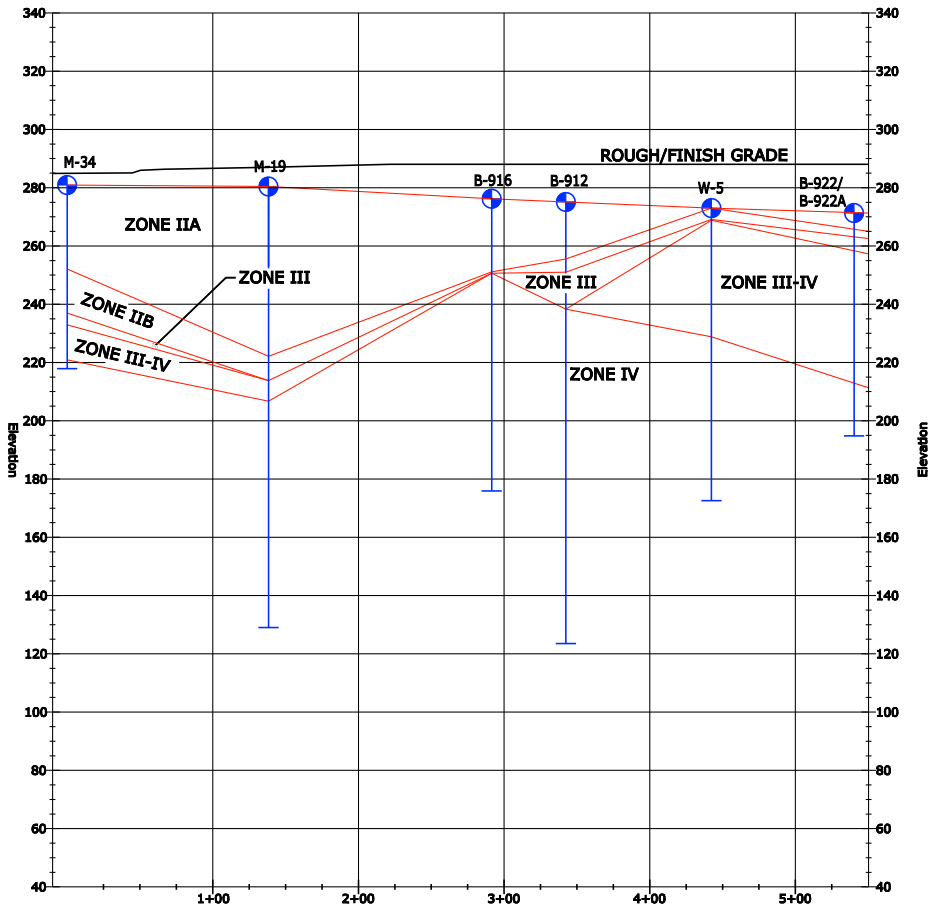

NOTE:
THE CONVERSION FROM NAVD88 DATUM ELEVATIONS
TO NGVD29 DATUM ELEVATIONS IS +0.86 FT

SUBSURFACE PROFILE K-K

0 40 80 160 240FT

VERTICAL EXAGGERATION = 2:1

NAPS COL 2.0-29-A **Figure 2.5.4-217 Unit 3 Boring Locations – Power Block**

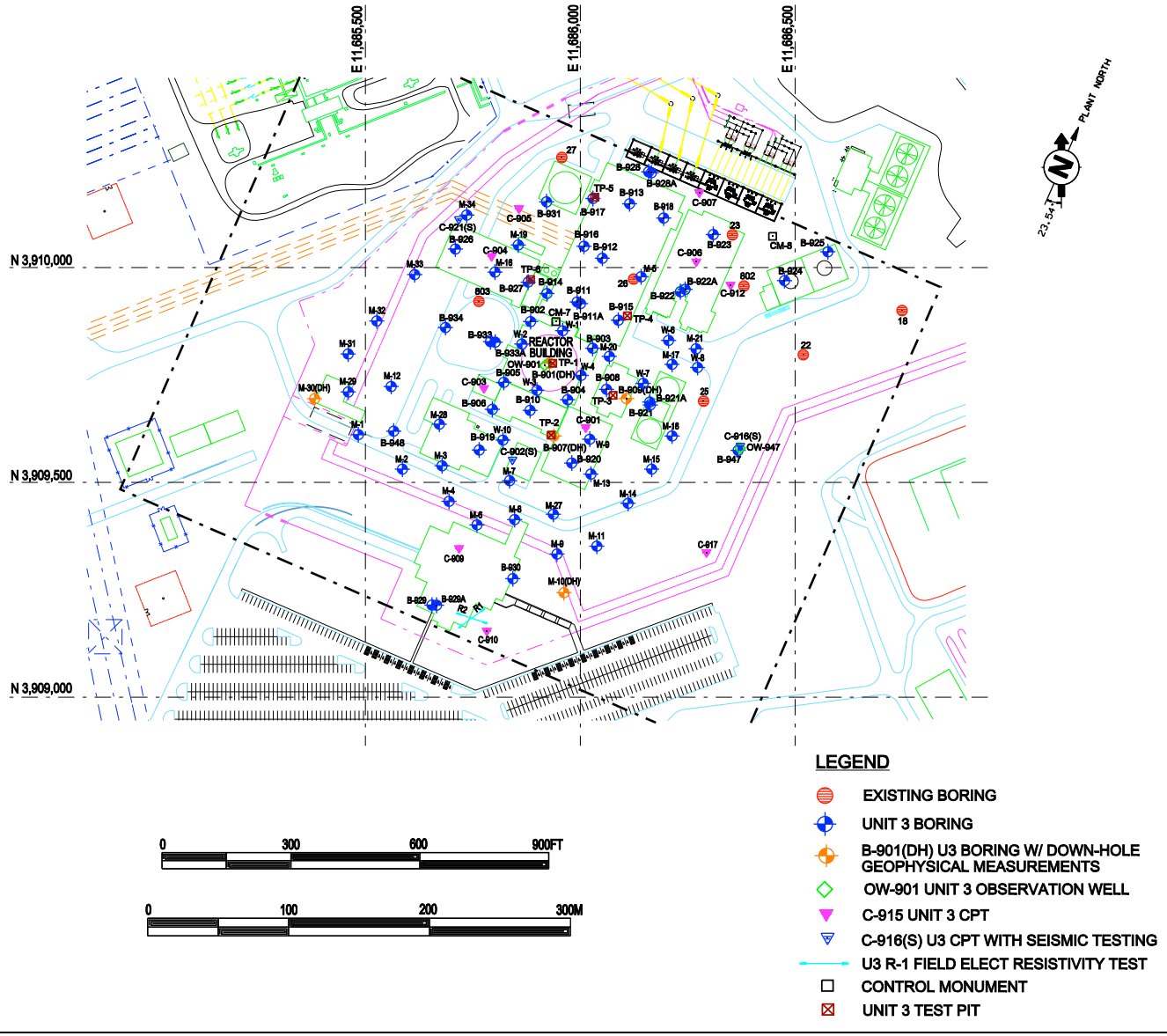

NAPS COL 2.0-29-A **Figure 2.5.4-218 Unit 3 Boring Locations – Site**

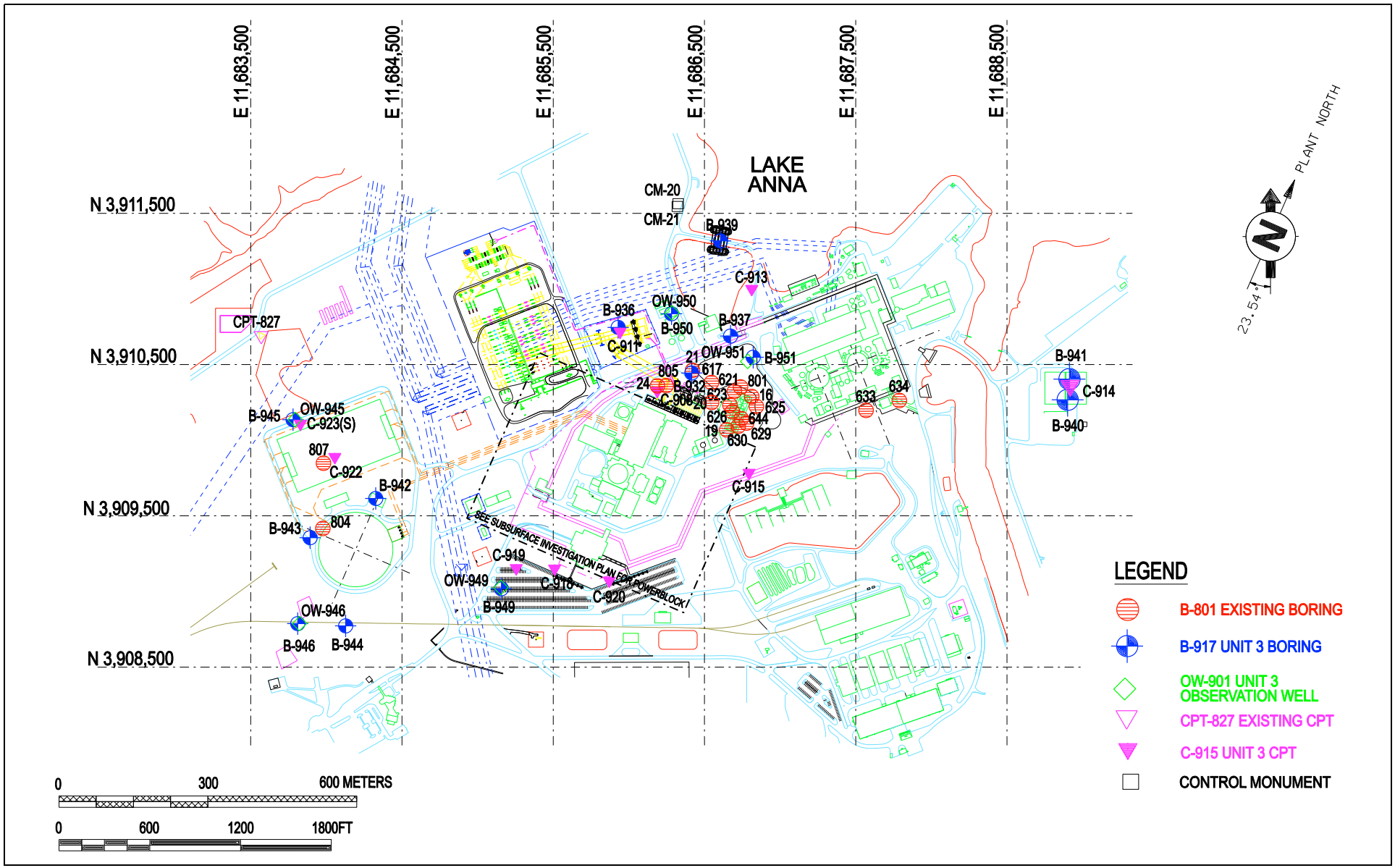

NAPS COL 2.0-29-A **Figure 2.5.4-219 RCTS Test Results (Sheet 1 of 3) G/G_{max} and D vs. Strain, B-901 UD-1: 4.3 psi Confining Pressure**

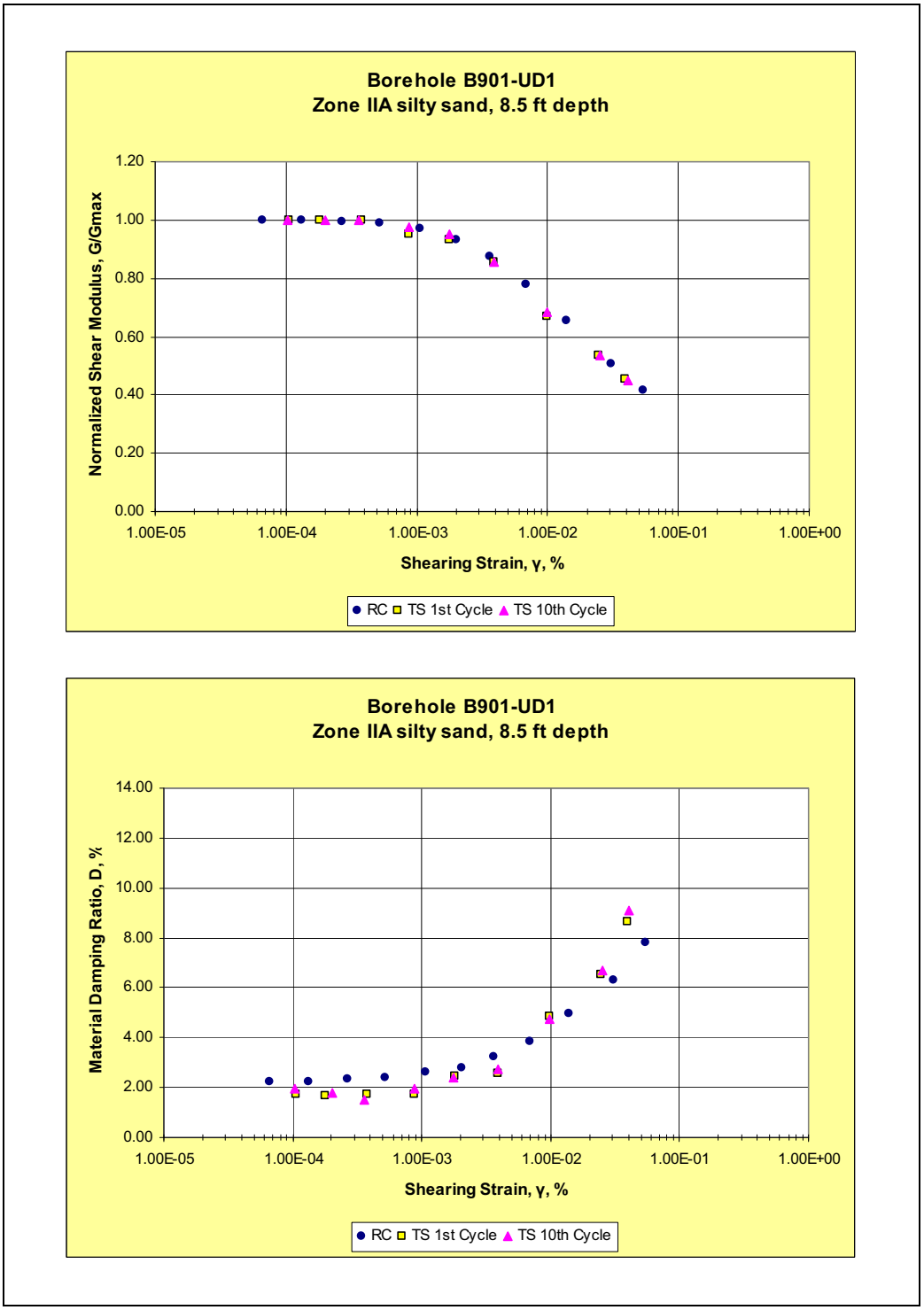

NAPS COL 2.0-29-A **Figure 2.5.4-219 RCTS Test Results (Sheet 2 of 3) G/G_{max} and D vs. Strain, B-911A UD-1: 5.6 psi Confining Pressure**

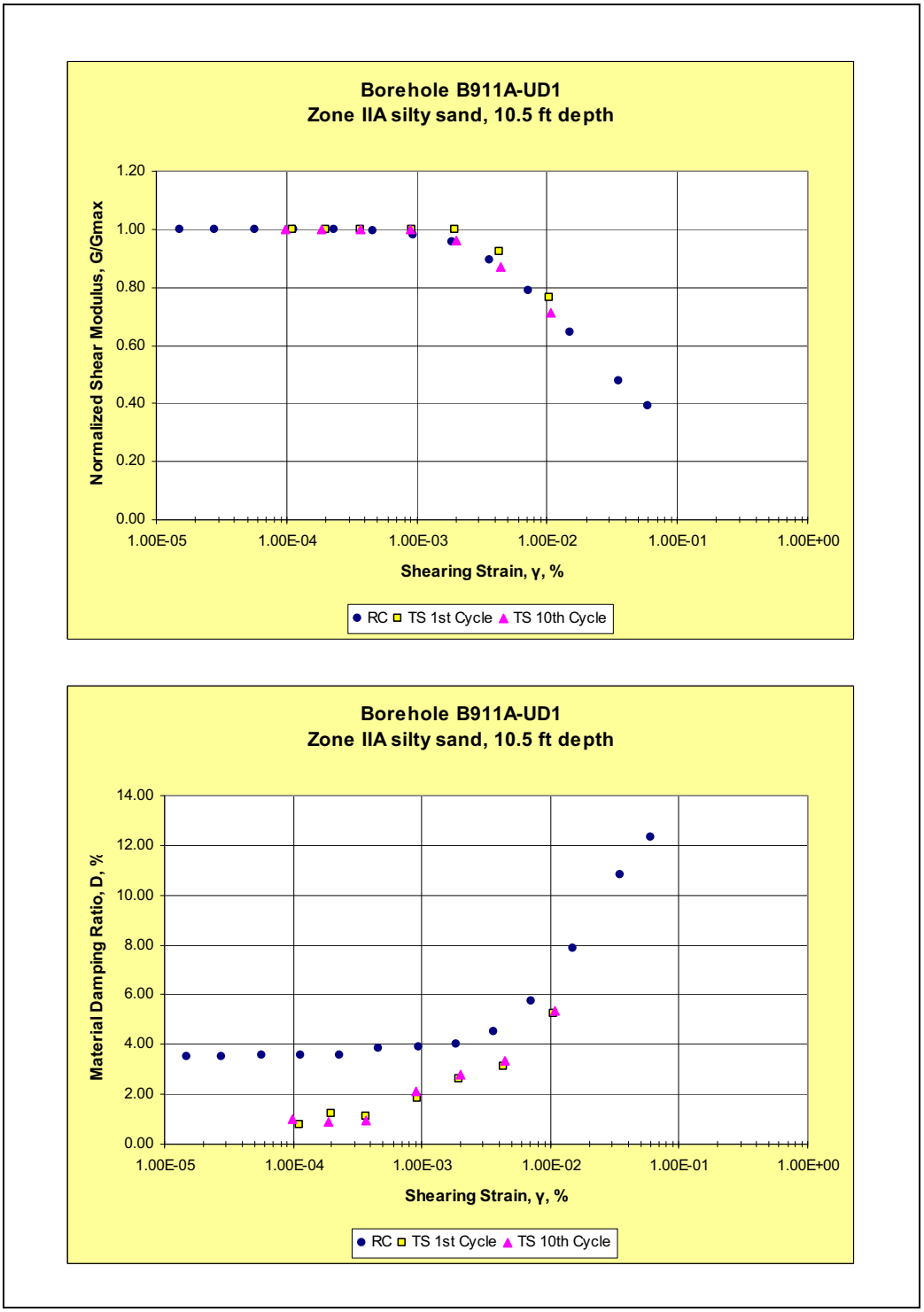

NAPS COL 2.0-29-A **Figure 2.5.4-219 RCTS Test Results (Sheet 3 of 3) G/G_{max} and D vs. Strain, B-911A PB-1: 11.4 psi Confining Pressure**

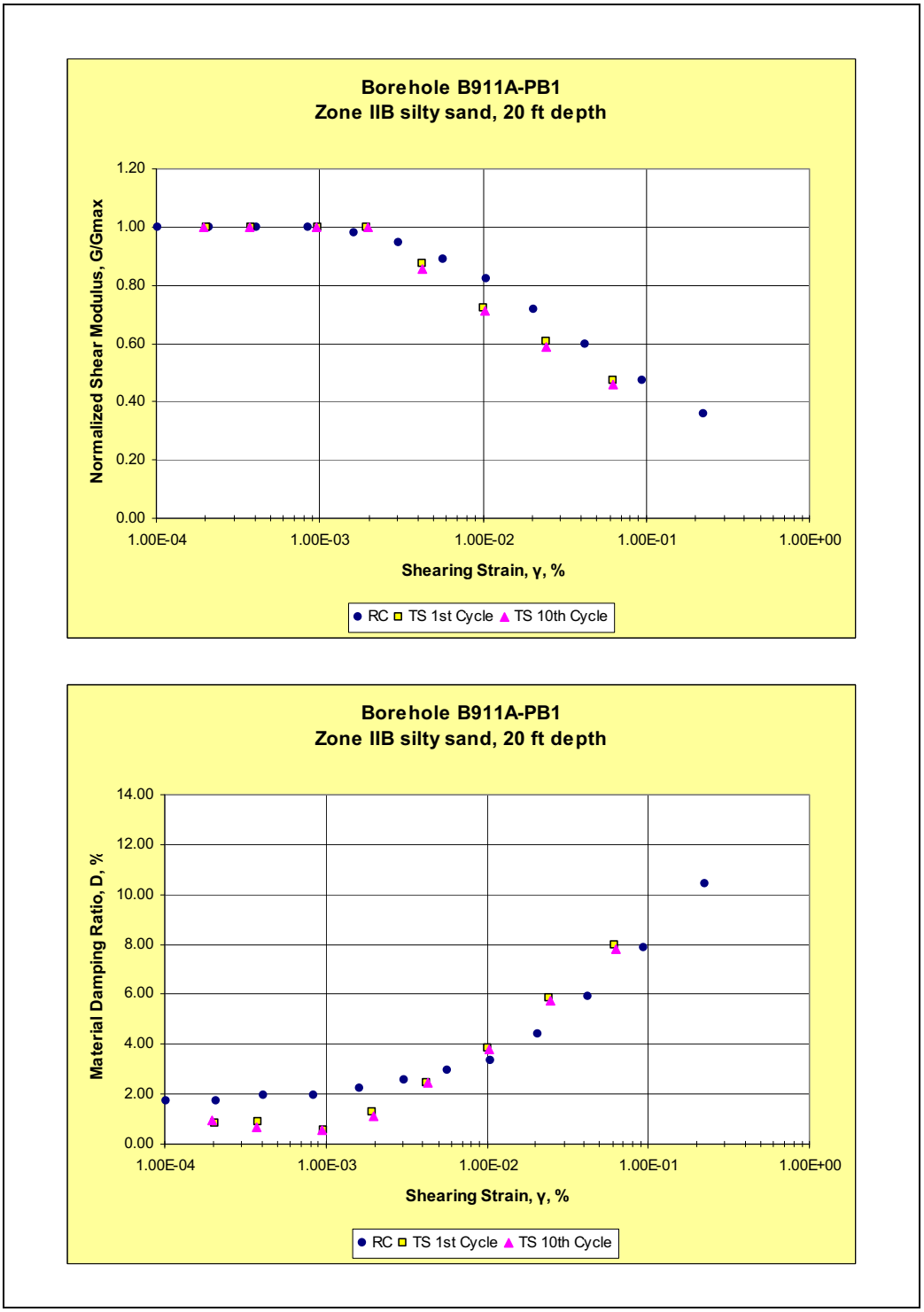

NAPS COL 2.0-29-A **Figure 2.5.4-220 Rock Quality Designation versus Elevation**

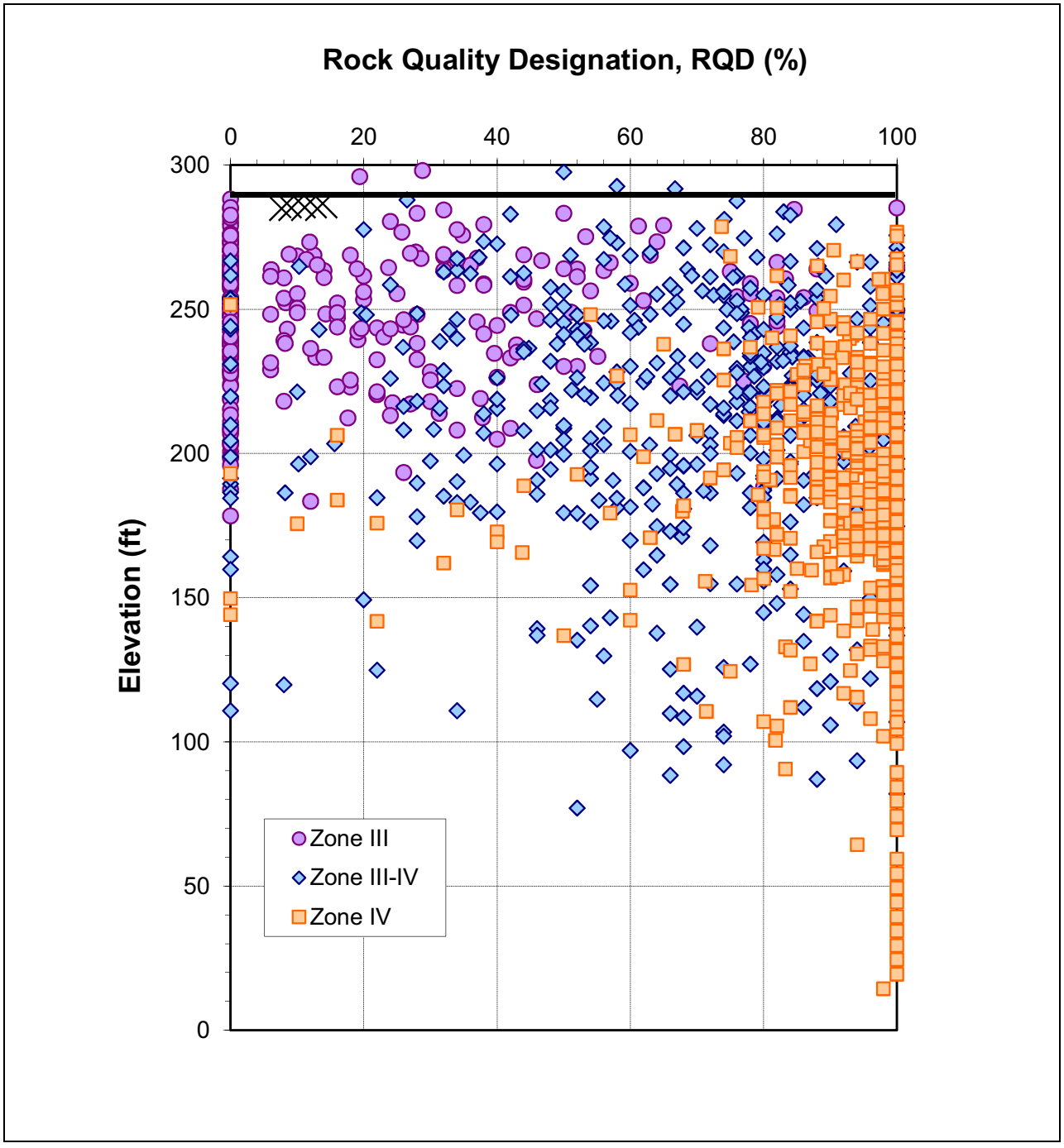

NAPS COL 2.0-29-A **Figure 2.5.4-221 Fines Content of Saprolite versus Depth**

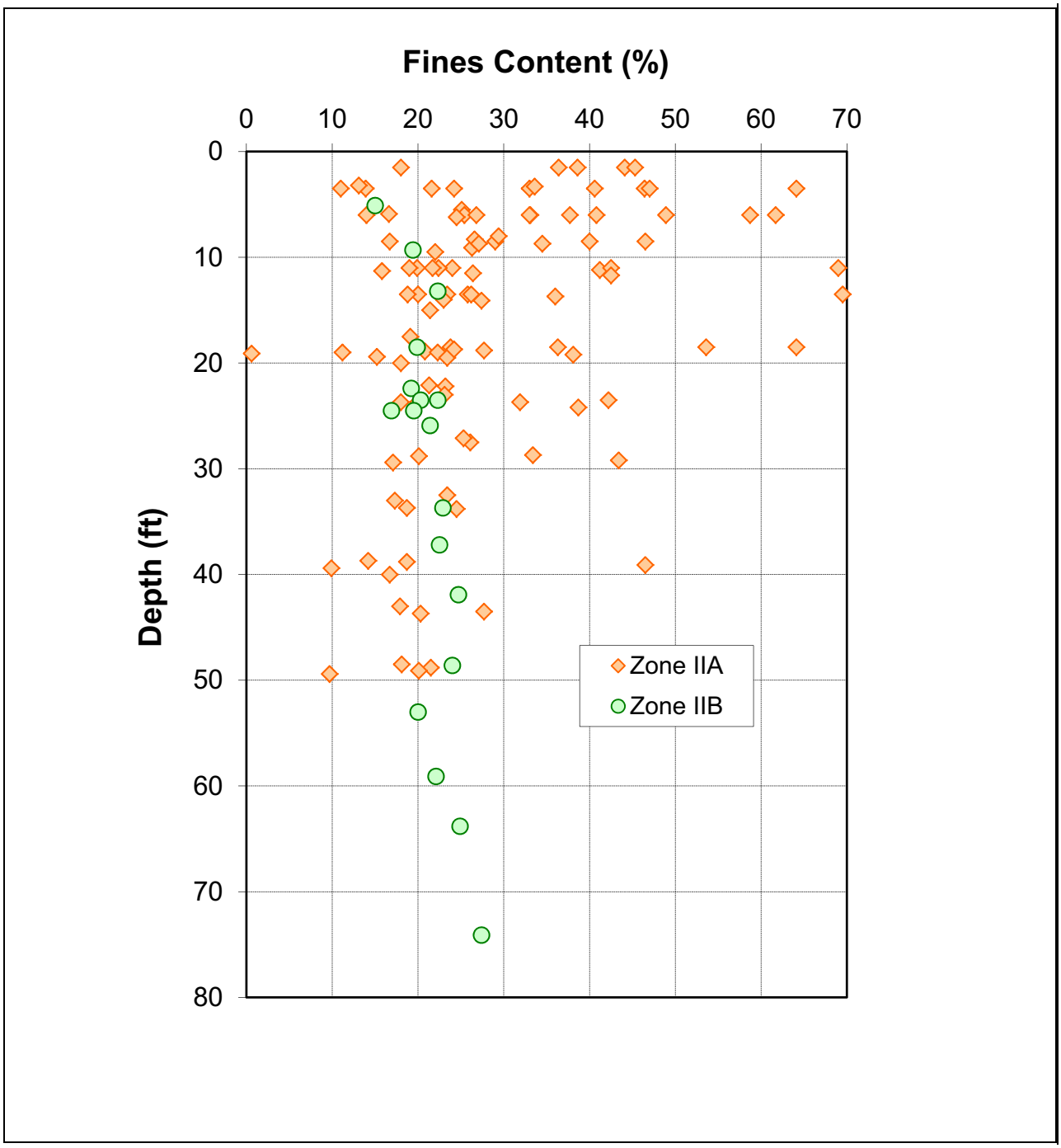

NAPS COL 2.0-29-A **Figure 2.5.4-222 Measured SPT N-Value versus Depth**

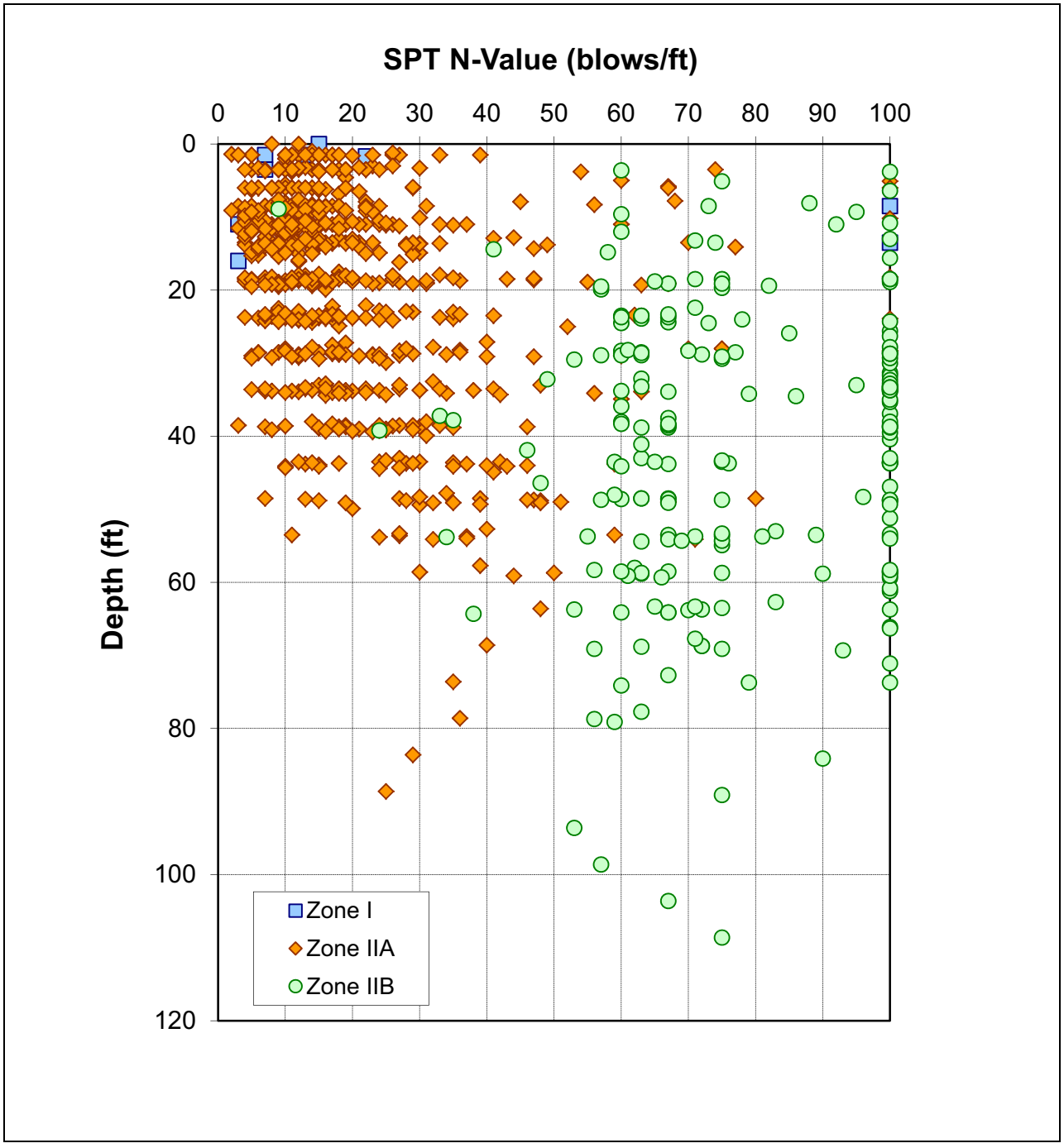

NAPS COL 2.0-29-A **Figure 2.5.4-223 Measured Soil Shear Wave Velocity versus Depth**

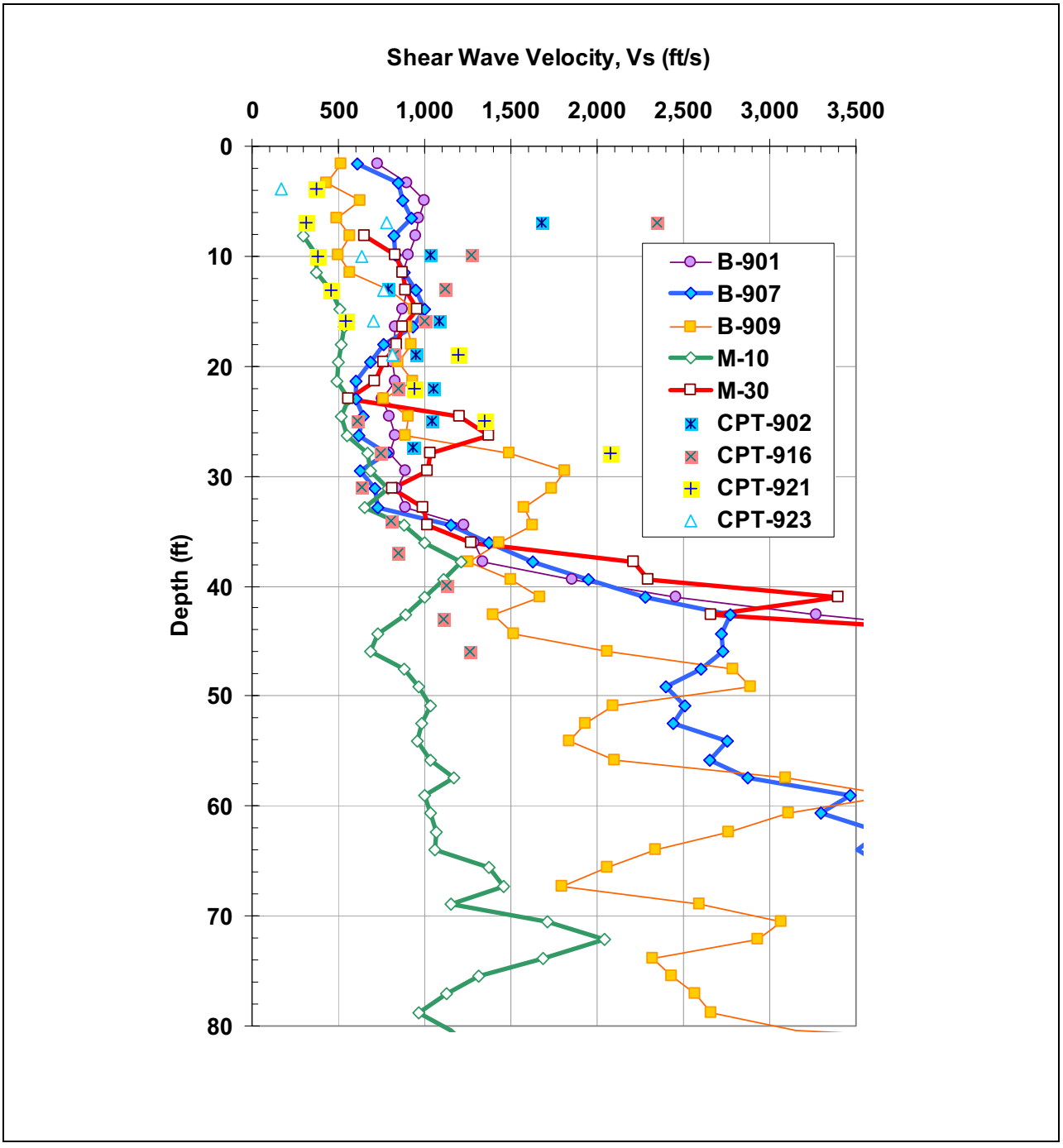

NAPS COL 2.0-29-A **Figure 2.5.4-224 Relationship between CBR and Molded Dry Density**

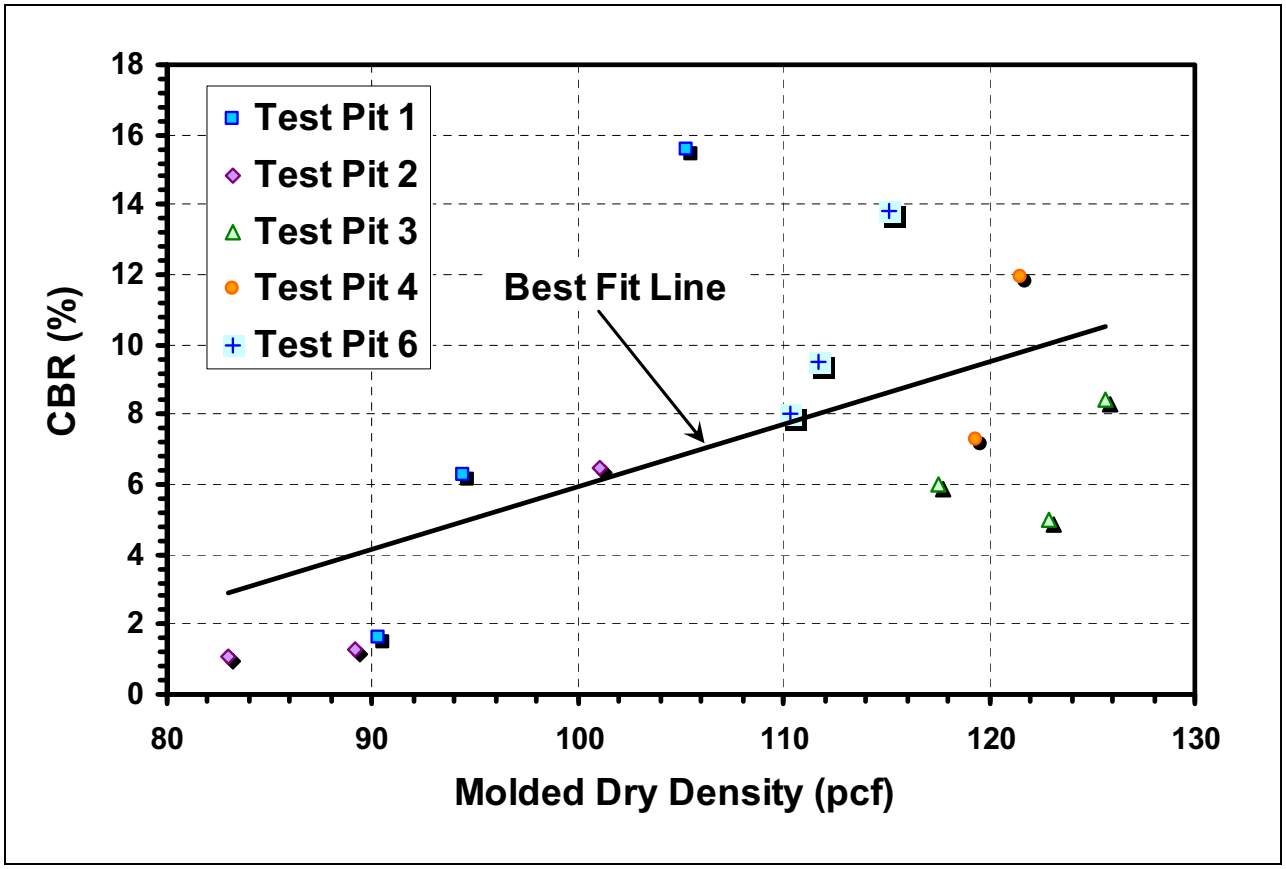

BASIS: NEW

NAPS ESP COL 2.5-3 Figure 2.5.4-225 Subsurface Profile A-A with Foundation Outline

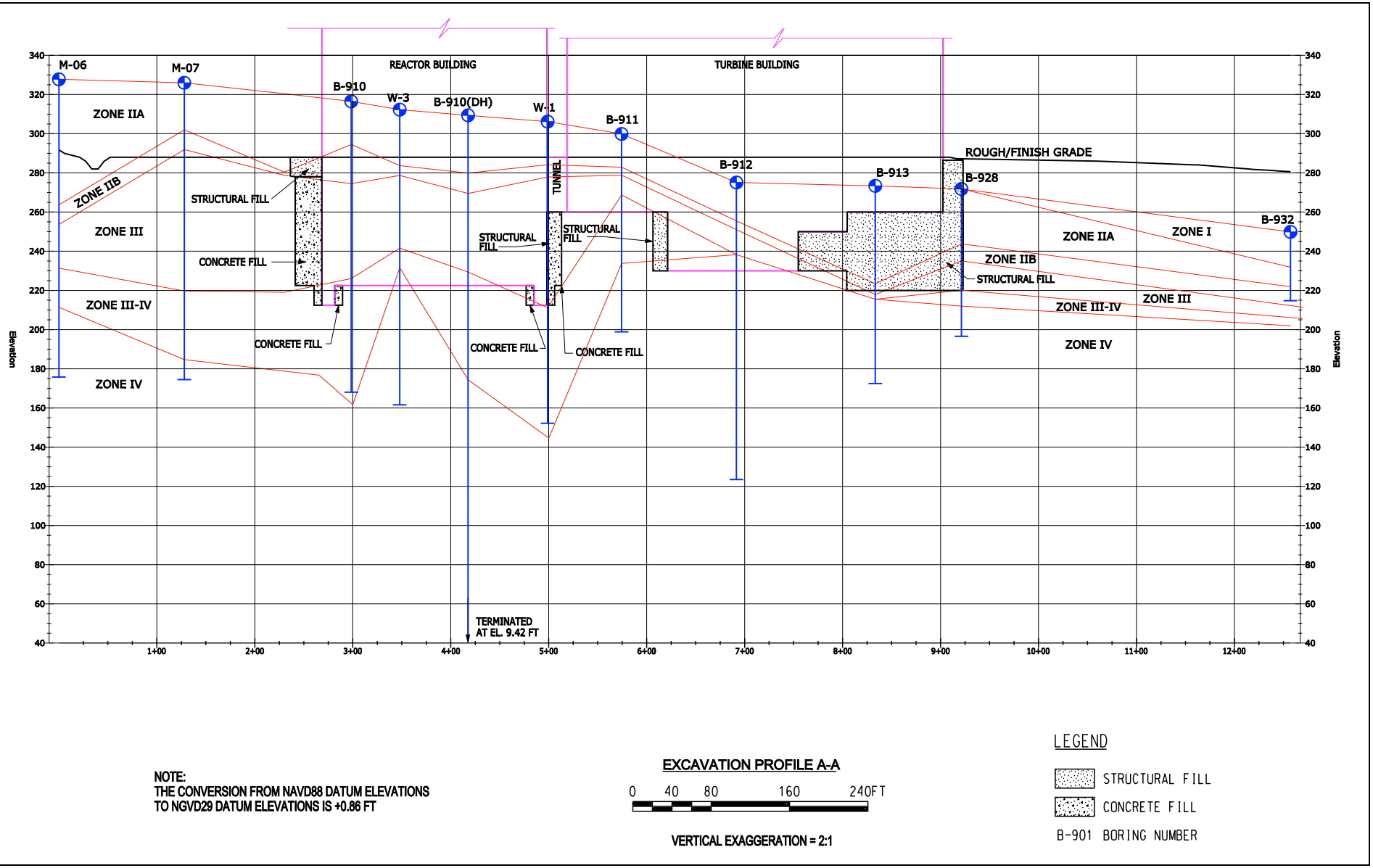

BASIS: NEW

NAPS ESP COL 2.5-3 Figure 2.5.4-226 Subsurface Profile B-B with Foundation Outline

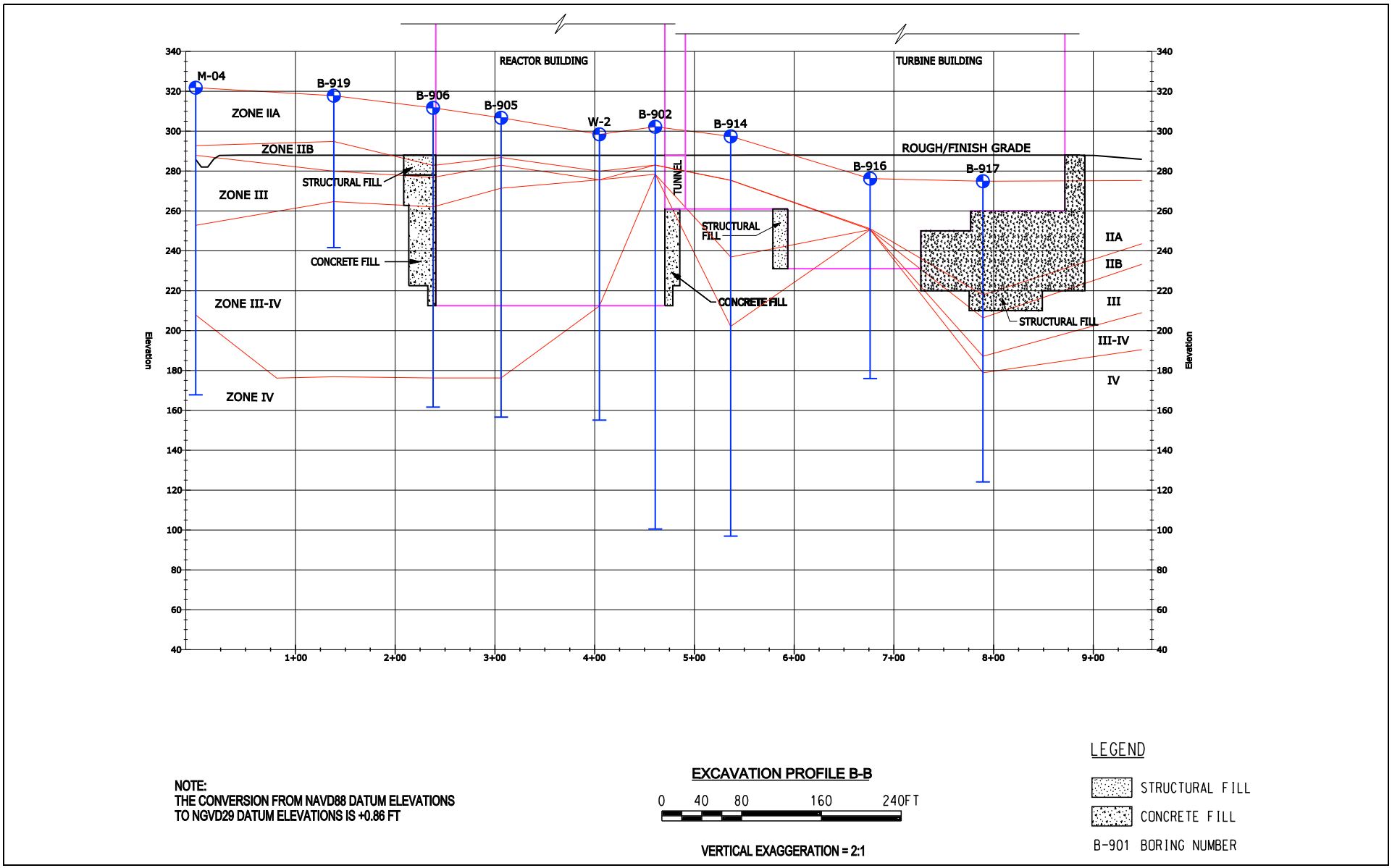

BASIS: NEW

NAPS ESP COL 2.5-3 Figure 2.5.4-227 Subsurface Profile C-C with Foundation Outline

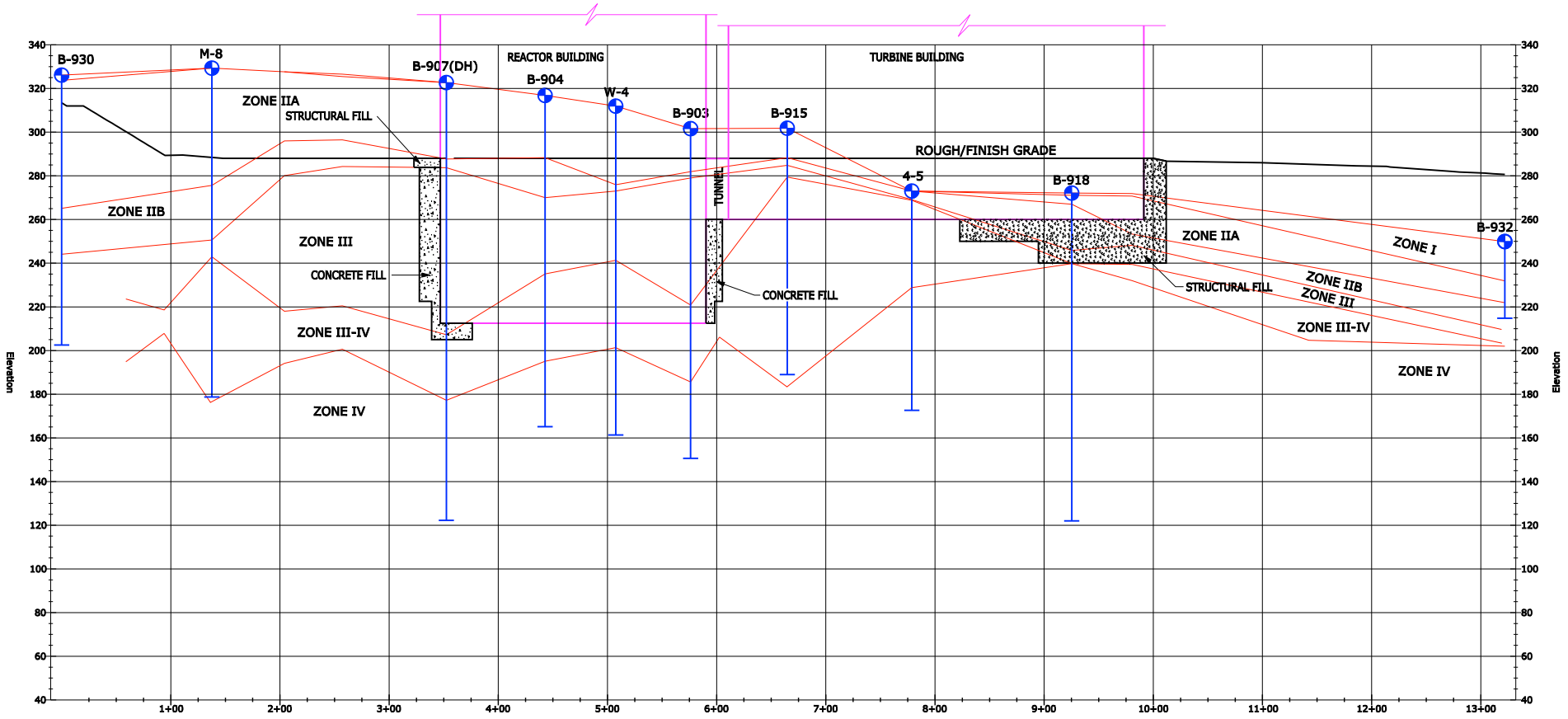

BASIS: NEW

NAPS ESP COL 2.5-3 Figure 2.5.4-228 Subsurface Profile D-D with Foundation Outline

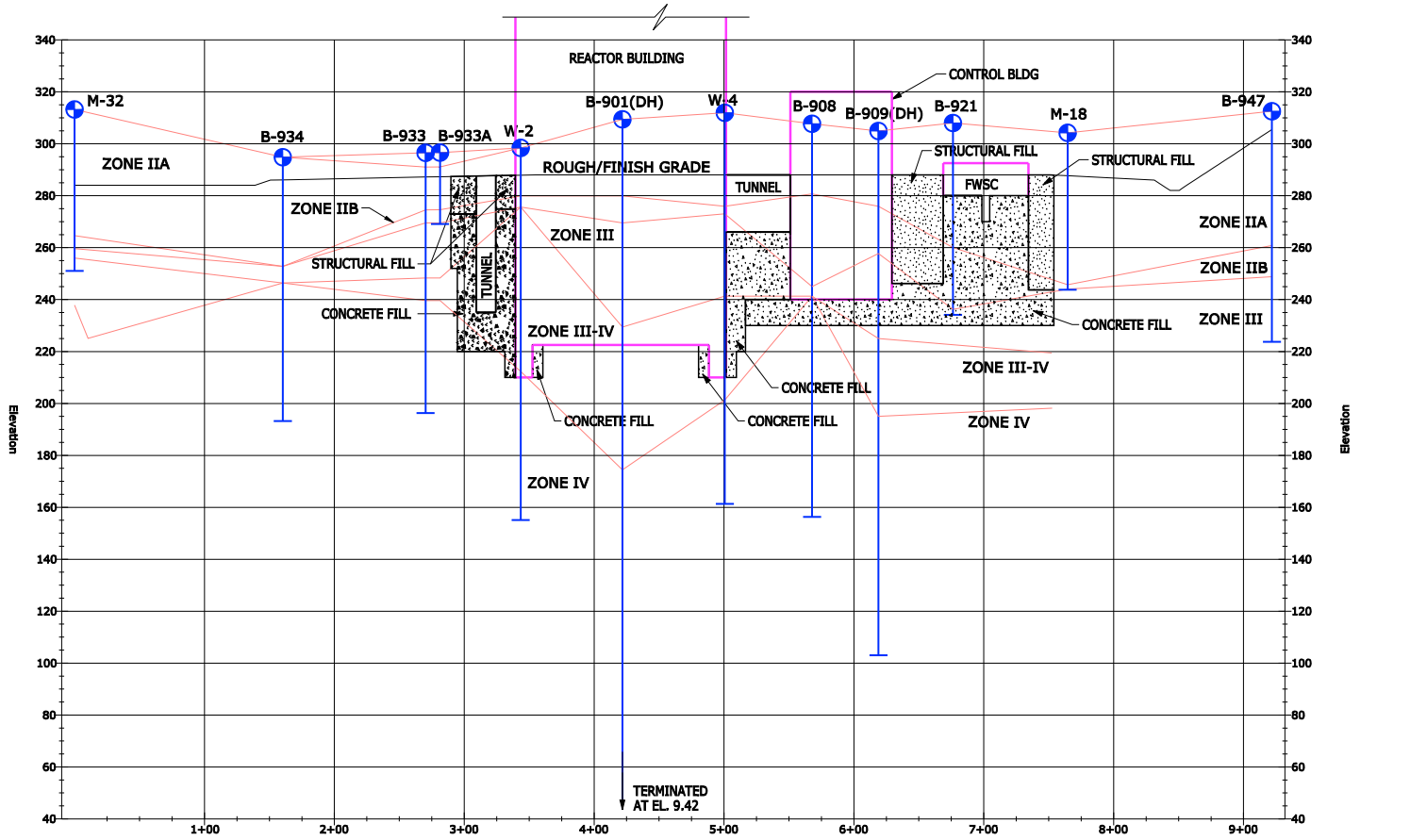

NOTE:
THE CONVERSION FROM NAVD88 DATUM ELEVATIONS TO NGVD29 DATUM ELEVATIONS IS +0.86 FT

EXCAVATION PROFILE D-D

0 40 80 160 240FT

VERTICAL EXAGGERATION = 2:1

LEGEND

STRUCTURAL FILL

CONCRETE FILL

B-901 BORING NUMBER

NAPS ESP COL 2.5-3 Figure 2.5.4-229 Subsurface Profile E-E with Foundation Outline

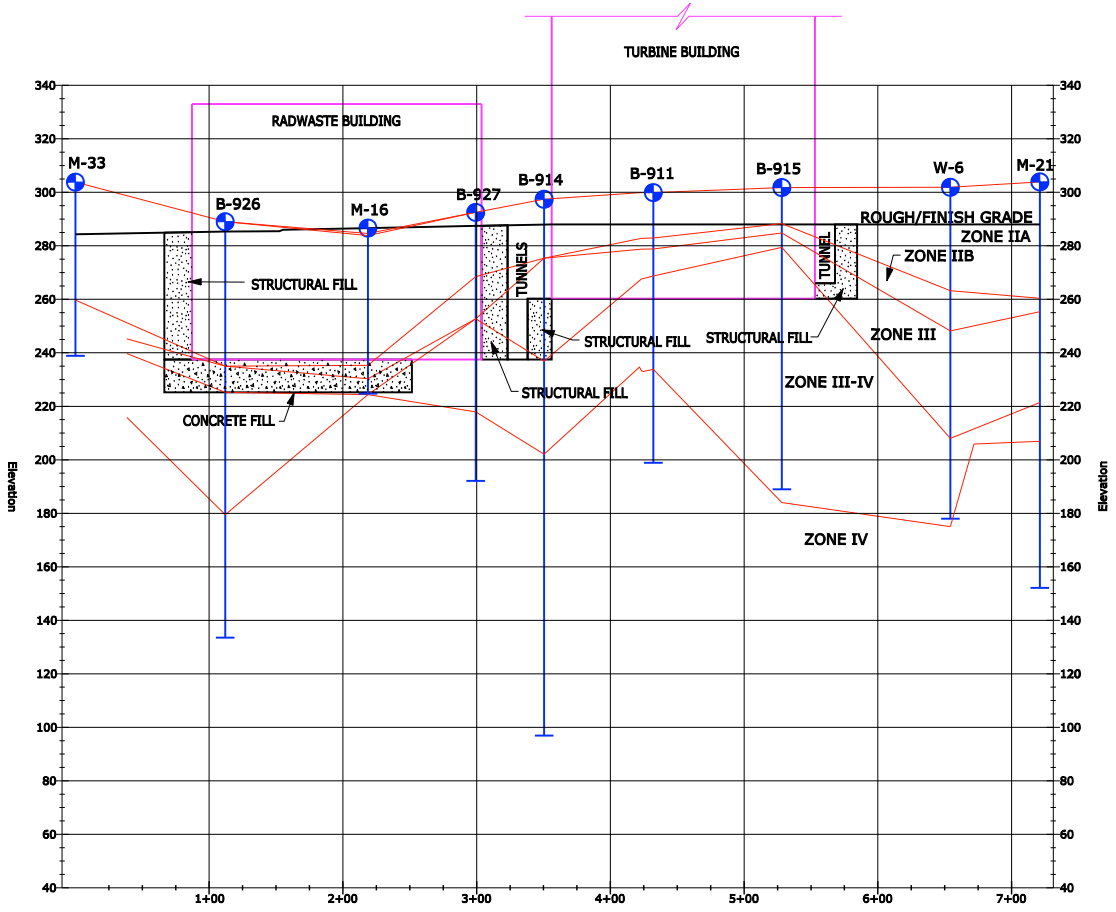

NOTE:
THE CONVERSION FROM NAVD88 DATUM ELEVATIONS TO NGVD29 DATUM ELEVATIONS IS +0.86 FT

EXCAVATION PROFILE E-E

0 40 80 160 240FT

VERTICAL EXAGGERATION = 2:1

LEGEND

STRUCTURAL FILL

CONCRETE FILL

B-901 BORING NUMBER

NAPS ESP COL 2.5-3 Figure 2.5.4-230 Subsurface Profile F-F with Foundation Outline

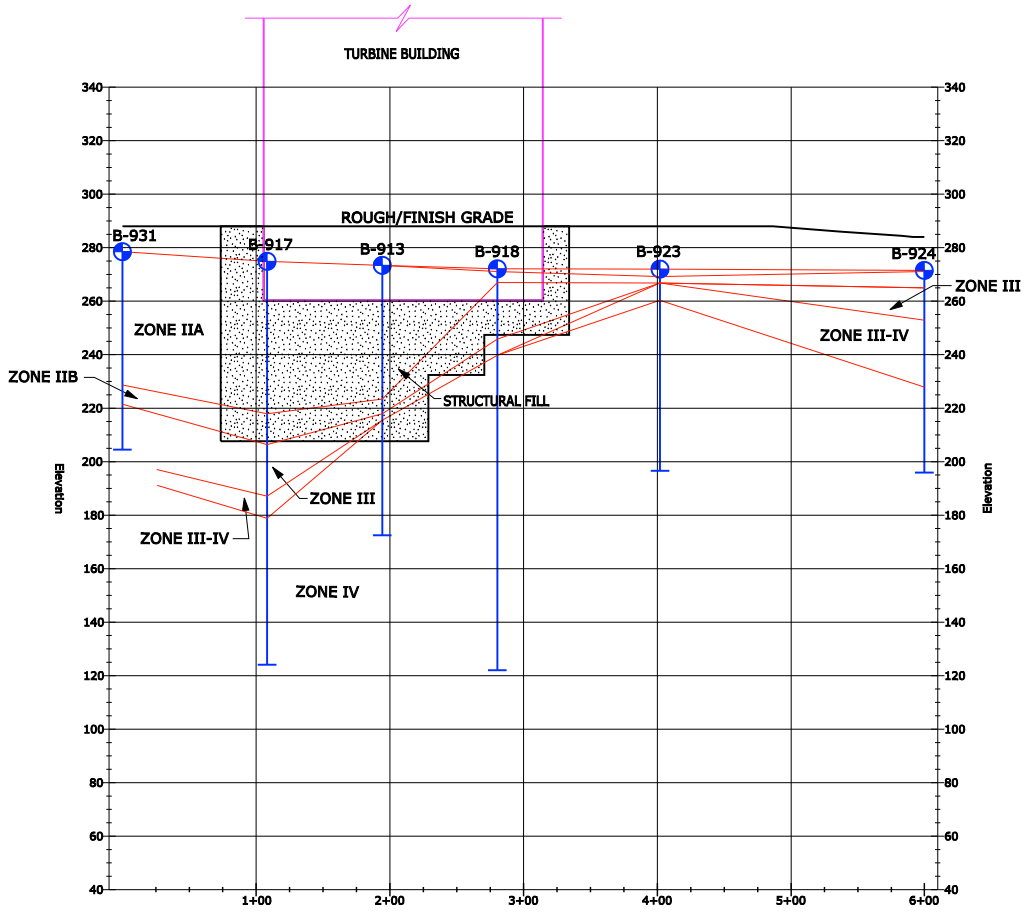

NOTE:
THE CONVERSION FROM NAVD88 DATUM ELEVATIONS TO NGVD29 DATUM ELEVATIONS IS +0.86 FT

EXCAVATION PROFILE F-F

0 40 80 160 240FT

VERTICAL EXAGGERATION = 2:1

LEGEND

STRUCTURAL FILL

CONCRETE FILL

B-901 BORING NUMBER

BASIS: NEW

NAPS ESP COL 2.5-3 Figure 2.5.4-231 Subsurface Profile G-G with Foundation Outline

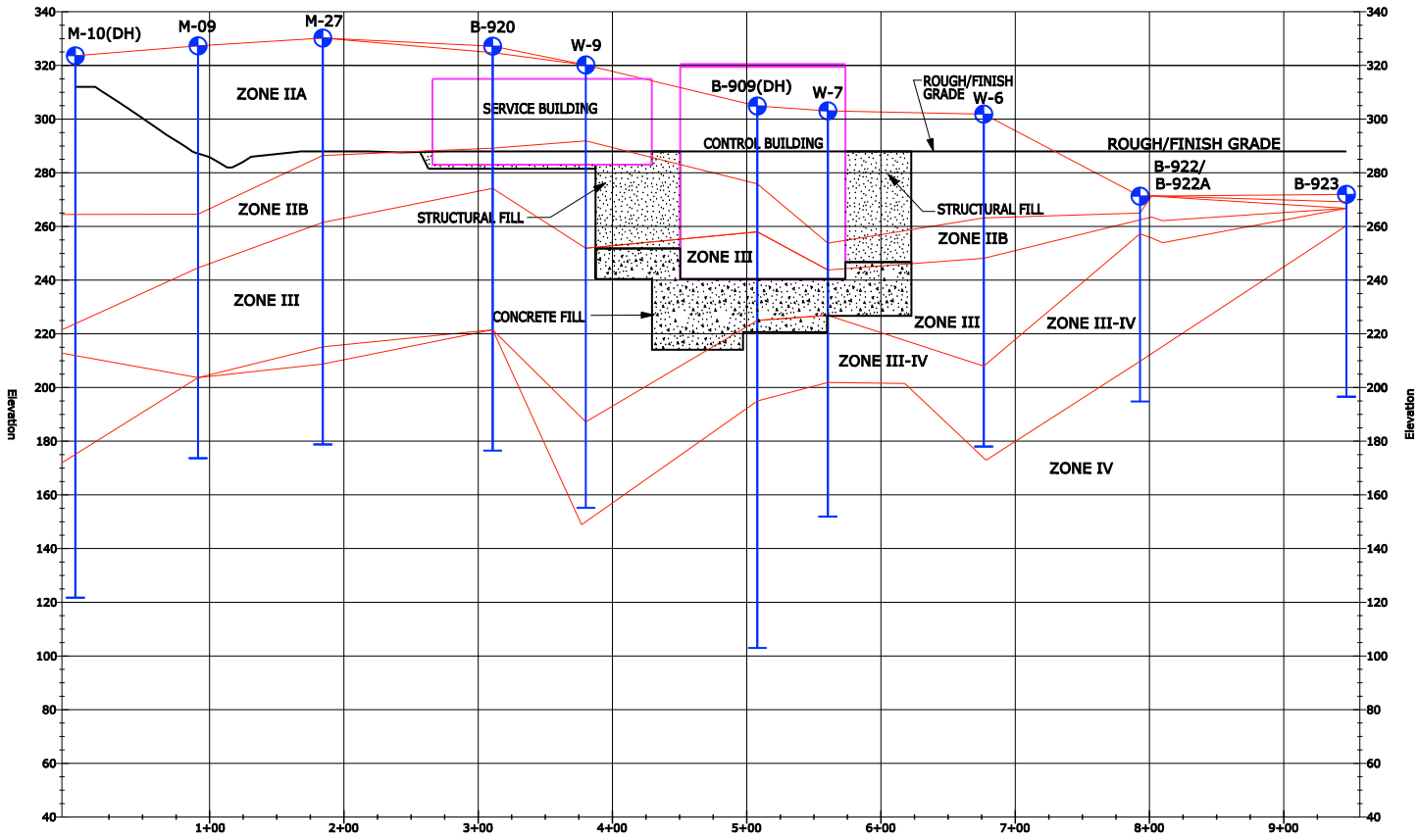

NOTE:
THE CONVERSION FROM NAVD88 DATUM ELEVATIONS TO NGVD29 DATUM ELEVATIONS IS +0.86 FT

EXCAVATION PROFILE G-G

0 40 80 160 240FT

VERTICAL EXAGGERATION = 2:1

LEGEND

STRUCTURAL FILL

CONCRETE FILL

B-901 BORING NUMBER

NAPS ESP COL 2.5-3 Figure 2.5.4-232 Subsurface Profile H-H with Foundation Outline

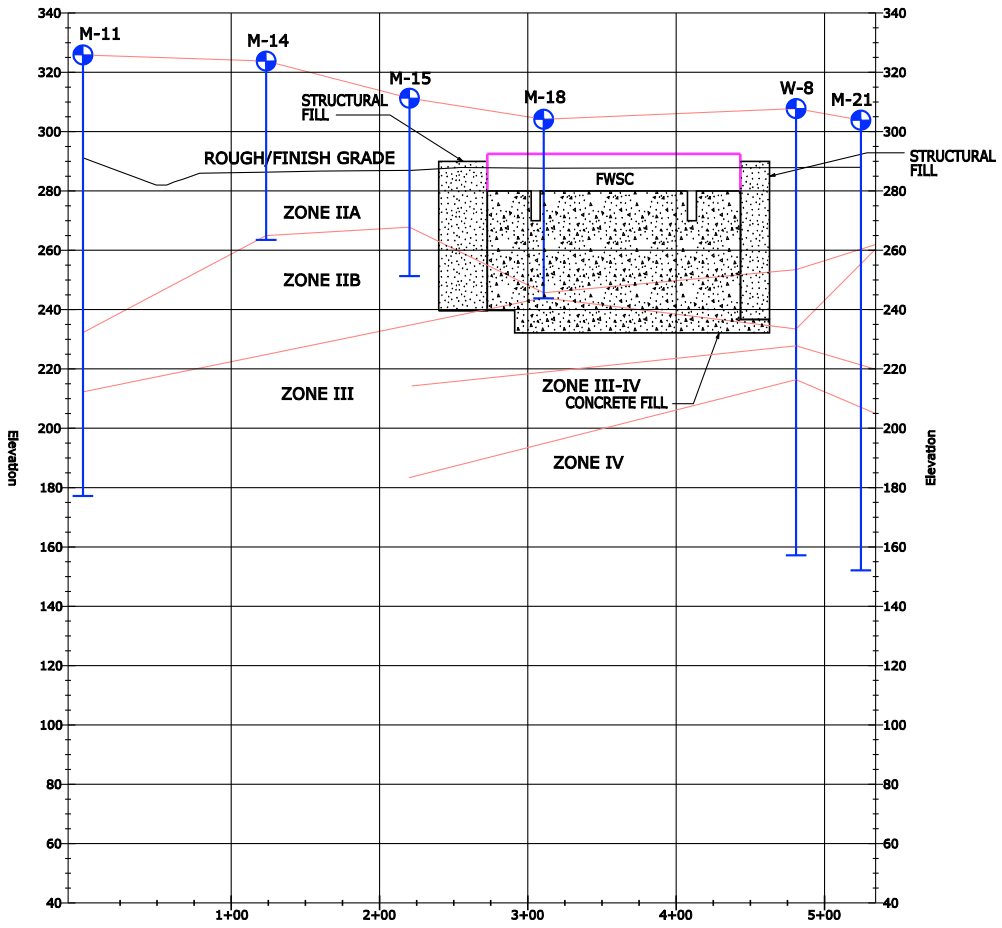

NOTE:
THE CONVERSION FROM NAVD88 DATUM ELEVATIONS TO NGVD29 DATUM ELEVATIONS IS +0.86 FT

EXCAVATION PROFILE H-H

0 40 80 160 240FT

VERTICAL EXAGGERATION = 2:1

LEGEND

STRUCTURAL FILL

CONCRETE FILL

B-901 BORING NUMBER

NAPS ESP COL 2.5-3 Figure 2.5.4-233 Subsurface Profile J-J with Foundation Outline

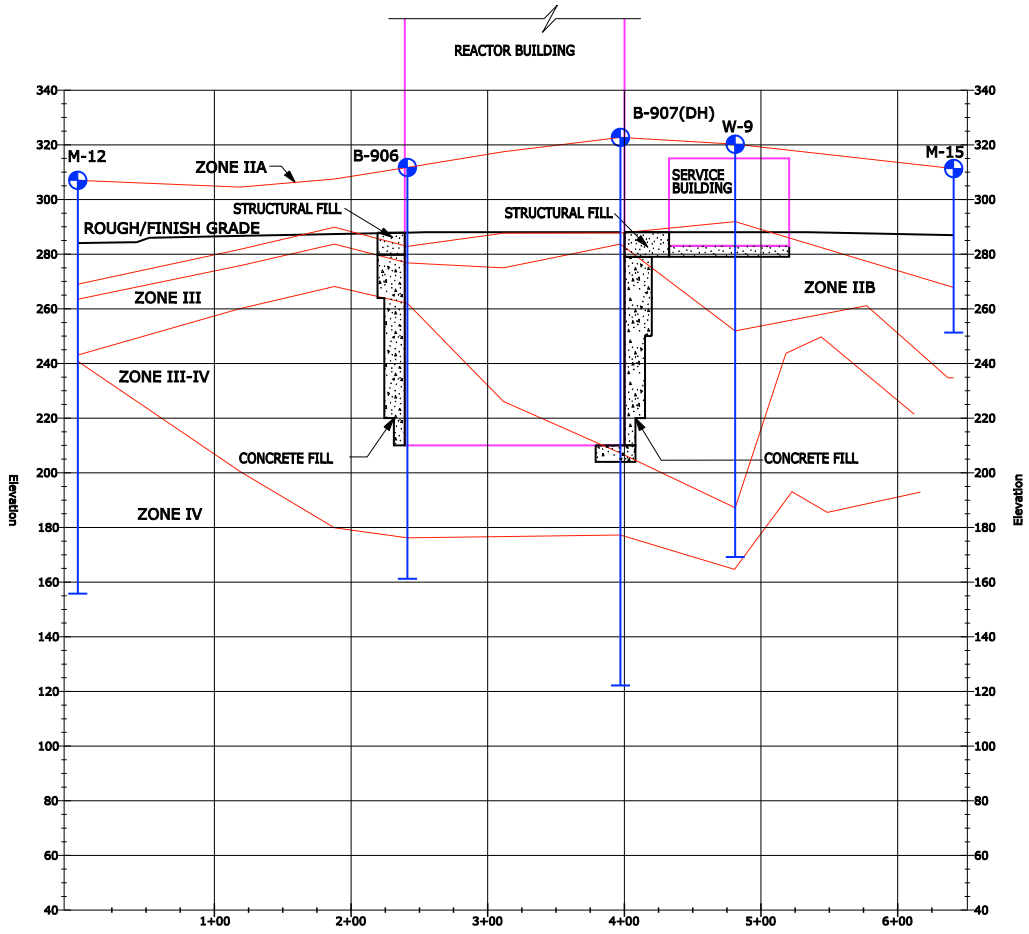

NOTE:
THE CONVERSION FROM NAVD88 DATUM ELEVATIONS TO NGVD29 DATUM ELEVATIONS IS +0.86 FT

EXCAVATION PROFILE J-J

0 40 80 160 240FT

VERTICAL EXAGGERATION = 2:1

LEGEND

STRUCTURAL FILL

CONCRETE FILL

B-901 BORING NUMBER

NAPS ESP COL 2.5-3 Figure 2.5.4-234 Subsurface Profile K-K with Foundation Outline

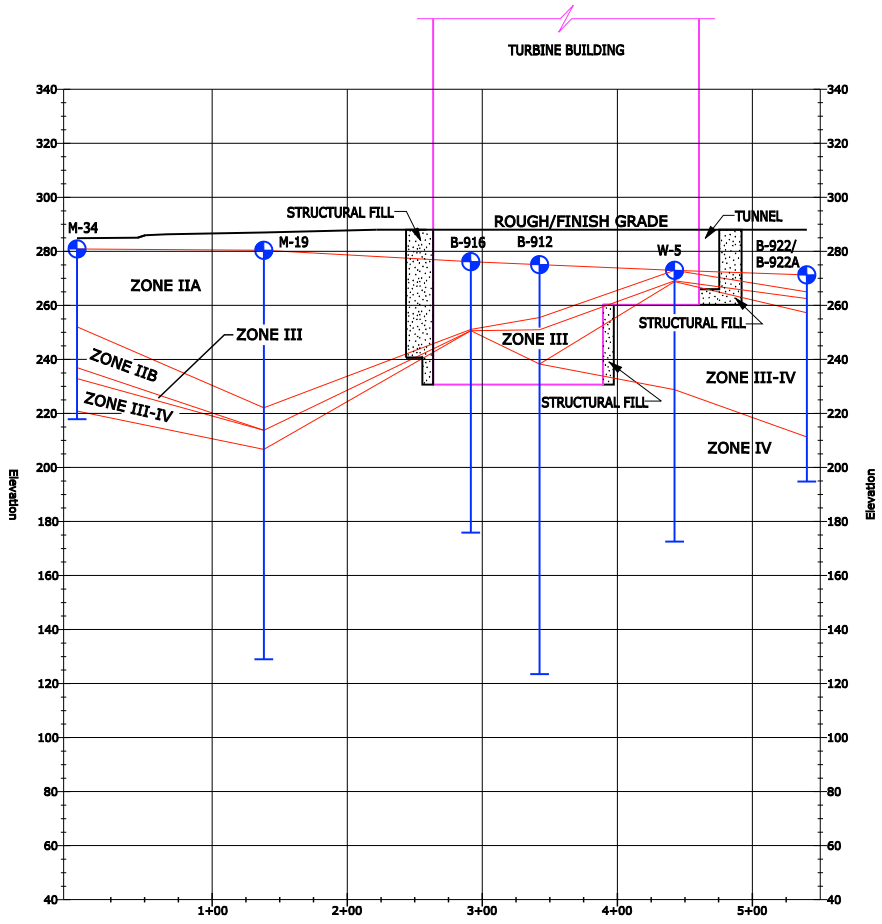

NOTE:
THE CONVERSION FROM NAVD88 DATUM ELEVATIONS TO NGVD29 DATUM ELEVATIONS IS +0.86 FT

EXCAVATION PROFILE K-K

0 40 80 160 240FT

VERTICAL EXAGGERATION = 2:1

LEGEND

STRUCTURAL FILL

CONCRETE FILL

BORING NUMBER

B-901

NAPS 2.0-29-A

Figure 2.5.4-235 Measured Compression Wave Velocity versus Depth

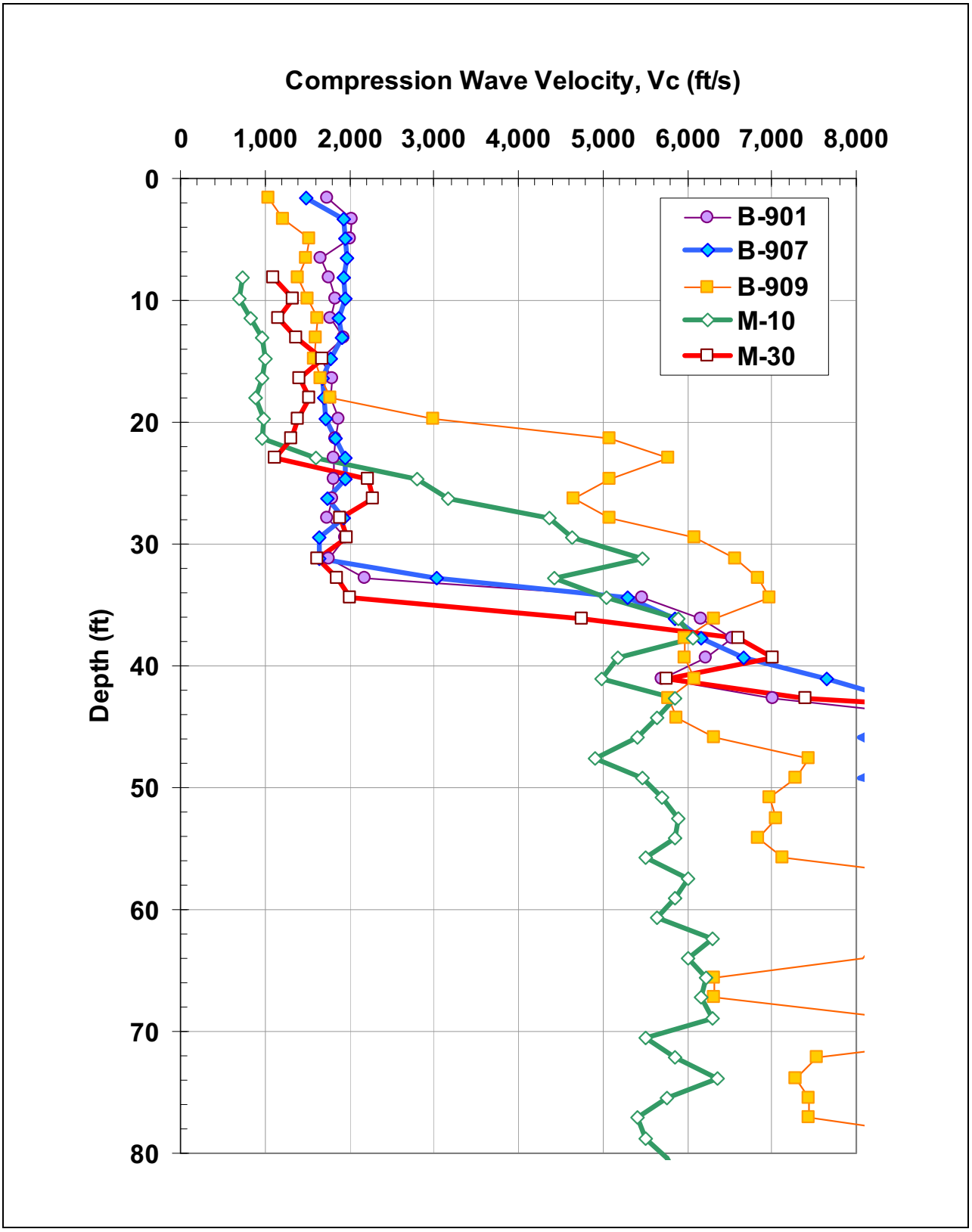

NAPS 2.0-29-A

Figure 2.5.4-236 Soil Poisson's Ratio versus Depth

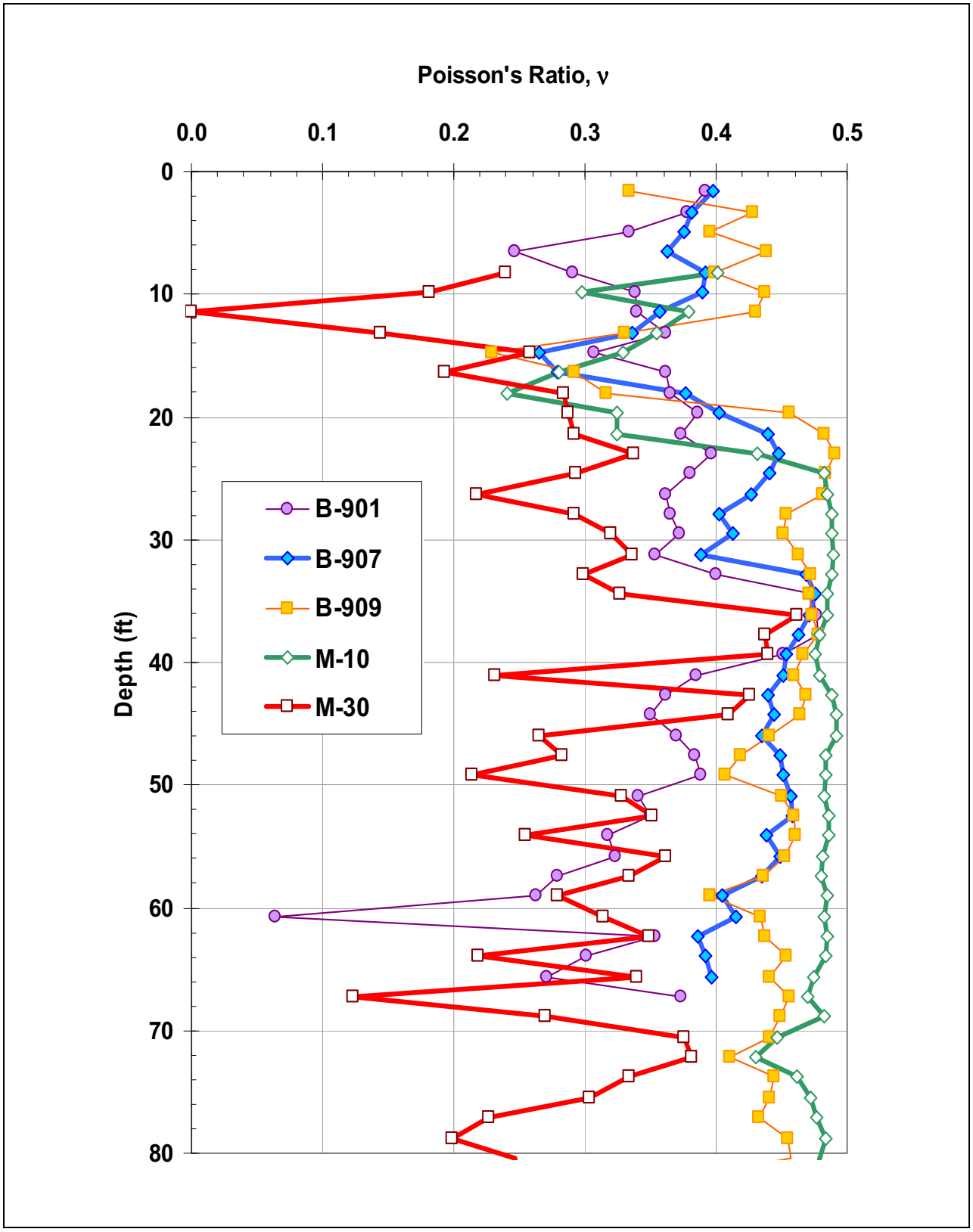

NAPS 2.0-29-A **Figure 2.5.4-237 Bedrock Shear Wave Velocity versus Elevation**

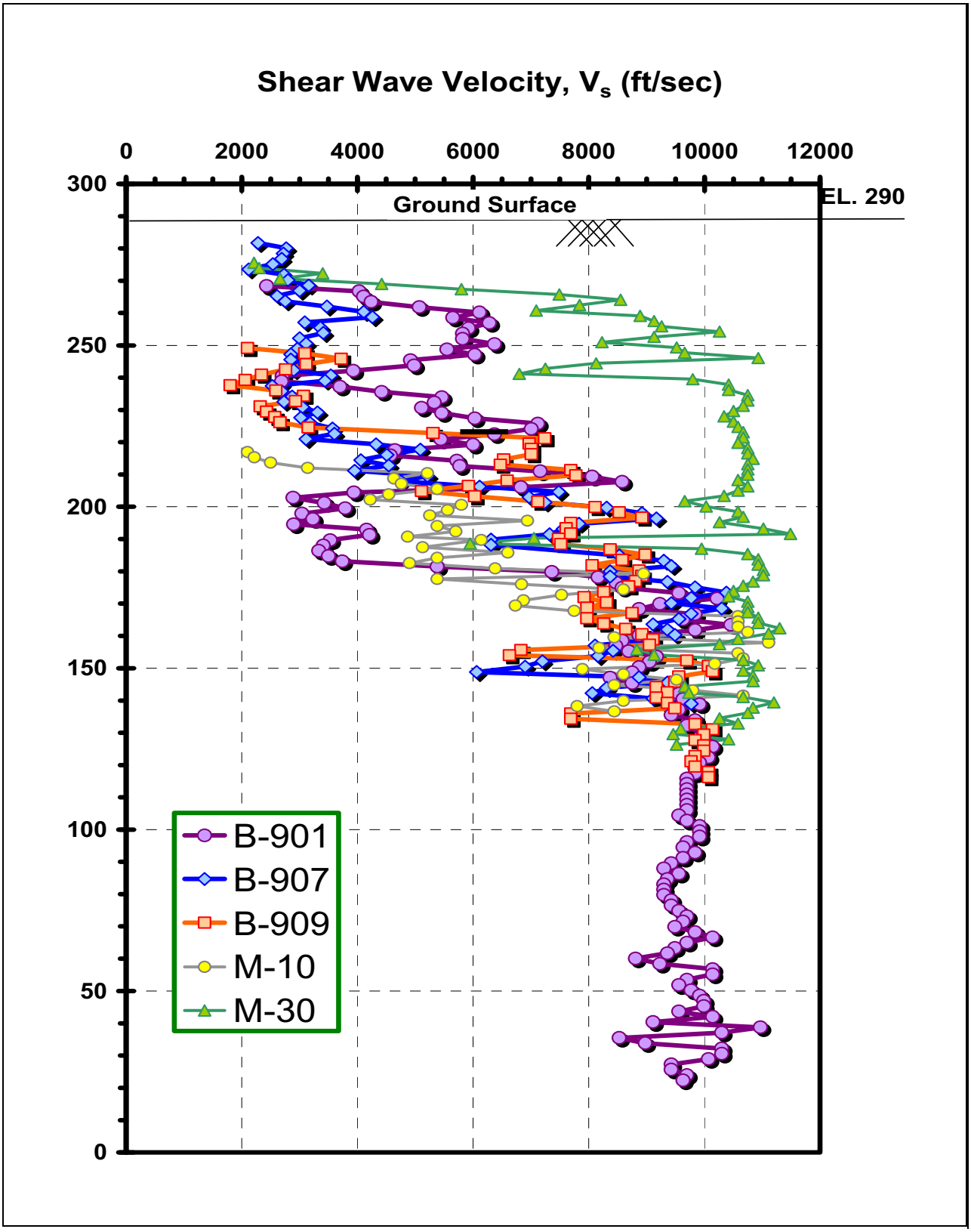

NAPS 2.0-29-A

Figure 2.5.4-238 Bedrock Compression Wave Velocity versus Elevation

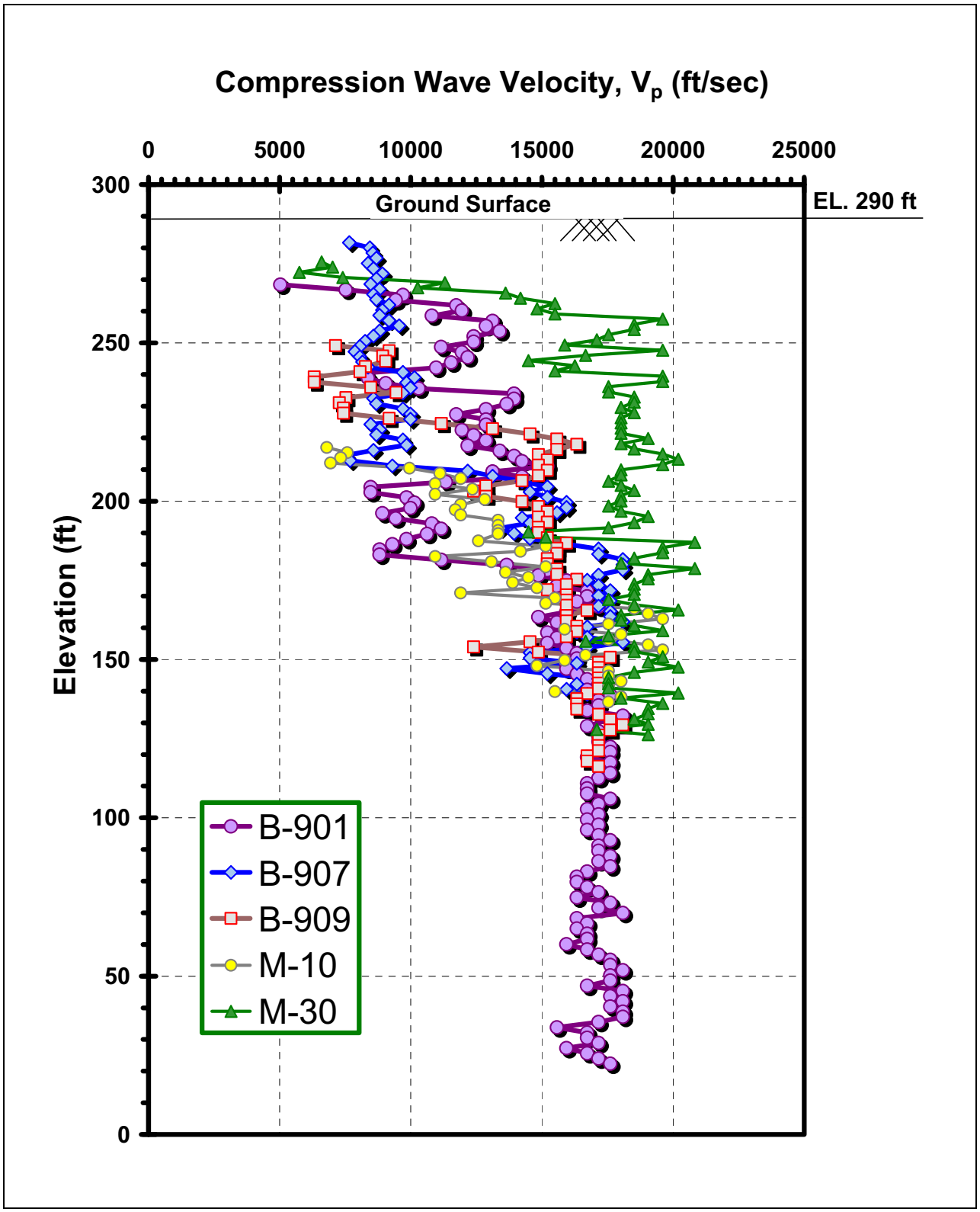

NAPS 2.0-29-A **Figure 2.5.4-239 Bedrock Poisson's Ratio versus Elevation**

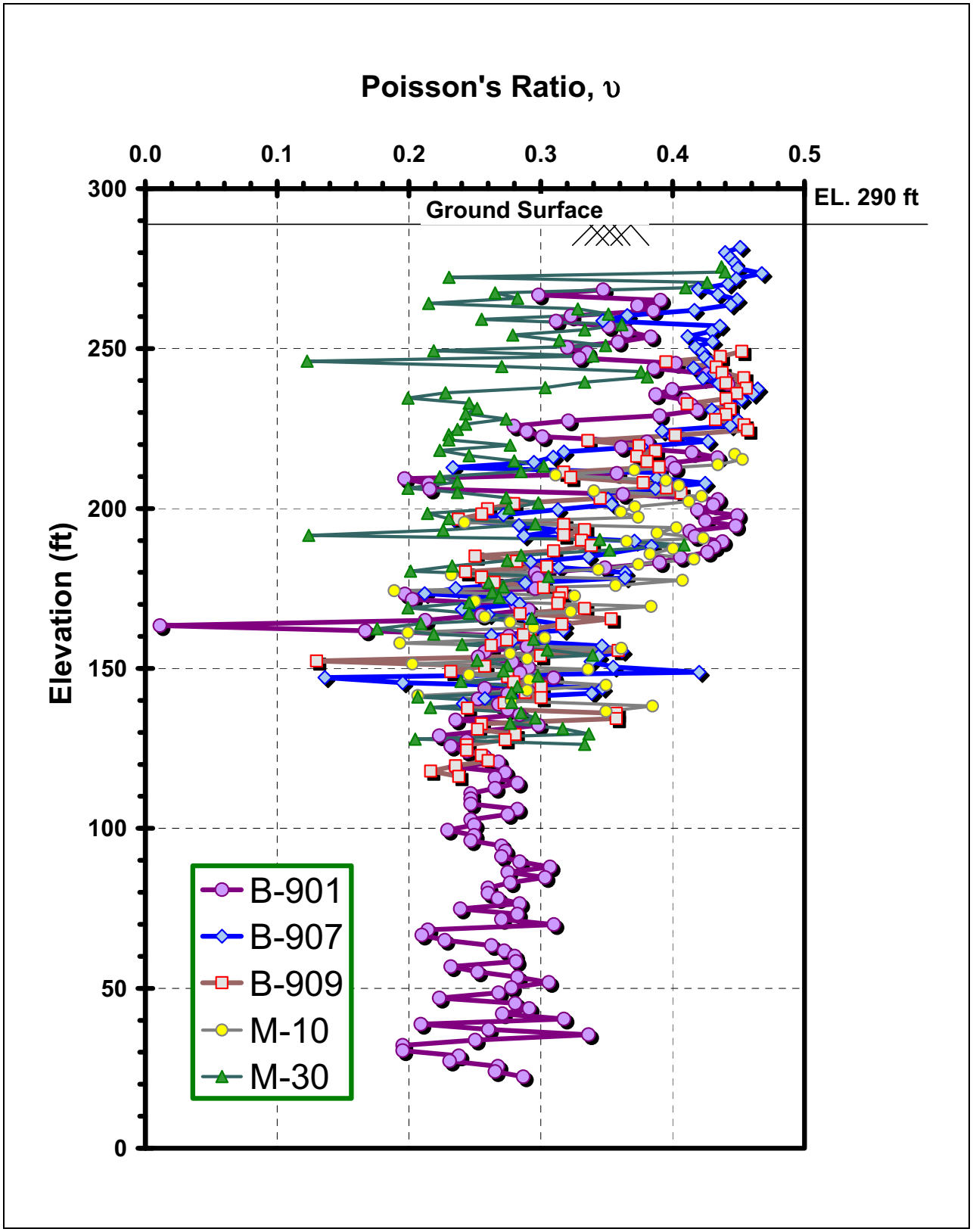

NAPS ESP COL 2.5-9 **Figure 2.5.4-240 VDOT Size No. 21A**

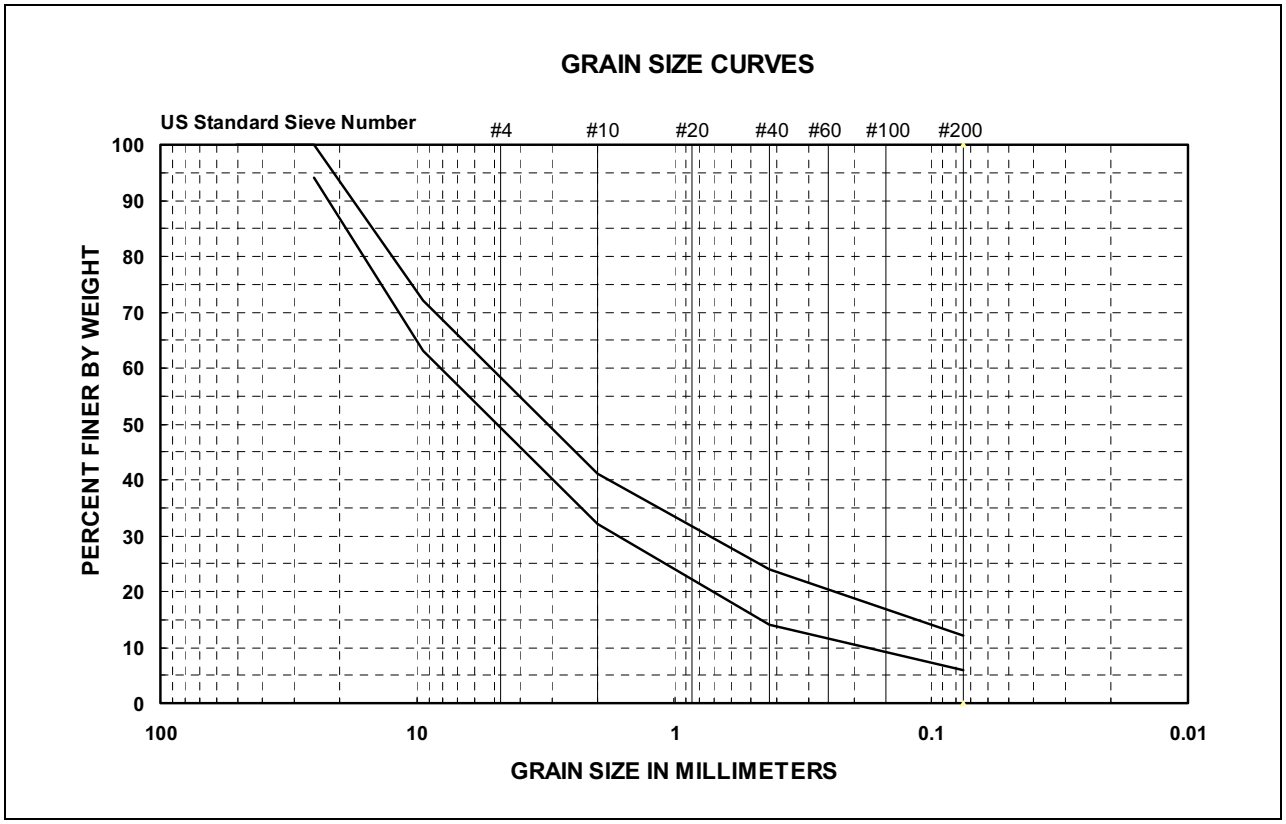

NAPS ESP COL 2.5-9 Figure 2.5.4-241 Bedrock Shear Wave Velocity Profiles 1 & 2 versus Elevation

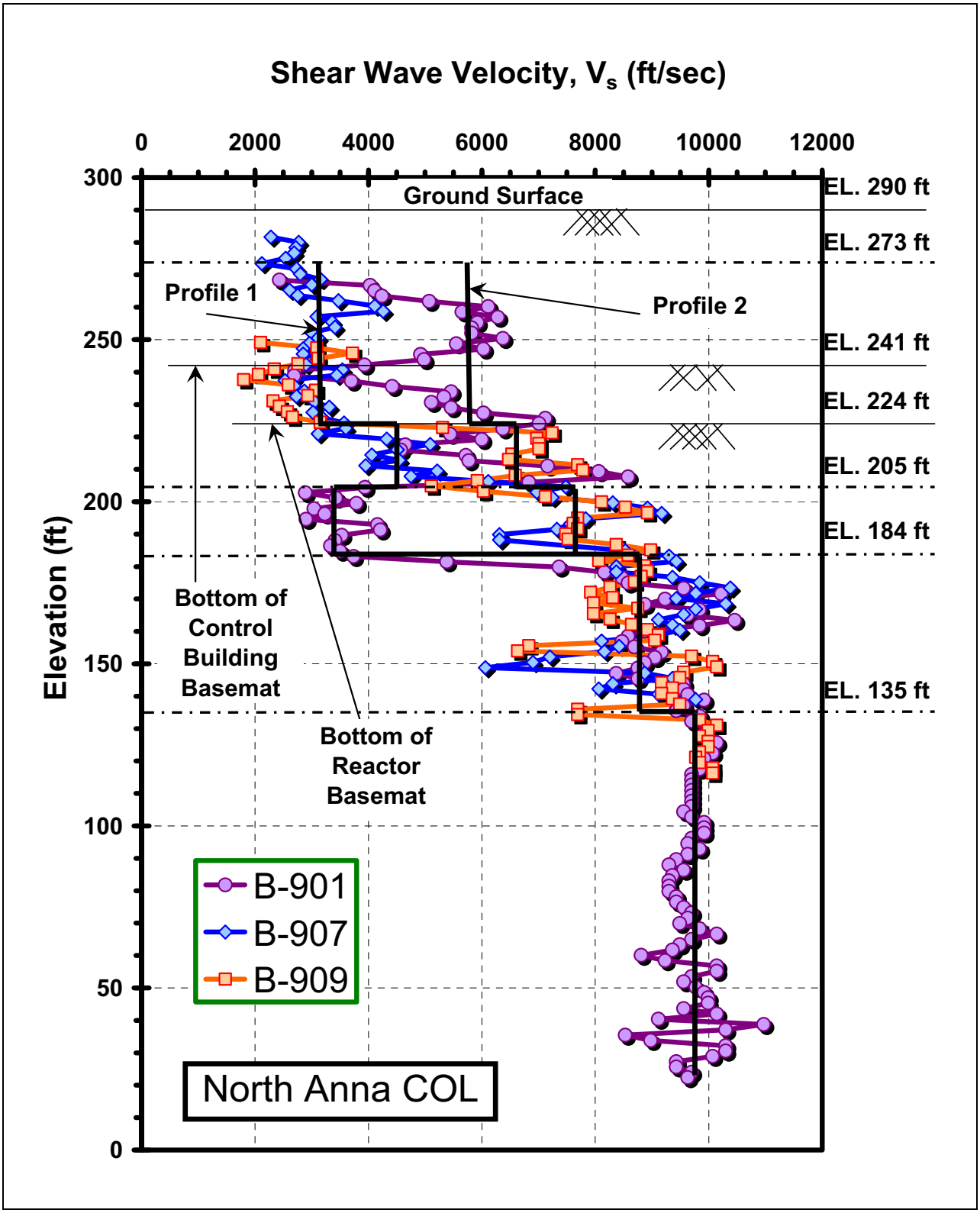

NAPS ESP COL 2.5-9 **Figure 2.5.4-242 Best Estimate Shear Wave Velocity Profiles for RB/FB and CB**

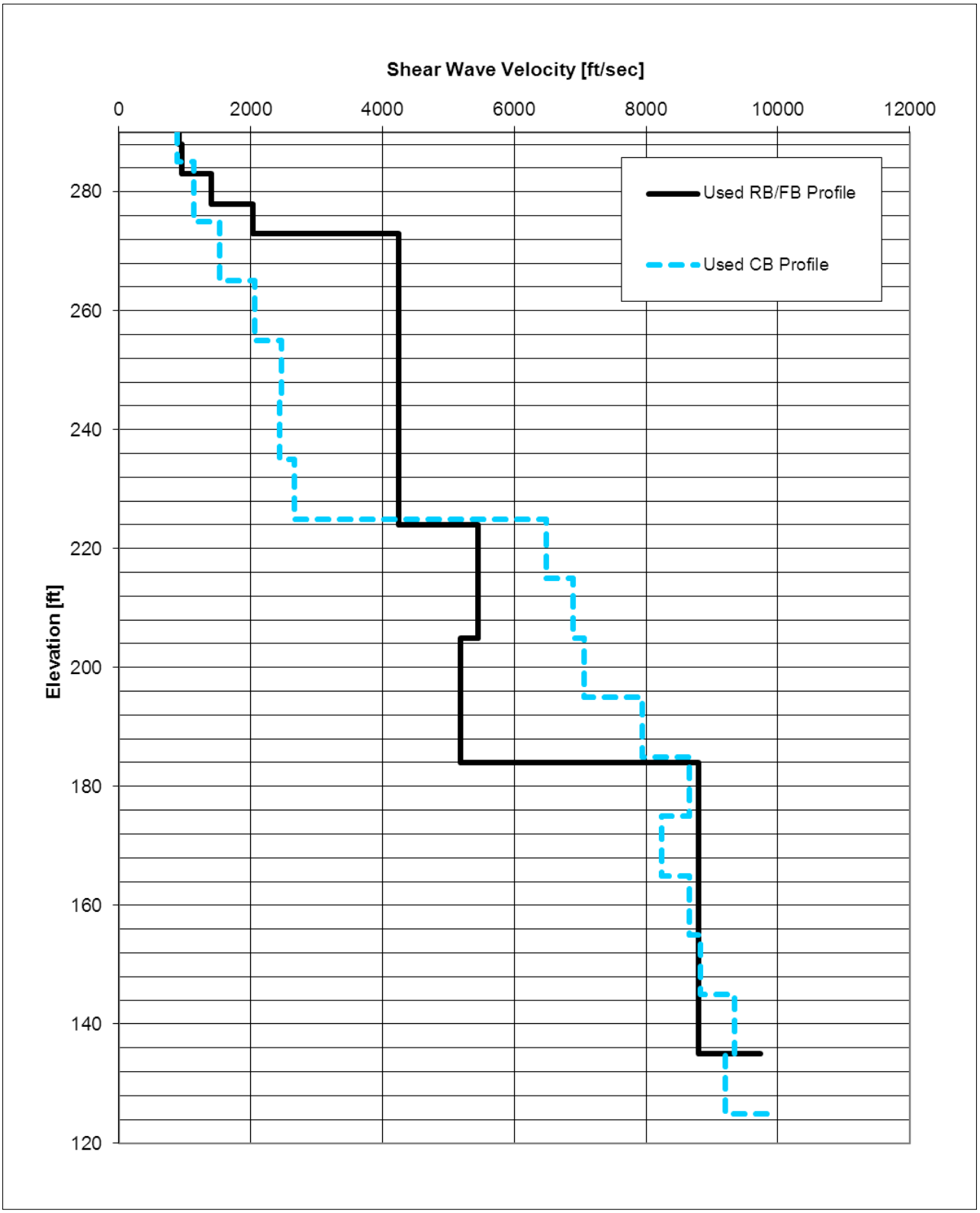

NAPS ESP COL 2.5-9 Figure 2.5.4-243 Best Estimate Shear Wave Velocity Profile for FWSC

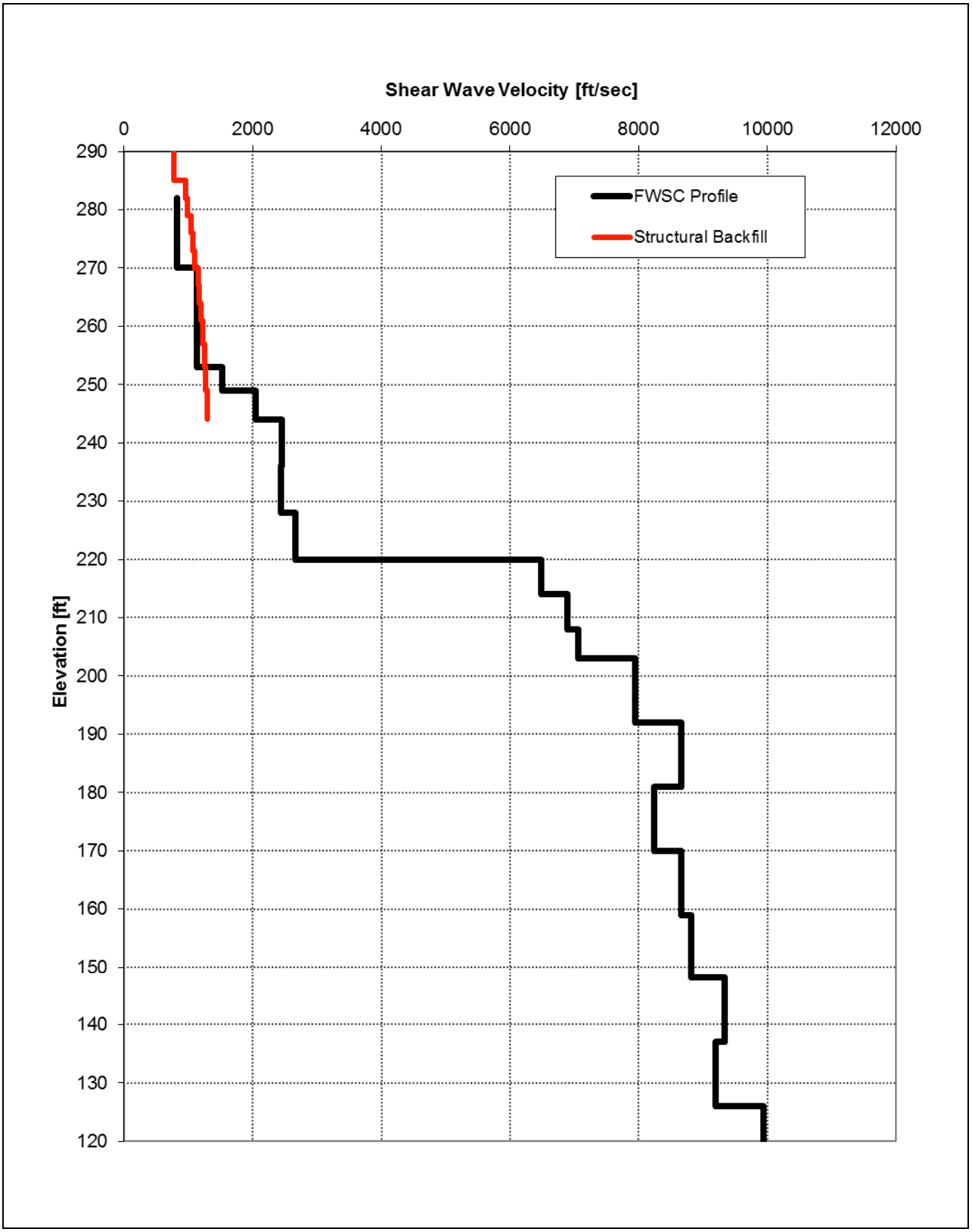

NAPS ESP COL 2.5-9 **Figure 2.5.4-244 Best Estimate Shear Wave Velocity Profile for Free-Field Slope**

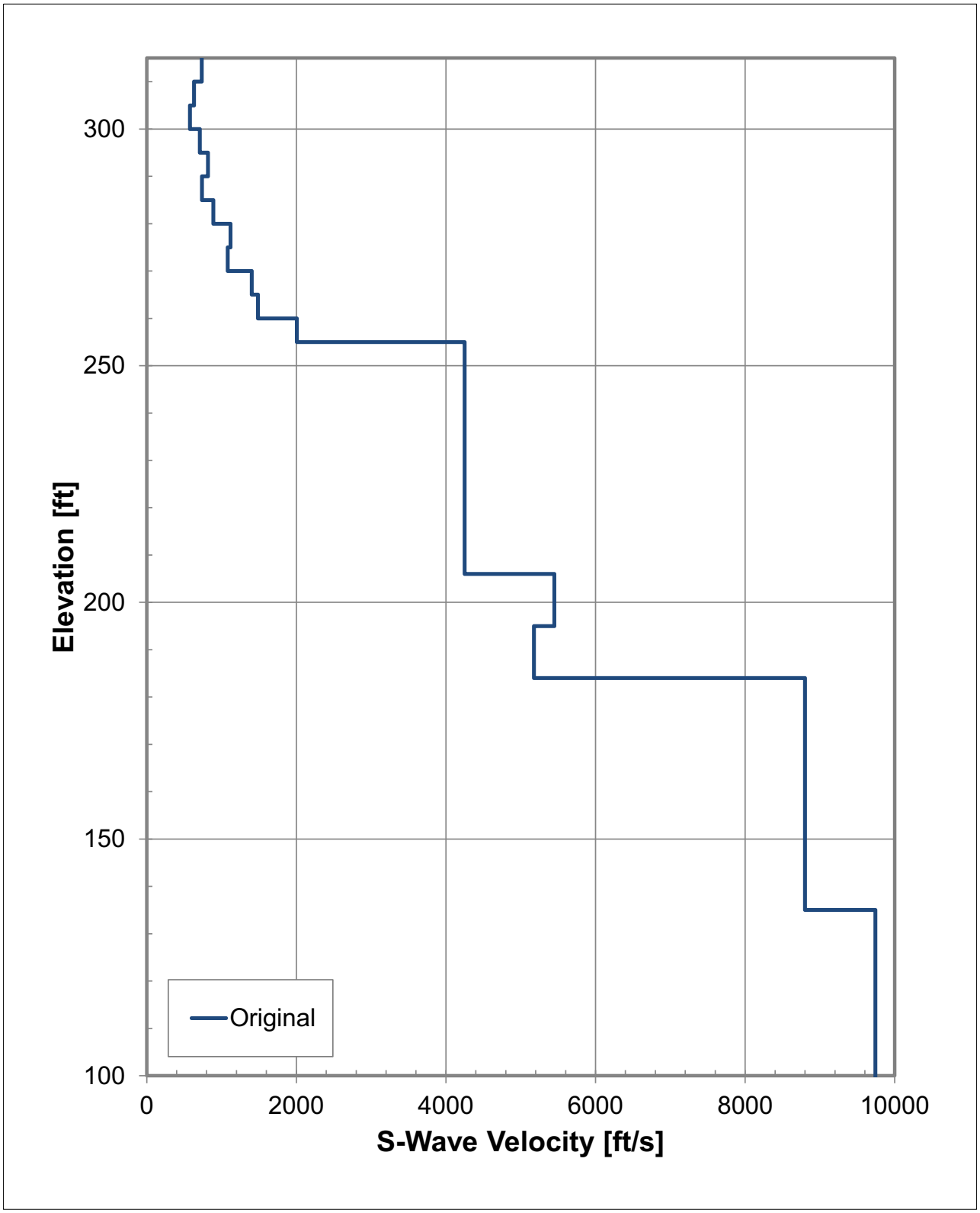

NAPS ESP COL 2.5-9 Figure 2.5.4-245 Best Estimate Shear Wave Velocity Profile for Structural Fill

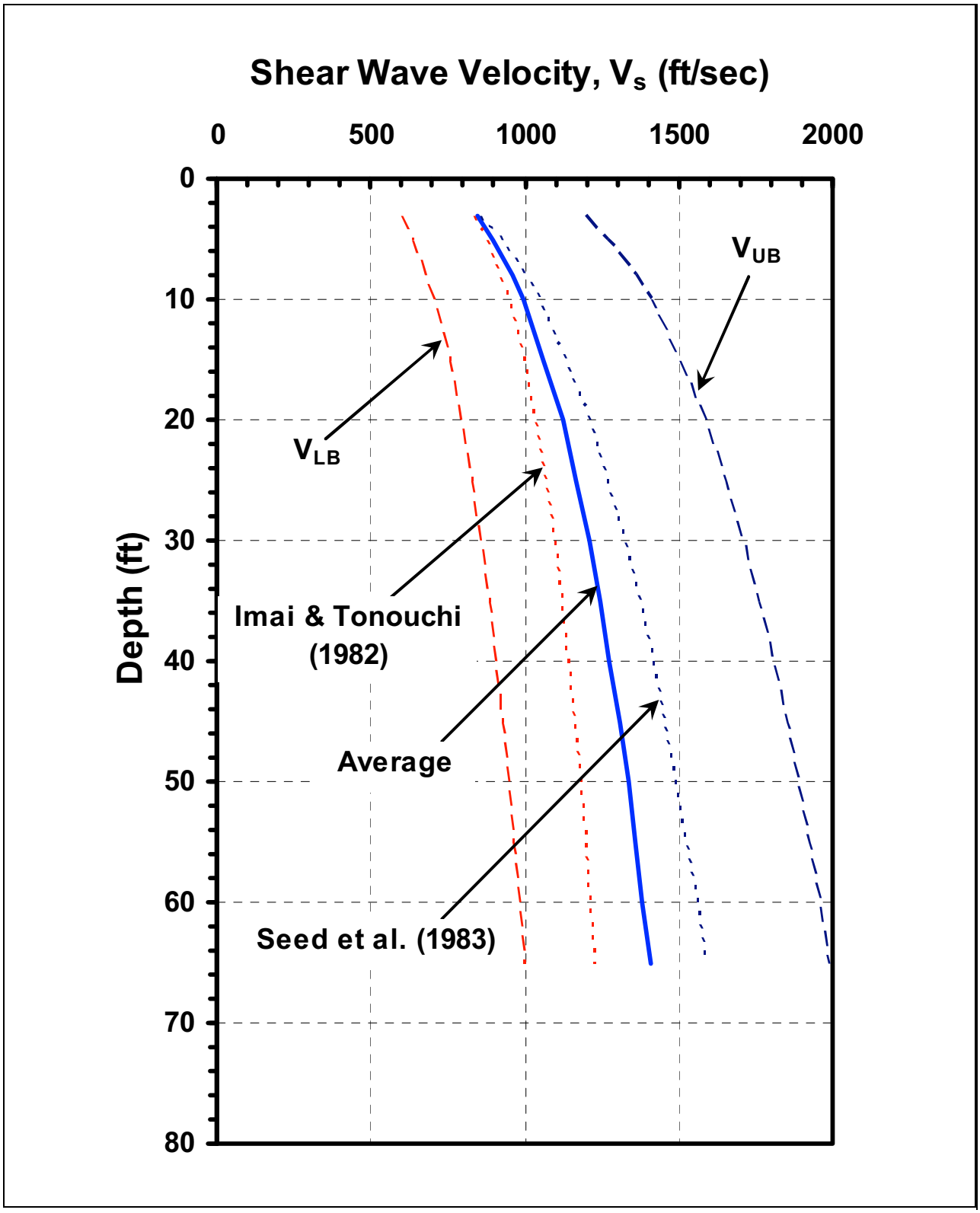

NAPS ESP COL 2.5-9 **Figure 2.5.4-246 Best Estimate Shear Wave Velocity Profile for Structural Fill in 5-Foot Intervals**

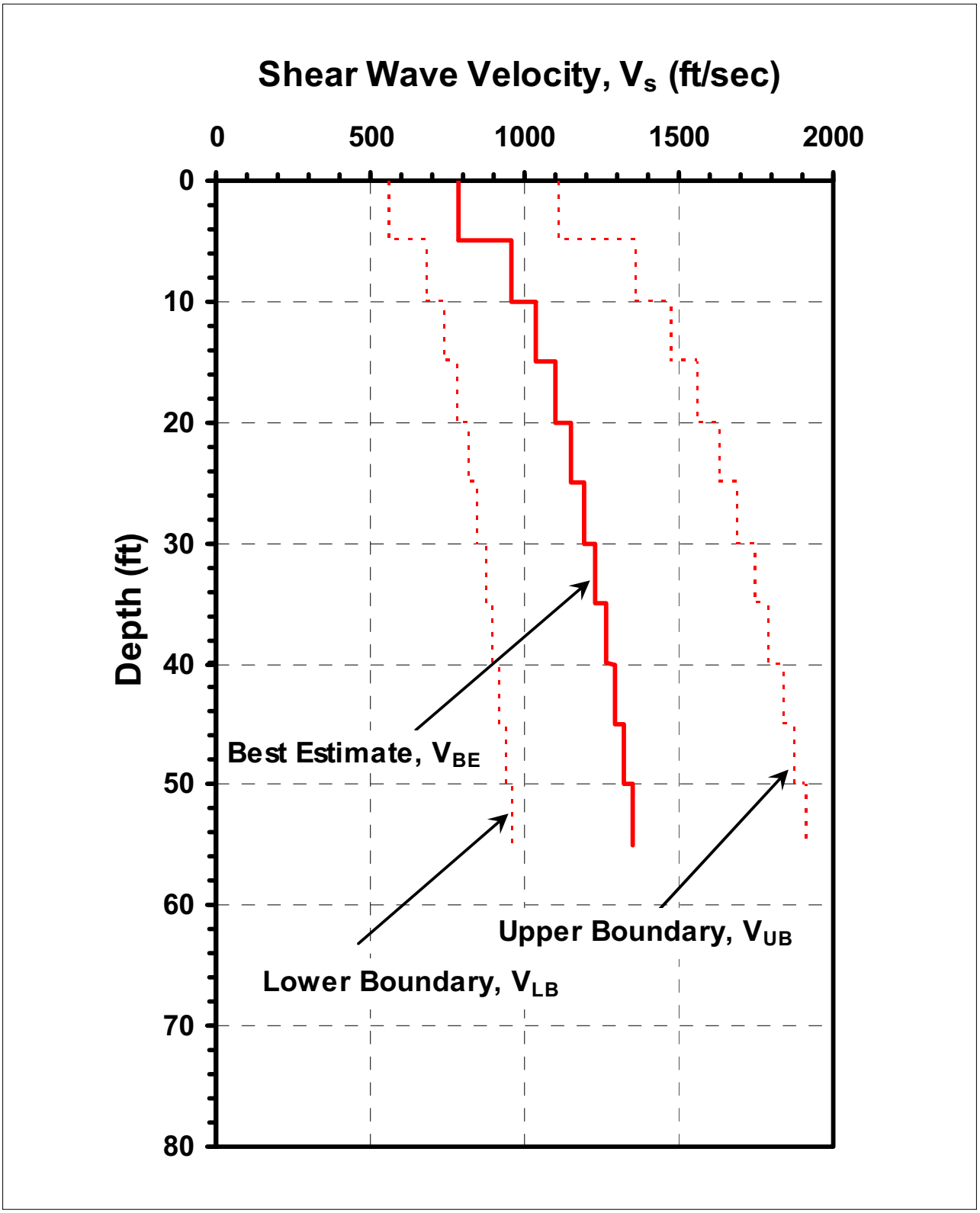

NAPS COL 2.0-29-A **Figure 2.5.4-247 Shear Modulus Reduction Design Curves**

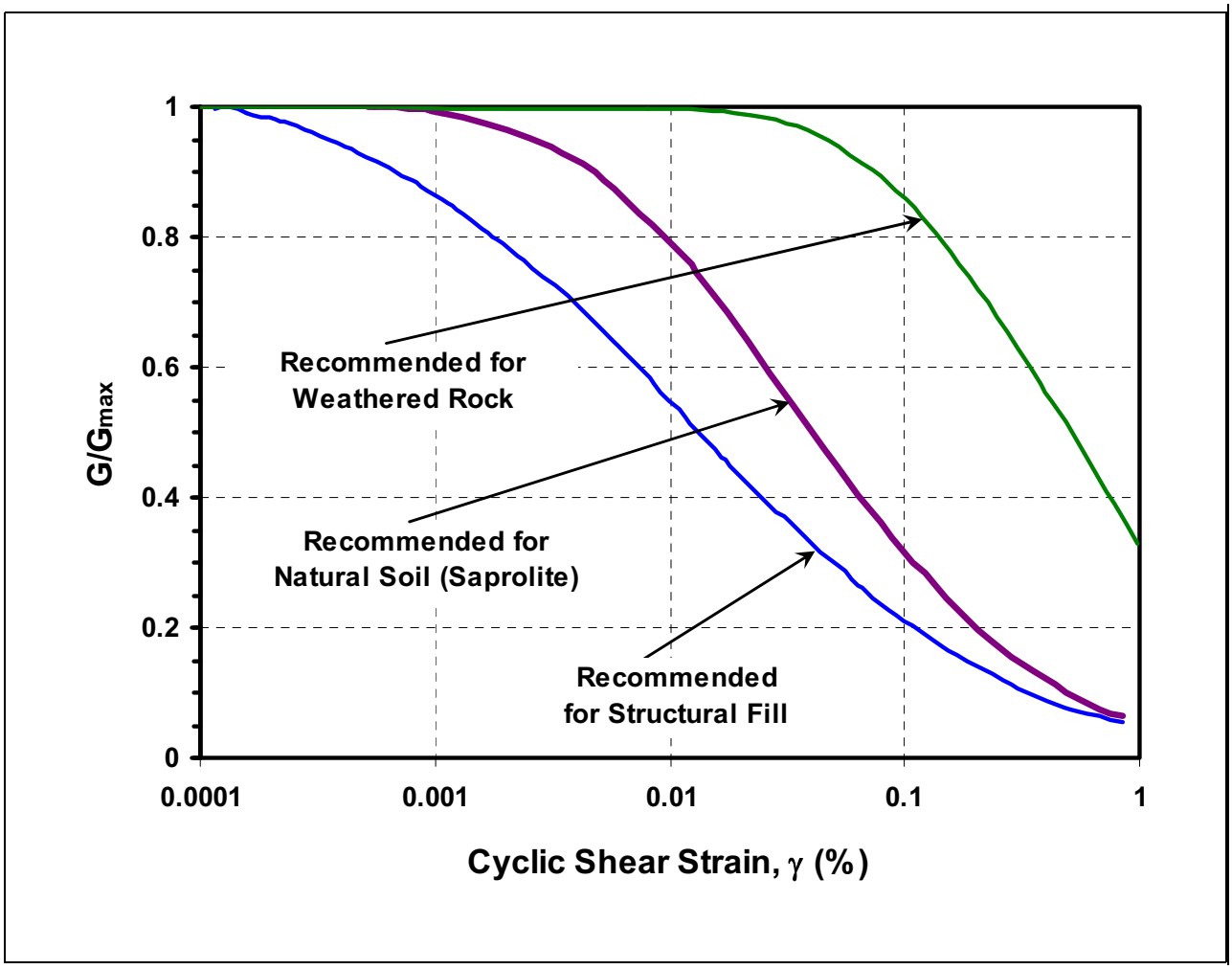

NAPS COL 2.0-29-A **Figure 2.5.4-248 RCTS Results with G/G_{max} and D Curve G/G_{max} vs. Strain, B-901 UD-1: 4.3 psi Confining Pressure (Sheet 1 of 3)**

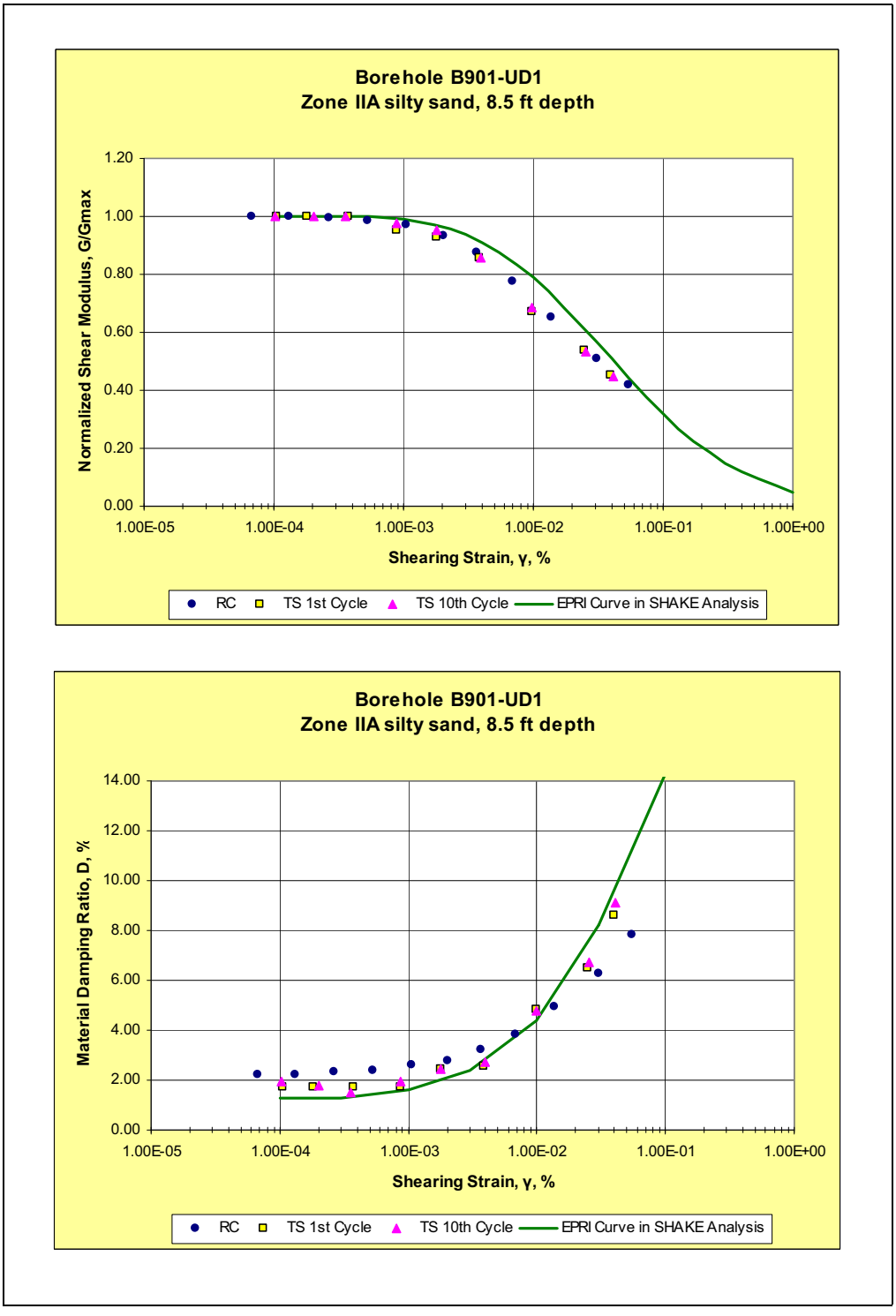

NAPS COL 2.0-29-A **Figure 2.5.4-248 RCTS Results with G/G_{max} and D Curve G/G_{max} vs. Strain, B-911A UD-1: 5.6 psi Confining Pressure (Sheet 2 of 3)**

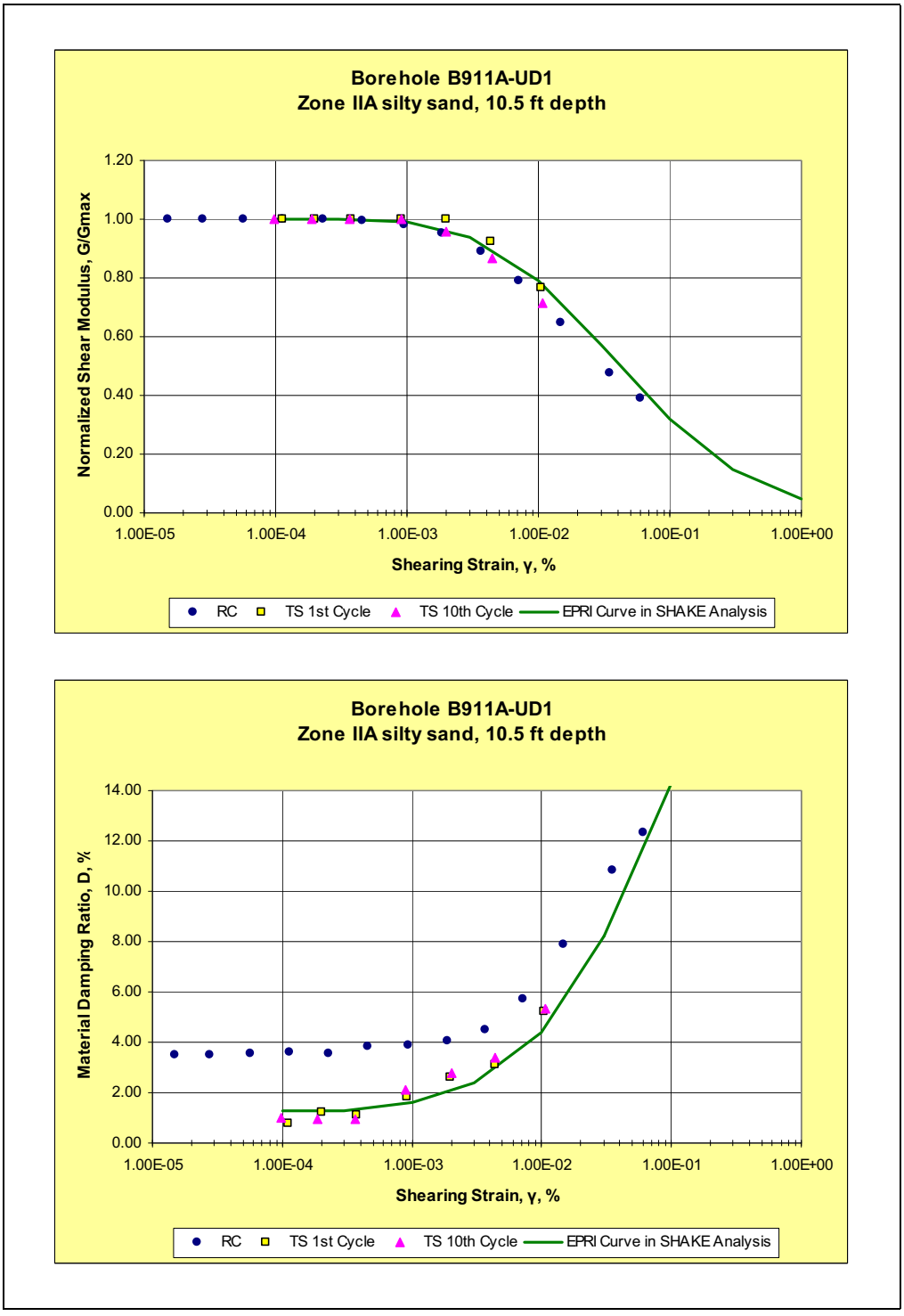

NAPS COL 2.0-29-A **Figure 2.5.4-248 RCTS Results with G/G_{max} and D Curve G/G_{max} vs. Strain, B-911A PB-1: 11.4 psi Confining Pressure (Sheet 3 of 3)**

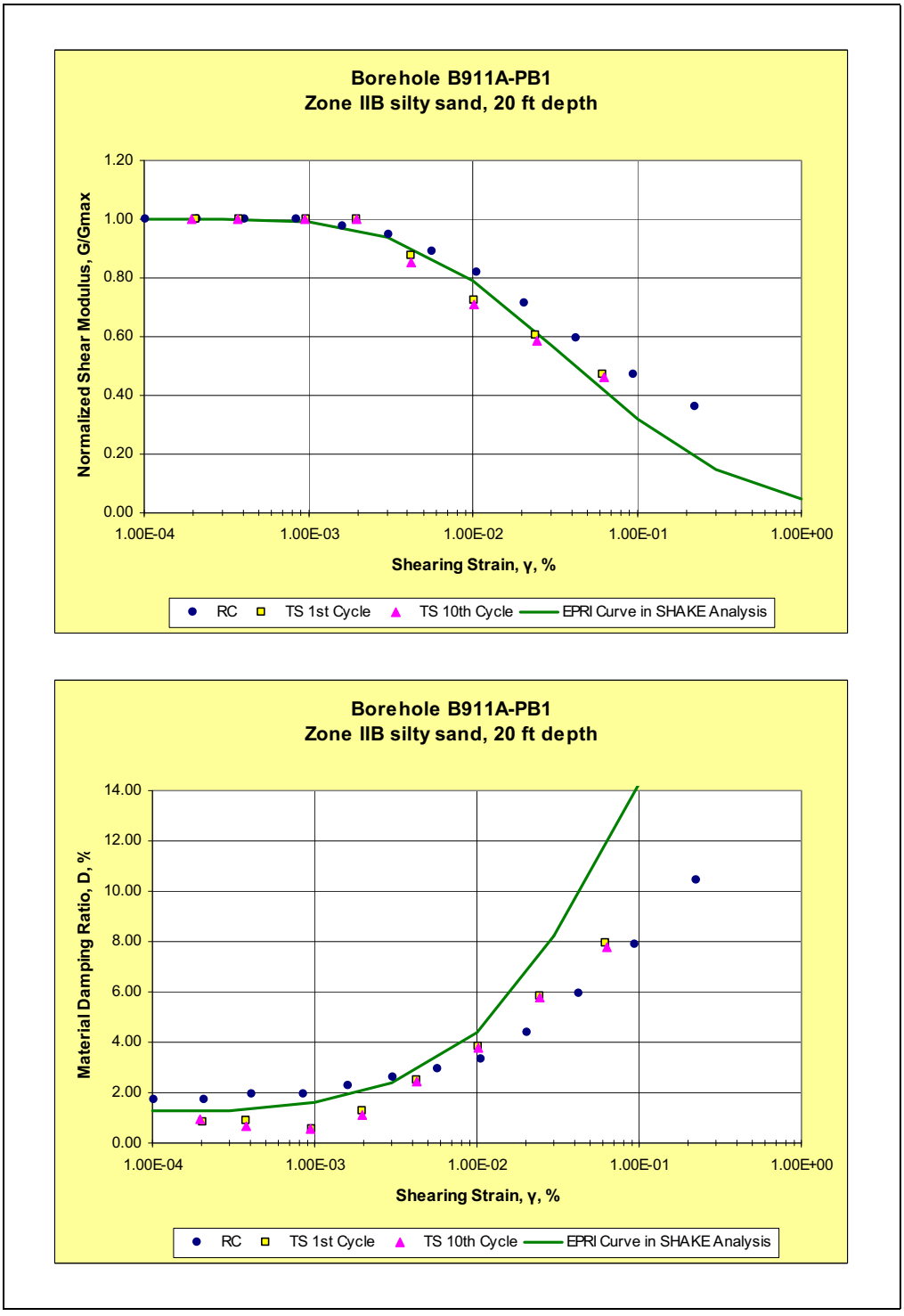

NAPS COL 2.0-29-A **Figure 2.5.4-249 Damping Ratio versus Cyclic Shear Strain**

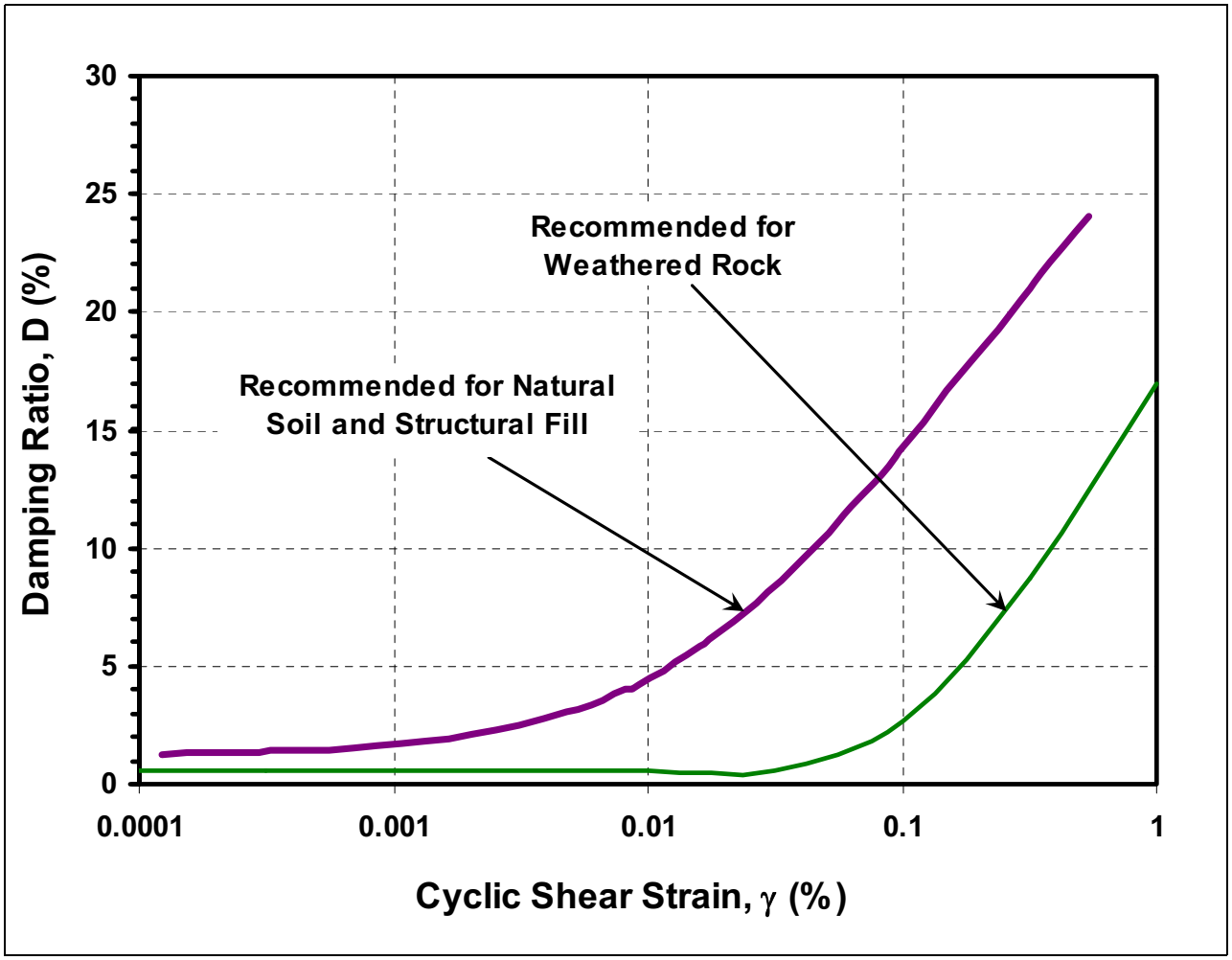

NAPS ESP COL 2.5-5 **Figure 2.5.4-250 Maximum Acceleration versus Depth for Free-Field Slope**

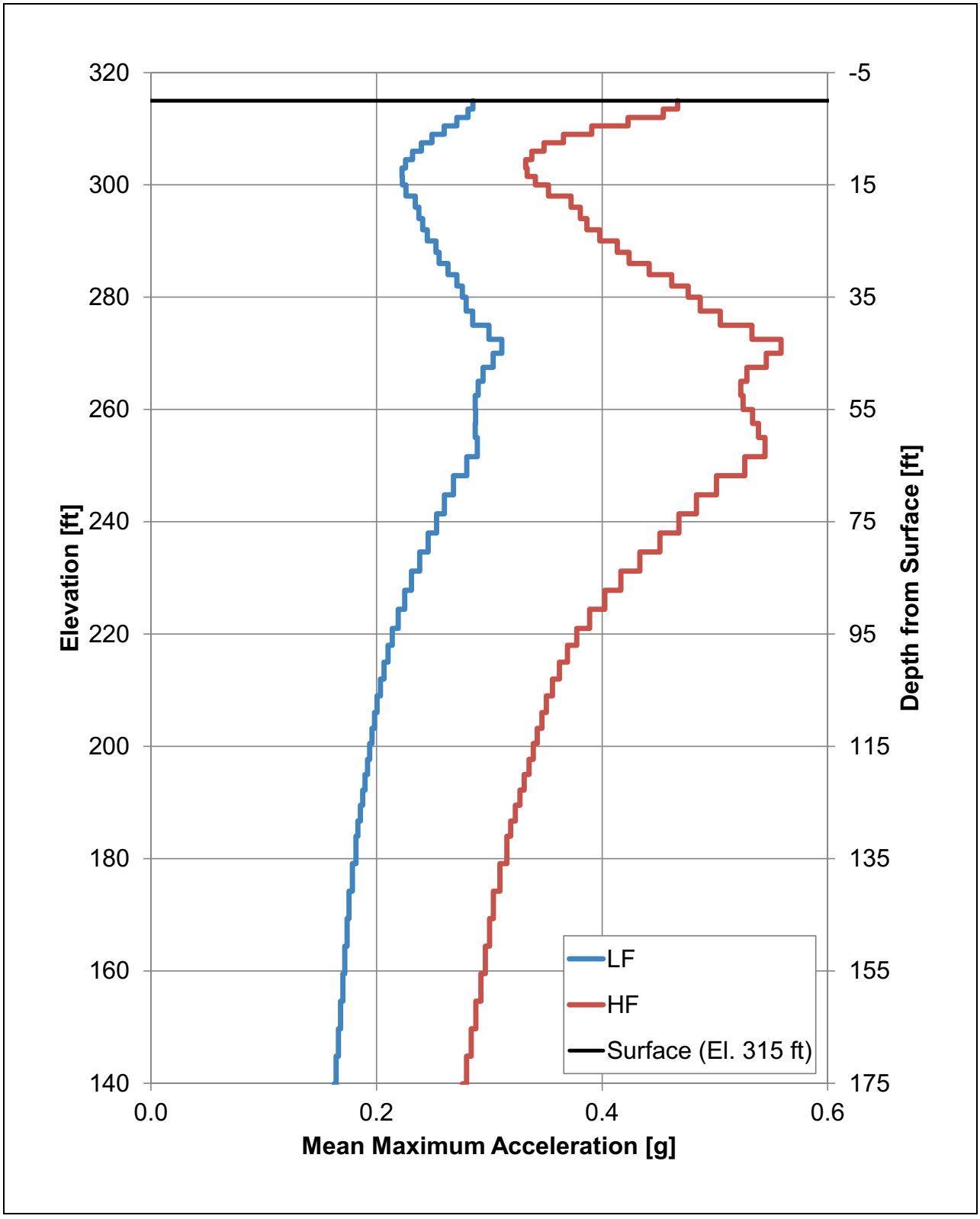

NAPS ESP COL 2.5-6 **Figure 2.5.4-251 Subsurface Profiles Below the Seismic Category I Structures: (a) Reactor/Fuel Building; (b) Control Building; (c) FWSC**

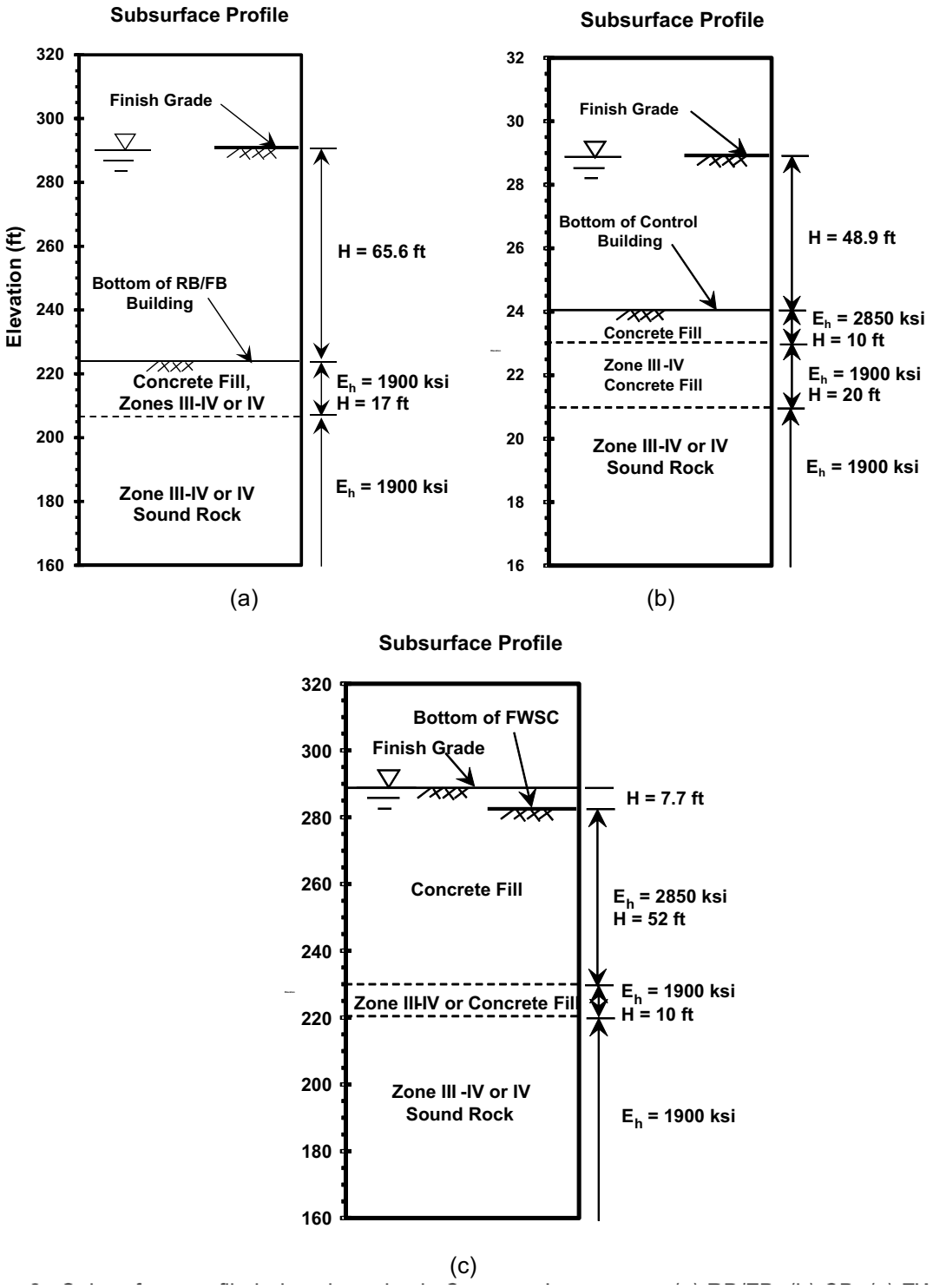

NAPS ESP COL 2.5-6 **Figure 2.5.4-252 Subsurface Profiles Below Non-Seismic Category I Structures: (a) Turbine Building; (b) Radwaste Building; (c) Service Building; (d) Ancillary Diesel Building**

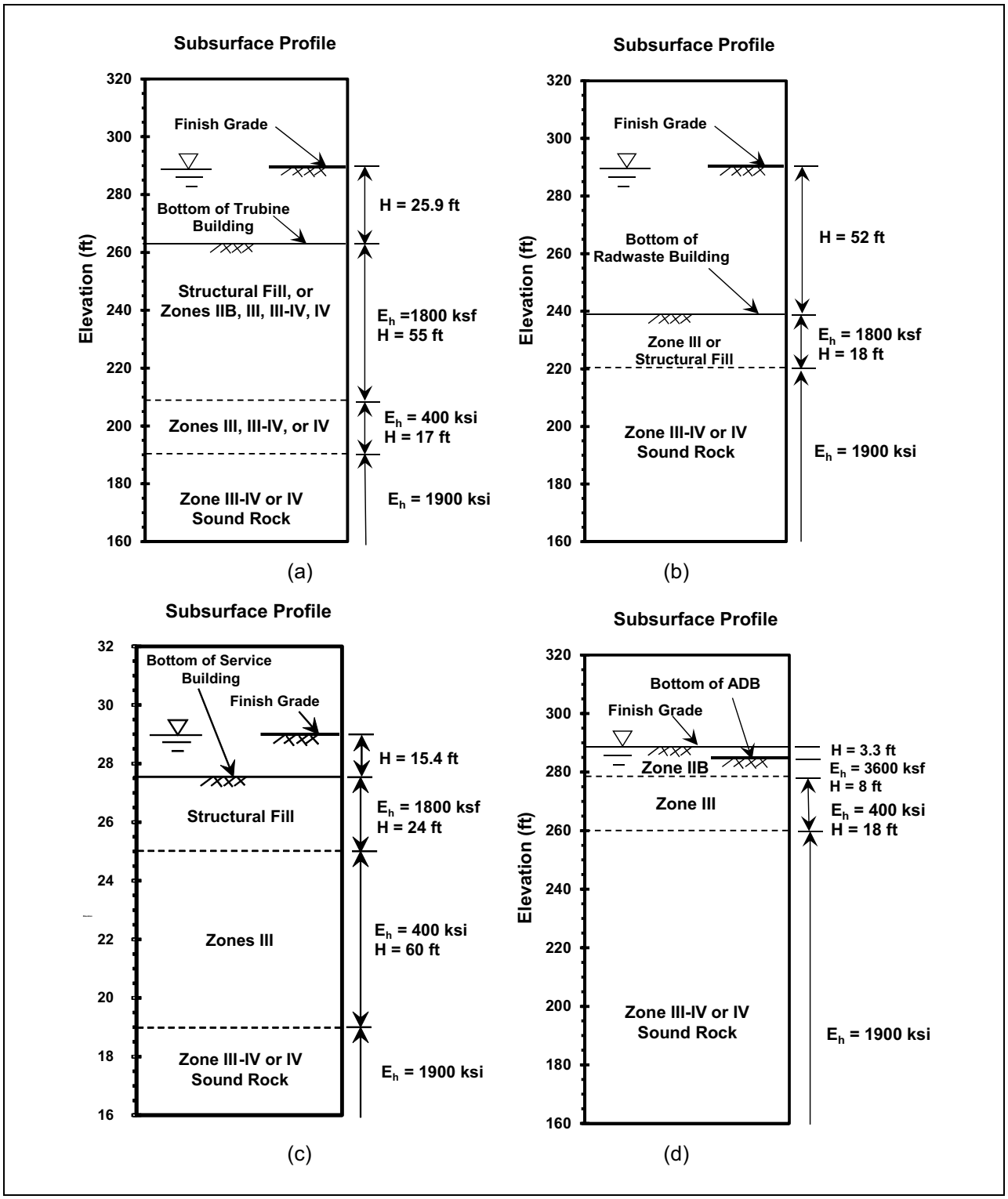

NAPS ESP COL 2.5-6 Figure 2.5.4-253 Lateral Pressure on Yielding Wall (Active Case)

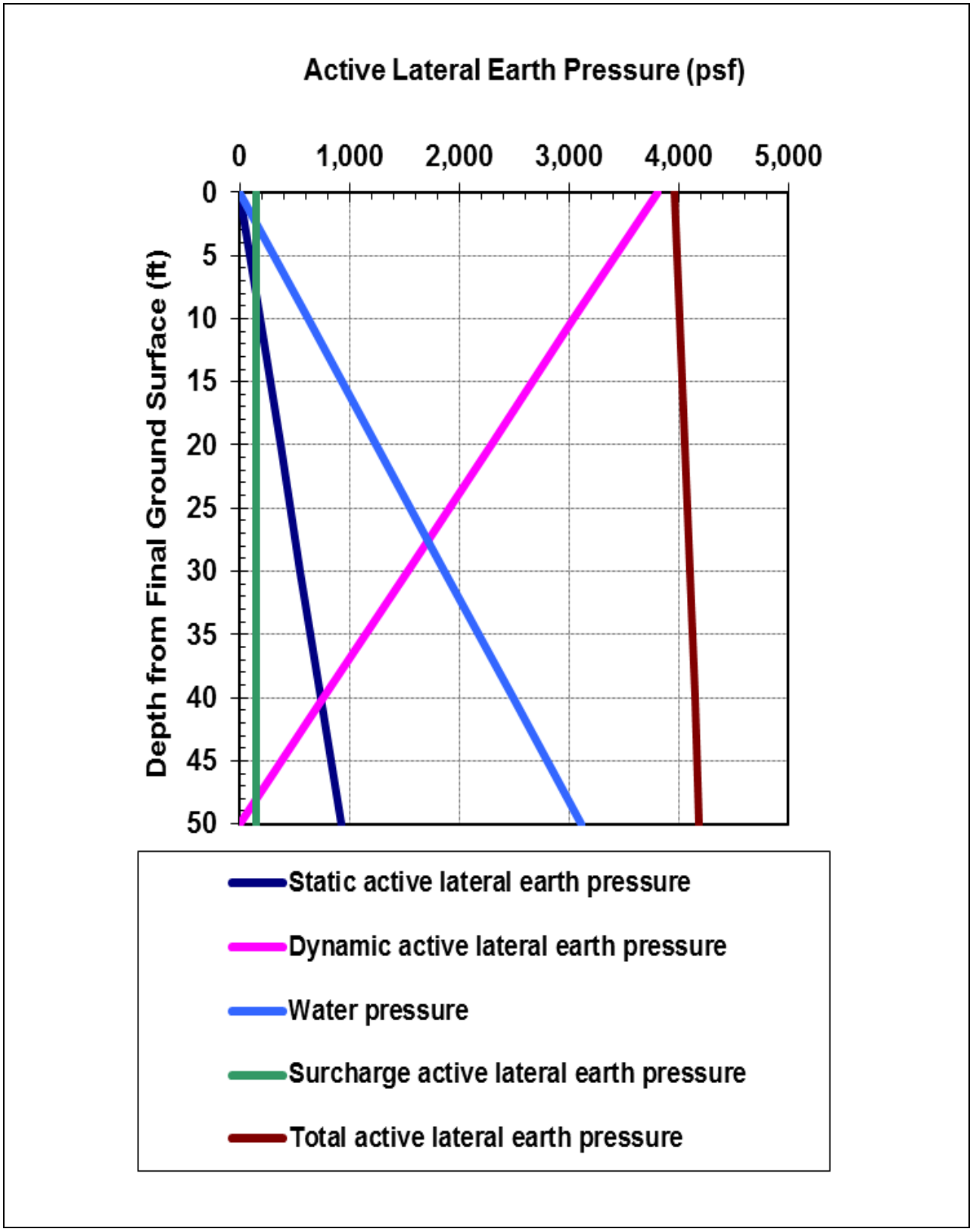

NAPS ESP COL 2.5-6 Figure 2.5.4-254 Lateral Pressure on Non-Yielding Wall (At-Rest Case)

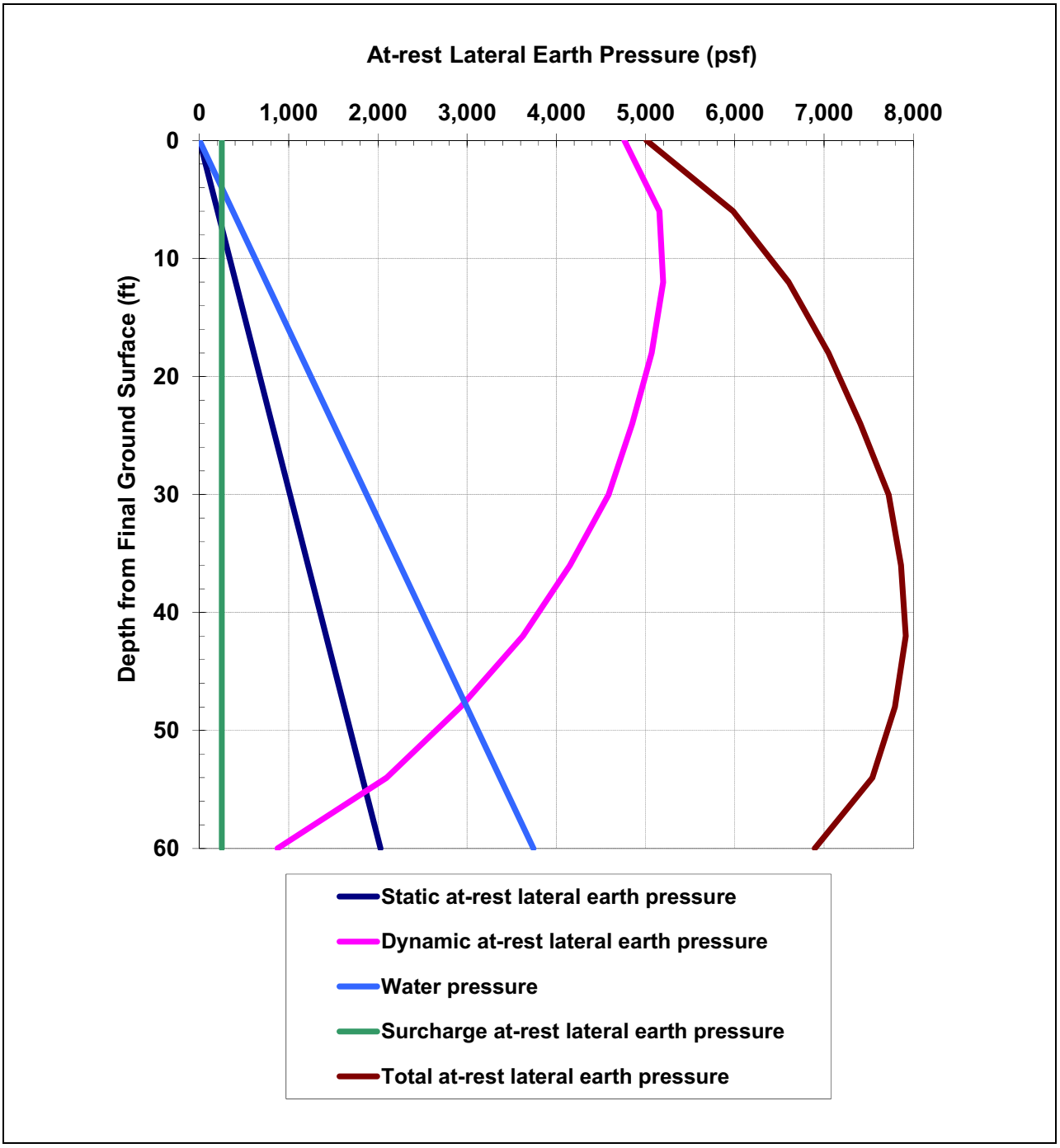

2.5.5 Stability of Slopes

NAPS COL 2.0-30-A

The information needed to address DCD COL Item 2.0-30-A is included in the following sections.

SSAR Section 2.5.5 is incorporated by reference with the following variances and/or supplements.

NAPS ESP VAR 2.5-1

SSAR Section 2.5.5 addressed the stability of slopes at the North Anna ESP site. However, the information presented in this FSAR section replaces the analyses presented in SSAR Section 2.5.5 because the slopes being considered have changed, and, for the seismic slope stability analysis, the peak ground acceleration (PGA) being applied is different. The method of analysis remains essentially the same. In summary, the slopes considered herein are lower, less steep, and have a smaller applied seismic acceleration than the slopes analyzed in SSAR Section 2.5.5. As a result, the slopes addressed in this section have a higher computed factor of safety against failure, and are stable under both long-term static and short-term seismic conditions.

This section presents information on the stability of permanent slopes at the Unit 3 site. The information was developed from a review of reports prepared for the existing units and the originally planned Units 3 and 4, geotechnical literature, the ESP subsurface investigation, and the Unit 3 subsurface investigation. The review included the site-specific reports from the UFSAR (SSAR Reference 5), and reports prepared by Dames and Moore regarding the design and construction of the existing units (SSAR Reference 7) and the originally planned Units 3 and 4 (SSAR Reference 8).

a. **Description of Slopes**

The grading plan for Unit 3 is shown in Figure 2.5.5-201. The design plant grade for the power block area is at Elevation 290 ft with elevations around the perimeter of this area ranging from about Elevation 289 ft to 284 ft to allow for adequate surface drainage. To the northeast of the power block area, going towards the existing Units 1 and 2, ground surface elevation reduces by an approximately 5 percent slope down to Elevation 280 ft at the Service Water Building. (Directions in this section are with respect to plant north.) Stormwater management pond #1 is between these structures and the boundary of Units 1 and 2 with yard grade at Elevation 270 ft. As existing grade falls off from the power block

area northeast towards Units 1 and 2 some backfilling will be required to achieve final grade. As much as 30 ft of backfill will be needed to bring grade up to the planned ground surface area of the originally planned Units 3 and 4, where ground level is presently at around Elevation 250 ft.

All of the Seismic Category I structures at Unit 3 are founded directly on Zone III-IV or Zone IV rock or on concrete fill placed on rock. Foundation support for Seismic Category II structures can also include structural fill and Zone III rock. This is illustrated in the cross sections shown in Figures 2.5.4-225 through 2.5-234. The locations of these cross sections are shown in Figure 2.5.4-206. The concrete fill has a minimum strength of 2500 psi. Thus, there are no slopes that contribute to the support of any Unit 3 Seismic Category I and II structure or any other major power block structure.

The only slopes that could impact Unit 3 are cut slopes that surround and ascend from the southern and eastern edges of the plant, comprising existing and new cut slopes. As discussed in Section 2.5.5b, material from sloughing or collapse of certain of these slopes could impact adjacent facilities.

The existing slopes (see Slope ES in Figure 2.5.5-201 and refer to Section 2.5.5.1.1) run in a southwest-northeast direction, to the east of the originally planned Units 3 and 4 and existing Units 1 and 2. These slopes were excavated during construction of Units 1 and 2. Based on previous topographic maps, this slope was described in the SSAR as a 2h:1v slope, 55 ft high. A more recent topographic survey performed for Unit 3 shows that the slope is actually about 2.4h:1v with a maximum height of 52 ft (from Elevation 271 ft to Elevation 323 ft). Based on the final grade for Unit 3, the maximum height of this existing slope within the vicinity of any new structures is about 45 ft (from Elevation 278 ft to Elevation 323 ft).

The new cut slopes are east and south of the power block (see for example Slope DD in Figure 2.5.5-201 and refer to Section 2.5.5.1.2), and as the slopes turn to the northeast, they merge into the existing slopes. These new slopes are cut at a 3-horizontal to 1-vertical (3h:1v) slope into the existing natural ground surrounding the plant, with a 15-ft wide bench constructed at about 10 ft height below the top of the slope. These slopes reach a maximum height of 39 ft (from about Elevation 281 ft up to Elevation 320 ft) east of the power block. A typical maximum-height cross-section through this slope is shown as Slope DD

in Figure 2.5.5-201.

The maximum depth of the stormwater management pond to the northeast of the main plant area is 20 ft (from Elevation 280 ft down to Elevation 260 ft). This pond is cut at a 3h:1v slope.

SSAR Section 2.5.5 refers to slopes resulting from the nonsafety-related deepened intake channel. In fact, the intake channel for Unit 3 will not be deepened, and thus there will be no new slopes associated with the intake channel.

As shown in Figures 2.5.4-225 through 2.5.4-234, temporary excavation for Unit 3 construction will be performed using vertical walls.

b. **Impact of Slope Instability**

Instability of the stormwater management pond sides does not impact the safety of the plant, nor any of the other plant structures, and therefore these slopes are not addressed further here. Failure of any temporary slope or excavation created for construction of the plant cannot adversely affect the safety of the nuclear power plant facilities, and likewise are not addressed further here.

The existing 2.4h:1v slope (Slope ES) was excavated during construction of the Units 1 and 2, and is almost entirely in cut material. The top of this slope is about 200 ft from the top of the existing service water reservoir (SWR) embankment, and thus any potential instability of the slope will have no impact on the stability of the SWR embankment. However, material from sloughing or collapse of these slopes could possibly impact the new diesel tanks and/or service water cooling tower. However, the toe of the slope is over 100 ft from the new diesel tanks and even farther from the closest point on the service water cooling tower. Slope ES is a representative section along the approximately 700 ft length of the existing slope.

Instability of the new 3h:1v slope to the east of the FWSC (Slope DD) does not impact the foundation stability of this Seismic Category I facility since the facility is founded on concrete fill on top of Zone III-IV bedrock. However, material from sloughing or collapse of this slope could possibly impact the facility, because the base of this new 39 ft high slope is about 55 ft from the FWSC. As can be seen from Figure 2.5.5-201, the new slopes extend to the south and then southwest of Slope DD and then west past the administration building, which is built into the slope. Although these slopes are of similar height to Slope DD, they are much

farther away from the Seismic Category I structures, and sloughing or collapse of these slopes would not impact any of the Seismic Category I structures. Thus, Slope DD is considered the critical slope in the area.

The stability of the existing slope closest to the new service water cooling tower and diesel tanks (Slope ES), and the stability of the new slope closest to the FWSC (Slope DD) are addressed in the following subsections.

2.5.5.1 Slope characteristics

2.5.5.1.1 Existing Slope Characteristics

The location and direction of the existing 45 ft high, 2.4h:1v slope to the north of the Units 1 and 2 SWR (Slope ES) is shown in plan view in Figure 2.5.5-201; the location is also shown in the photograph in SSAR Figure 2.5-66. The photograph in SSAR Figure 2.5-67 shows the existing slope clearly, descending from the SWR to close to the excavation for the originally planned Unit 3 and 4 containment buildings. The structure behind the slope on the SWR embankment is the Units 1 and 2 valve house, which was initially designed to be the originally planned Units 3 and 4 pump house. An approximate cross-section through the existing slope is shown in Figure 2.5.5-202.

As shown in a section view in Figure 2.5.5-202, a boring (B-18) was drilled close to the toe of the slope. This boring, made for the Units 1 and 2 investigation, is located in plan view in Figure 2.5.4-217. During the Unit 3 subsurface investigation, CPT C-915 (located in plan view in Figure 2.5.4-218) was performed near to the top of the slope. Also during the Unit 3 investigation, boring B-947 was drilled to the southwest of C-915, but at a similar elevation within the same original terrain as C-915. CPT C-916 and observation well OW-947 were located adjacent to B-947. The locations of boring B-18 and CPT C-915 are included in Figure 2.5.5-202, along with the groundwater levels extrapolated from the values measured in OW-947. The boring and CPT logs are presented in Section 2.5.5.3.

2.5.5.1.2 New Slope Characteristics

NAPS ESP COL 2.5-11

The location of the new 39 ft high, 3h:1v slope to the east of the FWSC (Slope DD) is shown in plan view in Figure 2.5.5-201. An approximate cross-section through the new slope is shown in Figure 2.5.5-203. As shown in Figure 2.5.4-217, boring B-947 was drilled relatively close to the

final location of the top of the slope during the Unit 3 subsurface investigation. CPT C-916 and observation well OW-947 were located adjacent to B-947. The boring and CPT logs are presented in Section 2.5.5.3. The stability analysis performed for Slope DD (Section 2.5.5.2.4) conservatively neglected the 15-ft wide bench in the slope. For consistency, this bench is not shown in Figure 2.5.5-203.

NAPS COL 2.0-30-A

2.5.5.1.3 Slope Subsurface Conditions

The site soils and bedrock are described in detail in Section 2.5.4.2.2. As can be seen from Figures 2.5.5-202 and 2.5.5-203, the materials in the existing and new slopes, respectively, consist mostly of Zone IIA saprolites. Saprolites are a further stage of weathering beyond weathered rock. They have been derived by in-place disintegration and decomposition and have not been transported. Saprolites are classified as soils but still contain the relict structure of the parent rock, and they also typically still contain some core stone of the parent rock. The North Anna saprolites in many instances maintain the foliation (banded texture) characteristics of the parent rock. The majority of the saprolites in the Unit 3 area are classified as silty sands, although there are also sands, clayey sands, sandy silts, clayey silts and clays, depending very much on their degree of weathering. The fabric is strongly anisotropic. The texture shows angular geometrically interlocking grains with a lack of void network, very unlike the well-pronounced voids found in marine or alluvial sands and silts. The Zone IIA saprolites comprise a large majority of the saprolitic materials onsite. Most of the saprolites obtained from the borings in the slope area are medium dense to dense silty sands. The underlying Zone IIB saprolites are generally very dense silty sands.

Boring B-18 in Figure 2.5.5-202 indicates top of bedrock levels rising significantly towards the toe of the existing slope, with top of weathered rock close to the slope surface at the B-18 location at around Elevation 290 ft. This is consistent with the top of bedrock levels shown in Figure 2.5-2, from SSAR Reference 5. For the new slope shown in Figure 2.5.5-203, the top of weathered rock is closer to Elevation 250 ft. The bedrock at North Anna ranges from moderately to severely weathered (Zone III) as encountered in B-18, to fresh to slightly weathered (Zone IV) at greater depths. The bedrock throughout the North Anna site is classified as a gneiss, which is a metamorphic rock that exhibits foliation in which light and dark bands alternate. It is

composed of feldspar, quartz, and one or more other minerals such as mica and hornblende.

The engineering properties of the site soils and bedrock are described in Section 2.5.4.2.5 and are tabulated in Table 2.5.4-208. These properties are based on extensive field and laboratory testing described in Section 2.5.4.2.

The liquefaction characteristics of all of the Zone IIA saprolites are thoroughly examined in Section 2.5.4.8. That section concludes that the results of the liquefaction analysis indicate that only a very limited amount of the Zone IIA saprolitic soil has a potential for liquefaction based on the Unit 3 seismic parameters. The liquefaction analysis did not take into account the beneficial effects of structure, fabric, and mineralogy of the saprolitic soils.

Details of the soils encountered in the new and existing slopes are outlined in the following paragraphs.

New Slope Subsurface Conditions

Boring B-947, close to the top of the new slope, indicates a predominantly silty sand profile, alternating with layers of silt in the top 15 ft (boring and CPT logs are presented in Section 2.5.5.3). Grain size analyses performed on 10 samples ranging in depth from 5 ft to 43 ft (see Section 2.5.5.3) showed fines contents varying from about 14 to 70 percent, with a median of about 29 percent. The bottom 10 ft of soil has an adjusted SPT N-value of over 50 blows/ft, which is characteristic of Zone IIB saprolite. The overlying soils are Zone IIA saprolites. Interpretation of CPT C-916 (performed adjacent to B-947) based on friction ratio, indicates mainly silty clays and clays, and thus, for these saprolites, this interpretation indicates a less granular composition than shown in the grain size tests.

For stability analyses of the new slope presented in Section 2.5.5.2, based on the results of B-947 and C-916, the new slope has the properties of Zone IIA silty sand saprolite given in Table 2.5.4-208 down to about 35 to 50 ft below existing ground level. The bottom 10 ft of saprolite above weathered rock has the Zone IIB saprolite properties given in Table 2.5.4-208.

The log of CPT-915 (located close to the top of the existing slope) is very similar to the log of CPT-916 in the top 30 ft. CPT-915 continues in a similar pattern below 30 ft down to 50 ft where it shows significantly

increased tip resistance. Below 30 ft, C-916 shows higher tip resistance values than C-915 down to 50 ft depth.

Existing Slope Subsurface Conditions

Boring B-18 provides information on the subsurface materials at the toe of the slope, namely, weathered rock. There are no borings at or near the top of the slope, only CPT C-915. However, as noted in Section 2.5.5.1.1, boring B-947 was drilled to the southwest of C-915, but at a similar elevation within the same original terrain as C-915. B-947 shows a predominantly silty sand profile. Grain size analysis conducted on 10 samples ranging from 5 ft depth to 43 ft depth from B-947 showed fines contents with a median of about 29 percent. The log of CPT C-915 is similar to the log of CPT C-916 (immediately adjacent to B-947) and indicates a mainly silty clay and clay profile, in contrast with the actual silty sand samples obtained from B-947. CPTs provide valuable information on the soil by measuring co ne tip resistance, sleeve friction, and pore-water pressure at very closely-spaced depth intervals throughout the soil profile. However, no samples were obtained with the CPT and so there is no direct evidence of the type of soil being measured. Instead, the soil type is selected based mainly on the friction ratio, which is the ratio, expressed as a percentage, of the measured sleeve friction to the tip resistance. The interpretation of soil type from friction ratio is empirical, based on historical correlations between ratio and soil type identified from adjacent borings. However, like most empirical correlations in geotechnical engineering, it is not exact for all soil types, and this was the case in C-916 (and presumably C-915). Thus, the silty sand profile in B-947 was the profile used in the slope stability analysis of the existing slope.

For the stability analysis of the existing slope presented in Section 2.5.5.2, as noted above, the existing slope has the properties of Zone IIA silty sand saprolite given in Table 2.5.4-208. This material extends down to about 53 ft below the ground level beyond the top of the slope. The thickness of Zone IIB saprolite below the Zone IIA material becomes less towards the toe of the slope and this layer eventually pinches out as the top of weathered rock rises, as shown in Figure 2.5.5-202. The Zone IIB saprolite and the weathered rock have the properties given in Table 2.5.4-208.

2.5.5.1.4 Slope Phreatic Surface

The phreatic surfaces shown in Figure 2.5.5-202 (existing slope ES) and Figure 2.5.5-203 (new slope DD) have been developed from the water table levels measured in OW-947 and derived in Section 2.4.12. The depth of this phreatic surface precludes any potential for liquefaction of the near-surface soils in the slope.

2.5.5.2 Design Criteria and Analyses

2.5.5.2.1 Required Factor of Safety

Minimum required factors of safety for stability of slopes under long-term static (non-seismic) loading and for dynamic (seismic) loading are 1.5 and 1.1, respectively.

2.5.5.2.2 Stability of Existing Slope

The photograph in SSAR Figure 2.5-67 of the existing 2.4h:1v slope to the north of the SWR was taken over 20 years ago. The condition of the slope is essentially the same today. It was thoroughly inspected during the ESP site investigation. The slope shows no signs of distress.

2.5.5.2.3 Analysis of Existing Slope

The static and dynamic stability of the existing slope to the north of the SWR was analyzed using the computer program SLOPE/W (Reference 2.5-219).

a. **Long-Term Static Analysis**

The SLOPE/W Program used the Bishop method of slices (SSAR Reference 185) for analysis of the long-term static condition. As noted in Section 2.5.5.1.3, the analysis assumed the saprolite was predominantly coarse grained. The effective strength parameters given in Table 2.5.4-208 are an angle of internal friction ϕ' = 33 degrees and effective cohesion c' = 0.125 ksf for the Zone IIA saprolite and ϕ' = 40 degrees and effective cohesion c' = 0 ksf for the Zone IIB saprolite. The underlying weathered rock used c = 70 ksf, approximately half of the value for unconfined compressive strength given in Table 2.5.4-208.

The input to the analysis and the results are shown in Figure 2.5.5-204. The computed factor of safety is 2.29. This value is above the minimum 1.5 factor of safety required.

b. **Seismic Slope Stability Analysis**

NAPS ESP COL 2.5-10

The pseudo-static approach is used as a first approximation for the seismic analysis of slopes. In this approach, the horizontal and vertical seismic forces are assumed to act on the slope in a static manner, that is, as a constant static force. This is an obviously conservative approach, since the actual seismic event occurs for only a short period of time, and during that time, the forces alternate their direction at a relatively high frequency. Also, the pseudo-static analysis tends to be run using the peak seismic acceleration; the mean acceleration during the design seismic event can be significantly less than the peak value. A pseudo-static analysis using peak acceleration values can be a useful tool in a limit analysis where the peak acceleration is relatively low. In such analyses, the computed factor of safety may well exceed the minimum of 1.1, thus requiring no further analysis. However, where the peak seismic acceleration values are high, the pseudo-static analysis produces unreasonably low safety factor values.

The pseudo-static analysis was run on the existing 45 ft high slope (Slope ES) using SLOPE/W with the Bishop method of slices. For the low frequency earthquake, the peak horizontal acceleration used was about 0.26g. This is the average peak acceleration in the top 45 ft of soil shown in Table 2.5.5-201. (The maximum horizontal acceleration is 0.31g at about 42 ft depth.) The vertical acceleration used was about 0.13g. The computed factor of safety was 1.30, more than the minimum 1.1 required. For the high frequency earthquake, the equivalent peak horizontal acceleration used was 0.42g with a vertical acceleration of 0.21g. (The maximum horizontal acceleration is 0.56g at about 42 ft depth.) The computed factor of safety was about 1.04, less than the minimum 1.1 required. The input to the analysis, and the results, are shown in Figure 2.5.5-205 for the low frequency earthquake and Figure 2.5.5-206 for the high frequency earthquake.

Seed (SSAR Reference 186), in the 19th Rankine Lecture, addressed the over-conservatism intrinsic in the pseudo-static analysis. He looked at the more rational approach proposed by Newmark (SSAR Reference 187), where the effective acceleration time-history is integrated to determine velocities and displacements of the slope. He also examined dams in California that had been subjected to seismic forces, including several dams that survived the 1906 San Francisco earthquake. Based on his studies, he concluded that for embankments

that consist of materials that do not tend to build up large pore pressures or lose significant percentages of their shear strength during seismic shaking, seismic coefficients of only 0.15g are adequate to ensure acceptable embankment performance for earthquakes up to Magnitude M = 8.25 with PGAs of 0.75g. For earthquakes in the range of M = 6.5, Seed recommends a horizontal seismic coefficient of only 0.1g with a vertical seismic coefficient of zero. Note that it is the magnitude of the earthquake that determines the acceleration to be used here; magnitude is not part of the input to the pseudo-static analysis.

The liquefaction analysis of the Zone IIA saprolite indicated that only a limited amount of the material has a potential for liquefaction. Also, because of its age, fabric and interlocking angular grain structure, this material does not lose a significant proportion of its shear strength during shaking. Thus, for the low frequency earthquake, with a design Magnitude M = 7.2, the pseudo-static analysis should be limited to a horizontal acceleration of 0.15g. A pseudo-static design using an inertia force of 0.1g is adequate for the high frequency earthquake.

The pseudo-static analysis was run again using SLOPE/W. This time the horizontal accelerations used were 0.1g and 0.15g, with zero vertical acceleration. The computed factors of safety were 1.76 and 1.57, respectively, greater than the minimum 1.1 required. The input to the analysis, and the results, for the 0.1g and 0.15g cases are shown in Figures 2.5.5-207 and 2.5.5-208, respectively.

Other researchers have also recommended substantially reducing the peak acceleration when applying the pseudo-static analysis. Kramer (SSAR Reference 188) recommends using an acceleration of 50 percent of the peak acceleration. For the low frequency earthquake, where the average peak acceleration in the top 45 ft is about 0.26g, the horizontal input using Kramer's recommendations was about 0.13g and the vertical input was about 0.065g. This results in a factor of safety of 1.65. Using the average peak acceleration for the high frequency earthquake in the top 45 ft of 0.42g, the horizontal input using Kramer's recommendation was 0.21g and the vertical input was 0.105g. This level of input provides a factor of safety against slope failure of 1.41. Thus the low and high frequency inputs give factors of safety above the minimum 1.1 required. The input to the analysis, and the results, for the low frequency and high frequency cases are shown in Figures 2.5.5-209 and 2.5.5-210, respectively.

In the preceding analyses (both long-term static, and seismic), the only case that gave a factor of safety lower than the required minimum was the pseudo-static analysis using the high frequency peak acceleration. As noted above, the pseudo-static analysis does not take into account the frequency of the motion nor the magnitude of the earthquake. For high frequency, low magnitude earthquakes, (as is the case at North Anna) the pseudo-static analysis is particularly conservative. Thus, it is concluded that the existing 2.4h:1v slope to the north of the SWR remains stable under long-term static and design seismic conditions.

NAPS COL 2.0-30-A

2.5.5.2.4 Analysis of New Slope

The static and dynamic stability of the new 39-ft high 3h:1v slope (Slope DD) to the east of the FWSC was analyzed using the computer program SLOPE/W (Reference 2.5-219).

a. **Long-Term Static Analysis**

The SLOPE/W Program used the Bishop method of slices (SSAR Reference 185) for analysis of the long-term static condition. As noted in Section 2.5.5.1.3, the properties assumed for the Zone IIA and Zone IIB saprolite were the same as those for the existing slope that was analyzed.

The input to the analysis and the results are shown in Figure 2.5.5-211. The computed factor of safety is 2.27. This value is above the minimum 1.5 factor of safety required.

b. **Seismic Slope Stability Analysis**

NAPS ESP COL 2.5-10

The pseudo-static analysis was run on the new 39 ft high slope using SLOPE/W with the Bishop method of slices. For the low frequency earthquake, the average peak horizontal acceleration in the top 39 ft used was about 0.25g with a vertical acceleration of about 0.125g. (The maximum horizontal acceleration is 0.31g at about 42 ft depth.) The computed factor of safety was 1.24, greater than the minimum 1.1 required. For the high frequency earthquake, the peak horizontal acceleration used was about 0.41g. This is the average peak acceleration in the top 39 ft of soil shown in Table 2.5.5-201. (The maximum horizontal acceleration is 0.56g at the ground surface.) The vertical acceleration used was about 0.205g. The computed factor of safety was 1.00, less than the minimum 1.1 required. The input to the analysis, and the results, for the low frequency and high frequency cases

are shown in Figures 2.5.5-212 and 2.5.5-213, respectively.

The pseudo-static analysis was run again using SLOPE/W and Seed's (SSAR Reference 186) approach described in Section 2.5.5.2.3. Again the horizontal accelerations used were 0.1g and 0.15g for the high and low frequency cases, respectively, with zero vertical acceleration. The computed factors of safety were 1.64 and 1.43, respectively, greater than the minimum 1.1. The input to the analysis, and the results, for the 0.1g and 0.15g cases are shown in Figures 2.5.5-214 and 2.5.5-215, respectively.

The pseudo-static analysis was then run using SLOPE/W and Kramer's (SSAR Reference 188) recommendations described in Section 2.5.5.2.3. For the low frequency earthquake, where the average peak acceleration in the top 39 ft is about 0.25g, the horizontal input using Kramer's recommendations was about 0.125g and the vertical input was about 0.063g. Using the average peak acceleration for the high frequency earthquake in the top 39 ft of about 0.41g, the horizontal input using Kramer's recommendation was 0.205g and the vertical input was 0.103g. These levels of input provide a factor of safety against slope failure of 1.59 and 1.34 for the low and high frequency cases, respectively, greater than the minimum 1.1 required. The input to the analysis, and the results, for the low frequency and high frequency cases are shown in Figures 2.5.5-216 and 2.5.5-217, respectively.

The results of the stability analyses for the new slope are almost identical to those for the existing slope, and the conclusion about stability is the same, i.e., the new 3h:1v slope to the east of the FWSC remains stable under long-term static and design seismic conditions.

NAPS COL 2.0-30-A

2.5.5.3 Logs of Borings

2.5.5.3.1 Boring Logs

As noted in Section 2.5.5.1, boring B-18 was drilled close to the toe of the existing 2.4h:1v slope to the north of the SWR and boring B-947 was drilled near the top of the proposed new 3h:1v slope east of the FWSC. The logs of borings B-18 and B-947 are reproduced in Figures 2.5.5-218 and 2.5.5-219, respectively.

2.5.5.3.2 CPT Logs

As noted in Section 2.5.5.1, CPT C-915 was drilled close to the top of the existing 2.4h:1v slope to the north of the SWR and CPT C-916 was drilled

adjacent to B-947 near the top of the new 3h:1v slope east of the FWSC. The logs of CPTs C-915 and C-916 are reproduced in Figures 2.5.5-220 and 2.5.5-221, respectively.

2.5.5.3.3 Observation Wells

As noted in Section 2.5.5.1, observation well OW-947 was installed adjacent to boring B-947 near the top of the new 3h:1v slope east of the FWSC. The log of OW-947 is reproduced in Figure 2.5.5-222. Water levels measured in this well over a 12-month period are shown in Table 2.5.5-202.

2.5.5.3.4 Laboratory Test Results

The grain size tests results for the saprolites in boring B-947 and noted in Section 2.5.5.1 are provided in Table 2.5.5-203. Details of these test results are provided in Appendix 2.5.4AA.

2.5.5.4 Compacted Fill

The existing 2.4h:1v slope described and analyzed in the previous sections is a cut slope and does not contain fill materials in any significant quantity.

As shown in Figure 2.5.5-203, the grading plan results in the top approximately 8 ft of the new 3h:1v slope east of the FWSC being new fill. This is not structural fill since it is used only for site grading and consists of re-compacted saprolitic soils obtained from plant excavations. These are described in Section 2.5.4.5. For slope stability analysis, this fill has been given the same properties as the in-situ Zone IIA saprolite.

2.5.5.5 Conclusions

Existing slopes and embankments that are not impacted by Unit 3 (such as the SWR embankments) do not require analysis for Unit 3 and are not addressed here. New slopes, such as in the stormwater management pond #1 that will not impact the safety of the plant or any other structure if they fail also do not require analysis and are not addressed here. Failure of any temporary slope or excavation created for construction of Unit 3 cannot adversely affect the safety of Unit 3, consequently, this is not addressed further here.

The only existing slope which, by its failure, could adversely affect the safety of Unit 3, because of its proximity, is the 45 ft high, 2.4h:1v slope that descends from north of the SWR down to southeast of the existing

excavation made for the originally planned Units 3 and 4. The slope is made almost entirely in cut material. The stability of this existing slope was analyzed using the computer program SLOPE/W. The only case that gave a factor of safety lower than the required minimum was the pseudo-static analysis using the high frequency peak ground acceleration. This analysis does not take into account the frequency of the motion or the magnitude of the earthquake. For high frequency, low magnitude earthquakes, (as is the case at North Anna) the pseudo-static analysis is particularly conservative. Thus, based on less conservative analysis, it is concluded that this slope remains stable under long-term static and design seismic conditions.

The results of the stability analyses for the new 3h:1v slope to the east of the FWSC are almost identical to those for the existing slope described above, and the conclusion about stability is the same, i.e., the new slope remains stable under long-term static and design seismic conditions.

NAPS ESP COL 2.5-10 **Table 2.5.5-201 Maximum Acceleration Results**

Depth (ft)	Low Frequency Max. Acc. (g)	High Frequency Max. Acc. (g)
0.0	0.285	0.467
1.5	0.281	0.454
3.0	0.271	0.423
4.5	0.260	0.391
6.0	0.249	0.366
7.5	0.240	0.349
9.0	0.232	0.338
10.5	0.226	0.332
12.0	0.223	0.334
13.5	0.223	0.341
15.0	0.226	0.352
17.0	0.234	0.372
19.0	0.237	0.381
21.0	0.241	0.386
23.0	0.245	0.398
25.0	0.253	0.413
27.0	0.255	0.424
29.0	0.263	0.442
31.0	0.271	0.462
33.0	0.276	0.476
35.0	0.280	0.487
37.5	0.285	0.505
40.0	0.300	0.533
42.5	0.311	0.559
45.0	0.303	0.546
47.5	0.294	0.528
50.0	0.290	0.523
52.5	0.288	0.525
55.0	0.288	0.533

NAPS COL 2.0-30-A

Table 2.5.5-202 Water Level Measurements for Well OW-947

Date	Groundwater Elevation, Ft
11/29/2006	297.61
2/28/2007	297.81
5/30/2007	297.92
8/29/2007	296.00

NAPS COL 2.0-30-A

Table 2.5.5-203 Grain-Size Test Results for Boring B-947

Sample No.	Depth (Ft)	Gravel (%)	Sand (%)	Fines (%)	Silt (%)	Clay (%)
B-947-3	4.5–6.0	0.0	38.3	61.7	23.5	38.2
B-947-4	8.5–10.0	0.0	60.0	40.0	-	-
B-947-5	9.5–11.0	1.6	55.9	42.5	21.1	21.4
B-947-6	13.5–15.0	0.0	30.5	69.5	-	-
B-947-7	17.2–18.7	0.0	75.8	24.2	-	-
B-947-8	22.2–23.7	0.6	79.4	20.0	10.7	9.3
B-947-9	28.7–30.2	0.0	66.6	33.4	-	-
B-947-10	33.7–35.2	0.0	81.3	18.7	-	-
B-947-11	38.7–40.2	0.0	85.8	14.2	-	-
B-947-12	42.2–43.7	0.0	79.7	20.3	13.4	6.9

BASIS: NEW

NAPS COL 2.0-30-A **Figure 2.5.5-201 Location of Evaluated Slopes**

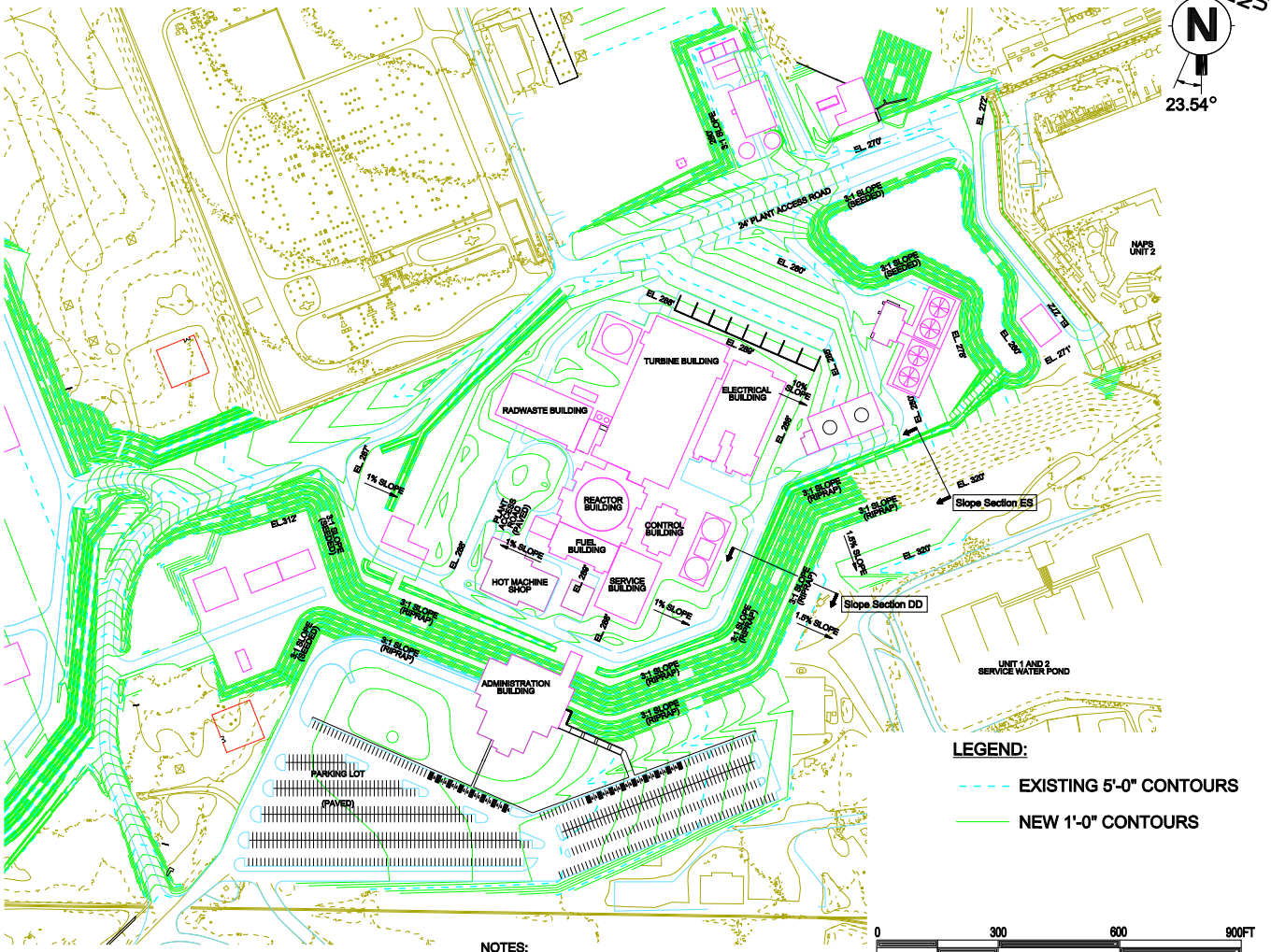

BASIS: NEW

NAPS COL 2.0-30-A **Figure 2.5.5-202 Cross-Section of Existing Slope (ES)**

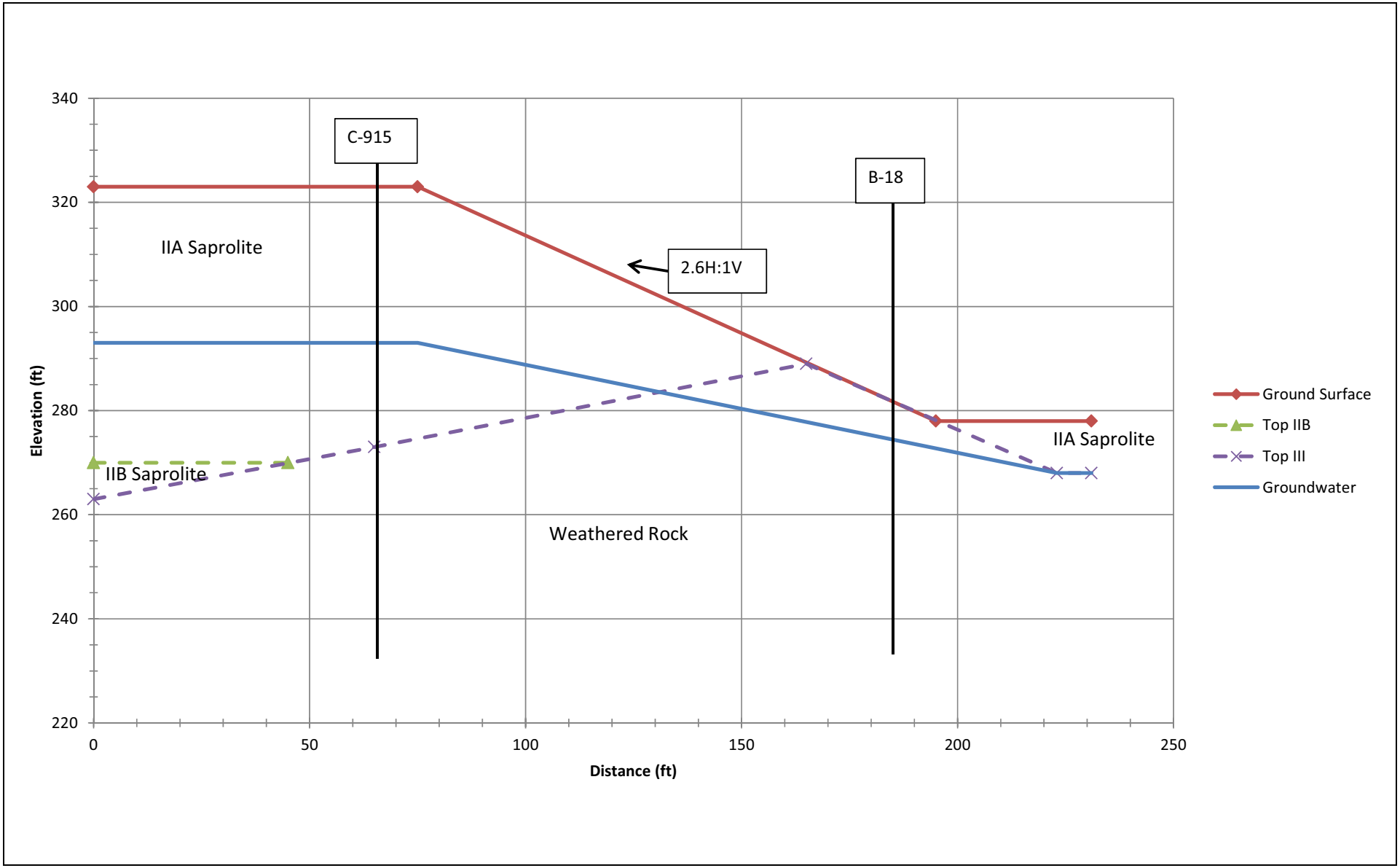

BASIS: NEW

NAPS ESP COL 2.5-11 Figure 2.5.5-203 Cross-Section of Slope DD

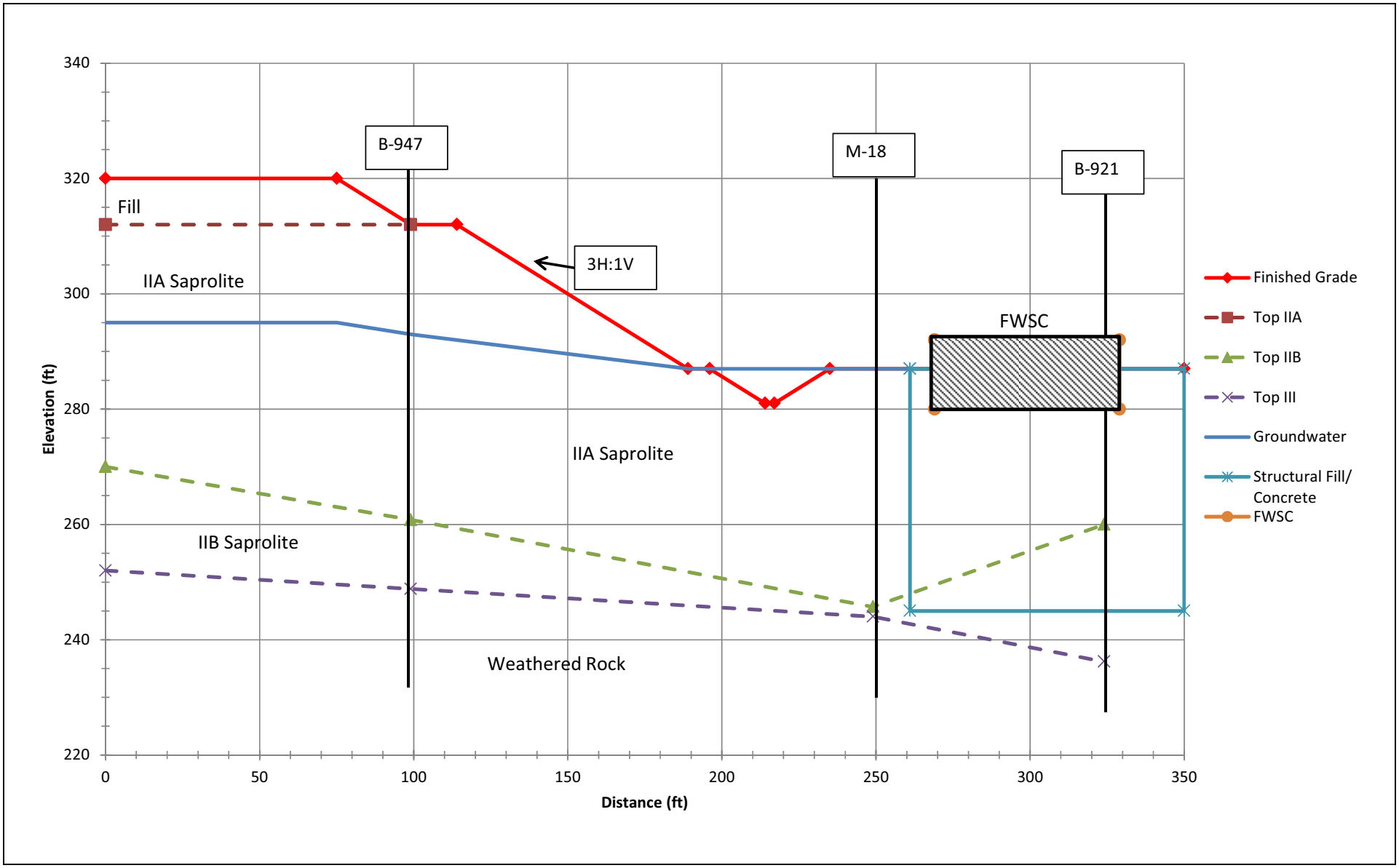

BASIS: NEW

NAPS COL 2.0-30-A **Figure 2.5.5-204 Slope Stability Analysis; Existing Slope; Long-Term Static**

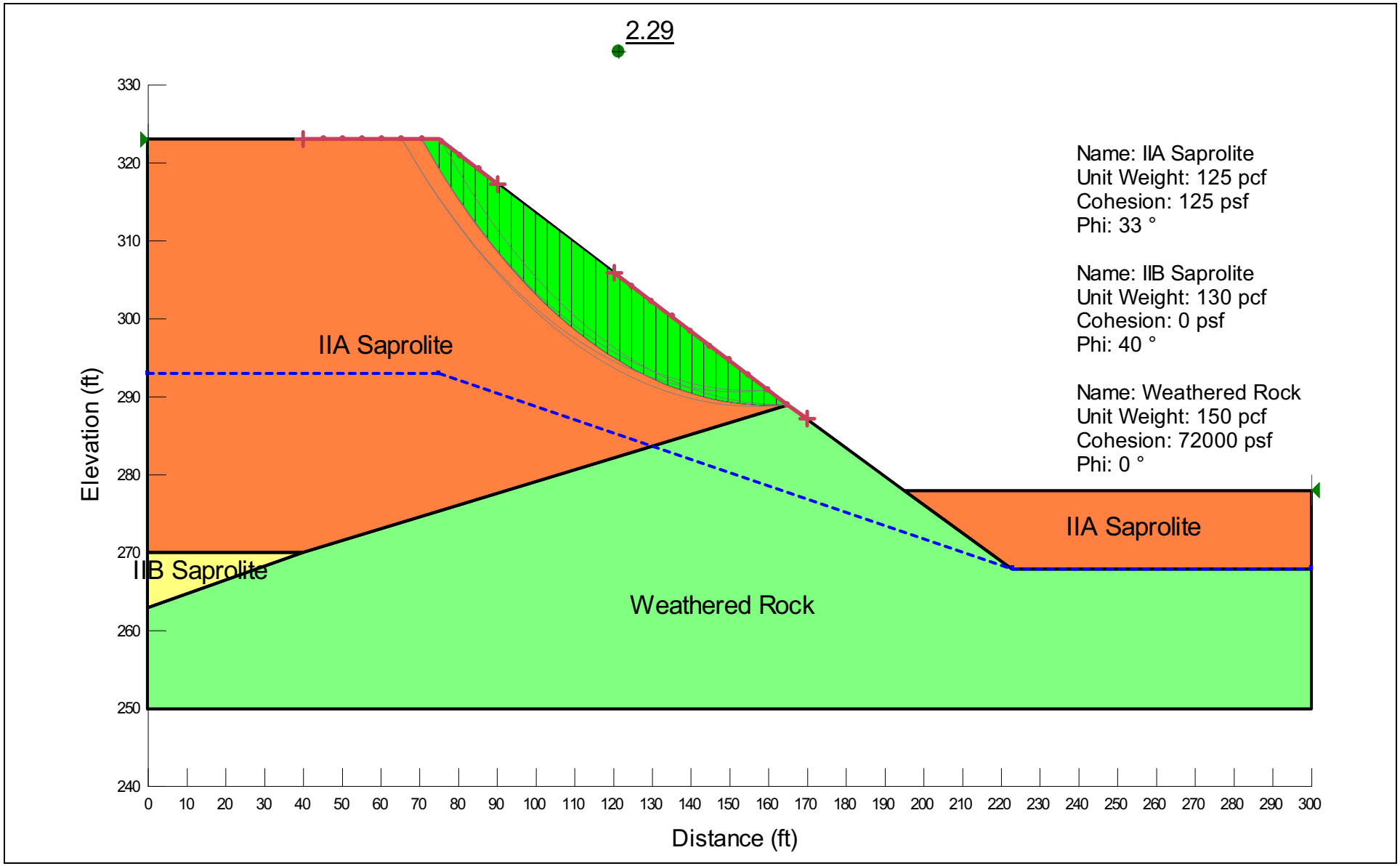

NAPS ESP COL 2.5-10 Figure 2.5.5-205 Slope Stability Analysis; Existing Slope; Pseudo-Static; LF

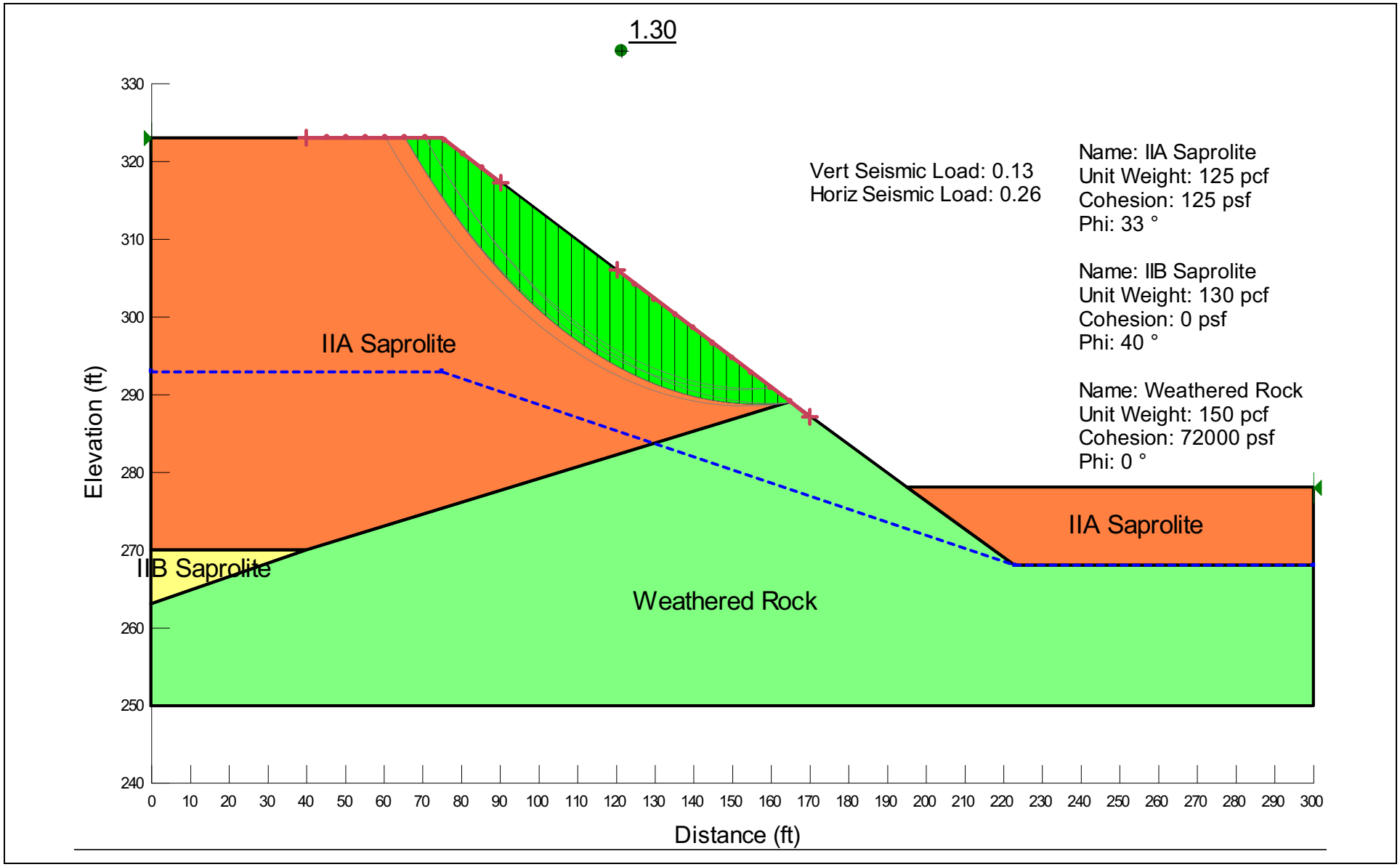

NAPS ESP COL 2.5-10 Figure 2.5.5-206 Slope Stability Analysis; Existing Slope; Pseudo-Static; HF

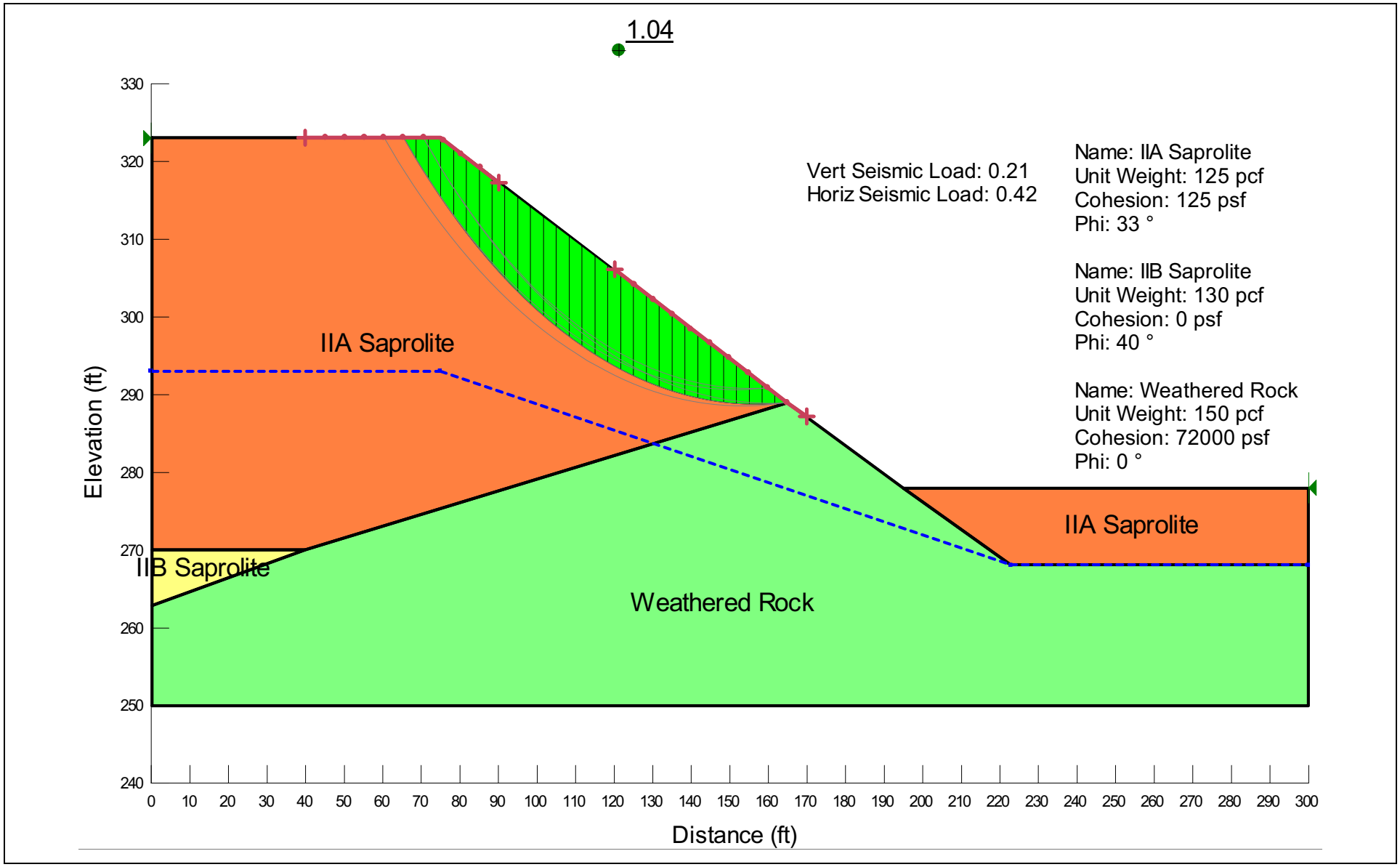

BASIS: NEW

NAPS ESP COL 2.5-10 Figure 2.5.5-207 Slope Stability Analysis; Existing Slope; Seed Approach; Acceleration of 0.1g

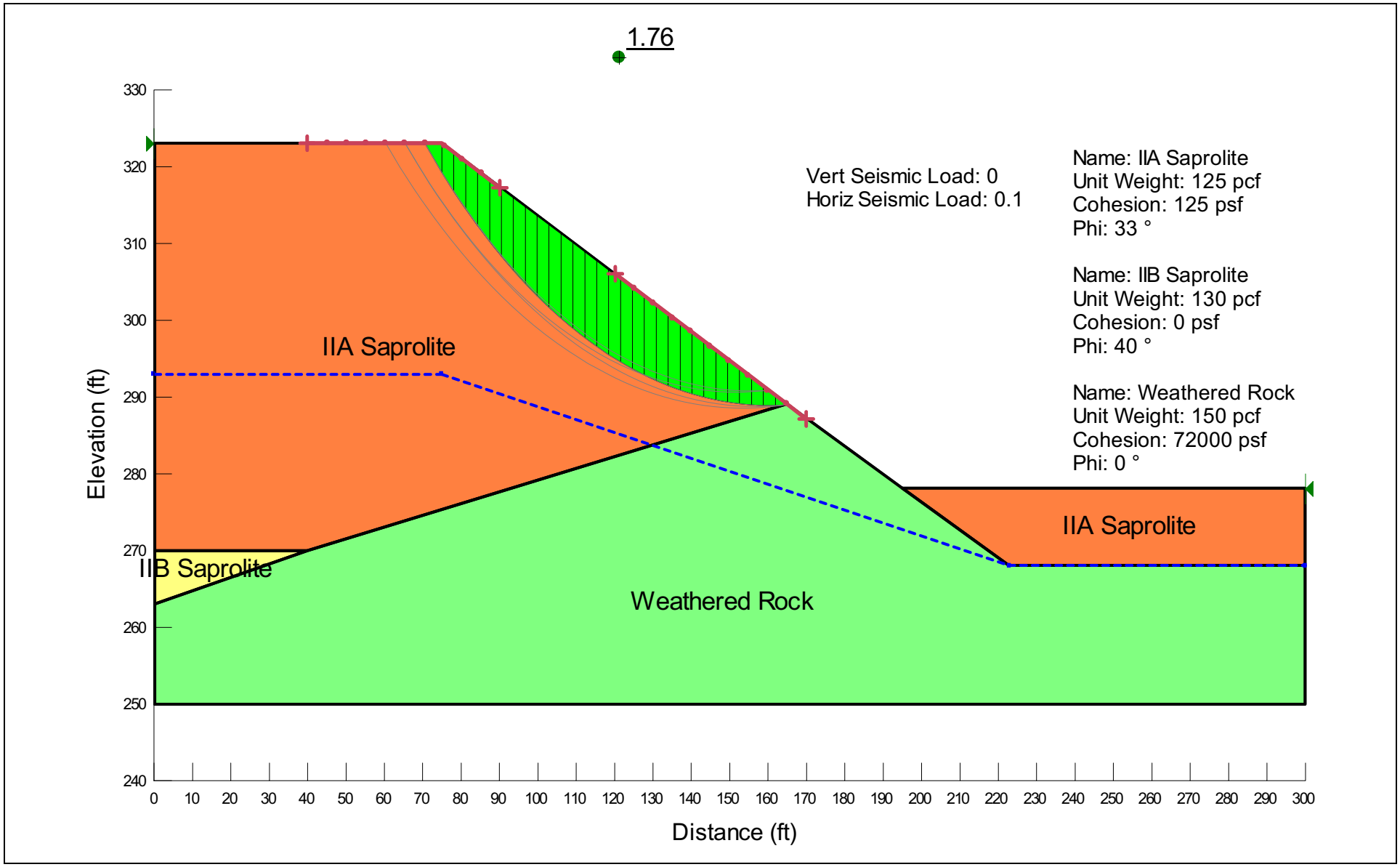

NAPS ESP COL 2.5-10 Figure 2.5.5-208 Slope Stability Analysis; Existing Slope; Seed Approach; Acceleration of 0.15g

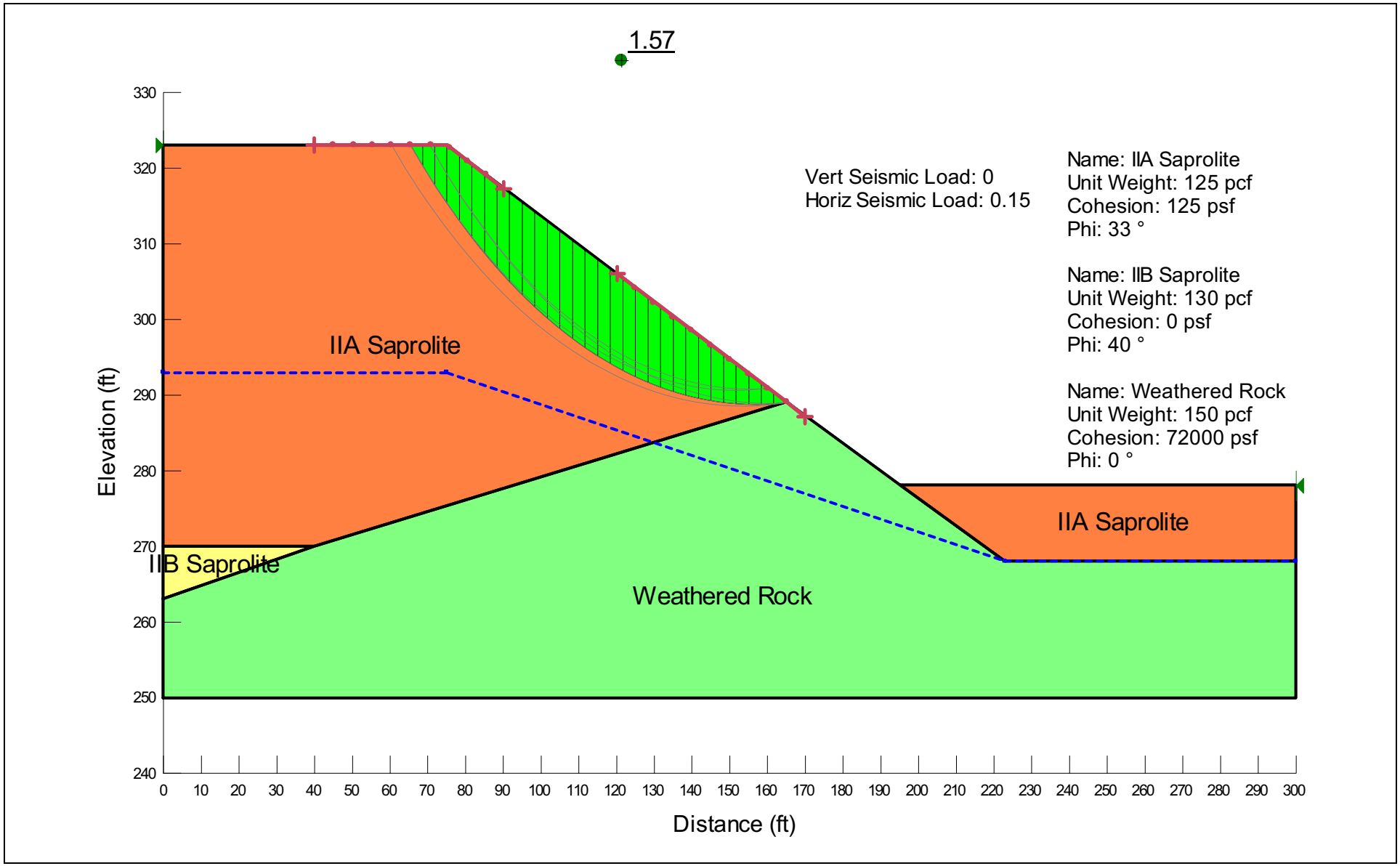

BASIS: NEW

NAPS ESP COL 2.5-10 Figure 2.5.5-209 Slope Stability Analysis; Existing Slope; Kramer Approach; LF

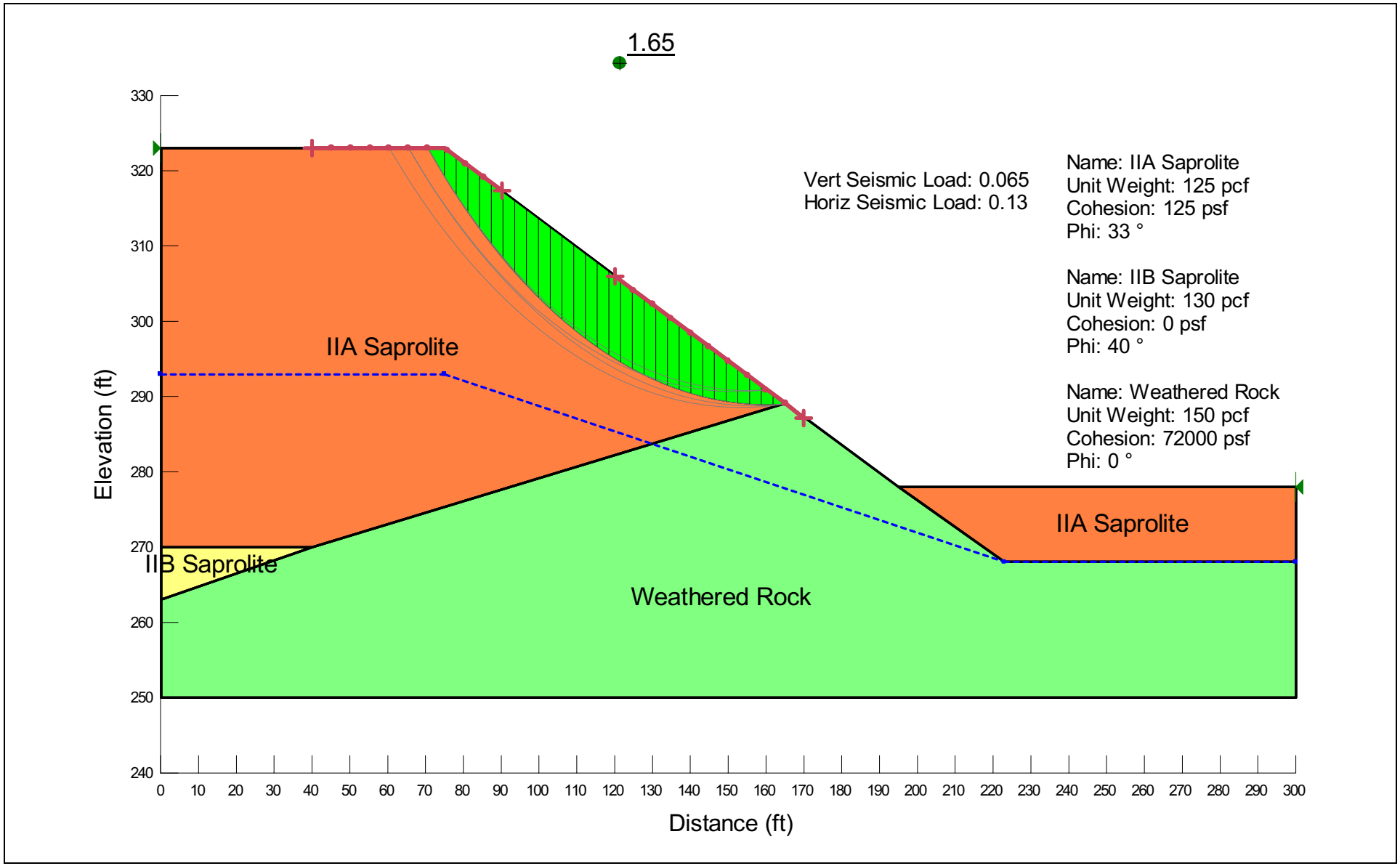

NAPS ESP COL 2.5-10 Figure 2.5.5-210 Slope Stability Analysis; Existing Slope; Kramer Approach; HF

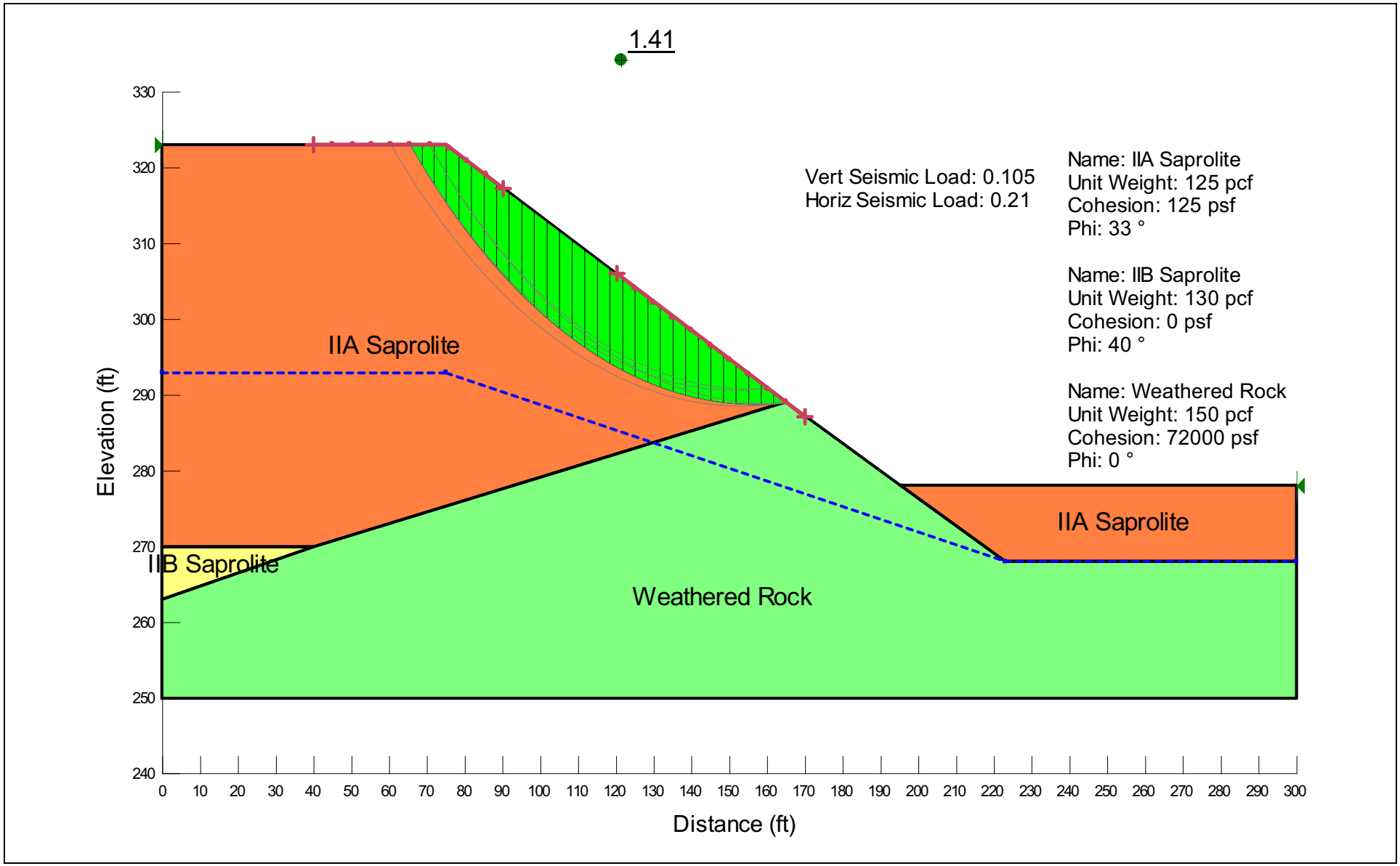

BASIS: NEW

NAPS COL 2.0-30-A **Figure 2.5.5-211 Slope Stability Analysis; Slope DD; Long-Term Static**

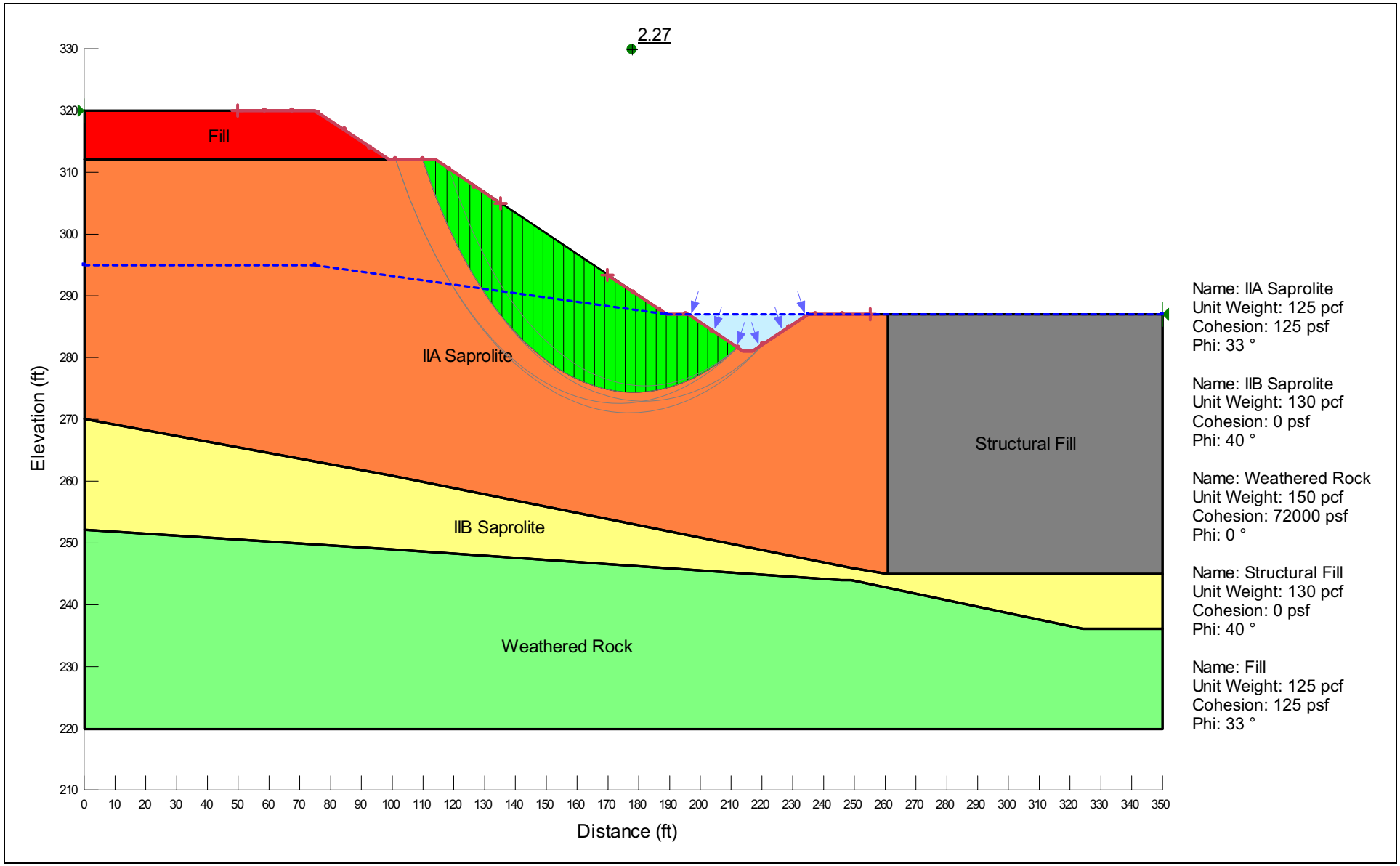

BASIS: NEW

NAPS ESP COL 2.5-10 Figure 2.5.5-212 Slope Stability Analysis; Slope DD; Pseudo-Static; LF

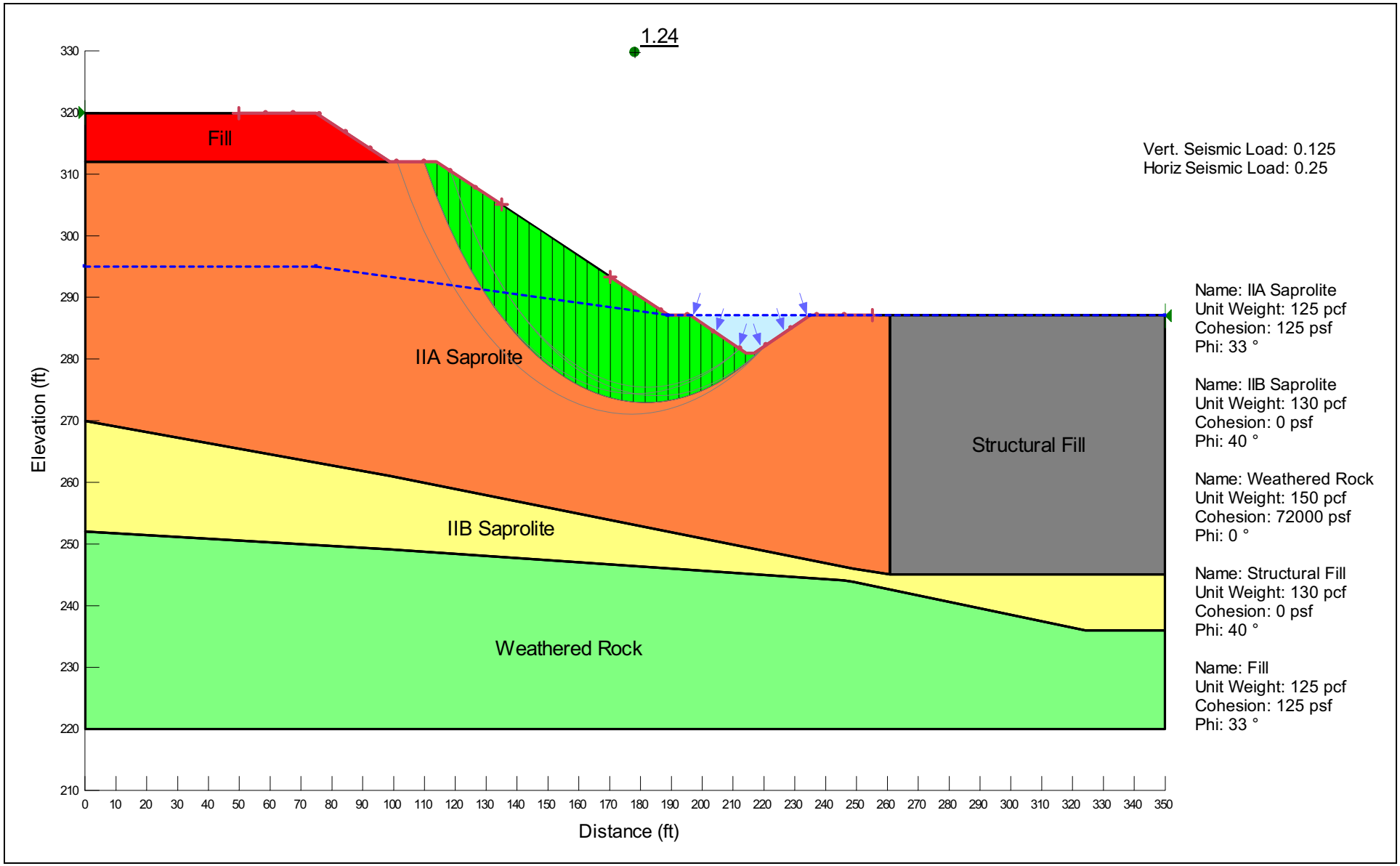

BASIS: NEW

NAPS ESP COL 2.5-10 Figure 2.5.5-213 Slope Stability Analysis; Slope DD; Pseudo-Static; HF

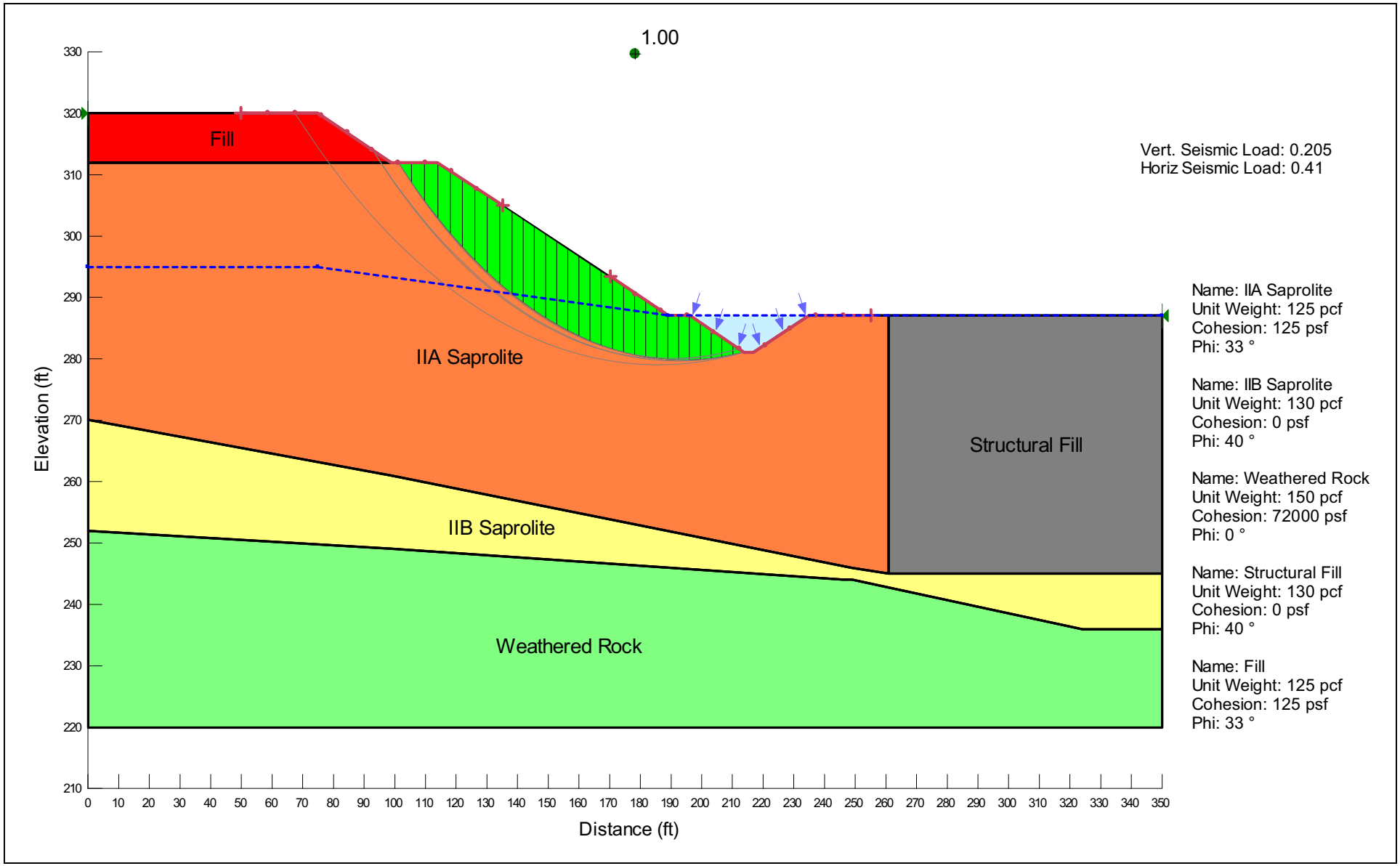

BASIS: NEW

NAPS ESP COL 2.5-10 Figure 2.5.5-214 Slope Stability Analysis; Slope DD; Seed Approach; Acceleration of 0.1g

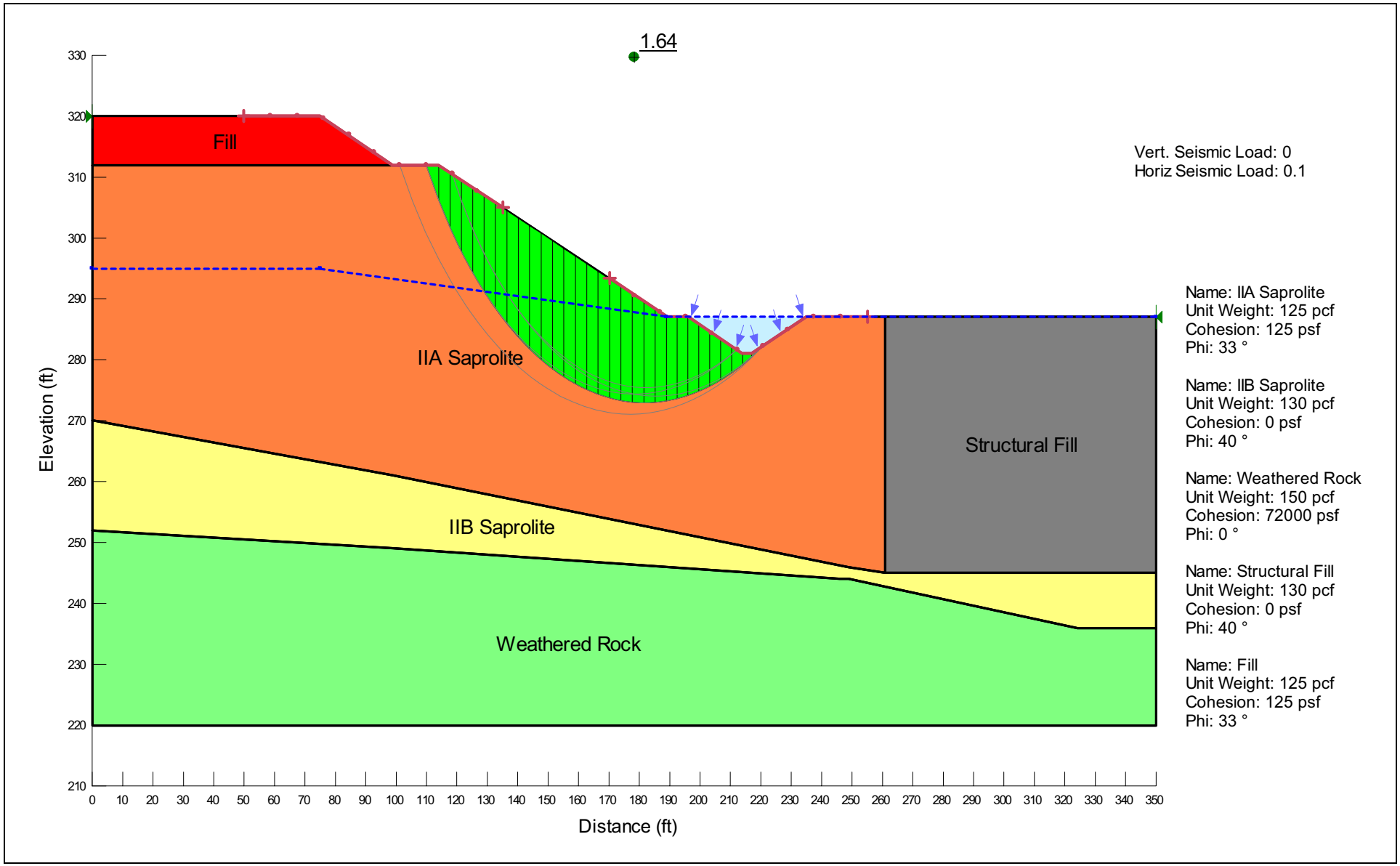

BASIS: NEW

NAPS ESP COL 2.5-10 Figure 2.5.5-215 Slope Stability Analysis; Slope DD; Seed Approach; Acceleration of 0.15g

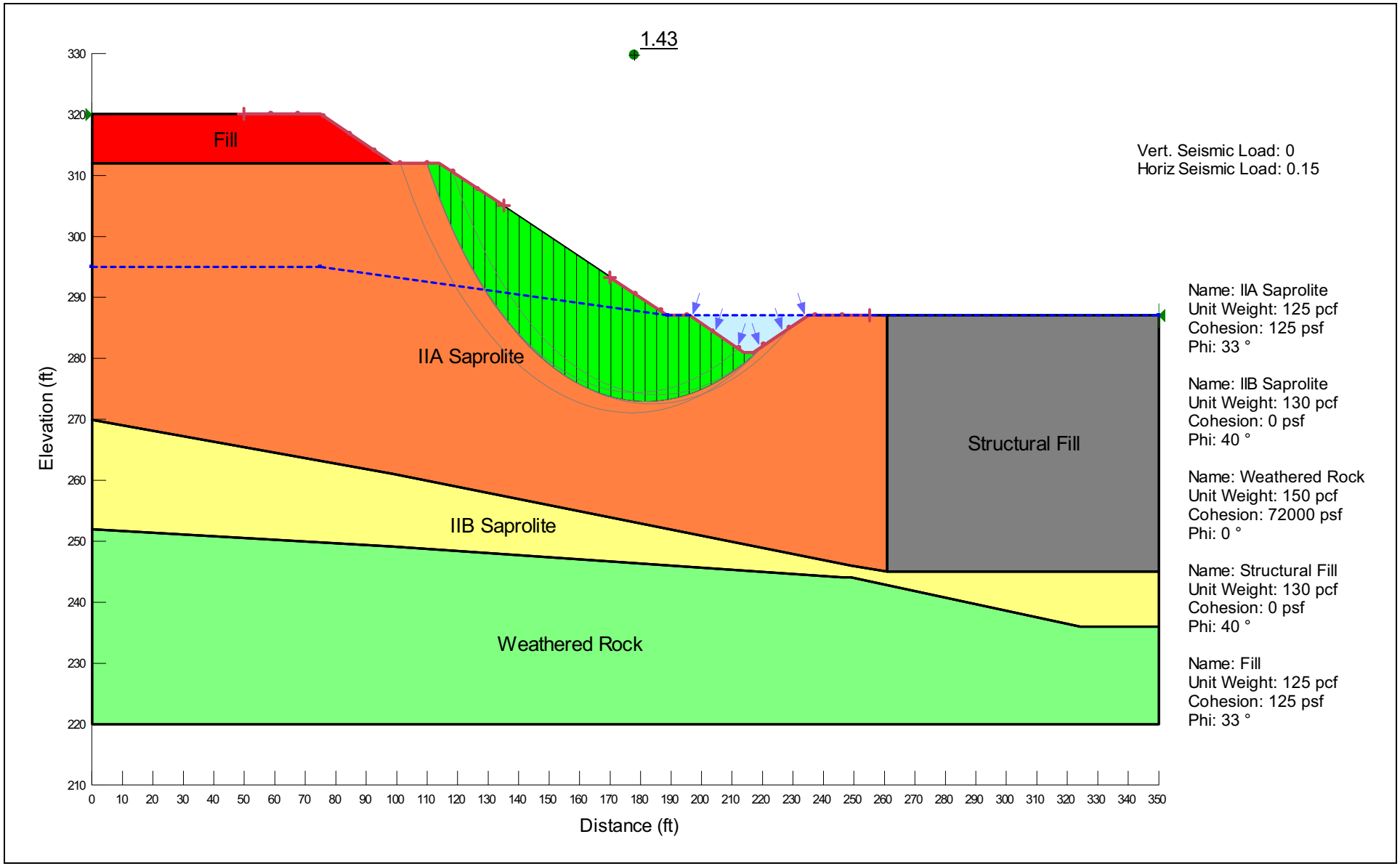

BASIS: NEW

NAPS ESP COL 2.5-10 Figure 2.5.5-216 Slope Stability Analysis; Slope DD; Kramer Approach; LF

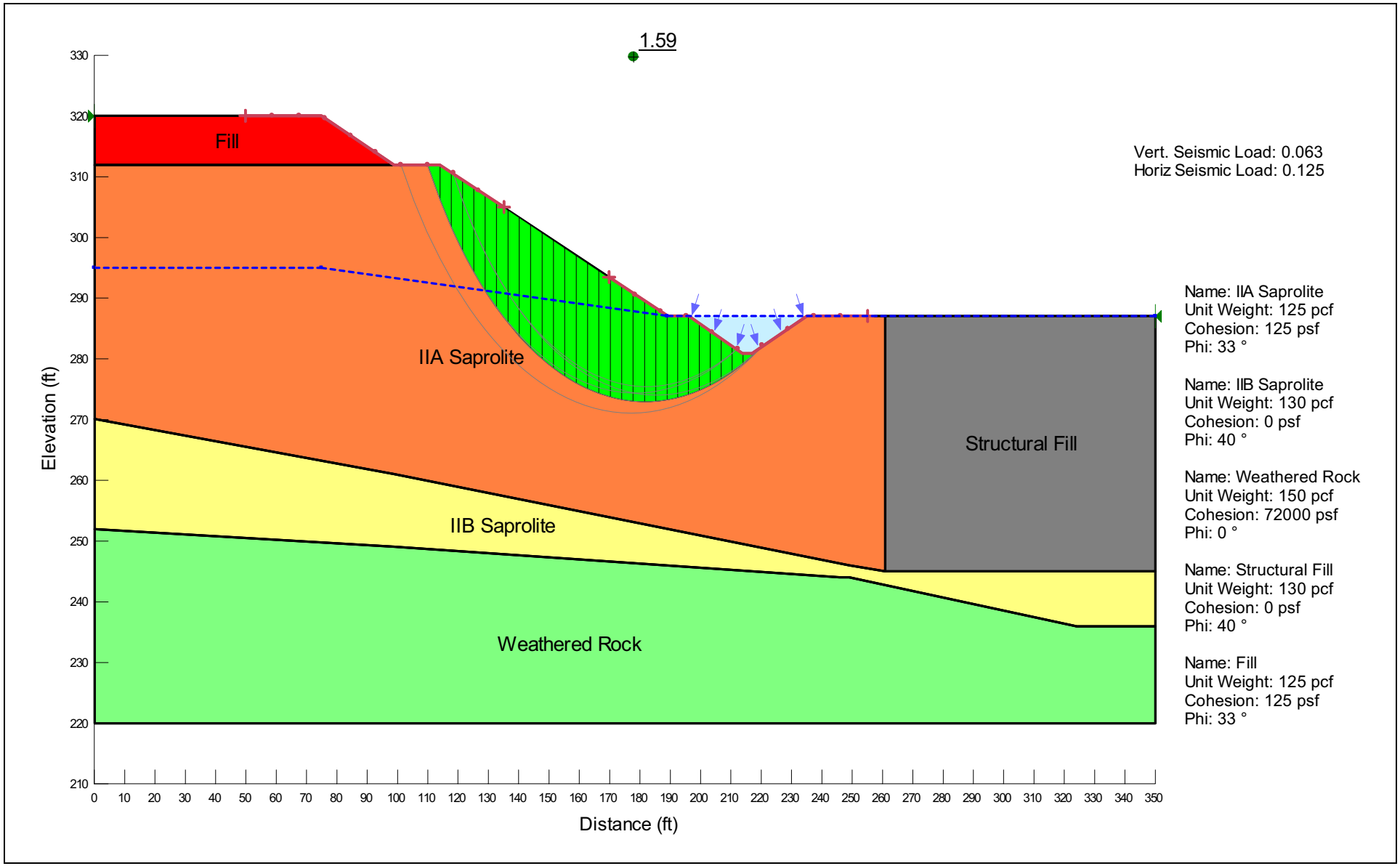

BASIS: NEW

NAPS ESP COL 2.5-10 Figure 2.5.5-217 Slope Stability Analysis; Slope DD; Kramer Approach; HF

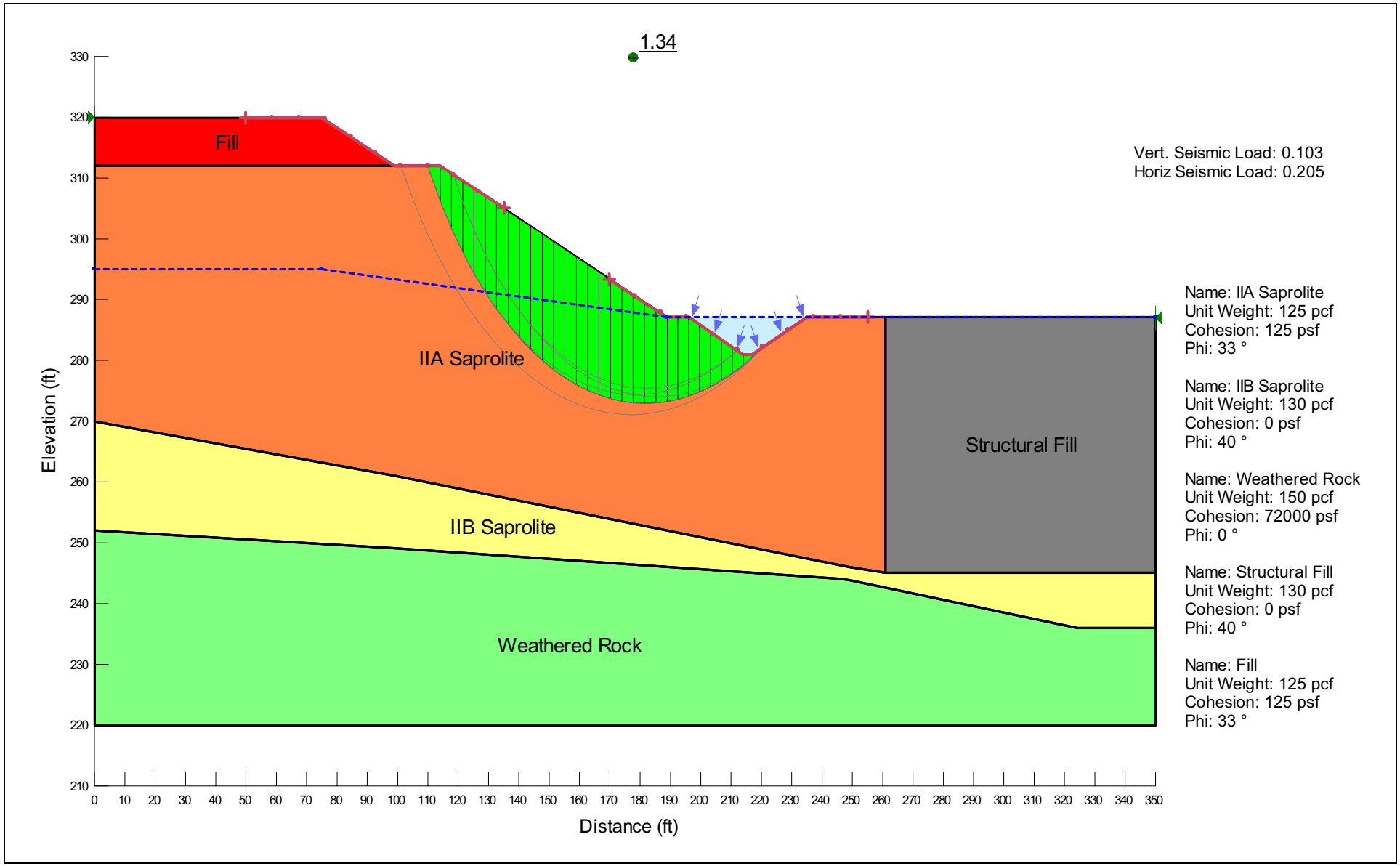

NAPS COL 2.0-30-A **Figure 2.5.5-218 Log of Boring B-18**

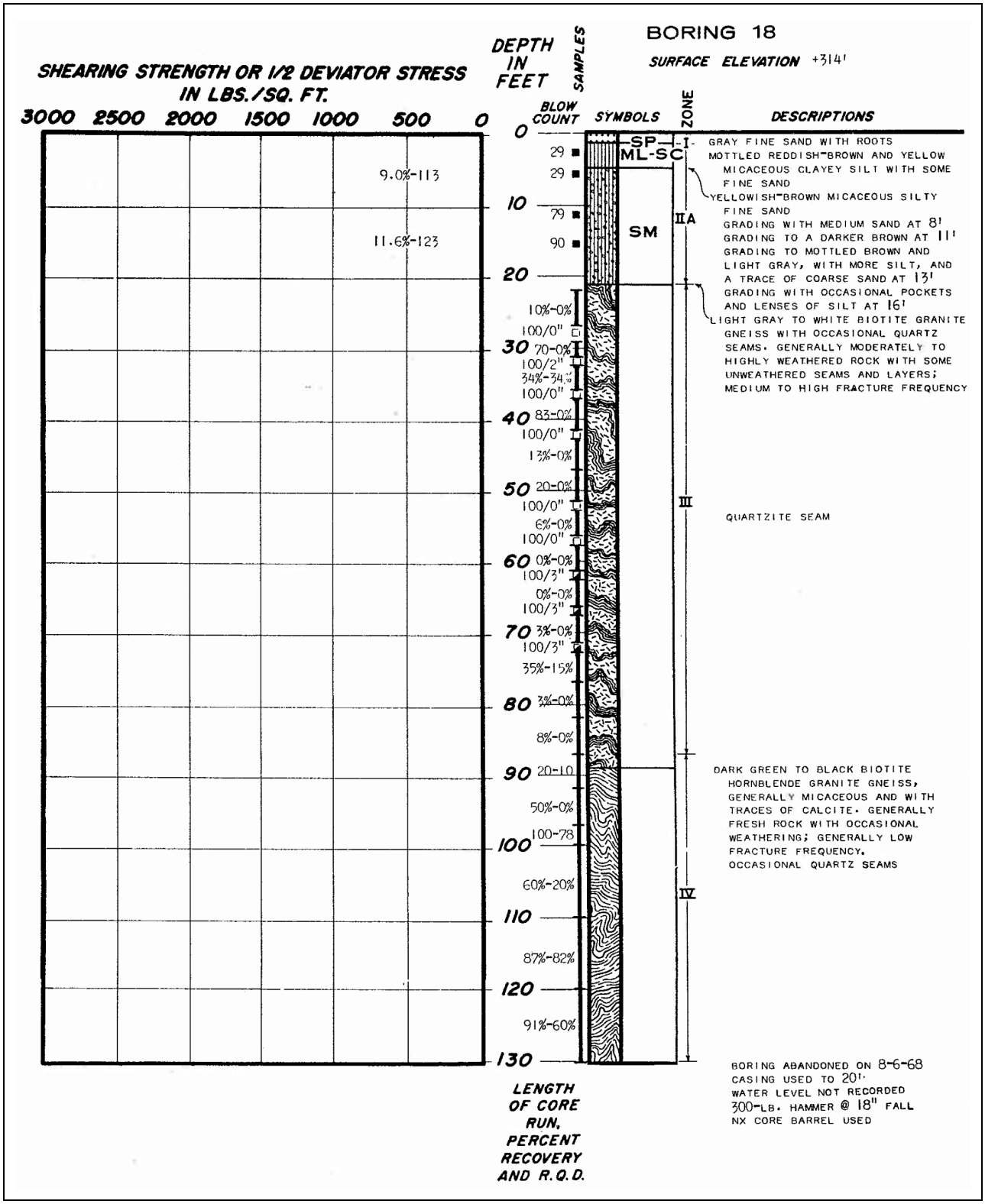

NAPS COL 2.0-30-A **Figure 2.5.5-219 Log of Boring B-947**

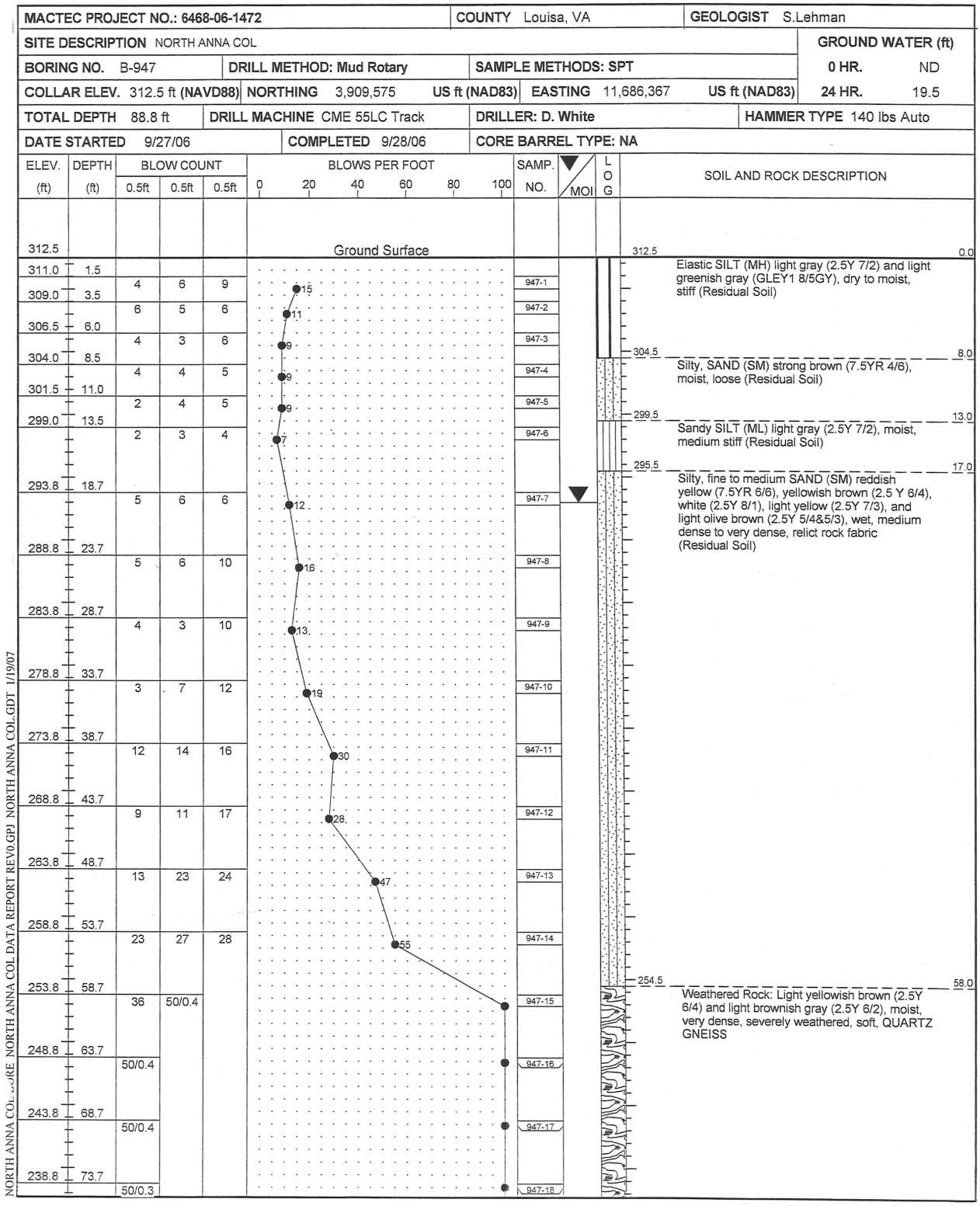

NAPS COL 2.0-30-A **Figure 2.5.5-219 Log of Boring B-947** *(continued)*

MACTEC PROJECT NO.: 6468-06-1472	**COUNTY** Louisa, VA	**GEOLOGIST** S.Lehman	
SITE DESCRIPTION NORTH ANNA COL			**GROUND WATER (ft)**
BORING NO. B-947	**DRILL METHOD: Mud Rotary**	**SAMPLE METHODS: SPT**	**0 HR.** ND
COLLAR ELEV. 312.5 ft **(NAVD88)**	**NORTHING** 3,909,575 **US ft (NAD83)**	**EASTING** 11,686,367 **US ft (NAD83)**	**24 HR.** 19.5
TOTAL DEPTH 88.8 ft	**DRILL MACHINE** CME 55LC Track	**DRILLER: D. White**	**HAMMER TYPE** 140 lbs Auto
DATE STARTED 9/27/06	**COMPLETED** 9/28/06	**CORE BARREL TYPE: NA**	

ELEV. (ft)	DEPTH (ft)	BLOW COUNT 0.5ft	0.5ft	0.5ft	BLOWS PER FOOT 0 20 40 60 80 100	SAMP. NO.	MOI	LOG	SOIL AND ROCK DESCRIPTION
237.7					Continued from previous page				
233.8	78.7	50/0.2				947-19			Weathered Rock: Light yellowish brown (2.5Y 6/4) and light brownish gray (2.5Y 6/2), moist, very dense, severely weathered, soft, QUARTZ GNEISS *(continued)*
228.8	83.7	50/0.1				947-20			
223.8	88.7	50/0.1				947-21			223.7 — Boring terminated at 88.8 ft in Weathered Rock: Very dense, severely weathered, soft, QUARTZ GNEISS — 88.8

NORTH ANNA COL CORE NORTH ANNA COL DATA REPORT REV0.GPJ NORTH ANNA COL.GDT 1/19/07

BASIS: NEW

NAPS COL 2.0-30-A **Figure 2.5.5-220 Log of CPT C-915**

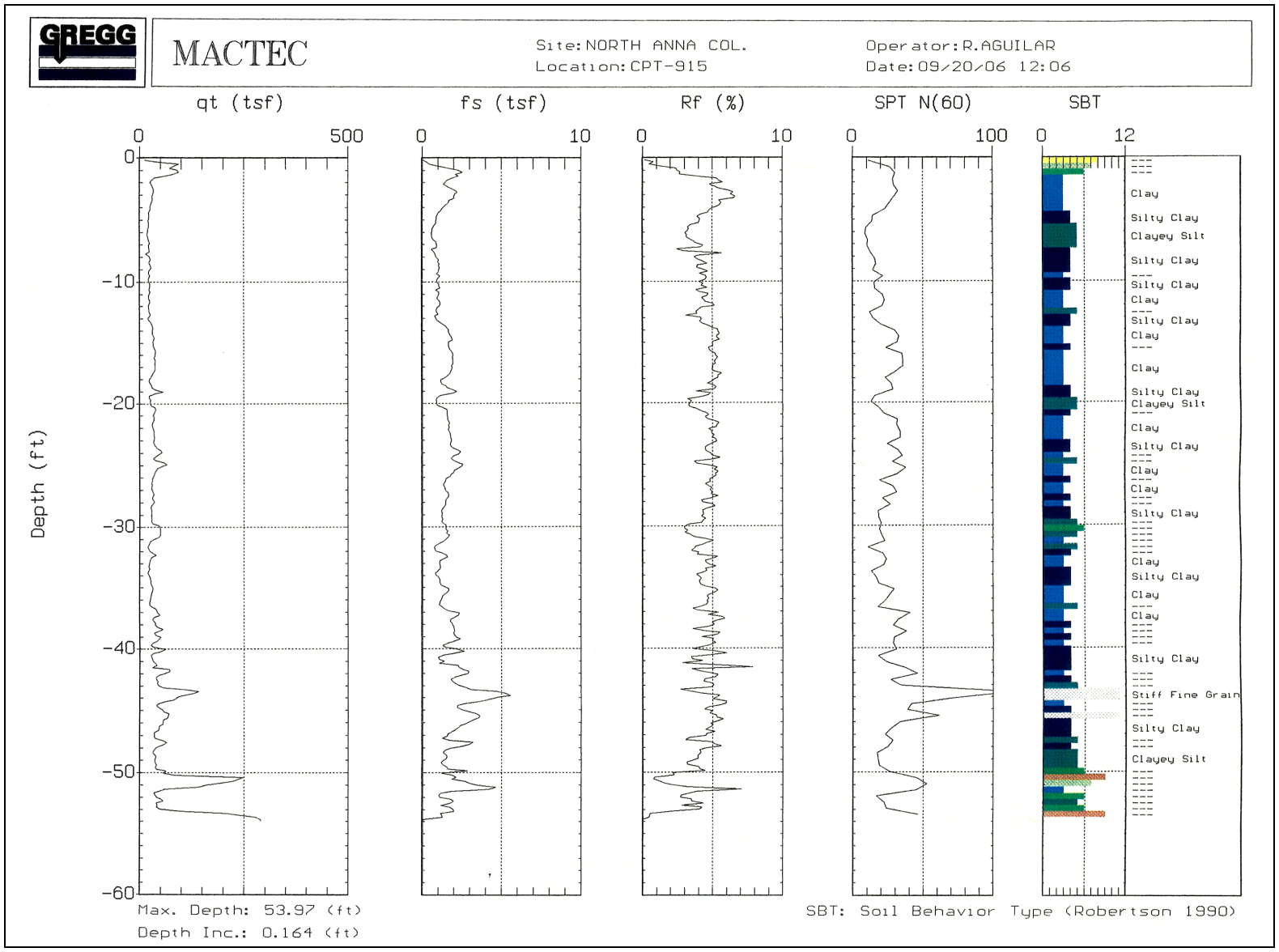

BASIS: NEW

NAPS COL 2.0-30-A **Figure 2.5.5-221 Log of CPT C-916**

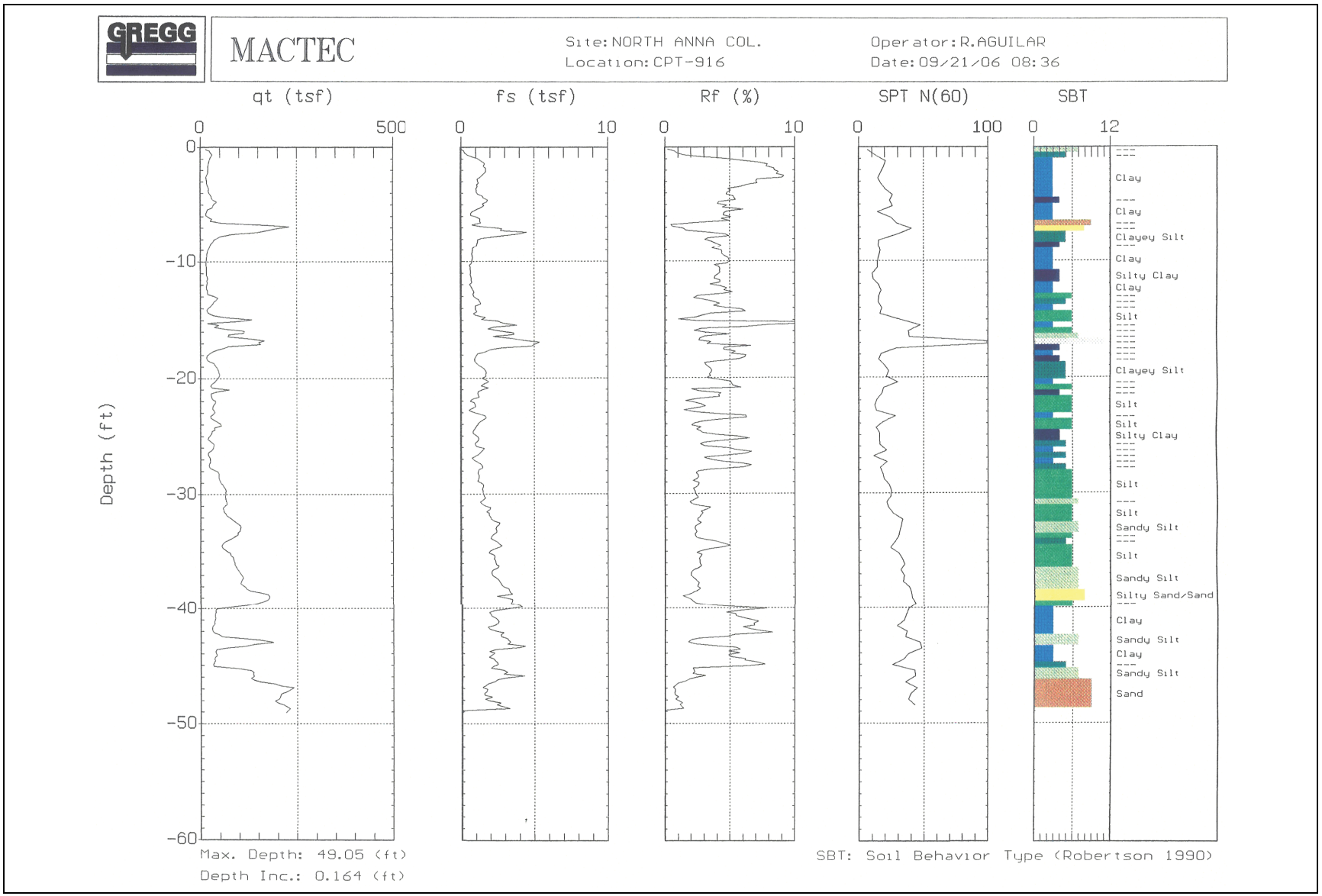

NAPS COL 2.0-30-A **Figure 2.5.5-222 Log of Well OW-947**

OBSERVATION WELL INSTALLATION RECORD

JOB NAME	NORTH ANNA COL	JOB NUMBER	6468-06-1472
WELL NUMBER	OW-947	INSTALLATION DATE	11-06-06
LOCATION (NAD83)	N = 3,909,579.58 E = 11,686,371.84		
GROUND SURFACE ELEVATION* (NAVD88)	313.30	REFERENCE POINT ELEVATION** (NAVD88)	315.08
GRANULAR BACKFILL MATERIAL	Southern Silica #1 & #3 Sand*	SLOT SIZE	.010
SCREEN MATERIAL	PVC Schd. 40-Standard	SCREEN DIAMETER	2 in.
RISER MATERIAL	PVC Schd. 40-Standard	RISER DIAMETER	2 in.
DRILLING TECHNIQUE	Hollow-stem auger 4.25" I.D.	DRILLING CONTRACTOR	MACTEC
BOREHOLE DIAMETER	Approximately 8"	MACTEC FIELD REPRESENTATIVE	Kim Charles-Smith
LOCK BRAND	Master	SIZE/MODEL	N/A
KEY CODE/COMBINATION	#3206		

* Both #1 and #3 sand met the technical specifications for use as granular backfill material. MACTEC used #3 sand to backfill the sump portion of observation well OW-947, and #1 sand for the remaining portion of the well boring.

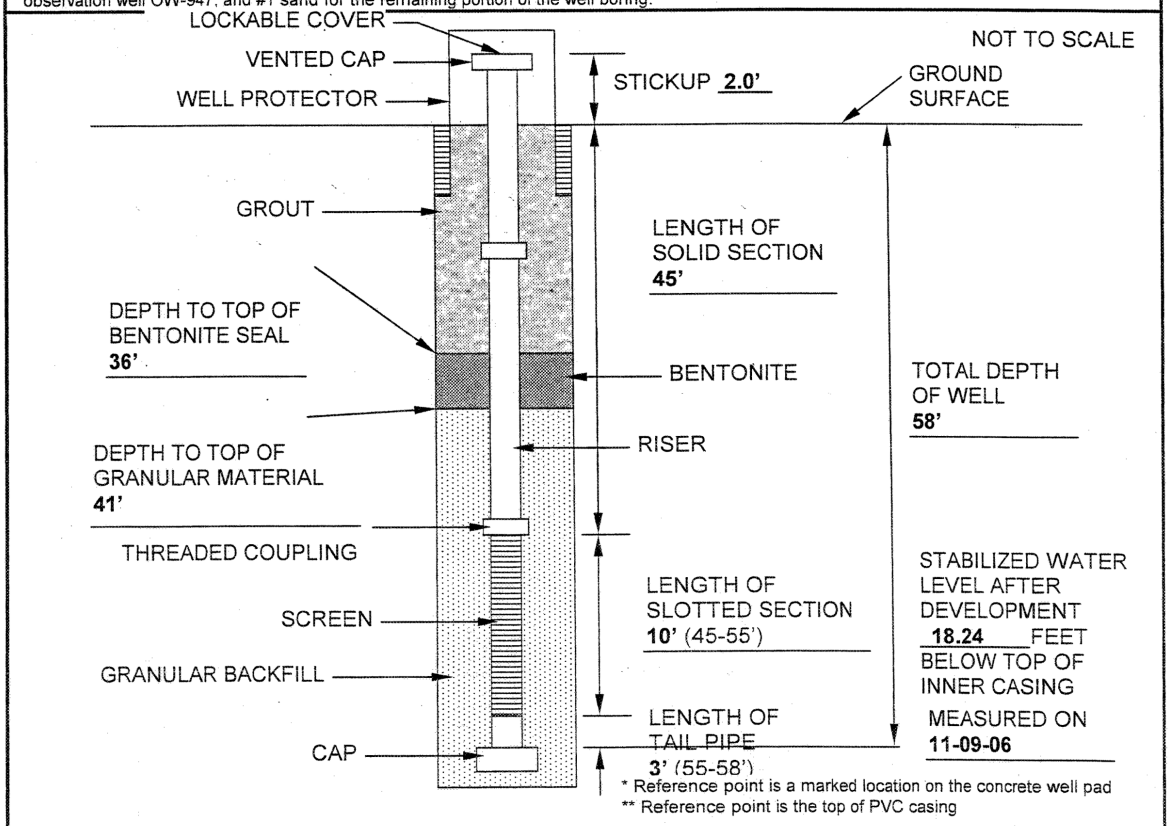

NORTH ANNA POWER STATION
MINERAL, VIRGINIA
COL PROJECT
Dominion Purchase Order 7015798

MACTEC
MACTEC Engineering and Consulting, Inc.
3301 Atlantic Avenue
Raleigh, North Carolina 27604

OBSERVATION WELL INSTALLATION RECORD

2.5.6 Embankments and Dams

SSAR Section 2.5.6 is incorporated by reference with the following supplement.

This SSAR section is supplemented as follows with a new paragraph on Unit 3 embankments and dams.

NAPS COL 2.0-30-A

Because Lake Anna is only used as a source of makeup water for Unit 3, the North Anna Dam, which is designed and constructed to meet requirements for a Seismic Category I structure in support of the existing Units 1 and 2, was not re-analyzed as part of this FSAR. Construction of Unit 3 does not adversely affect the slopes of the SWR for Units 1 and 2. There is an existing slope to the north of the SWR and a new slope to the east of the FWSC. These slopes are described and analyzed in Section 2.5.5.

Section 2.5 References

2.5-201 North Anna Early Site Permit Application, Rev. 9, Dominion Nuclear North Anna LLC, September 2006.

2.5-202 U.S. NRC. NUREG-0800, “Standard Review Plan for the Review of Safety Analysis Reports for Nuclear Power Plants,” Section 2.5.4, Revision 3, March 2007.

2.5-203 U.S. NRC. RG 1.206, “Combined License Applications for Nuclear Power Plants (LWR Edition),” June 2007.

2.5-204 ASME NQA-1 Subpart 2.20. “Quality Assurance Program Requirements for Nuclear Facilities,” 1994.

2.5-205 ASTM International. ASTM D 4220-95, Standard Practice for Preserving and Transporting Soil Samples, West Conshohocken, PA, 1995.

2.5-206 ASTM International. ASTM D 4633-05, Standard Test Method for Energy Measurement for Dynamic Penetrometers, West Conshohocken, PA, 2005.

2.5-207 ASTM International. ASTM D 4630-96, Standard Test Method for Determining Transmissivity and Storage Coefficient of Low-Permeability Rocks by In Situ Measurements Using the Constant Head Injection Test, West Conshohocken, PA, 1996.

2.5-208 U.S. Army Engineer Waterways Experiment Station, CE. Rock Testing Handbook, RTH 381-80, Vicksburg, Mississippi.

2.5-209 ASTM International. ASTM D 2487-06, Standard Practice for Classification of Soils for Engineering Purposes (Unified Soil Classification System), West Conshohocken, PA, 2006.

2.5-210 ASTM International. ASTM G 57-06, Standard Test Method for Field Measurement of Soil Resistivity Using the Wenner Four-Electrode Method, West Conshohocken, PA, 2006.

2.5-211 SHAKE2000, Equivalent Linear Seismic Response Analysis of Horizontally Layered Sites, Version 1.1, 2006.

2.5-212 Seed, H. B., I. M. Idriss, and I. Arango, “Evaluation of Liquefaction Potential Using Field Performance Data,” Journal of Geotechnical Engineering, ASCE, 109(3), 1983.

2.5-213 Imai, T. and K. Tonouchi, “Correlation of N-Value with S-Wave Velocity and Shear Modulus,” Proceedings, Second European Symposium on Penetration Testing, No. 1, Balkema, Amsterdam, 1982.

2.5-214 U.S. NRC. RG 1.198, “Procedures and Criteria for Assessing Seismic Soil Liquefaction at Nuclear Plants,” November 2003.

2.5-215 American Concrete Institute. “Code Requirements for Nuclear Safety-Related Structures,” ACI 349-01, 2001.

2.5-216 Poulos, H.G., and E. H. Davis, Elastic Solutions for Soil and Rock Mechanics, John Wiley and Sons, Inc., New York, 1974.

2.5-217 Seed, H. B., and R. V. Whitman, “Design of Earth Retaining Structures for Dynamic Loads,” Specialty Conference on Lateral Stresses in the Ground and Design of Earth Retaining Structures, ASCE, New York, 1970.

2.5-218 ASCE 4-98, Seismic Analysis of Safety-Related Nuclear Structures and Commentary, ASCE, Reston, VA, 2000.

2.5-219 Geo-Slope International Ltd. SLOPE/W Version 6.13, Calgary, Alberta, Canada, 2004.

2.5-220 ASTM International, ASTM D 1587-00, Standard Practice for Thin-Walled Tube Sampling of Soils for Geotechnical Purposes, West Conshohocken, PA, 2000.

2.5-221 ASME NQA-1, Table 5.6, “Quality Assurance Program Requirements for Nuclear Facilities,” 1994.

2.5-222 Bechtel Standard Computer program P-SHAKE (GE315), Version 2.0, “A Computer Program for Conducting Equivalent Linear Seismic Response Analyses of Horizontally Layered Soil Deposits Based on Random Vibration Theory,” Revision 1, September 2009.

2.5-223 U.S. NRC, U.S. DOE, and EPRI, NUREG-2115, “Central and Eastern United States Seismic Source Characterization for Nuclear Facilities,” January 2012.

2.5-224 EPRI, “CEUS Ground Motion Project Final Report,” Report TR-1009684, December 2004.

2.5-225 EPRI and U.S. DOE, “Program on Technology Innovation: Truncation of the Lognormal Distribution and Value of the Standard Deviation for Ground Motion Models in the Central and Eastern United States,” Report 1014381, 2006.

2.5-226 U.S. NRC, RG 1.208, “A Performance-Based Approach to Define the Site-Specific Earthquake Ground Motion,” March 2007.

2.5-227 EPRI, “Seismic Hazard Methodology for the Central and Eastern United States,” EPRI-NP-4726, 10 Volumes, 1988.

2.5-228 EPRI, “Probabilistic Seismic Hazard Evaluations at Nuclear Plant Sites in the Central and Eastern United States: Resolution of the Charleston Earthquake Issue,” EPRI Technical Report EPRI NP-6395-D, 1989.

2.5-229 U.S. NRC, NUREG/CR-5250, “Seismic Hazard Characterization of 69 Nuclear Plant Sites East of the Rocky Mountains,” Volumes 1–8, January 1989.

2.5-230 U.S. NRC, NUREG-1488, “Revised Livermore Seismic Hazard Estimates for Sixty-Nine Nuclear Power Plant Sites East of the Rocky Mountains,” April 1994.

2.5-231 Lawrence Livermore National Laboratory, “Eastern Seismic Hazard Characterization Update,” UCRL-ID-115111, June 1993.

2.5-232 Horton, J. W., M. C. Chapman, A. M. Carter, M. W. Carter, R. W. Harrison, R. B. Herrmann, and S. L. Snyder, “Faults Delineated by Aftershocks Associated with the 2011 Central

Virginia Earthquake and their Tectonic Setting," Geological Society of America, Southeast Section Meeting, Abstracts with Programs, Volume 44 (4), 2012.

2.5-233 Carter, M. W., M. L. Blanpied, A. L. Leeds, E. L. Harp, D. E. McNamara, R. W. Harrison, and J. S. Schindler, "USGS Response to the Mineral, Virginia MW 5.8 Earthquake of 23 August 2011," Geological Society of America, Southeast Section Meeting, Abstract with Programs, Volume 44 (4), 13, 2012.

2.5-234 Cramer, C. H., J. R. Kutliroff, and D. T. Dangkua, "The 2011 M5.7 Mineral, VA and M5.6 Sparks, OK Earthquake Ground Motions and Stress Drops: An Important Contribution to the NGA East Ground Motion Database," Seismological Society of America, Seismological Research Letters, Volume 83, 420, March/April 2012.

2.5-235 Chapman, M.C., "The Rupture Process of the August 23, 2011 Louisa County, Virginia Earthquake," Seismological Society of America Abstract, Seismological Research Letters, Volume 83, 403, March/April 2012.

2.5-236 Li, Y., "Seismic Investigations of Mineral, VA earthquake Impact to the North Anna Nuclear Power Plant," Seismological Society of America Abstract, Seismological Research Letters, Volume 83, 404, March/April 2012.

2.5-237 USGS, Website, Earthquake Hazards Program, Magnitude 5.8—Virginia, 2011 August 23, 17:51:04 UTC, available at http://earthquake.usgs.gov/earthquakes/recenteqsww/Quakes/se082311a.php, accessed on May 8, 2012

2.5-238 Wolin, E., S. Stein, F. Pazzaglia, A. Meltzer, A. Kafka, and C. Berti, "Mineral, Virginia earthquake illustrates seismicity of a passive-aggressive margin," Geophysical Research Letters 39, L02305, 7pp, 2012.

2.5-239 Brown, L.D., J. A. Hole, D. A. Quiros, K. Davenport, L. Han, C. Chen, W. Mooney, M. Chapman, "Aftershock Imaging with Dense Arrays (AIDA) after the August 23, 2011, Mw 5.8, Virginia Earthquake: Results from a Prototype Rapid Deployment of Large Numbers of Seismometers for High

Resolution Source Characterization, Structural imaging and 4D Monitoring," Seismological Society of America Abstract, Seismological Research Letters, Volume 83, 403, March/April 2012.

2.5-240 Shao, G., J. G. F. Crempien, R. J. Archuleta, C. Ji, "Finite source modeling and stress drop of the 2011 M5.8 Virginia Earthquake based on seismic waveforms," Seismological Society of America Abstract, Seismological Research Letters, Volume 83, 404, March/April 2012.

2.5-241 Saint Louis University, Website: http://www.eas.slu.edu/eqc/eqc_significant/2011_Virginia/aftershock.html, accessed on May 8, 2012.

2.5-242 Virginia Tech Seismological Observatory, Website, Index of /outreach/vtso/anonftp/events/2011/Louisa_aftershocks available at http://www.geol.vt.edu/outreach/vtso/anonftp/events/2011/Louisa_aftershocks/loc_total.dat, accessed on February 23, 2012.

2.5-243 Green, R.A., and S. Lasley, "Liquefaction Resulting from the 2011 Central Virginia Earthquake," Geological Society of America, Southeast Section Meeting, Abstracts with Programs, Volume 44 (4), 2012.

2.5-244 USGS, Website, M 5.8 Central Virginia Earthquake of 23 August 2011, United States Geological Survey, Earthquake Summary Map, 2011 available at http://earthquake.usgs.gov/earthquakes/eqarchives/poster/2011, accessed on February 13, 2012.

2.5-245 Dicken, C.L., S. W. Nicholoson, J. D. Horton, S. A. Kinney, G. Gunther, M. P. Foose, and J. A. L. Mueller, "Preliminary integrated geologic map databases for the United States: Delaware, Maryland, New York, Pennsylvania, and Virginia," U.S. Geological Survey Open-File Report 2005-1325, 2005 (revised 2008).

2.5-246 Hughes, S. and J. Hibbard, "Relict Paleozoic Faults in the Epicentral Area of the August 23, 2011 Virginia Earthquake; Geology In the Ferncliff, VA Quadrangle," Geological Society of America, Southeast Section Meeting, Abstracts with Programs, Volume 44 (4), 2012. (Presentation also available on the

Geological Society of America, Website, https://gsa.confex.com/gsa/2012SE/finalprogram/abstract_202175.htm, accessed on April 11, 2012).

2.5-247 Electric Power Research Institute [EPRI] (1986). “Seismic Hazard Methodology for the Central and Eastern United States, Tectonic Interpretations,” Volumes 5-10, EPRI Report NP-4726, Palo Alto, California, July 1986.

2.5-248 Electric Power Research Institute [EPRI] (1988). “Seismic Hazard Methodology for the Central and Eastern United States, Volume 1, Part 1: Theory; Volume 1, Part 2: Methodology (Revision 1).” EPRI Report NP-4726-A, Rev. 1, Palo Alto, California, November 1988.

2.5-249 Electric Power Research Institute [EPRI] (1989a). “Seismic Hazard Methodology for Central and Eastern United States, Volume 3: User’s Manual (Revision 1).” EPRI Report NP-4726-CCML-A, Palo Alto, California, February 1989.

2.5-250 Electric Power Research Institute [EPRI] (1989c). “EQHAZARD Primer,” prepared by Risk Engineering for Seismicity Owners Group and EPRI, EPRI Report NP-6452-D, Palo Alto, California, June 1989.

2.5-251 Seeber, L., and Armbruster, J.G., 1991, The NCEER-91 Earthquake Catalog: Improved Intensity-Based Magnitudes and Recurrence Relations for U.S. Earthquakes East of New Madrid: Technical Report NCEER-91-0021, National Center for Earthquake Engineering Research, State University of New York at Buffalo.

2.5-252 Mueller, C., Hopper, M., and Frankel, A., 1997, Preparation of Earthquake Catalogs for the National Seismic Hazard Maps—Contiguous 48 States: U.S. Geological Survey Open-File Report 97-464, 36 pp.

2.5-253 Petersen, M.D., A. D. Frankel, S. C. Harmsen, C. S. Mueller, K. M. Haller, R. L. Wheeler, R. L. Wesson, Y. Zeng, O. S. Boyd, D. M. Perkins, N. Luco, E. H. Field, C. J. Wills, and K. S. Rukstales (2008). “Documentation for the 2008 Update of the United States National Seismic Hazard Maps,” U.S. Geological Survey, Open-File Report 2008–1128, v. 1.1, 128p, 2008.

2.5-254 Adams, J., and Halchuk, S., 2003, Fourth Generation Seismic Hazard Maps of Canada: Values for over 650 Canadian Localities Intended for the 2005 National Building Code of Canada: Geological Survey of Canada, Open File 4459, 155 pp.

2.5-255 Gutenberg, B., and C.F. Richter (1956). Earthquake magnitude, intensity, energy and acceleration: Bulletin of the Seismological Society of America, v. 46, no. 2, pp. 105-145.

2.5-256 Smith, W.E.T. (1962). Earthquakes of eastern Canada and adjacent areas: 1534–1927: Publications of the Dominion Observatory, v. XXVI, no. 5, pp. 271-302.

2.5-257 Smith, W.E.T. (1966). Earthquakes of eastern Canada and adjacent areas: 1928–1959: Publications of the Dominion Observatory, v. XXXII, no. 3, pp. 87-121.

2.5-258 Atkinson, G.M. (2004a). Empirical attenuation of ground-motion spectral amplitudes in southeastern Canada and the northeastern United States: Bulletin of the Seismological Society of America, v. 94, no. 3, pp. 1079-1095.

2.5-259 Atkinson, G.M. (2004b). Erratum to —Empirical attenuation of ground-motion spectral amplitudes in southeastern Canada and the northeastern United States: Bulletin of the Seismological Society of America, v. 94, no. 6, pp. 2419-2423.

2.5-260 Boatwright, J. (1994). Regional propagation characteristics and source parameters of earthquakes in northeastern North America: Bulletin of the Seismological Society of America, v. 84, no. 1, pp. 1-15.

2.5-261 Moulis, A. (2002) The Development of a Moment-Magnitude Based Earthquake Catalog for the Northeastern United States: M.S. thesis, Boston College.

2.5-262 Hanks, T.C., and H. Kanamori, 1979, “A moment magnitude scale,” Journal of Geophysical Research, v. 84, no. B5, pp. 2348-2350.

2.5-263 Tinti, S., and F. Mulargia (1985). Effects of magnitude uncertainties on estimating the parameters in the Gutenberg-Richter frequency-magnitude law. Bulletin of the Seismological Society of America, v. 75, no. 6, pp. 1681-1697.

2.5-264 Gardner, J. K. and L. Knopoff (1974). “Is the sequence of earthquakes in Southern California, with aftershocks removed, Poissonian?” Bull. Seism. Soc. Am., v. 64, no. 5, 1363–1367.

2.5-265 Gutenberg, B. and C. F. Richter (1944). “Frequency of earthquakes in California,” Bulletin of Seismological Society of America, v. 34, no. 4, 185–188.

2.5-266 Stepp, J.C. (1972). Analysis of completeness of the earthquake sample in the Puget Sound area and its effect on statistical estimates of earthquake hazard: Proceedings of the International Conference on Microzonation, v. 2, pp. 897-909.

2.5-267 Herrmann, R. (2012). Personal (email) communication to J. Marrone, Subject “Re: Magnitude types in the NAMT listing.” dated January 2, 2012.

2.5-268 U.S. Geological Survey [USGS] (2012). Earthquake Hazards, Magnitude 5.8 Virginia, 2011 August 23, 17:51:04 UTC; http://earthquake.usgs.gov/earthquakes/recenteqsww/Quakes/se082311a.php, acquired November 9, 2012.

2.5-269 Bollinger, G. A., M. S. Sibol, and M. C. Chapman (1992). Maximum magnitude estimation for an intraplate setting-Example: The Giles County, Virginia, Seismic Zone, Seismological Research Letters, v. 63, no. 2, p.139-152.

2.5-270 Bollinger, G. A., and M. G. Hopper (1971). Virginia’s Two Largest Earthquakes- December 22, 1875 and May 31, 1897, Bulletin of the Seismological Society of America, v. 61, no. 4, p. 1033-1039.

2.5-271 Saint Louis University (SLU) Earthquake Center, Earthquake source parameters (for the 2011 Virginia Earthquake), St. Louis University Earthquake Center, website, http://www.eas.slu.edu/eqc/eqc_mt/MECH.NA/20110823175105/index.html, accessed 11/5/2012, 2012.

2.5-272 Atkinson, G.M., and D.J. Wald (2007). "Did You Feel It?" intensity data—A surprisingly good measure of earthquake ground motion: Seismological Research Letters, v. 78, no. 3, p. 362–368.

2.5-273 Assatourians, K. and G. M. Atkinson (2011). Ground Motion Characteristics of the 2011 Virginia and 1988 Quebec M5.8 Earthquakes (abs), American Geophysical Union, Fall meeting 2011, abstract #S14B-04

2.5-274 Hough, S. (2012). Initial Assessment of the Intensity Distribution of the 2011 Mw 5.8 Mineral, Virginia, Earthquake. Seismological Research Letters, Vol. 83, N. 4, p 649-657.

2.5-275 Nuttli, O. W., G. A. Bollinger, and D. W. Griffiths (1979). On the relation between modified Mercalli intensity and body-wave magnitude, Bull. Seism. Soc. Am., v. 69, no. 3, 893–909.

2.5-276 Bollinger, G. A., and R. L. Wheeler (1983). The Giles County, Virginia, Seismic Zone, Science, v. 219, no. 4588, 1063-1065, doi 10/1126/science. 219.4588.1063.

2.5-277 Walsh, L., Montesi, L.G.J., Sauber, J.M., Watters, T.R., Kim, W.Y., Martin, A.J., Anderson, R., (2012). Stress Changes in the Greater DC Metropolitan Area as a Result of the 2010 Germantown, MD and 2011 Mineral, VA, Intraplate Earthquakes, Seismological Research Letters, v. 83, no. 1, p. 217.

2.5-278 Kanamori, H. and L. Rivera (2008). Source inversion of W phase: speeding up seismic tsunami warning: Geophysical Journal International, v. 175, p. 222-238.

2.5-279 Kinemetrics (2011). Letter and Electronic file transmittal from Kinemetrics to Dominion dated August 31st, 2011, Bechtel SDN 25659-000-L0-GZC-00001.

2.5-280 Center for Engineering Strong Motion Data [CESMD], 2012 Web site source: http://www.strongmotioncenter.org/cgi-bin/CESMD/iqrStationMap.pl?ID=MineralVirginia_23Aug2011_usse082311a, accessed January 23, 2013.

2.5-281 Senior Seismic Hazard Analysis Committee (SSHAC), Recommendations for Probabilistic Seismic Hazard Analysis — Guidance on Uncertainty and Use of Experts: Prepared by SSHAC, NUREG/CR-6372, 256 p., 1997.

2.5-282 Hanks, T.C., Abrahamson, N.A., Boore, D.M., Coppersmith, K.J, and Knepprath, N.E., Implementation of the SSHAC Guidelines for Level 3 and 4 PSHAs—Experience Gained from Actual Applications: U.S. Geological Survey Open-File Report 2009-1093, 66 p., 2009.

2.5-283 Kammerer, A.M. and Ake, J.P., Practical Implementation Guidelines for SSHAC Level 3 and 4 Hazard Studies: U.S. Nuclear Regulatory Commission NUREG-2117, 235 p., 2012.

2.5-284 Ellsworth, W.L., Matthews, M.V., Nadeau, R.M., Nishenko, S.P., Reasenberg, P.A., and Simpson, R.W., A physically-based earthquake recurrence model for estimation of long-term earthquake probabilities, Proceedings of the Workshop on Earthquake Recurrence: State of the Art and Directions for the Future, Istituto Nazionale de Geofisica. Rome, Italy, February 22-25, 1999.

2.5-285 Matthews, M.V., Ellsworth, W.L., and Reasenberg, P.A., A Brownian model for recurrent earthquakes: Bulletin of the Seismological Society of America, v. 92, pp. 2233-2250, 2002.

2.5-286 Johnston, A.C., Coppersmith, K.J., Kanter, L.R., and Cornell, C.A., The Earthquakes of Stable Continental Regions: Final Report Submitted to Electric Power Research Institute (EPRI): TR-102261, 5-volume proprietary report prepared for Electric Power Research Institute, Palo Alto, California, 1994.

2.5-287 Kijko, A., Estimation of the Maximum Earthquake Magnitude, Mmax: Pure and Applied Geophysics, v. 161, pp. 1-27, 2004.

2.5-288 Schulte, S.M., and Mooney, W.D., An Updated Global Earthquake Catalog for Stable Continental Regions: Reassessing the Correlation with Ancient Rifts, Geophysical Journal International, v. 161, pp. 707-721, 2005.

2.5-289 Prowell, D.C., Cretaceous and Cenozic tectonism on the Atlantic coastal margin, in Sheridan, R.E., and Grow, J.A., eds., The Atlantic continental margin, U.S.: Boulder, Colorado, Geological Society of America, The Geology of North America, v. I-2, p. 557-564, 1988.

2.5-290 Manspeizer, W., DeBoer, J., Costain, J.K., Froelich, A.J., Çoruh, C., Olsen, P.E., McHone, G.J., Puffer, J.H., and Prowell, D.C., Post-Paleozoic activity, in Hatcher, R.D., Jr., Thomas,

W.A., and Viele, G.W., eds., The Appalachian-Oachita Orogen in the United States: Boulder, Colorado, Geological Society of America, The Geology of North America, v. F-2, p. 319-374, 1989.

2.5-291 Crone, A.J., and Wheeler, R.L., Data for Quaternary Faults, Liquefaction Features, and Possible Tectonic Features in the Central and Eastern United States, East of the Rocky Mountain Front: U.S. Geological Survey Open-File Report 00-0260, 342 p., 2000.

2.5-292 LASE Study Group, Deep structure of the US East Coast passive margin from large aperture seismic experiments, Marine and Petroleum Geology, v. 3, pp. 234-242, 1986.

2.5-293 Austin, J.A., Jr., Stoffa, P.L., Phillips, J.D., Oh, J., Sawyer, D.S., Purdy, G.M., Reiter, E., and Makris, J., Crustal structure of the Southeast Georgia embayment-Carolina trough: Preliminary results of a composite seismic image of a continental suture(?) and a volcanic passive margin, Geology, v.18, pp. 1023-1027, 1990.

2.5-294 Wheeler, R.L., Earthquakes and the Cratonward Limit of Iapetan faulting in eastern North America: Geology, v. 23, no. 2, pp. 105-108, 1995.

2.5-295 Mooney, W.D., and Ritsema, J., Mmax and Lithospheric Structure in Central and Eastern North America [abstract]: Proceedings, Meeting of Central and Eastern U.S. (CEUS) Earthquake Hazards Program, October 28-29, 2009, Memphis, TN, U.S. Geological Survey Memphis, TN, office, p. 25, 2009.

2.5-296 Tremblay, A., Long, B., and Massé, M., Supracrustal faults of the St. Lawrence rift system, Québec: Kinematics and geometry as revealed by field mapping and marine seismic reflection data: Tectonophysics, v. 369, pp. 231-252, 2003.

2.5-297 Lemieux, Y., Tremblay, A., and Lavoie, D., Structural analysis of supracrustal faults in the Charlevoix area, Quebec: Relation to impact cratering and the St-Laurent fault system: Canadian Journal of Earth Sciences, v. 40, pp. 221-235, 2003.

2.5-298 Rocher, M., Tremblay, A., Lavoie, D., and Campeau, A., Brittle fault evolution of the Montréal area (St Lawrence Lowlands, Canada): Rift-related structural inheritance and tectonism approached by palaeostress analysis: Geological Magazine, v. 140, pp. 157-172, 2003

2.5-299 Rimando, R.E., and Benn, K., Evolution of faulting and paleo-stress field within the Ottawa graben, Canada: Journal of Geodynamics, v. 39, pp. 337-360, 2005.

2.5-300 McBride, J.H., Leetaru, H.E., Bauer, R.A., Tingey, B.E., and Schmidt, S.E.A., Deep faulting and structural reactivation beneath the southern Illinois basin: Precambrian Research, v. 157, pp. 289-313, doi:10.1016/j.precamres.2007.02.020, 2007.

2.5-301 Obermeier, S.F., Weems, R.E., Jacobson, R.B., and Gohn, G.S., Liquefaction Evidence for Repeated Holocene Earthquakes in the Coastal Region of South Carolina: Annals of the New York Academy of Sciences, v. 558, pp. 183-195, 1989.

2.5-302 Weems, R.E., and Obermeier, S.F., The 1886 Charleston earthquake—An Overview of Geological Studies: *in* Proceedings of the U.S. Nuclear Regulatory Commission Seventeenth Water Reactor Safety Information Meeting, NUREG/CP-0105, v. 2, pp. 289-313, 1990.

2.5-303 Amick, D., Gelinas, R., Maurath, G., Cannon, R., Moore, D., Billington, E., and Kemppinen, H., Paleoliquefaction Features along the Atlantic Seaboard: U.S. Nuclear Regulatory Commission, NUREG/CR-5613 RA, 146 p., 1990a.

2.5-304 Amick, D., Maurath, G., and Gelinas, R., Characteristics of Seismically Induced Liquefaction Sites and Features Located in the Vicinity of the 1886 Charleston, South Carolina Earthquake: Seismological Research Letters, v. 61, no. 2, pp. 117-130, 1990b.

2.5-305 Talwani, P., and Schaeffer, W., Recurrence rates of Large Earthquakes in the South Carolina Coastal Plain based on Paleoliquefaction Data: Journal of Geophysical Research, v. 106, pp. 6621-6642, 2001.

2.5-306 Talwani, P., Dura-Gomez, I., Gassman, S., Hasek, M., and Chapman, A., Studies related to the Discovery of a Prehistoric Sandblow in the Epicentral Area of the 1886 Charleston SC Earthquake: Trenching and Geotechnical Investigations: Program and Abstracts, Eastern Section of the Seismological Society of America, p. 50, 2008.

2.5-307 Chapman, M.C., and Beale, J.N., Mesozoic and Cenozoic Faulting Imaged at the Epicenter of the 1886 Charleston, South Carolina Earthquake, Bulletin of the Seismological Society of America, v. 98, pp. 2533-2542, 2008.

2.5-308 Chapman, M.C., and Beale, J.N., On the Geologic Structure at the Epicenter of the 1886 Charleston, South Carolina, Earthquake, Bulletin of the Seismological Society of America, v. 100, no. 3, pp. 1010-1030, 2010.

2.5-309 Hu, K., Gassman, S.L., and Talwani, P., In-situ Properties of Soils at Paleoliquefaction Sites in the South Carolina Coastal Plain: Seismological Research Letters, v. 73, pp. 964-978, 2002a.

2.5-310 Hu, K., Gassman, S.L., and Talwani, P., Magnitudes of Prehistoric Earthquakes in the South Carolina Coastal Plain from Geotechnical Data: Seismological Research Letters, v. 73, pp. 979-991, 2002b.

2.5-311 Leon, E., Gassman, S.L., and Talwani, P., Effect of Soil Aging on Assessing Magnitudes and Accelerations of Prehistoric Earthquakes, Earthquake Spectra, v. 21, pp. 737-759, 2005.

2.5-312 Gassman, S., Talwani, P., and Hasek, M., Magnitudes of Charleston, South Carolina Earthquakes from In Situ Geotechnical Data: presentation given at meeting of CEUS Earthquake Hazards Program, U.S. Geological Survey, October 28-29, Memphis, Tenn, 2009.

2.5-313 Saucier, R., Geoarchaeological Evidence of Strong Prehistoric Earthquakes in the New Madrid (Missouri) Seismic Zone: Geology, v. 19, pp. 296-298, 1991.

2.5-314 Tuttle, M.P., and Schweig, E.S., Towards a Paleoearthquake Chronology of the New Madrid Seismic Zone: U.S. Geological Survey, Earthquake Hazards Program, Progress Report (99HQGR0022), 28 p., 2001.

2.5-315 Tuttle, M.P., Schweig, E.S., Sims, J.D., Lafferty, R.H., Wolf, L.W., and Haynes, M.I., The Earthquake Potential of the New Madrid Seismic Zone: Bulletin of the Seismological Society of America, v. 92, no. 6, pp. 2080-2089, 2002.

2.5-316 Tuttle, M.P., Schweig, E., III, Campbell, J., Thomas, P.M., Sims, J.D., and Lafferty, R.H., III, Evidence for New Madrid earthquakes in A.D. 300 and 2350 B.C.: Seismological Research Letters, v. 76, no. 4, pp. 489-501, 2005.

2.5-317 Schweig, E.S., and Ellis, M.A., Reconciling Short Recurrence Intervals with Minor Deformation in the New Madrid Seismic Zone: Science, v. 264, pp. 1308-1311, 1994.

2.5-318 Van Arsdale, R.B., Displacement History and Slip Rate on the Reelfoot Fault of the New Madrid Seismic Zone: Engineering Geology, v. 55, no. 4, pp. 219-226, 2000.

2.5-319 Holbrook, J., Autin, W.J., Rittenour, T.M., Marshak, S., and Goble, R.J., Stratigraphic Evidence for Millennial-Scale Temporal Clustering of Earthquakes on a Continental-Interior Fault: Holocene Mississippi River Floodplain Deposits, New Madrid Seismic Zone, USA: Tectonophysics, v. 420, pp. 431-454, 2006.

2.5-320 Calais, E., Mattioli, G., DeMets, C., Nocquet, J.M., Stein, S., Newman, A., and Rydelek, P., Tectonic Strain in the Interior of the North American Plate, Nature, v. 438, doi: 10.1038/nature04428, 2005.

2.5-321 Smalley, R., Jr., Ellis, M.A., Paul, J., and VanArsdale, R.B., Space Geodetic Evidence for Rapid Strain Rates in the New Madrid Seismic Zone of the Central USA: Nature, v. 435, pp.1088-1090, doi:10.1038/nature03642, 2005.

2.5-322 Bakun, W.H., and Hopper, M.G., Magnitudes and locations of the 1811-1812 New Madrid, Missouri, and the 1886 Charleston, South Carolina, earthquakes: Bulletin of the Seismological Society of America, v. 94, no. 1. pp. 64-75, 2004.

2.5-323 Hough, S.E., and Page, M., Toward a Consistent Model for Strain Accrual and Release for the New Madrid, Central United States: Journal of Geophysical Research, v. 116, no. B03311, doi:10.1029/2010JB007783, 2011.

2.5-324 Obermeier, S.F., Bleurer, N.K., Munson, C.A., Munson, P.J., Marin, W.S., McWilliams, K.M., Tabaczynski, D.A., Odum J.K., Rubin, M., and Eggert, D.L., Evidence of strong earthquake shaking in the lower Wabash Valley from prehistoric liquefaction features: *Science*, v. 251, pp. 1061-1063, 1991.

2.5-325 Munson, P.J., Obermeier, S.M., Munson, C.A., and Hajic, E.R., Liquefaction evidence for Holocene and latest Pleistocene in the southern halves of Indiana and Illinois—A preliminary overview: Seismological Research Letters, v. 68, no. 4, pp. 523-536, 1997.

2.5-326 Pond, E.C., and Martin, J.R., Estimated magnitudes and accelerations associated with prehistoric earthquakes in the Wabash Valley region of the central United States: in Kolata, D.R., and Hildenbrand, T.G. (editors), Investigations of the Illinois Basin Earthquake Region, Seismological Research Letters, v. 68, pp. 611-623, 1997.

2.5-327 Obermeier, S.F., Liquefaction evidence for strong earthquakes of Holocene and latest Pleistocene ages in the states of Indiana and Illinois, USA: Engineering Geology, Elsevier Science, v. 50, pp. 227-254, 1998.

2.5-328 McNulty, W.E., and Obermeier, S.F., Liquefaction evidence for at least two strong Holocene paleoearthquakes in central and southwestern Illinois, USA: Environmental and Engineering Geoscience, v. 5, no. 2, pp. 133-146, 1999.

2.5-329 Tuttle, M., Chester, J., Lafferty, R., Dyer-Williams, K., and Cande, B., Paleoseismology Study Northwest of the New Madrid Seismic Zone: U.S. Nuclear Regulatory Commission, NUREG/CR-5730, 98 pp., 1999.

2.5-330 Virginia Tech Seismological Observatory (VTSO), Louisa County Earthquake: August 23, 2011, website http://www.geol.vt.edu/outreach/vtso/2011/0823-louisa accessed 2/16/2012.

2.5-331 Walsh, L.S., Montesi, L.G., Sauber, J.M., Watters, T.R., Kim, W., Martin, A.J., and Anderson, R., Comparing the stress change characteristics and aftershock decay rate of the 2011

Mineral, VA earthquake with similar earthquakes from a variety of tectonic settings, Abstract S11B-2241 presented at 2011 Fall Meeting, AGU, San Francisco, Calif., 5-9 Dec, 2011.

2.5-332 Ellsworth, W.L., Imanishi, K., Aist, T., Luetgert, J.H., and Pratt, T.L., The Mw5.8 Virginia earthquake of August 23, 2011: A high stress drop event in a critically stressed crust, 83rd Annual Meeting of the Eastern Section of the Seismological Society of America, October 16-18, Little Rock, Arkansas, 2011.

2.5-333 Earthquake Engineering Research Institute (EERI), The Mw 5.8 Virginia earthquake of August 23, 2011, EERI Special Earthquake Report, December 2011.

2.5-334 Geotechnical Extreme Events Reconnaissance (GEER), Geotechnical quick report on the affected region of the 23 August 2011 M5.8 Central Virginia earthquake near Mineral, Virginia, GEER Association Report No. GEER-026, 2011.

2.5-335 Chapman, M.C., Munsey, J.W., Powell, C.A., Whisner, S.C., and Whisner, J., The eastern Tennessee seismic zone: Summary after 20 years of network monitoring: Seismological Research Letters, v. 73, no. 2, p. 245, 2002.

2.5-336 Obermeier, S.F., Vaughn, J.D., and Hatcher, R.D., Field Trip Guide: Paleoseismic Features in and near Douglas Reservoir, East Tennessee Seismic Zone, Northeastern Tennessee, 25 p., 2010.

2.5-337 Vaughn, J. D., Obermeier, S. F., Hatcher, R. D., Howard, C. W., Mills, H. H., and Whisner, S. C., Evidence for One or More Major Late-Quaternary Earthquakes and Surface Faulting in the East Tennessee Seismic Zone, Seismological Research Letters, v. 81, no. 2, p. 323, 2010.

2.5-338 Howard, C.W., Derryberry, P.M., Hatcher, R.D. Jr., Vaughn, J.D., and Obermeier, S.F., Detailed geologic maps of two sites south of Dandridge, Tennessee, record evidence of polyphase paleoseismic activity in the East Tennessee seismic zone: Abstract from the 60th Annual Meeting of the Southeastern Section of the Geological Society of America, paper no. 16-1, 2011.

2.5-339 Warrell, K.F., Hatcher, R.D. Jr., Blankenship, S.A., Howard, C.W., Derryberry, P.M., Wunderlich, A.L., Obermeier, S.O., Counts, R.C., and Vaughn, J.D., Detailed geologic mapping of paleoseismic features: an added tool for seismic hazard assessment in the east Tennessee seismic zone, Abstract from the 61st Annual Meeting of the Southeastern Section of the Geological Society of America, paper no. 8-3, 2012.

2.5-340 Hurd, O., Stress measurement update for the Central and Eastern United States, conducted as part of the CEUS SSC project, 5 pp., 2010.

2.5-341 Shumway, A.M., Focal mechanisms in the northeast New Madrid seismic zone: Seismological Research Letters, v. 79, no. 3, pp. 469-477, 2008.

2.5-342 Horton, S.P., Kim, W.Y., and Withers, M., The 6 June 2003 Bardwell, Kentucky, earthquake sequence: Evidence for a locally perturbed stress field in the Mississippi embayment: Bulletin of the Seismological Society of America, v. 95, pp. 431-445, 2005.

2.5-343 Chapman, M.C., Powell, C.A., Vlahovic, G., and Sibol, M.S., A statistical analysis of earthquake focal mechanisms and epicenter locations in the eastern Tennessee seismic zone: Bulletin of the Seismological Society of America, v. 87, no. 6, pp. 1522-1536, 1997.

2.5-344 Kim, W.-Y., and Chapman, M., The 9 December 2003 central Virginia earthquake sequence: A compound earthquake in the Central Virginia seismic zone: Bulletin of the Seismological Society of America, v. 95, no. 6, pp. 2428-2445, 2005.

2.5-345 Mazzotti, S., Strain (and Stress) Constraints on Seismicity in the St. Lawrence Valley: presentation given at CEUS SSC Project Workshop #2, February 18-20, Palo Alto, Calif, 2009.

2.5-346 Dineva, S., Eaton, D., and Mereu, R., Seismicity of the southern Great Lakes: Revised earthquake hypocenters and possible tectonic controls: Bulletin of the Seismological Society of America, v. 94, no. 5, pp. 1902-1918, 2004.

2.5-347 Kim, W.-Y., The 18 June 2002 Caborn, Indiana, earthquake: Reactivation of ancient rift in the Wabash Valley seismic zone? Bulletin of the Seismological Society of America, v. 93, no. 5, pp. 2201-2211, 2003.

2.5-348 Seeber, L., Armbruster, J.G., Kim, W.-Y., and Barstow, N., The 1994 Cacoosing Valley earthquakes near Reading, Pennsylvania: A shallow rupture triggered by quarry unloading, Journal of Geophysical Research, v. 103, no. B10, pp. 24,505-24,521, 1998.

2.5-349 Heidbach, O., Tingay, M., Barth, A., Reinecker, J., Kurfess, D., and Müller, B., The World Stress Map database release 2008, http://dc-app3-14.gfz-potsdam.de, 2008.

2.5-350 van Lanen, X., and Mooney, W.D., Integrated geologic and geophysical studies of North American continental intraplate seismicity: in Stein, S., and Mazzotti, S. (editors), Continental Intraplate Earthquakes: Science, Hazard, and Policy Issues, Geological Society of America Special Paper 425, pp. 101-112, 2007.

2.5-351 Talwani, P., The Source and Magnitude of the Charleston Earthquakes: presentation given at CEUS SSC Project Workshop #2, February 18-20, Palo Alto, Calif, 2009.

2.5-352 Zoback, M.L., Stress field constraints on intraplate seismicity in eastern North America: Journal of Geophysical Research, v. 97, no. B8, pp. 11,761-11,782, 1992.

2.5-353 Sibson, R.H., and Xie, G., Dip range for intracontinental reverse fault ruptures: Truth not stranger than friction? Bulletin of the Seismological Society of America, v. 88, no. 4, pp. 1014-1022, 1998.

2.5-354 Marshak, S., and Paulsen, T., Structural style, regional distribution, and seismic implications of midcontinent fault-and-fold zones, United States: Seismological Research Letters, v. 68, no. 4. pp. 511-520, 1997.

2.5-355 Sibson, R.H., Roughness at the base of the seismogenic zone: Contributing factors: Journal of Geophysical Research, v. 89, pp. 5791-5799, 1984.

2.5-356 Sibson, R.H., Au-quartz mineralization near the base of the continental seismogenic zone: Geological Society, London, Special Publications, v. 272, no. 1, pp. 519-532, 2007.

2.5-357 Mai, P.M., Spudich, P., and Boatwright, J., Hypocenter locations in finite-source rupture models: Bulletin of the Seismological Society of America, v. 95, no. 3, pp. 965-980, 2005.

2.5-358 Sykes, L.R., Armbruster, J.G., Kim, W.-K., and Seeber, L., Observations and tectonic setting of historic and instrumentally located earthquakes in the greater New York City–Philadelphia area: Bulletin of the Seismological Society of America, v. 98, no. 4, pp. 1696-1719, 2008.

2.5-359 Somerville, P., Collins, N., Abrahamson, N., Graves, R., and Saikia, C., Ground Motion Attenuation Relations for the Central and Eastern United States, Final Report, June 30, 2001: external research project funded by U.S. Geological Survey Award No. 99HQGR0098, 38 pp, 2001.

2.5-360 Wesnousky, S.G., Displacement and geometrical characteristics of earthquake surface ruptures: Issues and implications for seismic-hazard analysis and the process of earthquake rupture: Bulletin of the Seismological Society of America, v. 98, no. 4, pp. 1609-1632, 2008.

2.5-361 NAGRA (Nationale Genossenschaft für die Lagerung radioaktiver Abfälle), Probabilistic Seismic Hazard Analysis for Swiss Nuclear Power Plant Sites (PEGASOS Project), Volume 1, Final Report, Wettingen, Switzerland, July 31, 2004.

2.5-362 Keller, M.R., Robinson, E.S., and Glover III, L., 1985, Seismicity, seismic reflection, gravity, and geology of the central Virginia seismic zone: Part 3. Gravity: Geological Society of America Bulletin, v. 96, pp. 1,580-1,584.

2.5-363 de Witt, W., and Bayer, K.C., 1986, Seismicity, seismic reflection, gravity, and geology of the Central Virginia Seismic Zone: Part 3. Gravity: Discussion and reply: Geological Society of America Bulletin, v. 97, Discussion, pp. 1285-1286.

2.5-364 Steltenpohl, M.G., Zietz, I., Horton, J.W., Jr., and Daniels, D.L., 2010, New York–Alabama lineament: A buried right-slip fault bordering the Appalachians and mid-continent North America: Geology, v. 38, no. 6, pp. 571-574.

2.5-365 Bollinger, G.A., and Wheeler, R.L., 1988, The Giles County, Virginia, Seismogenic Zone—Seismological Results and Geological Interpretations: U.S. Geological Survey Professional Paper 1355, 85 pp.

2.5-366 Law, R.D., Pope, M.C., Wirgart, R.H., Eriksson, K.A., Carpenter, D., Robinson, E.S., and Bollinger, G.A., 1993, Geologically recent near-surface folding and faulting in the Valley and Ridge Province: New exposures of extensional faults in alluvial sediments, Giles County, SW Virginia [abstract]: Eos, Transactions of the American Geophysical Union, v. 74, no. 16, p. 282.

2.5-367 Chapman, M.C., and Krimgold, F., 1994, Seismic Hazard Assessment for Virginia: report prepared for the Virginia Department of Emergency Services and the Federal Emergency Management Agency, Virginia Tech Seismological Observatory, Blacksburg, Va., 62 pp.

2.5-368 Law, R.D., Pope, M.C., Wirgart, R.H., Eriksson, K.A., Robinson, E.S., Sayer, S., Phinney, E.J., and Bollinger, G.A., 1994, Geologically recent near-surface faulting and folding in Giles County, southwest Virginia: New exposures of extensional and apparent reverse faults in alluvial sediments between Pembroke and Pearisburg: Proceedings of the U.S. Nuclear Regulatory Commission for 1994, Twenty-First Water Reactor Safety Information Meeting, October 25-27, 1993, Bethesda, Maryland, NUREG/CP-0133, v. 3, pp. 415-432.

2.5-369 Law, R.D., Robinson, E.S., Cyrnak, J.S., Sayer, S., Williams, R.T., Callis, J., and Pope, M., 1997, Geologically-recent faulting and folding of alluvial sediments near Pearisburg, Giles County, Virginia—Tectonic faulting or karst subsidence in origin? [abstract]: Eos, Transactions of the American Geophysical Union, v. 78, no. 17 (supplement), p. S316.

2.5-370 Obermeier, S.F., 1995, Paleoseismic liquefaction studies—Central U.S. and Pacific Northwestern U.S.: in Jacobsen, M.L. (compiler), National Earthquake Hazards Reduction Program Annual Project Summaries: XXXVI, Volume II, U.S. Geological Survey Open-File Report 95-210, pp. 606-609.

2.5-371 Seeber, L., and Armbruster, J.G., 1993, Natural and induced seismicity in the Lake Erie–Lake Ontario region: Reactivation of ancient faults with little neotectonic displacement: Géographie physique et Quaternaire, v. 47, no. 3, pp. 363-378.

2.5-372 Wheeler, R.L., and Crone, A.J., 2001, Known and suggested Quaternary faulting in the midcontinent United States: Engineering Geology, v. 62, pp. 51-78.

2.5-373 Niemi, T.M., Ferris, A.N., and Abers, G.A., 2004, Investigation of microearthquakes, macroseismic data, and liquefaction associated with the 1867 Wamego earthquake in eastern Kansas: Bulletin of the Seismological Society of America, v. 94, no. 6, pp. 2317-2329.

2.5-374 Adams, J., and Basham, P., 1991, The seismicity and seismotectonics of eastern Canada: in Slemmons, D.B., Engdahl, E.R., Zoback, M.D., and Blackwell, D.D. (editors), *Neotectonics of North America*, Geological Society of America, Decade Map, Volume 1.

2.5-375 Lamontagne, M., and Ranalli, G., 1997, Faults and spatial clustering of earthquakes near La Malbaie, Charlevoix seismic zone, Canada: Seismological Research Letters, v. 68, no. 2, pp. 337-352.

2.5-376 Harrison, R.W., A Preliminary Assessment of Neotectonic Features in the Central Virginia Seismic Zone, Geological Society of America, Abstracts with Programs, v. 44, no. 4, p. 14, 2012.

2.5-377 Spears, D.B., Geologic Framework of the Central Virginia Seismic Zone, Geological Society of America, Abstracts with Programs, v. 44, no. 4, p. 14, 2012.

2.5-378 McGuire, R.K., Seismic Hazard and Risk Analysis, Earthquake Engineering Research Institute, Monograph MNO-10, 2004.

2.5-379 Building Seismic Safety Council, “NEHRP [National Earthquake Hazards Reduction Program] Recommended Provisions for Seismic Regulations for New Buildings and Other Structures,” FEMA Rept. P-750, 2009 edition, Washington DC, 2009.

2.5-380 U.S. Nuclear Regulatory Commission (2010). Interim Staff Guidance on Ensuring Hazard-Consistent Seismic Input for Site Response and Soil Structure Interaction Analyses, DC/COL-ISG-17, March 2010.

2.5-381 Toro, G.R. (1995). Probabilistic Models of Site Velocity Profiles for Generic and Site-Specific Ground Motion Amplification Studies. Published as Appendix C in Silva, W.J., N. Abrahamson, G. Toro and C. Constantino. (1996). "Description and validation of the stochastic ground motion model." Report Submitted to Brookhaven National Laboratory, Associated Universities, Inc. Upton, New York 11973, Contract No. 770573.

2.5-382 Idriss, I. M., and Sun, J. I. (1992). SHAKE91: A Computer Program for Conducting Equivalent Linear Seismic Response Analyses of Horizontally Layered Soil Deposits, Dept. of Civil and Environmental Engineering, Center for Geotechnical Modeling, Univ. of California, Davis.

2.5-383 Kramer, Steven L. (1996). Geotechnical earthquake engineering, Prentice-Hall, ISBN 0-13-374943-6.

2.5-384 American Society of Civil Engineers [ASCE] and Structural Engineering Institute [SEI] (2005). “Seismic Design Criteria for Structures, Systems, and Components in Nuclear Facilities.” ASCE/SEI Standard 43-05, 1/1/2005, 103p.

2.5-385 McGuire, R.K., W. J. Silva, and C. J. Costantino (2001). “Technical Basis for Revision of Regulatory Guidance on Design Ground Motions, Hazard- and Risk-consistent Ground Motion Spectra Guidelines,” prepared for Nuclear Regulatory Commission, NUREG/CR-6728.

2.5-386 Graizer, V., C.G. Munson, and Y. Li (2013). “North Anna Nuclear Power Plant Strong-Motion Records of the Mineral, Virginia, Earthquake of 23 August 2011,” Seismological Research Letters, Volume 84, Number 3 May/June 2013, 551-557.

2.5-387 Electric Power Research Institute [EPRI] (1993). “Guidelines for Determining Design Basis Ground Motions,” Volumes 1-5, EPRI TR-102293, Electric Power Research Institute, Palo Alto, California.

2.5-388 Gülerce, Z, and N. Abrahamson (2011) [GA11], “Site-Specific Design Spectra for Vertical Ground Motion,” Earthquake Spectra, Volume 27, No. 4, pages 1023–1047.

2.5-389 Reinbold, D.J., and Johnston, A.C., 1987, Historical Seismicity in the Southern Appalachian Seismic Zone: U.S. Geological Survey Open-File Report 87-433, 40 pp.

Table 2.5-201 [Deleted] (Replaced by Table 2.5.2-228)
Table 2.5-202 [Deleted] (Replaced by Tables 2.5.2-223 and 2.5.2-225)
Table 2.5-203 [Deleted] (Replaced by Tables 2.5.2-222 and 2.5.2-224)
Table 2.5-204 [Deleted] (Replaced by Table 2.5.2-227)
Table 2.5-205 Renumbered as Table 2.5.4-201
Table 2.5-206 Renumbered as Table 2.5.4-202
Table 2.5-207 Renumbered as Table 2.5.4-203
Table 2.5-208 Renumbered as Table 2.5.4-204
Table 2.5-209 Renumbered as Table 2.5.4-205
Table 2.5-210 Renumbered as Tables 2.5.4-206a, 2.5.4-206b, and 2.5.4-206c
Table 2.5-211 Renumbered as Table 2.5.4-207)
Table 2.5-212 Renumbered as Table 2.5.4-208
Table 2.5-213 Renumbered as Table 2.5.4-209
Table 2.5-214 Renumbered as Table 2.5.4-210
Table 2.5-215 [Deleted] (Replaced by Table 2.5.4-211)
Table 2.5-216 Renumbered as Table 2.5.4-212
Table 2.5-217 [Deleted] (Replaced by Table 2.5.5-201)
Table 2.5-218 Renumbered to Table 2.5.5-202
Table 2.5-219 Renumbered to Table 2.5.5-203
Figure 2.5-201 [Deleted]
Figure 2.5-202 [Deleted]
Figure 2.5-203 [Deleted]
Figure 2.5-204 [Deleted]
Figure 2.5-205 [Deleted] (Replaced by Figure 2.5.2-313)
Figure 2.5-206 [Deleted] (Replaced by Figures 2.5.2-308 and 2.5.2-310)
Figure 2.5-207 [Deleted] (Replaced by Figures 2.5.2-307 and 2.5.2-309)
Figure 2.5-208 [Deleted] (Replaced by Figure 2.5.2-312)
Figure 2.5-209 [Deleted] (Replaced by Figure 2.5.4-201)
Figure 2.5-210 [Deleted] (Replaced by Figure 2.5.4-202)
Figure 2.5-211 [Deleted] (Replaced by Figure 2.5.4-203)
Figure 2.5-212 [Deleted] (Replaced by Figure 2.5.4-204)
Figure 2.5-213 [Deleted] (Replaced by Figure 2.5.4-205)
Figure 2.5-214 [Deleted] (Replaced by Figure 2.5.4-206)
Figure 2.5-215 [Deleted] (Replaced by Figure 2.5.4-207)
Figure 2.5-216 [Deleted] (Replaced by Figure 2.5.4-208)

Figure 2.5-217 [Deleted] (Replaced by Figure 2.5.4-209)
Figure 2.5-218 [Deleted] (Replaced by Figure 2.5.4-210)
Figure 2.5-219 [Deleted] (Replaced by Figure 2.5.4-211)
Figure 2.5-220 [Deleted] (Replaced by Figure 2.5.4-212)
Figure 2.5-221 [Deleted] (Replaced by Figure 2.5.4-217)
Figure 2.5-222 [Deleted] (Replaced by Figure 2.5.4-218)
Figure 2.5-223 Renumbered as Figure 2.5.4-219
Figure 2.5-224 [Deleted] (Replaced by Figure 2.5.4-220)
Figure 2.5-225 [Deleted] (Replaced by Figure 2.5.4-221)
Figure 2.5-226 [Deleted] (Replaced by Figure 2.5.4-222)
Figure 2.5-227 [Deleted] (Replaced by Figure 2.5.4-223)
Figure 2.5-228 [Deleted] (Replaced by Figure 2.5.4-224)
Figure 2.5-229 [Deleted] (Replaced by Figure 2.5.4-225)
Figure 2.5-230 [Deleted] (Replaced by Figure 2.5.4-226)
Figure 2.5-231 [Deleted] (Replaced by Figure 2.5.4-227)
Figure 2.5-232 [Deleted] (Replaced by Figure 2.5.4-228)
Figure 2.5-233 [Deleted] (Replaced by Figure 2.5.4-229)
Figure 2.5-234 [Deleted] (Replaced by Figure 2.5.4-230)
Figure 2.5-235 [Deleted] (Replaced by Figure 2.5.4-235)
Figure 2.5-236 [Deleted] (Replaced by Figure 2.5.4-236)
Figure 2.5-237 [Deleted] (Replaced by Figure 2.5.4-237)
Figure 2.5-238 [Deleted] (Replaced by Figure 2.5.4-238)
Figure 2.5-239 [Deleted] (Replaced by Figure 2.5.4-239)
Figure 2.5-240 [Deleted] (Replaced by Figure 2.5.4-241)
Figure 2.5-241 [Deleted] (Replaced by Figure 2.5.4-242)
Figure 2.5-242 [Deleted] (Replaced by Figure 2.5.4-243)
Figure 2.5-243 [Deleted] (Replaced by Figure 2.5.4-244)
Figure 2.5-244 Re-titled and renumbered as Figure 2.5.4-245
Figure 2.5-245 [Deleted] (Replaced by Figure 2.5.4-246)
Figure 2.5-246 Renumbered as Figure 2.5.4-247
Figure 2.5-247 Renumbered as Figure 2.5.4-248
Figure 2.5-248 Renumbered as Figure 2.5.4-249
Figure 2.5-249 [Deleted] (Replaced by Figure 2.5.4-250)
Figure 2.5-250 [Deleted]
Figure 2.5-251 [Deleted] (Replaced by Figure 2.5.4-251)
Figure 2.5-252 [Deleted] (Replaced by Figure 2.5.4-252)
Figure 2.5-253 [Deleted] (Replaced by Figure 2.5.4-253)
Figure 2.5-254 [Deleted] (Replaced by Figure 2.5.4-254)
Figure 2.5-255 Deleted] (Replaced by Figure 2.5.5-201)

Figure 2.5-256 [Deleted] (Replaced by Figure 2.5.5-202)
Figure 2.5-257 [Deleted] (Replaced by Figure 2.5.5-203)
Figure 2.5-258 [Deleted] (Replaced by Figure 2.5.5-204)
Figure 2.5-259 [Deleted] (Replaced by Figure 2.5.5-205)
Figure 2.5-260 [Deleted] (Replaced by Figure 2.5.5-206)
Figure 2.5-261 [Deleted] (Replaced by Figure 2.5.5-207)
Figure 2.5-262 [Deleted] (Replaced by Figure 2.5.5-208)
Figure 2.5-263 [Deleted] (Replaced by Figure 2.5.5-209)
Figure 2.5-264 [Deleted] (Replaced by Figure 2.5.5-210)
Figure 2.5-265 [Deleted] (Replaced by Figure 2.5.5-211)
Figure 2.5-266 [Deleted] (Replaced by Figure 2.5.5-212)
Figure 2.5-267 [Deleted] (Replaced by Figure 2.5.5-213)
Figure 2.5-268 [Deleted] (Replaced by Figure 2.5.5-214)
Figure 2.5-269 [Deleted] (Replaced by Figure 2.5.5-215)
Figure 2.5-270 [Deleted] (Replaced by Figure 2.5.5-216)
Figure 2.5-271 [Deleted] (Replaced by Figure 2.5.5-217)
Figure 2.5-272 Renumbered as Figure 2.5.5-218
Figure 2.5-273 [Deleted] (Replaced by Figure 2.5.5-219)
Figure 2.5-274 [Deleted] (Replaced by Figure 2.5.5-220)
Figure 2.5-275 [Deleted] (Replaced by Figure 2.5.5-221)
Figure 2.5-276 [Deleted] (Replaced by Figure 2.5.5-222)
Figure 2.5-277 Renumbered as Figure 2.5.4-240

Appendix 2A ARCON96 Source/Receptor Inputs

This section of the referenced DCD is incorporated by reference with the following departures and/or supplements.

2A.2.1 Meteorological Data

Add the following as the last sentence of this section.

NAPS COL 2A.2-1-A

Instrumentation heights used in the analysis are described in SSAR Section 2.3.3.1.3. Meteorological data from 1996 to 1998 as described in SSAR Section 2.3 is used in the analysis.

2A.2.3 ARCON96 ESBWR Inputs

Replace the last sentence of the first paragraph with the following.

NAPS COL 2A.2-1-A

These directions are adjusted by the difference in angle (approximately 23.5 degrees east of true North); Unit 3 receptor to source directions are shown in Table 2A-4R.

2A.2.4 Confirmation of the ESBWR χ/Q Values

Replace this section with the following.

NAPS COL 2A.2-1-A

DCD Figure 2A-1 shows the locations of the sources and receptors for ESBWR control room determinations, also used in the Unit 3 evaluations. The dimensions of the diffuse source planes provided in DCD Table 2A-3 are determined as directed by RG 1.194, Regulatory Position 3.2.4.5, for the nearest receptor locations. ARCON96 calculations are performed for source/receptor pairs compared in Table 2.0-201. The calculations used design inputs listed in DCD Table 2A-3, directions in Table 2A-4R, and site-specific meteorological data. Results of the site-specific analysis are provided in Tables 2.3-201 through 2.3-204, and Table 2.3-206.

2A.2.5 Confirmation of the Reactor Building χ/Q Values

Replace this section with the following.

NAPS COL 2A.2-2-A

During refueling, doors or personnel air locks on the plant east sides of the Reactor Building or Fuel Building could act as a point source that could result in χ/Q values that would result in a dose greater than a bounding dose consequence reported in the Fuel Handling Accident Analysis Results (DCD Table 15.4-4). Therefore, these doors and

personnel air locks are administratively controlled to remain closed during movement of irradiated fuel bundles.

2A.3 COL Information

2A.2-1-A **Confirmation of the ESBWR χ/Q Values**

NAPS COL 2A.2-1-A This COL item is addressed in Section 2.3.4.3 and in Section 2A.2.4.

2A.2-2-A **Confirmation of the Reactor Building χ/Q Values**

NAPS COL 2A.2-2-A This COL item is addressed in Section 2A.2.5.

NAPS ESP COL 2.3-2
NAPS COL 2A.2-1-A

Table 2A-4R ARCON96 Direction Design Inputs Used for the Determination of On-Site χ/Q Values

Source/Receptor	Direction (degrees from true North)
RB to CBL	294
RB to EN	284
RB to ES	304
RB to N	308
RB to TSCB	236
RB to TSCA	240
PCCS to CBL	333
PCCS to EN	309
PCCS to ES	328
PCCS to N	332
PCCS to TSCB	238
PCCS to TSCA	241
TB to CBL	7
TB to EN	348
TB to ES	355
TB to N	360
TB to TSCB	256
TB to TSCA	260
TB-TD to CBL	5
TB-TD to EN	355
TB-TD to TSCB	301
FB to CBL	252
FB to EN	258
FB to ES	272
FB to N	276
RW to N	328
RB-VS to CBL	271
RB-VS to ES	285
RB-VS to N	286
TB-VS to CBL	20

NAPS ESP COL 2.3-2
NAPS COL 2A.2-1-A

Table 2A-4R ARCON96 Direction Design Inputs Used for the Determination of On-Site χ/Q Values

Source/Receptor	Direction (degrees from true North)
TB-VS to EN	5
TB-VS to N	12
RW-VS to CBL	326
RW-VS to EN	314
RW-VS to N	328
BPN to CBL	346
BPN to EN	309
BPN to ES	330
BPN to N	339
BPS to CBL	243
BPS to EN	253
BPS to ES	279
BPS to N	283

Appendix 2B Ventilation Stack Pathway Information for Long-Term χ/Q Values

This section of the referenced DCD is incorporated by reference with no departures or supplements.